
Quantum Noise and Quantum Walks

By

ANDREU ANGLÉS CASTILLO



VNIVERSITAT DE VALÈNCIA

PROGRAMA DE DOCTORAT EN FÍSICA - 3126
Departament de Física Teòrica

JULY 2023

Advisors:

Prof. Armando Pérez Cañellas
Prof. Mari Carmen Bañuls Polo
Prof. Inés de Vega Rodrigo

El tiempo se lo lleva lo numérico

Inés de Vega

Abstract

The first part of the thesis is dedicated to the field of open quantum systems. An open quantum system is a quantum system subject to the action of an environment with which it interacts. Firstly, we introduce the basic concepts of this theory, such as irreversible temporal evolution, Markovianity, and master equations. In the first study conducted in this field, we investigate how a non-equilibrium environment, composed of two systems at different temperatures, affects the dynamics of a two-level system. We derive a master equation to describe the evolution of the two-level system, and through certain approximations, we obtain analytical results for the decay rates appearing in it. These expressions allow us to anticipate that the system's dynamics will be governed by two timescales: a short one in which the system will prethermalize to a non-asymptotic thermal state, and a long one during which the system will evolve towards the true thermal state. In this work, we also examine the effect of these composite environments on the direction of heat flows when they are connected through a two-level system.

In the second chapter, we present the types of noise affecting two-level systems that make up quantum computers, known as qubits. Firstly, we briefly review the possible noise channels affecting qubits and present two very simple models that use master equations to describe the qubits' dynamics. It is theorized that the main source of noise in solid-state qubits

is due to the presence of two-level systems (TLS) around the qubits with which they interact. We first present a semiclassical noise model, considering the qubit as a quantum system, but the two-level systems inducing noise are treated as classical fluctuators. We study noise mitigation techniques on this model and compare their effectiveness. Next, we introduce a purely quantum model, considering the two-level systems around the qubit as quantum systems. These two-level systems are also interacting with a medium at a finite temperature, inducing decoherence on them. We explore the energy structure of the qubit-TLS system, and under the secular approximation, we study the main transitions and draw a physical picture of the process.

The second part of the thesis focuses on the field of quantum walkers (QW). We introduce the basic scheme and its classical analogue. Next, we show how the continuous limit of the QW leads to the Dirac equation and how inhomogeneous coins can give rise to more interesting dynamics in the continuum limit, such as spinors in electromagnetic fields or curved spacetimes. In the first study conducted in this field, we consider a time-inhomogeneous coin, which means a stochastic coin that can perform different operations with different probabilities at each time step. We find that in the continuum limit, these QWs simulate dissipative dynamics described by a Lindblad equation. We conduct a numerical study of the dynamics of a spinor described by this equation and identify two regimes: an initial regime of ballistic propagation and a second regime of diffusion. Finally, we also extend the study to coins with temporal noise that smoothly depends on the position.

The next work in this part employs a 2-dimensional QW, which in the continuum limit, simulates the Dirac equation in curved spacetimes to simulate the Randall-Sundrum model. This model proposes an extra dimension to explain the mass hierarchy problem. The extra dimension is finite and has 4-dimensional branes at each end. One of the branes is

postulated to contain the matter of the Standard Model, while gravity occupies the entire space. The QW that simulates this model accurately reproduces the phenomenology of the model, as the spinor representing the QW tends towards the position of the brane of the Standard Model. Additionally, we study the evolution of entanglement entropy between the spin and position of the QW, as well as the composition of energy modes of the walker.

The last work in this part studies a QW with a non-linear coin that depends on the walker's components. This map can be experimentally implemented using the components of an electric field propagating in a nonlinear optical medium of the Kerr type. One characteristic of these media is the formation of solitons. Firstly, we study the continuous limit of this QW and perform a stability analysis of stationary homogeneous solutions, which allows us to systematically explore the QW numerically and anticipate soliton formation. Under certain approximations, also supported by the numerical studies, we obtain an analytical solution describing the solitons. The numerical study corroborates this solution and also reveals the existence of dark solitons. Finally, we explore the stability of solitons in the presence of constant electric fields. We find that non-linearity helps reduce the soliton dispersion caused by the electric field but does not stop it.

Agraïments

Vull començar agraint a Armando, el meu tutor de tesi, perquè sense ell no haguera pogut tirar avant esta tesi. Armando sempre ha estat disponible per a qualsevol dubte tant científic com no personal, i això ha ajudat a que el doctorat fora una molt bona experiència. Tambien agradecer a Mari Carmen y Inés por el esfuerzo que han puesto en esta tesis a pesar de la distancia y por acogerme durante mi visita a Múnich.

També voldria agrair a tots aquells que han contribuït al meu aprenentatge en el món de la investigació. Gracias a Pablo por contar conmigo para realizar el primer trabajo de la tesis cuando aun no me dedicaba a tiempo completo a la tesis. També agrair a Manel per la oportunitat de provar l'investigació en un camp de la física diferent al que ha constituït aquesta tesi. Thank you Miha for resolving all the questions that came up to me in the field on Quantum Computing, now I have a much better understanding of the technology. Finalment, agrair a Eugenio per proposar un tema molt interessant que a trobat el seu lloc en aquesta tesi i la seua disponibilitat per a poder discutir qualsevol detall que ha anat apareixent. En resum, gracies a tots per mostrar-me que la investigació científica es pot nodrir de la col·laboració.

Estic molt agraït d'haver tingut un grup de companys i amics al voltant

que estaven passant pel mateix procés, sense aquesta gent a prop, amb la que parlar de les penes i glories per les que passem, l'experiència no hauria sigut tant bona. Gracies a Silvia, Rafa, Andreu, Dani, Sergi, Pau, Renan i Carlos per compartir aquests dinars i cafès tant a la cafeteria de Campus com a la de Farmàcia (la millor). També agrair a Pepe, Marina i Kevin, amb els que porte compartint trajectòria des de la carrera, pels eventuais dinar i xarraetes en les diferents activitats ens les que ens hem seguit trobant tant dins com fora del ambient acadèmic.

Per últim, però no menys important, agrair a tota la gent que m'ha donat suport, estima i bons moments. En primer lloc, a la meua família que m'ha educat, donat suport i cuidat, gracies a vosaltres soc qui soc. Meu criat en un ambient molt sa i amb valors, amb un germà amb el que tinc confiança cega i se que sempre em donarà suport. En segon lloc, agrair a la meua segona família, Abel, Joan, Lidón, Marta, Pau, Sara i Xavi, la qual m'ha cuidat i han contribuït a fer-me millor persona, espere que puga seguir sent així per molts anys. Agrair també als meus amics de tota la vida (literalment), Guillem, Pedro i Rocio, amb qui vaig començar a compartir els meus sentiments i emocions per primera vegada i han estat sempre al meu costat per al que fora. També vull agrair a tota la gent que he anat coneixent durant aquest anys en València, i m'han fet passar molts bons moments, a David (per les bones viaciades), Adriana, Sílvia, Ana, Andreu, Martí, Iker, Vero, Mar, Vicky (aunque la conocí en Casteshón) i algú més que segurament en deixe.

En fi, he estat molt a gust durant aquesta etapa gracies a tots vosaltres. Amb estima,

Andreu

Author's Declaration

I declare that the work presented in this thesis was carried out in accordance with the requirements of the University's Regulations and Code of Practice for Research Degree Program.

The contents of this thesis are based on the following papers, in order of appearance, and the journal versions have been added in section [Publications](#).

[P.1] *Prethermalization of quantum systems interacting with non-equilibrium environments* Andreu Anglés-Castillo, Mari Carmen Bañuls, Armando Pérez and Inés De Vega; New Journal of Physics, Volume 22, August 2020

[P.2] *A quantum walk simulation of extra dimensions with warped geometry*; Andreu Anglés-Castillo and Armando Pérez; Scientific Reports volume 12, Article number: 1926 (2022)

[P.3] *Quantum simulation of quantum relativistic diffusion via quantum walks*; Pablo Arnault, Adrian Macquet, Andreu Anglés-Castillo, Iván Márquez-Martín, Vicente Pina-Canelles, Armando Pérez, Giuseppe Di Molfetta, Pablo Arrighi and Fabrice Debbaesch; Journal of Physics A: Mathematical and Theoretical, Volume 53, Number 20

- [P.4] *Solitons in a photonic nonlinear quantum walk: lessons from the continuum*; Andreu Anglés-Castillo, Armando Pérez and Eugenio Roldán; [arXiv:2308.01014](https://arxiv.org/abs/2308.01014)

Also remark that the following article has also been produced during the doctoral studies, but, since it belongs to another field of physics, its contents and theoretical framework is not presented in this thesis.

- *On the deceleration of Fanaroff-Riley Class I jets: mass loading of magnetized jets by stellar winds*; Andreu Anglés-Castillo, Manel Perucho, José María Martí, Robert A. Laing; Monthly Notices of the Royal Astronomical Society, Volume 500, Issue 1, January 2021, Pages 1512–1530.

The text presented here should be understood as a dissertation submitted to the University of Valencia as required to obtain the degree of Doctor of Philosophy in Physics.

Except where indicated by specific reference in the text, this is the candidate's own work, done in collaboration with, and/or with the assistance of, the candidate's supervisors and collaborators. Any views expressed in the thesis are those of the author.

València, August 15, 2023
Andreu Anglés-Castillo

Contents

I	Quantum Noise	3
1	The theory of Open Quantum Systems	5
1.1	Introduction	5
1.2	Time evolution in open quantum systems	6
1.3	Markovianity	14
1.4	Non-Markovianity	19
1.5	Weak coupling Master Equation	22
1.6	Stationary states	30
1.7	Heat fluxes in open systems	32
1.8	Prethermalization (Publication [P.1])	33
2	Noise in Quantum Computing	35
2.1	Introduction	35
2.2	Quantum Errors and Noise	38
2.3	Dissipative noise model: thermalization	42
2.4	Markovian pure dephasing	45
2.5	Non-Markovian pure dephasing: semiclassical model	47
2.6	Non-Markovian pure dephasing: quantum model	58

II Quantum Walks	69
3 Discrete Time Quantum Walks	71
3.1 Introduction	71
3.2 The Random Walk on the line: Classical and Quantum . .	73
3.3 QW in momentum space	79
3.4 The continuum limit of the discrete time Quantum Walk . .	81
3.5 Inhomogeneous coin operator	84
3.6 QW simulation of warped geometry in high energy theories (Publication [P.2])	86
3.7 Relativistic diffusion as the continuum limit of a stochastic QW (Publication [P.3])	89
3.8 Non-linear coin operator and solitons (Publication [P.4]) . .	90
Appendices	93
A.1 Derivation ME dissipative noise model	93
A.2 Derivation ME pure dephasing noise model	95
Resum en valencià	97
Bibliography	125
Publications	141
P.1 Prethermalization of quantum systems interacting with non- equilibrium environments	141
P.2 A quantum walk simulation of extra dimensions with warped geometry	158
P.3 Quantum simulation of quantum relativistic diffusion via quantum walks	170
P.4 Solitons in a photonic nonlinear quantum walk: lessons from the continuum	209

Part I

Quantum Noise

Open Quantum Systems and their use in qubit noise models

Chapter 1

The theory of Open Quantum Systems

1.1 Introduction

Quantum Mechanics (QM) is the most fundamental theory of nature that we currently know. Since its conception in the 1920s it has proven a successful theory at different complexity levels, from correctly describing the energy levels of the hydrogen atom to predicting the existence of the elementary particles that constitute the building blocks of matter. Even though the theory has proven successful, whenever there is an increasingly high level of complexity, approximate or perturbative methods need to be employed.

Quantum systems are hardly ever completely isolated, we refer to them as open systems, and they should be considered in interaction with a surrounding environment, which will most likely affect the dynamics of the open system. The number of degrees of freedom of the environment are generally much higher than those of the open system. One could resort to

exact methods to solve the evolution of the whole isolated system, composed by the open system and its environment. In practice this task rapidly becomes unfeasible.

The theory of open quantum systems (OQS) has developed the tools to describe the open system without the need to give an exact description of the environmental degrees of freedom. The use of the theory of open quantum systems has been successful in the field of quantum optics, where for instance a lossy cavity can modify the rates at which transitions occur and modify the steady state of the system. The theory of OQSs has experienced a rise in popularity due to its applicability in quantum technological scenarios, where the phenomena of decoherence and dissipation are well captured by the formalism, and it constitutes a test bed for the study of mitigation and control techniques. The following sections are devoted to evolution dynamics of OQSs. Specifically in Section 1.2 we explore the general features of the evolution that the OQS undergoes and introduce the concept of Markovianity and non-Markovianity in Sections 1.3 and 1.4, respectively. In Section 1.5 we derived a weak coupling master equation and in the following sections we briefly study its asymptotic and thermodynamic properties. Finally, in Section 1.8, we comment on how this theory is the basis for the work done in [P.1]. In Chapter 2 of this part we delve deeper into the field of quantum computing, and explore how the theory of OQS can be employed to explore dissipative dynamics and to model noise sources.

1.2 Time evolution in open quantum systems

Let us consider the general situation where the open system S is coupled to an environment E . The total Hilbert space is the tensor product of the Hilbert space of each subsystem $\mathcal{H} = \mathcal{H}_S \otimes \mathcal{H}_E$. The whole system is described by the free Hamiltonians of each subsystem, H_S for the open

system and H_E for the environment, plus the interaction Hamiltonian H_I between both. The evolution of both system and environment is given by the total Hamiltonian $H = H_S + H_E + H_I$ so that the state of the whole system at time t is

$$|\psi(t)\rangle = e^{-iH(t-t_0)} |\psi(t_0)\rangle , \quad (1.1)$$

where $|\psi(t_0)\rangle$ is the initial state of the composite system and we define $U(t, t_0) = \exp[-iH(t - t_0)]$, the unitary evolution operator. This unitary evolution is given by the Schrödinger equation¹

$$i \frac{d}{dt} |\psi(t)\rangle = H |\psi(t)\rangle . \quad (1.2)$$

Finally, the open system is completely described by the partial trace with respect to the environment of the final state

$$\rho_S(t) = \text{Tr}_E \{ \rho_{SE}(t) \} = \text{Tr}_E \left\{ U(t, t_0) \rho_{SE}(t_0) U^\dagger(t, t_0) \right\} , \quad (1.3)$$

where $\rho_{SE}(t_0) = |\psi(t_0)\rangle \langle \psi(t_0)|$. In practice this procedure, described by the top right path of Fig. 1.1, is not feasible and we need to resort to a representation of the evolution reduced to S . The mathematical object $\phi_{(t,t_0)}$ that describes the evolution of the initial state of the open system S up to time t is called a dynamical map and it encodes the effect of the environment onto the open system, a procedure which is described by the bottom left path of the diagram in Fig. 1.1.

We have not specified the initial relation between system and environment. In general they could be in an entangled initial state but in most problems they can be prepared in a separable/uncorrelated state

$$\rho_{SE}(0) = \rho_S(0) \otimes \rho_E(0) . \quad (1.4)$$

¹In natural units where $\hbar = 1$.

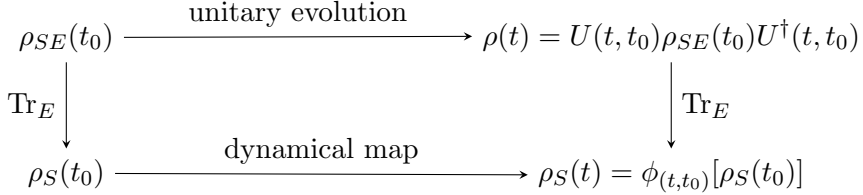


Figure 1.1: A diagram showing the action of the dynamical map $\phi(t)$. It is possible to either evolve the whole system, and trace out the environment to obtain the dynamics of the OQS, or alternatively the evolution of the OQS can be described by the dynamical map.

This assumption is correct in most quantum technological scenarios where the control systems interact much more strongly with the open system than the environment, so that in practice the correlations with the environment are washed out. We can write the spectral decomposition of the environment initial state as

$$\rho_E(0) = \sum_i \lambda_i |\lambda_i\rangle \langle \lambda_i|, \quad (1.5)$$

where $|\lambda_i\rangle$ are the eigenvectors of $\rho_E(0)$, which in general do not correspond with the eigenvectors of the environment Hamiltonian H_E . This is only the case when the initial state of the environment is in equilibrium state, i.e., $[H_E, \rho_E(0)] = 0$. If we plug this decomposition into Eq. (1.3)

$$\begin{aligned}
 \rho_S(t) &= \text{Tr}_E \left\{ U(t, t_0)\rho_S(t_0) \otimes \sum_i \lambda_i |\lambda_i\rangle \langle \lambda_i| U(t, t_0)^\dagger \right\} \\
 &= \sum_{i,j} \lambda_i \langle \lambda_j| U(t, t_0) |\lambda_i\rangle \rho_S(t_0) \langle \lambda_i| U(t, t_0)^\dagger |\lambda_j\rangle, \quad (1.6)
 \end{aligned}$$

after defining the Kraus operators $K_{i,j}(t, t_0) = \sqrt{\lambda_i} \langle \lambda_j| U(t, t_0) |\lambda_i\rangle$, which

act on \mathcal{H}_S , the dynamical map can be written as

$$\rho_S(t) = \mathcal{E}_{(t,t_0)}[\rho_S(t_0)] = \sum_{i,j} K_{i,j}(t, t_0) \rho_S(t_0) K_{i,j}^\dagger(t, t_0) , \quad (1.7)$$

where we denoted the dynamical map as $\mathcal{E}_{(t,t_0)}$ to differentiate a map that evolves states of the form of Eq. (1.4) from a general dynamical map $\phi_{(t,t_0)}$ acting on general entangled states. The Kraus operators fulfill the property

$$\sum_{i,j} K_{i,j}^\dagger(t, t_0) K_{i,j}(t, t_0) = \mathbb{I}_S , \quad (1.8)$$

that comes from the normalization condition of the quantum state. This representation of the evolution is also referred to as the operator sum representation of the dynamical map, and the indices on the operators can be grouped into a single one

$$\rho_S(t) = \sum_{\mu=\{i,j\}} K_\mu(t, 0) \rho_S(0) K_\mu^\dagger(t, 0) . \quad (1.9)$$

Relation (1.7) indicates that when the evolution of the reduced density matrix can be described by the means of Kraus operators, it can also be described by a map $\mathcal{E}_{(t,t_0)}$ acting on its initial state, which is often called a universal dynamical map (UDM).

If we did not impose condition (1.4) the initial state would be not be separable and the Kraus operators could depend on the initial state of the system, in which case the dynamical map would not be universal; in this case the same map cannot be applied to arbitrary states. Let us consider the general initial state

$$\rho_{SE}(t_0) = \rho_S(t_0) \otimes \rho_E(t_0) + \rho_{\text{cor}}(t_0) , \quad (1.10)$$

where $\rho_{\text{cor}}(t_0)$, which is not a quantum state, contains all correlations between system and environment, and $\text{Tr}_{S/E} \{ \rho_{\text{cor}}(t_0) \} = 0$. If we compute

the evolution of this state as in Eq. (1.3) we arrive at following expression for the dynamical map

$$\rho_S(t) = \phi_{(t,t_0)}[\rho_S(t_0)] = \mathcal{E}_{(t,t_0)}[\rho_S(t_0)] + \text{Tr}_E \left\{ U(t, t_0) \rho_{\text{cor}}(t_0) U(t, t_0)^\dagger \right\} , \quad (1.11)$$

where the first term is the dynamical map given by Kraus operators (1.7). Since the Kraus operators depend on the initial state of the environment (and on the unitary evolution operator), the dynamical map $\phi_{(t,t_0)}$ will depend on the initial state of the system $\rho_S(t_0)$ because of the term ρ_{cor} . See reference [1] for further details on the effect of the initial correlations.

The key properties of a map that can be expressed in Kraus form are that

- It preserves the trace

$$\begin{aligned} \text{Tr} \{ \rho_S(t) \} &= \text{Tr} \left\{ \sum_{\mu} K_{\mu}(t, t_0) \rho_S(t_0) K_{\mu}^{\dagger}(t, t_0) \right\} = \\ &= \text{Tr} \left\{ \sum_{\mu} K_{\mu}^{\dagger}(t, t_0) K_{\mu}(t, t_0) \rho_S(t_0) \right\} = \text{Tr} \{ \rho_S(t_0) \} . \end{aligned} \quad (1.12)$$

- It is linear

$$\sum_{\mu} K_{\mu}(a\rho_1 + b\rho_2)K_{\mu}^{\dagger} = a \sum_{\mu} K_{\mu}\rho_1 K_{\mu}^{\dagger} + b \sum_{\mu} K_{\mu}\rho_2 K_{\mu}^{\dagger} .$$

- It preserves positivity of operators. An operator is positive semidefinite if its eigenvalues are ≥ 0 . To show this property we can consider the spectral decomposition of a positive operator $O = \sum_i o_i |e_i\rangle \langle e_i|$ (with

$o_i \geq 0$) and see that, for any $|\phi\rangle \in \mathcal{H}_S$, the expectation value of the evolved operator O

$$\langle \phi | \sum_{\mu} K_{\mu} O K_{\mu}^{\dagger} | \phi \rangle = \sum_{\mu, k} o_k \langle \phi | K_{\mu} | e_k \rangle \langle e_k | K_{\mu}^{\dagger} | \phi \rangle \geq 0$$

is positive. While all Kraus maps preserve positivity not all positive maps have a Kraus representation [1, 2]. When a map obeys the previous properties and has a representation in terms of Kraus operators it is said to be completely positive. A completely positive (CP) map preserves positivity of operators on arbitrarily large Hilbert spaces $\mathcal{H}_S \otimes \mathcal{H}_{\text{extra}}$.

There is an equivalent way of determining if a dynamical map is UDM demonstrated by Kosakowski in [3, 4], which indicated that a dynamical map is a UDM if and only if it preserves the trace $\text{Tr} \{ \phi_{(t,t_0)} \rho(t_0) \} = \text{Tr} \{ \rho(t_0) \}$ and it is a contraction. A dynamical map is a contraction if

$$\frac{\| \phi_{(t,t_0)} \rho \|}{\| \rho \|} \leq 1, \quad \forall \rho \in \mathcal{H}_S, \forall t, \quad (1.13)$$

where $\| \rho \| = \text{Tr} \{ \sqrt{\rho^{\dagger} \rho} \}$ is the trace norm. The trace norm is a witness of the purity of the quantum state, therefore a contraction will cause the reduction of the purity of the quantum state, in other words, UDMs create mixed states. If a map would increase the purity of the quantum state it would be required that the trace norm of the quantum state increases and to do so the positivity of the dynamical map is lost. This observation will be critical to understand the concept of Markovianity, which is dealt with in Section 1.3.

Reversibility of the dynamical map

In general, when the open system evolution is given by a dynamical map its dynamics becomes irreversible, the exception being a dynamical map representing unitary dynamics. This phenomenon is tightly related to the entanglement generation between system and environment along the evolution. When two systems entangle, the information is no longer contained in the individual systems, but encoded in the global state of the composite system. Taking the partial trace of the environment is equivalent to averaging over the environmental degrees of freedom, then the reduced density matrix gives a classical probabilistic mixture of compatible quantum states of the system, since the actual quantum state is only correctly described globally. If the entanglement between system and environment is maximal, the reduced density matrix of the system becomes the maximally mixed state, and no information about the system or environment can be extracted by just measuring the system. This situation is most easily understood following the top right path of Fig. 1.1: the unitary dynamics entangles the system with the environment, and when the partial trace is taken over one of them the remaining state only preserves part of the information. An inverse map of this evolution $\phi_{(t,t_0)}^{-1}$, such that $\phi_{(t,t_0)}^{-1}[\phi_{(t,t_0)}[\rho]] = \phi_{(t,t_0)}[\phi_{(t,t_0)}^{-1}[\rho]] = \rho$, may exist but in general it will not be a UDM.

A reversible dynamical map is only possible when the evolution of the open system is unitary, that is, $\mathcal{U}_{(t,t_0)}[\rho(t_0)] = U_S(t, t_0)\rho(t_0)U_S^\dagger(t, t_0)$, such that, $U_S(t, t_0)U_S^\dagger(t, t_0) = U_S^\dagger(t, t_0)U_S(t, t_0) = \mathbb{I}_S$. We will denote by $\mathcal{U}_{(t,t_0)}$ the dynamical map of unitary evolutions. In this case the inverse dynamical map is simply $\mathcal{U}_{(t,t_0)}^{-1}[\rho_S(t_0)] = (\mathcal{U}_{(t,t_0)}[\rho_S(t_0)])^\dagger$, which still remains an UDM. During reversible evolutions a single Kraus operator that describes the map $\mathcal{U}_{(t,t_0)}$ can be found, and it is the unitary evolution operator $K_0(t, t_0) = U_S(t, t_0)$.

Dynamical map semigroup

A dynamical map is said to form a (continuous one-parameter) semigroup if it only depends on the time differences of the evolution $\phi_{(t_2, t_1)} = \phi_\tau$, with $\tau = t_2 - t_1 > 0$, and fulfills the following properties

$$\phi_t \circ \phi_s = \phi_{t+s} , \quad (1.14)$$

$$\phi_0 = \mathbb{I}_S , \quad (1.15)$$

where the composition acting on arbitrary density matrices is defined as $(\phi_t \circ \phi_s)[\rho] = \phi_t[\phi_s[\rho]]$. In a semigroup the inverse of an element might not exist, which, as stated before, is specially true for irreversible dynamical maps. A dynamical map semigroup is differentiable, and its derivative is given by

$$\frac{d\phi_t}{dt} = \mathcal{L}[\phi_t] , \quad (1.16)$$

where $\mathcal{L}[\cdot]$ is a superoperator that acts on ϕ_t . This differential equation together with condition (1.15) has a unique solution which is

$$\phi_t[\cdot] = e^{\mathcal{L}t}[\cdot] , \quad (1.17)$$

where $\mathcal{L}[\cdot]$ is called the generator of the semigroup and, to form a semigroup, must be constant in time. From this solution it is straightforward to see that condition (1.14) is fulfilled

$$\phi_t \circ \phi_s = e^{\mathcal{L}t} \circ e^{\mathcal{L}s} = e^{\mathcal{L}(t+s)} = \phi_{t+s} . \quad (1.18)$$

The explicit form of the generator \mathcal{L} depends on the particular physical problem, and its derivation can be obtained through different approximate methods. In Section 1.5 we will obtain an explicit form of the generator through a perturbative expansion in the weak coupling between system and environment. For the simple case of a closed system the generator is simply

$$\mathcal{L}[O] = -i[H, O] , \quad (1.19)$$

where we defined its action on an arbitrary operator O . And for this particular case the solution (1.17) becomes

$$\phi_{(t-t_0)}[\rho(t_0)] = U(t-t_0)\rho(t_0)U^\dagger(t-t_0) , \quad (1.20)$$

where $U(t-t_0) = e^{-iH(t-t_0)}$.

If the generator $\mathcal{L}(t)$ is allowed to be time dependent, the solution to the new differential equation

$$\frac{d\phi_t}{dt} = \mathcal{L}(t)[\phi_t] , \quad (1.21)$$

is formally expressed as the time ordered exponential

$$\phi_{(t,t_0)} = \mathcal{T} e^{\int_{t_0}^t \mathcal{L}(t') dt'} , \quad (1.22)$$

where now the dynamical map not only depends on the final time, but also on the initial time, and the semigroup property (1.14) is no longer fulfilled. Despite the fact that time dependent generators do not lead to dynamical maps that satisfy the semigroup properties, they can still be expressed in the operator sum representation.

1.3 Markovianity

To first review the concept of quantum Markovian evolution, it is useful to review the concept of classical Markovianity. A classical stochastic process, where a random variable $X(t)$ takes different values x_i at each time t_i , is said to be a Markov process if the probability of finding x_n at time t_n is only conditioned on the previous values x_{n-1} at time t_{n-1} and not on any x_i obtained at time t_i with $i < n-1$. This is expressed in terms of conditional probabilities as

$$p(\{x_n, t_n\} | \{x_{n-1}, t_{n-1}\}, \dots, \{x_0, t_0\}) = p(\{x_n, t_n\} | \{x_{n-1}, t_{n-1}\}) . \quad (1.23)$$

This process is sometimes referred to as a memoryless process, where the next random value is independent of the past history of values of $X(t)$. The concept was presented in discrete time variables for illustrative purposes but can be straightforwardly extended to continuous time variables.

The parallelism with the quantum setting is drawn by translating the role played by probabilities to density operators $\rho(t)$, and the role of conditional probabilities to universal dynamical maps $\phi_{(t_2, t_1)}$. With this reasoning one could say that an open quantum system undergoes a Markovian evolution if it is described by UDMs (equivalent to a contractive map) and they obey the composition law

$$\phi_{(t_2, t_0)} = \phi_{(t_2, t_1)} \circ \phi_{(t_1, t_0)} , \quad (1.24)$$

where t_1 is an intermediate time of the evolution, so that $t_2 > t_1 > t_0$. This relation is referred as the divisibility condition. To understand the implications of this condition let us first look closely at the resulting state after the evolution up to t_1 . In order to have an evolution described by an operator sum representation, and hence a UDM, we required that the initial state of the evolution was in a separable state (1.4). After evolving for time t_1 there is, in general, a generation of correlations or entanglement between the system and environment. To compute the evolution between times $t_1 \rightarrow t_2$, an operator sum representation is not suitable since the state at time t_1 is not separable, and hence the evolution would not be represented by a UDM. Which may look surprising since the evolution from $t_0 \rightarrow t_2$ is also a UDM. The problem lies at the evolution between intermediate steps. Under some conditions where the effect of the system is negligible on the environment, a Born approximation can be taken under which system and environment are assumed to be in a product state, and the divisibility condition is able to be recovered.

Another way to look at this problem is from the point of view of irreversibility. We could write the evolution from $t_1 \rightarrow t_2$ as $\phi_{(t_2,t_1)} = \phi_{(t_1,t_0)}^{-1} \circ \phi_{(t_0,t_2)}$ if the inverse of $\phi_{(t_1,t_0)}$ existed, but as seen before, except under unitary dynamics, the map is irreversible and even if the inverse of the map existed, it would not be a UDM.

The physical significance of the failure to obey the divisibility property (1.24) is still debated nowadays, but a common interpretation is as follows. When system and environment interact there is a flow of information from system to environment, also represented by the increase of entanglement between both systems or, equivalently, a reduction of coherence of the open system. Usually, when the environment is not a big system, there can be revivals of coherence: the open system is restoring part of its initial information in which case the dynamical map becomes non-contractive. In this situation, the process is said to have memory where, after some time, information about the initial state of the system arises again. In the Markovian case, where the evolution is said to be memoryless, the system is monotonously losing information about its initial state.

This interpretation is tightly related to an alternative definition of Markovianity that involves the behaviour of the trace distance [5], where an evolution is Markovian if the trace distance (distinguishability) between any two states decreases monotonously. This interpretation relates the degree of non-Markovianity to the ability of any two arbitrary states to have memory of the initial state and thus recover part of the initial distinguishability. While this alternative interpretation is closely related to the contractive property of the dynamical map, it is not concerned about the divisibility property (1.24), a fact that is of special importance to draw the parallelism between quantum and classical Markov processes.

The property of the environment that leads to memoryless dynamics is

its capacity to destroy correlations. In general, large environments dissipate correlations fast, as they have short correlation times. The correlations that built up as a result of the interaction between system and environment decay faster than the time required for the system to display coherent dynamics, and in this situation the system is unable to retain its memory about the initial state, or even the previous states if the decay of correlations is extreme, in which case we might find a dynamical map that fulfills both conditions of Markovianity.

The divisibility condition stated in Eq. (1.24) is generalized for time dependent generators $\mathcal{L}(t)$, but if we restrict to the case of a constant generator and hence dynamical maps obeying the semigroup property (1.14) the condition is automatically fulfilled. A semigroup dynamical map only depends on the time differences of the interval $\tau_1 = t_1 - t_0$ and $\tau_2 = t_2 - t_1$ and the semigroup property ensures

$$\phi_{(\tau_1+\tau_2)} = \phi_{\tau_2} \circ \phi_{\tau_1} . \quad (1.25)$$

One could require the semigroup property to define a Markov process, but that would lead to a more strict definition. It was shown by Gorini, Kossakowski and Sudarshan [6] and independently by Lindblad [7] that any dynamical map semigroup could be generated by a constant generator of the form

$$\mathcal{L}\rho(t) = -i[H, \rho(t)] + \sum_k \gamma_k \left(L_k \rho(t) L_k^\dagger - \frac{1}{2} \{L_k^\dagger L_k, \rho(t)\} \right) , \quad (1.26)$$

where H is a Hermitian operator, γ_k are positive constants, and L_k are the so called Lindblad operators. The operator $H = H_S + \sum_k \Delta_k L_k^\dagger L_k$ represents the modified free Hamiltonian of the system due to the action of the environment, the L_k are related to the induced decay channels, which describe the dissipative part of the dynamics, and γ_k are the corresponding decay rates. A simple way of obtaining this generator, presented in

[8], is done by considering the infinitesimal version of the operator sum representation

$$\rho(t + dt) = \sum_{\mu} K_{\mu} \rho(t) K_{\mu}^{\dagger} , \quad (1.27)$$

where we may, in general, consider that there is one operator of order dt

$$K_0 = \mathbb{I}_S + dt(-iH + M) , \quad (1.28)$$

where H and M are Hermitian, and other operators K_{ν} with $\nu > 0$ of order \sqrt{dt} as

$$K_{\nu} = \sqrt{dt} L_{\nu} . \quad (1.29)$$

The completeness relation must hold

$$\mathbb{I} = \sum_{\mu} K_{\mu} K_{\mu}^{\dagger} = \mathbb{I} + dt \left(2M + \sum_{\nu > 0} L_{\nu}^{\dagger} L_{\nu} \right) + O(dt^2) , \quad (1.30)$$

so that

$$M = -\frac{1}{2} \sum_{\nu > 0} L_{\nu}^{\dagger} L_{\nu} . \quad (1.31)$$

Substituting these operators into the infinitesimal operator sum evolution in Eq. (1.27) we find that

$$\rho(t+dt) = \rho(t) + dt \left(-i[H, \rho(t)] + \sum_{\nu > 0} \left(L_{\nu} \rho(t) L_{\nu}^{\dagger} - \frac{1}{2} L_{\nu}^{\dagger} L_{\nu} \rho(t) - \frac{1}{2} \rho(t) L_{\nu}^{\dagger} L_{\nu} \right) \right) , \quad (1.32)$$

where employing the infinitesimal definition of the derivative we obtain

$$\frac{d\rho(t)}{dt} = \frac{\rho(t + dt) - \rho(t)}{dt} = \mathcal{L}\rho(t) , \quad (1.33)$$

where this generator is the same as the one in Eq. (1.26) with the decay rates absorbed into the operators L_{ν} .

This results would later be extended, see [2, 9] for a detailed derivation, to account for time dependent generators with a similar form

$$\mathcal{L}(t)\rho(t) = -i[H(t), \rho(t)] + \sum_k \gamma_k(t) \left(L_k(t)\rho(t)L_k^\dagger(t) - \frac{1}{2}\{L_k^\dagger(t)L_k(t), \rho(t)\} \right), \quad (1.34)$$

where now the Hermitian operator $H(t)$ is time-dependent, as well as the Lindblad operators $L_k(t)$ and rates $\gamma_k(t)$, with the only restriction of all the rates being non-negative at all times, such that the dynamical map describes a contractive evolution and obeys the more general Markov condition (1.24).

1.4 Non-Markovianity

Failure of dynamical maps to be a contraction ² and/or to obey the divisibility condition (1.24) deem them non-Markovian.

There have been many proposed witnesses or measures to quantify the degree of non-Markovianity, see [10] for a complete review of non-Markovian definitions and measures. Here we give the definitions of the ones employed in the works that make up this thesis.

1. **Bloch Volume Measure** This measure proposed in [11] is directly related to the contractive property of Markovian evolutions. It is a nice geometrical characterization of non-Markovianity based on the fact that the volume of accessible states through a Markovian evolution monotonously decreases. During the time intervals where this volumes increases a non-Markovianity is present, and the rate of volume increase is used as a quantifier of it. In the particular case of two dimensional systems, this characterization of the volume of

²Equivalent to being UDM or have an operator sum representation.

accessible states matches the volume of the region of accessible states represented by their Bloch vector. This characterization was employed in [P.1] to visualize the reduction of the volume of all possible states to a transient stationary state, and at the same time to find out that the master equation that we derived was Markovian.

2. **BLP Measure** This measure presented in [12] is very popular due to its easy computation and its close connection with memory effects on the open system. Non-Markovianity is quantified by the rate at which two arbitrary states ρ_1 and ρ_2 become more distinguishable. Distinguishability is measured with the help of the trace distance

$$D(\rho_1(t), \rho_2(t)) = \frac{1}{2} \text{Tr} \left\{ \sqrt{(\rho_1(t) - \rho_2(t))^\dagger (\rho_1(t) - \rho_2(t))} \right\} . \quad (1.35)$$

If during any point of the evolution it increases, it is a sign of recovery of memory and hence non-Markovianity. If we define the rate of change of trace distance as $\sigma(\rho_1, \rho_2, t) = \partial_t D(\rho_1(t), \rho_2(t))$ the proposed measure is

$$\mathcal{N} = \max_{\rho_1, \rho_2} \int_{\sigma > 0} dt \sigma(\rho_1, \rho_2, t) , \quad (1.36)$$

where the maximization is performed over all pairs of states ρ_1, ρ_2 .

3. **Negative decay rates in canonical form master equations** This characterization of non-Markovianity proposed in [13] takes advantage of the fact that time-nonlocal master equations that can in general be expressed as

$$\frac{d\rho_S(t)}{dt} = -i[H(t), \rho_S(t)] + \int_0^t d\tau K(t, \tau) \rho(\tau) , \quad (1.37)$$

where $K(t, s)$ is the memory kernel, are of non-Markovianity nature, unless the kernel is proportional to $\delta(t - \tau)$ in which case becomes

time-local. All time-local master equations with a generator (which is in general time dependent)

$$\frac{d\rho_S(t)}{dt} = \mathcal{L}(t)\rho(t) , \quad (1.38)$$

can be brought into a canonical form

$$\mathcal{L}(t)\rho(t) = -i[H(t), \rho(t)] + \sum_k \gamma_k(t) \left(L_k(t)\rho(t)L_k^\dagger(t) - \frac{1}{2}\{L_k^\dagger(t)L_k(t), \rho(t)\} \right) , \quad (1.39)$$

where the operators $L_k(t)$ obey the properties

$$\text{Tr} \{L_k(t)\} = 0 , \quad \text{Tr} \{L_i^\dagger(t)L_j(t)\} = \delta_{ij} . \quad (1.40)$$

There does not exist a unique way of writing a time-local master equation in the form of Eq. (1.39), there are (infinitely) many changes of basis of the Lindblad operators that preserve the Lindblad form. What makes this choice *canonical* is the requirement of conditions (1.40) that render the representation unique. As stated in the previous section an equation with this generator leads to divisible and completely positive evolution, as long as the decay rates are positive, so that it is suggested that the negativity of the decay rates in the canonical form is the suitable witness for non-Markovianity. The following quantitative measure is then defined

$$\mathcal{N} = - \int_{\gamma_k < 0} dt \sum_{\gamma_i(t) < 0} \gamma_i(t) , \quad (1.41)$$

where the integration is carried in the time intervals in which any of the decay rates is negative, and the sum only takes into account negative decay rates. This measure was employed in [P.1] where the derived master equation was brought into the canonical form. It was again corroborated that the map was Markovian since all the obtained decay rates were positive at all times.

1.5 Weak coupling Master Equation

In previous sections we have seen some examples of evolution equations that describe the evolution of the open system, for instance,

$$\frac{d\rho(t)}{dt} = \mathcal{L}\rho(t) , \quad (1.42)$$

where the generator was given by the Lindbladian (1.26). But, so far, we only focused on the properties they should have in order to induce a Markov process and have not paid any attention to physical situations and when to extract a closed equation for the density matrix from them. In this section we present the general physical situation under which a ME can be obtained and under which approximations, see references [14, 2] for similar derivations.

The general Hamiltonian describing the system plus environment is given by

$$H = H_S + H_I + H_E , \quad (1.43)$$

where H_S is the open system Hamiltonian, H_E the environment one, and H_I is the interaction Hamiltonian between system and environment. The general form that the interaction Hamiltonian can have is

$$H_I = \sum_{\mu} S_{\mu} \otimes B_{\mu} , \quad (1.44)$$

where S_{μ} are operators acting on the system and B_{μ} on the environment, and they are Hermitian. As the name of this Section suggests, the first assumption made to derive this ME is that the interaction between system and environment is small, so that a perturbative approach can be followed for the derivation. As stated before, the initial condition of the whole system is considered in a separable state

$$\rho(0) = \rho_S(0) \otimes \rho_E , \quad (1.45)$$

where the reduced density matrix of the system in the initial time is $\rho_S(0)$. We did not include a time dependence on the reduced density matrix of the environment since we further assume that it starts in a stationary state, such that, $[H_E, \rho_E] = 0$, and that it is much larger than the open system so that the perturbations that the system induces on the environment are negligible. The complete evolution is unitary and is given by the von Neumann equation

$$\frac{d\rho(t)}{dt} = -i[H, \rho(t)] . \quad (1.46)$$

To produce a perturbative approach in the interaction Hamiltonian, it is convenient to reformulate the problem in the interaction picture

$$\tilde{\rho}(t) = e^{i(H_S+H_E)t} \rho(t) e^{-i(H_S+H_E)t} , \quad (1.47)$$

so that the von Neumann equation becomes

$$\frac{d\tilde{\rho}(t)}{dt} = -i[\tilde{H}_I(t), \rho(t)] , \quad (1.48)$$

where

$$\begin{aligned} \tilde{H}_I(t) &= e^{i(H_S+H_E)t} H_I e^{-i(H_S+H_E)t} = \\ &= \sum_{\mu} e^{iH_S t} S_{\mu} e^{-iH_S t} \otimes e^{iH_E t} B_{\mu} e^{-iH_E t} \equiv \sum_{\mu} S_{\mu}(t) \otimes B_{\mu}(t) , \end{aligned} \quad (1.49)$$

is the interaction Hamiltonian in the interaction picture. The formal solution to this equation is

$$\tilde{\rho}(t) = \rho(0) - i \int_0^t dt' [\tilde{H}_I(t'), \tilde{\rho}(t')] , \quad (1.50)$$

and in order to develop a perturbative method we plug this solution in the interaction picture von Neumann equation to obtain

$$\frac{d\tilde{\rho}(t)}{dt} = -i[\tilde{H}_I(t), \rho(0)] - \int_0^t dt' [\tilde{H}_I(t), [\tilde{H}_I(t'), \tilde{\rho}(t')]] . \quad (1.51)$$

To obtain an equation for the system's density matrix we have to take the partial trace with respect to the environment of the previous equation

$$\begin{aligned} \frac{d\tilde{\rho}_S(t)}{dt} = & -i\text{Tr}_E \left\{ \left[\sum_{\mu} S_{\mu}(t) \otimes B_{\mu}(t), \tilde{\rho}_S(0) \otimes \tilde{\rho}_E \right] \right\} \\ & - \int_0^t dt' \text{Tr}_E \left\{ [\tilde{H}_I(t), [\tilde{H}_I(t'), \tilde{\rho}(t')]] \right\} , \end{aligned} \quad (1.52)$$

where $\tilde{\rho}_S(t) = \text{Tr}_E \{ \tilde{\rho}(t) \}$ and, in the first term, we employed the assumption (1.45). This term can be reduced to

$$-i \sum_{\mu} [S_{\mu}(t), \tilde{\rho}_S(0)] \text{Tr}_E \{ B_{\mu}(t) \tilde{\rho}_E \} . \quad (1.53)$$

Since we assumed that the environment is in equilibrium $[\rho_E, H_E] = 0$, the quantity $\langle B_{\mu} \rangle_{\text{eq}} = \text{Tr}_E \{ B_{\mu}(t) \tilde{\rho}_E \} = \text{Tr}_E \{ B_{\mu}(0) \rho_E \}$ is time independent. Through a redefinition of the interaction Hamiltonian $H'_I = H_I - \sum_{\mu} \langle B_{\mu} \rangle_{\text{eq}} S_{\mu}$ this term can be eliminated by also redefining the system Hamiltonian $H'_S = H_S + \sum \langle B_{\mu} \rangle_{\text{eq}} S_{\mu}$. For the sake of simplicity, we drop the prime notation in the following. The equation now reads

$$\frac{d\tilde{\rho}_S(t)}{dt} = - \int_0^t dt' \text{Tr}_E \left\{ [\tilde{H}_I(t), [\tilde{H}_I(t'), \tilde{\rho}(t')]] \right\} . \quad (1.54)$$

Up to this point, the equation remains exact, but it is a hard equation to solve since we still have the evolved total density matrix in the commutator and it is non-local in time, which implies that it is a non-Markovian evolution equation. By introducing further assumption it is possible to arrive to a time-local ME. The first approximation we are going to consider is the Born approximation, which assumes that, since the interaction between system and environment is so weak, and in general the environment is a system much bigger than the open system, it will almost be unperturbed by the

open system. This assumption implies that the evolved state of the whole system remains in a product state

$$\tilde{\rho}(t) \approx \tilde{\rho}_S(t) \otimes \rho_E . \quad (1.55)$$

There is some criticism [1] in the argumentation of this approximation. From the physical point of view, it can be questioned whether the state remains factorized but the parts of the system are still interacting. For that reason, it is argued that the above should be considered an ansatz to achieve a closed equation for the open system's density matrix, instead of a physical requirement for this equation to work. There are other approaches for deriving the same weak coupling ME that do not rely on this assumption, see [2, 1] for these alternative approaches.

Introducing this ansatz, the now approximate equation reads

$$\frac{d\tilde{\rho}_S(t)}{dt} = - \int_0^t dt' \text{Tr}_E \left\{ [\tilde{H}_I(t), [\tilde{H}_I(t'), \tilde{\rho}_S(t') \otimes \rho_E]] \right\} , \quad (1.56)$$

which, after expressing the interaction Hamiltonian as in Eq. (1.49), can be expanded as

$$\frac{d\tilde{\rho}_S(t)}{dt} = - \sum_{\mu, \nu} \int_0^t dt' (\text{Tr}_E \{ B_\mu(t) B_\nu(t') \rho_E \} [S_\mu(t), S_\nu(t') \tilde{\rho}_S(t')] + h.c.) , \quad (1.57)$$

where now we have been able to group the environment operators inside the trace. This defines the correlation function of the environment $C_{\mu, \nu}(t, t') = \text{Tr}_E \{ B_\mu(t) B_\nu(t') \rho_E \}$, and in this way we have obtained an equation using open system operators alone. The description of the environment has been reduced to a correlation function which encapsulates the correlations of the environment. Since the environment state is stationary, the correlation functions only depend on the time difference $C_{\mu, \nu}(t, t') = \text{Tr}_E \{ B_\mu(t - t') B_\nu \rho_E \} = C_{\mu, \nu}(t - t')$ where the cyclic property

of the trace and the commutation of ρ_E with the system evolution operator have been used. It is convenient to perform the change of variable $\tau = t - t'$, so that

$$\frac{d\tilde{\rho}_S(t)}{dt} = - \sum_{\mu,\nu} \int_0^t d\tau (C_{\mu,\nu}(\tau)[S_\mu(t), S_\nu(t-\tau)\tilde{\rho}_S(t-\tau)] + h.c.) , \quad (1.58)$$

and to transform it into a time-local master equation in which the Markov approximation is introduced. Let us quantify the interaction strength by the parameter g which is small. The approximation states that, since the difference of $\tilde{\rho}_S$ at time t and at time $t - \tau$ is of second order g^2

$$\tilde{\rho}_S(t - \tau) = \rho_S(t) + O(g^2) , \quad (1.59)$$

and since the change in $\rho_S(t - \tau)$ goes with terms of order $O(g^2)$ inside the integral we can safely neglect the higher orders and substitute $\tilde{\rho}_S(t - \tau) \approx \tilde{\rho}_S(t)$ in the equation

$$\frac{d\tilde{\rho}_S(t)}{dt} = - \sum_{\mu,\nu} \int_0^t d\tau (C_{\mu,\nu}(\tau)[S_\mu(t), S_\nu(t-\tau)\tilde{\rho}_S(t)] + h.c.) , \quad (1.60)$$

which becomes time-local. Even if, the above approximation is called Markovian, the dynamics is not necessarily Markovian. Recall the third measure of non-Markovianity that we introduced; since the equation is time local, it can be brought into a canonical master equation, but we do not have any guarantee that the decay rates stay positive along the evolution. Another further assumption that is in line with this approximation is to extend the limit of integration to infinity

$$\frac{d\tilde{\rho}_S(t)}{dt} = - \sum_{\mu,\nu} \int_0^\infty d\tau (C_{\mu,\nu}(\tau)[S_\mu(t), S_\nu(t-\tau)\tilde{\rho}_S(t)] + h.c.) , \quad (1.61)$$

and obtain the equation that is known as Redfield equation. These later approximation is correct as long as the relaxing dynamics of the system are

slower than τ_E , the time taken for the environment to wash out correlations. The time scale of the relaxation is given by the coupling strength between subsystems $\tau_R \sim O(g^{-2})$, so that, the validity of these approximations is set by

$$\tau_E \ll \tau_R . \quad (1.62)$$

We can undo the change of image by differentiating Eq. (1.47)

$$\frac{d\tilde{\rho}_S(t)}{dt} = e^{iH_S t} \frac{d\rho_S(t)}{dt} e^{-iH_S t} + i e^{iH_S t} [H_S, \rho_S(t)] e^{-iH_S t} , \quad (1.63)$$

so that by isolating the derivative in the Schrödinger picture we can obtain the Redfield equation in this picture

$$\frac{d\rho_S(t)}{dt} = -i[H_S, \rho_S(t)] - \sum_{\mu, \nu} \int_0^\infty d\tau (C_{\mu, \nu}(\tau) [S_\mu, S_\nu(-\tau) \rho_S(t)] + h.c.) . \quad (1.64)$$

If we define the time-independent operator

$$\Lambda_\mu = \sum_\nu \int_0^\infty d\tau C_{\mu, \nu}(\tau) S_\nu(-\tau) , \quad (1.65)$$

we can write the r.h.s. of equation in the form of a time-homogeneous generator

$$\frac{d\rho_S(t)}{dt} = -i[H_S, \rho_S(t)] - \sum_\mu [S_\mu, \Lambda_\mu \rho_S(t) - \rho_S(t) \Lambda_\mu^\dagger] \equiv \mathcal{L} \rho_S(t) . \quad (1.66)$$

While a constant generator satisfies the semigroup property (1.14), it is not ensured to produce a dynamical map contraction. In order to achieve a map that is purely Markovian, one more approximation has to be considered, the so called secular approximation.

To consider the secular approximation we have to rewrite Eq. (1.61) as the Bloch-Redfield equation [14, 2]. To do so we rewrite the system

operators S_μ in terms of the operators

$$S_\mu = \sum_{\omega} S_\mu(\omega) , \quad (1.67)$$

where ω are the energy differences in the system spectrum, and

$$S_\mu(\omega) = \sum_{\epsilon' - \epsilon = \omega} |\epsilon\rangle \langle \epsilon| S_\mu |\epsilon'\rangle \langle \epsilon'| , \quad (1.68)$$

with the set of $\{|\epsilon\rangle\}$ the eigenbasis of H_S , and ϵ their respective eigenvalues. The evolution of the system operators in the interaction picture now reads

$$S_\mu(t) = \sum_{\omega} e^{-i\omega t} S_\mu(\omega) = \sum_{\omega} e^{i\omega t} S_\mu^\dagger(\omega) , \quad (1.69)$$

where in the last equation we employed the Hermitian property of $S_\mu(t)$. We also note that

$$S_\mu(\omega) = S_\mu^\dagger(-\omega) , \quad (1.70)$$

which implies that

$$[H_S, S_\mu^\dagger(\omega) S_\nu(\omega)] = 0 . \quad (1.71)$$

In this new representation of the system operators we can rewrite Eq. (1.61) as

$$\frac{d\tilde{\rho}_S(t)}{dt} = \sum_{\omega, \omega'} \sum_{\mu, \nu} e^{i(\omega' - \omega)t} \Gamma_{\mu\nu}(\omega) (S_\nu(\omega) \tilde{\rho}_S(t) S_\mu^\dagger(\omega') - S_\mu^\dagger(\omega') S_\nu(\omega) \tilde{\rho}_S(t)) + h.c. , \quad (1.72)$$

which is the Bloch-Redfield equation, and where we defined

$$\Gamma_{\mu\nu}(\omega) = \int_0^\infty d\tau e^{i\omega\tau} C_{\mu\nu}(\tau) . \quad (1.73)$$

The secular approximation consists on discarding the oscillating terms in the systems operators, i.e., the terms where $\omega - \omega' \neq 0$. This approximation

works well as long as the time scales defined by $\tau_S = \min_{|\omega-\omega'|} |\omega - \omega'|^{-1}$ are short in comparison to the relaxation time scale τ_R , i.e.,

$$\tau_S \ll \tau_R . \quad (1.74)$$

After this approximation the equation becomes

$$\frac{d\tilde{\rho}_S(t)}{dt} = \sum_{\omega} \sum_{\mu,\nu} \Gamma_{\mu\nu}(\omega) (S_{\nu}(\omega) \tilde{\rho}_S(t) S_{\mu}^{\dagger}(\omega) - S_{\mu}^{\dagger}(\omega) S_{\nu}(\omega) \tilde{\rho}_S(t)) + h.c. , \quad (1.75)$$

which after expressing

$$\Gamma_{\mu\nu} = \frac{1}{2} \gamma_{\mu\nu}(\omega) + i\sigma_{\mu\nu}(\omega) , \quad (1.76)$$

in its real and imaginary parts, we arrive at a Markovian equation

$$\begin{aligned} \frac{d\rho_S(t)}{dt} = & -i[H_S + H_{LS}, \rho_S(t)] \\ & + \sum_{\omega} \sum_{\mu,\nu} \gamma_{\mu\nu}(\omega) (S_{\nu}(\omega) \rho_S(t) S_{\mu}^{\dagger}(\omega) - \frac{1}{2} \{S_{\mu}^{\dagger}(\omega) S_{\nu}(\omega), \rho_S(t)\}) , \end{aligned} \quad (1.77)$$

in the Schrödinger picture, where we defined the Lamb Shift

$$H_{LS} = \sum_{\omega} \sum_{\mu,\nu} \sigma_{\mu\nu}(\omega) S_{\mu}^{\dagger}(\omega) S_{\nu}(\omega) . \quad (1.78)$$

Finally this master equation rates $\gamma_{\mu\nu}$ form a matrix whose elements are

$$\gamma_{\mu\nu}(\omega) = \int_{-\infty}^{\infty} d\tau e^{i\omega\tau} C_{\mu\nu}(\tau) , \quad (1.79)$$

which according to Bochner's theorem [2] is a positive matrix. This matrix can be diagonalized to bring the equation back to a ME in the form of Eq. (1.26).

which is a positive quantity, and ensures that this resulting equation produces a Markov process.

1.6 Stationary states

The interaction of the open system with the environment leads to an asymptotic stationary state of the system if there exist any $\rho_{ss} = \lim_{t \rightarrow \infty} \rho_S(t)$ such that

$$\mathcal{L}\rho_{ss} = 0 . \quad (1.80)$$

If the process is a contraction, it is ensured that at least one of these states exists [1].

We now show that the steady state of the Markovian ME (1.77) of an environment in a thermal state is the thermal state of the system. The thermal state of a system is given by the canonical equilibrium distribution

$$\rho^{\text{th}}(\beta) = \frac{e^{-\beta H}}{\text{Tr} \{e^{-\beta H}\}} , \quad (1.81)$$

where $\beta = 1/T$ is the inverse temperature. If the environment is in a thermal state at inverse temperature β , the correlation functions obey the following relation

$$C_{\mu\nu}(t) = \text{Tr} \left\{ B_\mu(t) B_\nu \rho_E^{\text{th}} \right\} = \text{Tr} \left\{ B_\mu e^{-iH_E t} B_\nu e^{-\beta H_E} e^{iH_E t} \right\} / \mathbb{Z} , \quad (1.82)$$

where $\mathbb{Z} = \text{Tr} \{e^{-\beta H_E}\}$ and we employed the cyclic property of the trace. We can insert the identity $\mathbb{I}_E = e^{-\beta H_E} e^{\beta H_E}$ before the operator B_ν to obtain

$$C_{\mu\nu}(t) = \text{Tr} \left\{ B_\mu e^{-\beta H_E} / \mathbb{Z} e^{\beta H_E} e^{-iH_E t} B_\nu e^{-\beta H_E} e^{iH_E t} \right\} . \quad (1.83)$$

We can now group the exponentials around B_ν to write

$$C_{\mu\nu}(t) = \text{Tr} \left\{ B_\nu(-t - i\beta) B_\mu \rho_E^{\text{th}} \right\} = C_{\nu\mu}(-t - i\beta) , \quad (1.84)$$

which is the Kubo-Martin-Schwinger condition. This property can be translated to the decay rates of Eq. (1.77) as

$$\gamma_{\mu\nu}(-\omega) = e^{-\beta\omega} \gamma_{\nu\mu}(\omega) . \quad (1.85)$$

Let us assume that the steady state of the system is a thermal state at the temperature of the environment

$$\rho_S^{\text{th}}(\beta) = \frac{e^{-\beta H_S}}{\text{Tr}_S \{e^{-\beta H_S}\}} . \quad (1.86)$$

This is a stationary state of the ME (1.77) if the generator of this state obeys $\mathcal{L}\rho_S^{\text{th}}(\beta) = 0$, i.e.,

$$\begin{aligned} & -i[H_S + H_{LS}, \rho_S^{\text{th}}] + \sum_{\omega>0} \sum_{\mu,\nu} \gamma_{\mu\nu}(\omega) (S_\nu(\omega) \rho_S^{\text{th}} S_\mu^\dagger(\omega) - \frac{1}{2} \{S_\mu^\dagger(\omega) S_\nu(\omega), \rho_S^{\text{th}}\}) \\ & + \sum_{\omega>0} \sum_{\mu,\nu} \gamma_{\mu\nu}(-\omega) (S_\nu(-\omega) \rho_S^{\text{th}} S_\mu^\dagger(-\omega) - \frac{1}{2} \{S_\mu^\dagger(-\omega) S_\nu(-\omega), \rho_S^{\text{th}}\}) = 0 , \end{aligned} \quad (1.87)$$

where we split the sum in ω into two sums with positive and negative ω , and we assumed that there is not any degenerate eigenstate of the system Hamiltonian. If the system was degenerate, the asymptotic state could not be unique and/or stationary³. Since the thermal state commutes with H_S and we recall Eq. (1.71), which implies $[H_S, H_{LS}] = 0$, the first commutator of the generators of the thermal state is null.

Making use of the properties in Eqs. (1.70,1.85) we can rewrite

$$\begin{aligned} \mathcal{L}\rho_S^{\text{th}}(\beta) = & \sum_{\omega>0} \sum_{\mu,\nu} \gamma_{\mu\nu}(\omega) \left(S_\nu(\omega) \rho_S^{\text{th}} S_\mu^\dagger(\omega) - \frac{1}{2} \{S_\mu^\dagger(\omega) S_\nu(\omega), \rho_S^{\text{th}}\} \right. \\ & \left. + e^{-\beta\omega} [S_\mu^\dagger(\omega) \rho_S^{\text{th}} S_\nu(\omega) - \frac{1}{2} \{S_\nu(\omega) S_\mu^\dagger(\omega), \rho_S^{\text{th}}\}] \right) . \end{aligned} \quad (1.88)$$

Finally by employing the following property of the thermal state and system operators

$$\rho_S^{\text{th}} S_\mu(\omega) = e^{\beta\omega} S_\mu(\omega) \rho_S^{\text{th}} , \quad (1.89)$$

³If the system was degenerate, the dynamics could be reduced to a degenerate subspace and the system could be able to evolve in that subspace.

the first term of the first line can be made to cancel the last terms of the second line, and using the same properties, the remaining terms can also be made to cancel out showing that the thermal state of the system is an stationary state of the ME. The process through which environment and system reach thermal equilibrium is usually referred as thermalization. It is an important process that has to be studied and controlled as far as possible in quantum technological applications as it is one of the main processes through which the systems loses coherence. We will take a closer look to this phenomenon in the context of qubits in the next chapter and study the characteristic time scales involved.

1.7 Heat fluxes in open systems

The scenario presented in the previous section represents a stationary equilibrium state, i.e., the system has reached a thermodynamic equilibrium with the surrounding environment. The theory of open quantum systems is not limited to the presence of a unique environment, it can also describe the dynamics of a system connected to multiple environments, which may be at different temperatures. In those situations the open quantum system can still reach a steady state, but it will not be in equilibrium, since the gradient in temperatures will cause the appearance of currents through the system. In this situation we say that the open system has reached a non-equilibrium steady state. It might be also the case that the system is also subject to an external driving force, encapsulated by an explicit time dependence of the system's Hamiltonian $H_S(t)$. The energy variation of the system

$$\frac{dE_S}{dt} = \frac{d}{dt} \langle H_S(t) \rangle = \text{Tr} \left\{ \frac{\partial H_S(t)}{\partial t} \rho_S(t) \right\} + \text{Tr} \left\{ H_S(t) \frac{d\rho_S(t)}{dt} \right\} , \quad (1.90)$$

comes from the power of the driving forces (first term) and heat currents of surrounding environments (second term). We can define the current

produced by each environment as

$$\begin{aligned} \mathcal{J}_i(\rho_S(t)) &\equiv \text{Tr} \left\{ H_S(t) D^{(i)}(\rho_S(t)) \right\} \\ &= \text{Tr} \left\{ H_S(t) \sum_{\mu} \gamma_{\mu}^{(i)} (L_{\mu}^{(i)} \rho_S(t) L_{\mu}^{(i)\dagger} - \frac{1}{2} \{ L_{\mu}^{(i)\dagger} L_{\mu}^{(i)}, \rho_S(t) \}) \right\}, \end{aligned} \quad (1.91)$$

where the superindex (i) makes reference to the decay rates and operators of the different environments, and we defined the dissipator $D^{(i)}$ of each environment. In the steady state the heat flux through the system becomes constant so that $\frac{dE_S}{dt} = 0$, and the heat fluxes and driving power have to balance. For simplicity, let us analyze the case without driving

$$\left. \frac{dE_S}{dt} \right|_{\rho_S^{ss}} = 0 = \sum_i \text{Tr} \left\{ H_S D^{(i)}(\rho_S^{ss}) \right\} = \sum_i J_i(\rho_S^{ss}), \quad (1.92)$$

where the steady state is given by the condition $\mathcal{L}\rho_S^{ss} = 0 = \sum_i D^{(i)}(\rho_S^{ss})$, which implies that all currents in the steady state have to be compensated. This energy balance condition in the steady state is reminiscent of the first law of thermodynamic. The theory of quantum thermodynamics is much more extense, read for instance [15] for a basic review and emergence of the laws of thermodynamics or [16] for a review on quantum heat engines.

1.8 Prethermalization (Publication [P.1])

In [P.1] we employ the theory of open quantum systems to tackle the effect that a non-equilibrium environment has on the dynamics of a two level system. The environment is composed of two subsystems that are at different temperatures, i.e., the environment is not in equilibrium, but only one of the subsystems is in direct interaction with the open system. The

novelty of this work comes from the treatment of the composite environment, and determining the correct approximations, that go in the same spirit as the Markov approximation, used to obtain the evolution operators of the environment and their corresponding correlation functions. We derived a master equation which was brought into canonical form as in Eq. (1.39), which allowed us to determine if the evolution was Markovian or not by just looking at the derived canonical decay rates. We were also inspired by the Quantum Volume measure of non-Markovianity to perform a study over all possible states in a geometric or visual way which was enlightening. The main result of the work is that this type of environments induce quasi-stationary states that live for some time of the evolution, but which do not correspond to the true steady state of the dynamical map. This effect is an instance of prethermalization, a phenomenon present in weakly non-integrable systems, where at short times the dynamics is dominated by one part of the Hamiltonian, but at long time the weak break of integrability, caused by a weak term of the Hamiltonian, drives the system out to the true thermal state of the whole Hamiltonian. We present a rigorous definition for the appearance of prethermalization, and do a systematic study of the properties of the environment, namely its temperatures and couplings, that enhance the existence of this intermediate quasi-stationary state. Finally, we also explore the effect that this phenomenon may have on a system that is coupled to multiple of these environments. The presence of this intermediate quasi-stationary state can cause the switch of heat flow direction through the system multiple times during the evolution.

Chapter 2

Noise in Quantum Computing

2.1 Introduction

The statement that the quantum information of a system is lost when it gets entangled with its environment is a witness of the deep distinction between classical and quantum information. Expressed in another way, the information of a composite quantum system is not the sum of its parts. This profound characteristic of quantum mechanics was first brought to light by John Bell [17] in 1964, whose work led to the understanding that quantum information is encoded in non-local correlations between the different parts of a physical system. Another key difference between quantum and classical information is that the acquisition of information in a quantum system suffers from two problems: i) the measurement process in quantum mechanics is a probabilistic procedure; ii) it also causes the disturbance of system that is being measured.

Some time after these discoveries, it was pointed out in 1982 independently by Feynman [18] and Benioff [19], and by the unnoticed work of Yuri Manin [20], that quantum systems could perform computations. The most remarkable motivation was the complexity of simulating quantum systems classically. There is no fundamental restriction for classical machines to simulate quantum systems; in the end, it amounts to computing a rotation matrix and applying it to a vector in a Hilbert space, but the problem becomes exponentially harder for larger systems. This limitation motivated the use of quantum systems to simulate analogous quantum systems. A quantum simulator would be nothing other than a quantum system that can be very precisely manipulated to simulate other quantum systems.

The peculiar features of quantum information, which sets it apart from its classical counterpart, were indicative that quantum systems could have a profound impact not only on the simulation of quantum systems but on the foundations of computing. This became crystal clear with the appearance of Shor's factoring algorithm [21] in 1994, which showed that a quantum computer could factor a large number more efficiently than currently know algorithms, and Grover's algorithm [22], which is a quantum search algorithm with a quadratic increase in efficiency compared to best possible classical algorithms.

The quintessential paradigm of quantum information processing is performed over collections of two level systems [23] which, in analogy to the classical bit, are called qubits. The qubit is the most basic carrier of quantum information. A computation usually follows three steps: (i) qubit initialization to a known state, (ii) qubit manipulation, which consists on applying operations on single qubits or operations that involve (entangle) multiple qubits, and (iii) measurement. Since the outcomes of the measurement are probabilistic, it might be necessary to repeat the previous steps several times.

The most common framework to describe qubit manipulations is the quantum circuit model. In this model, qubits are represented as wires, and manipulations over them are represented by gates acting over these wires. These gates have a corresponding physical implementation that is performed on the physical qubit, but this abstraction allows one to remove all the physical details and focus on the quantum information processing or quantum algorithms alone. Since calibrating each possible operation on a qubit is an arduous experimental task, it is convenient to be able to represent all operations in terms of a small subset that can be controlled with high precision. If combinations of these gates allow one to perform any possible quantum operation, then it is said to be a universal set of gates. It can be shown [24, 25] that a set of single qubit gates and an entangling two qubit gate are universal. For instance, one of these sets is composed of the three single qubit rotations around the three orthogonal axes and the CNOT gate, which, conditioned on a control qubit state, flips the target qubit state.

The first proposal to physically implement qubits, which was able to perform a universal set of gates, was in 1994 when Peter Zoller and Ignacio Cirac proposed in their seminal paper [26] a system of cold trapped ions. After this initial proposal, there have been many quantum systems proposed that can be more controllable or have better scalability. One of the most popular and promising implementations is the so called superconducting qubits, which are realized with a circuit loop that, when cooled down to cryogenic temperatures, displays superconducting properties. The current in the circuits is made of Cooper pairs that can display the quantum properties of superposition and entanglement. Operations on these systems can be performed with the use of microwave pulses.

While the quantum systems designed to carry and process quantum information can be constructed, they are not free from interaction with

external parties. Entanglement is at the same time the bane and the boon of quantum computing. Entanglement between the different components of a quantum computer has to be maintained and protected, but entanglement with undesired external systems that do not take part in the computation has to be avoided. In this chapter, we are concerned with the latter and employ the theory of open quantum systems, introduced in the previous chapter, to study the effects of thermalization and pure dephasing of qubits. In Section 2.2 we introduce the types of errors that affect qubits and briefly comment on techniques to reduce them. In Sections 2.3 and 2.4 we introduce two simple models of thermalization and pure dephasing and employ Markovian master equations to describe the dynamics. Finally, in Sections 2.5 and 2.6 we introduce non-Markovian pure dephasing noise models, a semiclassical and a full quantum model, respectively.

2.2 Quantum Errors and Noise

The two most common errors that qubits suffer are bit flip and phase flip errors. If we define the basis of the qubit levels as $\{|0\rangle, |1\rangle\}$, in analogy to the two classical states 0 or 1, the bit flip error is represented by a certain probability p that the following occurs

$$\begin{aligned} |0\rangle &\longrightarrow |1\rangle , \\ |1\rangle &\longrightarrow |0\rangle . \end{aligned} \tag{2.1}$$

A general qubit state $\alpha |0\rangle + \beta |1\rangle$ under this type of noise would change with probability p to the state $\alpha |1\rangle + \beta |0\rangle$. The operator sum representation of this process has Kraus operators $K_0 = \sqrt{1-p}\mathbb{I}$ and $K_1 = \sqrt{p}\sigma_x$, where σ_x represents the Pauli matrix x . This type of error produces, in general, a change in energy of the qubit, which causes energy dissipation of the qubit into the environment. In Section 2.3 we study this type of error as a consequence of thermalization in more detail.

The other type of error that a qubit might suffer is the phase flip error, which is represented by the following process

$$\begin{aligned} |0\rangle &\longrightarrow |0\rangle , \\ |1\rangle &\longrightarrow -|1\rangle . \end{aligned} \tag{2.2}$$

A general qubit state $\alpha|0\rangle + \beta|1\rangle$ under this type of noise would change with probability p to the state $\alpha|0\rangle - \beta|1\rangle$, where the relative phase of qubit states changes. This process has Kraus operators $K_0 = \sqrt{1-p}\mathbb{I}$ and $K_1 = \sqrt{p}\sigma_z$, where σ_z represents the z Pauli matrix. This type of noise, which is exclusively quantum mechanical, implies a loss of quantum information without any loss of energy. This noise process causes the loss of coherence (or quantum superposition) of the quantum system, but does not change the statistics of measuring in the eigenbasis of the qubit. If we represent the state of the qubit by its density matrix, this noise process produces

$$\rho = \begin{pmatrix} |\alpha|^2 & \alpha\beta^* \\ \alpha^*\beta & |\beta|^2 \end{pmatrix} \xrightarrow{\text{noise}} K_0\rho K_0^\dagger + K_1\rho K_1^\dagger = \begin{pmatrix} |\alpha|^2 & (1-2p)\alpha\beta^* \\ (1-2p)\alpha^*\beta & |\beta|^2 \end{pmatrix}, \tag{2.3}$$

where we can see that the populations are not affected but the coherence (off-diagonal elements) has decreased (in modulus). If the qubit is subject to successive applications of this noise process, the off-diagonal elements will tend to 0 (unless $p = 1$ or $p = 0$, which represent unitary processes). This type of noise is also called pure dephasing. While this process only reduces coherence, the bit flip errors, apart from producing energy dissipation, also produce a reduction in coherence, which is a feature that we will explore in the following section.

This type of errors might occur when applying imperfect gates as well as when the qubits are idle, i.e., waiting for the following gate to be applied.

The accumulation of these errors can render the computation useless, as the information is being lost to the environment. There are two main ways to tackle this problem. On the one hand, if the noise process that produces the errors is well-known and characterized, mitigation techniques can be applied that try to undo the harmful effect of noise. Mitigation techniques try to compensate the effect of noise, for instance, by applying additional operations on the qubits without affecting the computation. We expand more on these techniques in the following subsection. On the other hand, the method that works for general errors is called quantum error correction (QEC) [27]. In a faulty classical computer, one could copy the information many times and perform the operation on all the copies, to then keep the result that happened with the highest frequency. In the quantum realm, due to the no-cloning theorem [28, 29], information cannot be copied and repeated, but it can be spread along multiple qubits to create a highly entangled state that contains the original information. Then, after performing the computation, part of the information will be lost, but since it was spread between multiple parties, as long as some of them remained unaffected, the correct answer can be reconstructed. The first code that was able to correct the two types of errors previously introduced, and hence to correct general one qubit errors, was introduced by Peter Shor [30] in 1995, and involved encoding the state of one qubit into nine qubits. This code requires full connectivity between all qubits, which is a feature that most quantum computing implementations do not possess, and just to carry out the encoding becomes a very demanding task. More modern error correcting codes have been developed, such as surface codes [31, 32, 33, 34] that are designed for qubits that are laid out in a two dimensional grid, which is a common feature of current solid state implementations.

The basic difference is that QEC involves the detection and correction of errors that occur during computation, while error mitigation schemes

allow errors to occur and try to compensate for the negative effects of these uncorrected errors in various ways. If an implementation of a quantum computer can surpass the thresholds stabilised by QEC codes, errors could in principle be completely eliminated. While error mitigation tries to reduce the impact of errors it cannot completely eliminate them. In the next subsection we introduce two basic mitigation techniques, whose efficiency is later studied in the presence of random telegraph noise, a type of coherent noise that can explain the decoherence dynamics of qubits.

Mitigation techniques

One such technique is dynamical decoupling [35, 36], which originated in the field of nuclear magnetic resonance (NMR) and consists of applying pulses at repeated time intervals that flip the state of the qubit. The purpose of this technique is to partially cancel the noise induced in one interval by the noise induced in the following one by flipping the state. The effect of the pulses is to refocus the state dispersion caused by the environment. In a pictorial description, before the pulse, the states drifts "in one direction" due to the noise, and by flipping their state, they drift "in the opposite direction," thus recovering part of the lost information. The technique works when the noise induced by the environment possesses time correlations, and if the time intervals of the pulses are smaller than the correlation time of the environment. There are more sophisticated versions of this technique [37, 38] which, instead of performing pulses at equally spaced time intervals, they are performed at specific time intervals that lead to improved fidelity. In reference [39], it was studied how these techniques improve the fidelity of the qubits, and it was observed that this effect was related to the suppression of the low-energy part of the environment spectrum. This technique is especially useful when the qubits are idle, i.e., no operation is being performed on them, and they are only subject to the

action of the environment.

During an algorithm the qubit is subject to gates that rotate the qubit state and modify the degree in which the qubit is affected by the noise. A strategy to mitigate the noise consists on making the single qubit rotations of the algorithm as random as possible in order to obtain an average effect of the noise. One such technique is the so-called Pauli twirling [40, 41, 42], which consists of applying random Pauli operators (\mathbb{I} , σ_x , σ_y , σ_z) in between the algorithm gates and then averaging over all possible realizations of these operations. This technique does not change the logical circuit, but randomizes the single qubit rotations.

2.3 Dissipative noise model: thermalization

A very simple model to describe the bit flip type of error is to have a qubit that interacts with an environment at an inverse temperature β_E that induces transitions between its eigenstates. Such a situation can be described with a Hamiltonian of the form

$$H = \frac{\omega_0}{2}\sigma_z + \sigma_+ \otimes B + \sigma_- \otimes B^\dagger + H_E , \quad (2.4)$$

where the first term is the qubit free Hamiltonian, whose levels have an energy difference of ω_0 , H_E is the free Hamiltonian of the environment, and the remaining two terms constitute the interaction Hamiltonian, where the coupling is absorbed in the system operator B . The raising and lower operators $\sigma_\pm = \sigma_x \pm i\sigma_y$ of the system induce excitation or decay of the qubit states

$$\begin{aligned} \sigma_+ |0\rangle &= |1\rangle , \\ \sigma_- |1\rangle &= |0\rangle . \end{aligned} \quad (2.5)$$

This system can be described using the Redfield master equation (1.66), and we leave the derivation to Appendix A.1. The master equation becomes

$$\begin{aligned} \frac{d}{dt}\rho_S(t) = & -i[H'_S, \rho_S(t)] + \gamma n(\omega_0, \beta_E) [\sigma_+ \rho_S(t) \sigma_- - \frac{1}{2} \{\sigma_- \sigma_+, \rho_S(t)\}] \\ & + \gamma (n(\omega_0, \beta_E) + 1) [\sigma_- \rho_S(t) \sigma_+ - \frac{1}{2} \{\sigma_+ \sigma_-, \rho_S(t)\}] , \end{aligned} \quad (2.6)$$

where H'_S is the renormalized system Hamiltonian (see Appendix A.1), γ is related to the strength of the coupling with the environment, and $n(\omega, \beta) = [e^{\beta\omega} - 1]^{-1}$ is the average thermal number at temperature β . If we define the density matrix components as $\rho_{ij}(t) = \langle i | \rho_S(t) | j \rangle$ with $\{i, j\} = \{0, 1\}$, we can write the following differential equation for them,

$$\dot{\rho}_{10}(t) = i\omega'_0 \rho_{10}(t) - \frac{\gamma}{2} [2n(\omega_0, \beta_E) + 1] \rho_{10}(t) , \quad (2.7)$$

$$\dot{\rho}_{11}(t) = \gamma n(\omega_0, \beta_E) [1 - \rho_{11}(t)] - \gamma [n(\omega_0, \beta_E) + 1] \rho_{11}(t) , \quad (2.8)$$

where we employed trace preservation of the density matrix $\rho_{11}(t) + \rho_{00}(t) = 1$.

Zero temperature

Let us first explore what occurs to a qubit coupled to an environment at 0 temperature, i.e., $n(\omega_0, \beta \rightarrow \infty) \rightarrow 0$. The second term of Eq. (2.6) becomes null, and we have a Lindbladian ME with Lindblad operators $L = \sigma_-$, meaning that the qubit will only be subject to spontaneous decay at a rate γ . The system of Eqs. (2.7, 2.8) then has the solution

$$\begin{pmatrix} \rho_{00}(t) & \rho_{01}(t) \\ \rho_{10}(t) & \rho_{11}(t) \end{pmatrix} = \begin{pmatrix} (1 - e^{-\gamma t}) + e^{-\gamma t} \rho_{00}(0) & e^{i\omega'_0 t - \gamma t/2} \rho_{01}(0) \\ e^{-i\omega'_0 t - \gamma t/2} \rho_{10}(0) & e^{-\gamma t} \rho_{11}(0) \end{pmatrix} . \quad (2.9)$$

We can define the timescale T_1 at which the populations decay $\rho_{11}(t) = e^{-t/T_1} \rho_{11}(0)$ and the timescale T_2 corresponding to the coherence decay

$|\rho_{01}(t)| = e^{-t/T_2}|\rho_{01}(0)|$, following a nomenclature extracted from NMR. In this scenario we observe that $T_2 = 2\gamma^{-1} = 2T_1$: the populations decay twice as fast as the coherence, and at long times only the state $|0\rangle$ is populated.

Finite temperature

When the temperature of the environment is finite, the decay times become shorter, becoming $T_1 = [\gamma(2n(\omega_0, \beta_E) + 1)\gamma]^{-1} = T_2/2$, and, while coherences have the same exponential decay, the populations change their stationary solution

$$\rho_{11}(t) = e^{-t/T_1}\rho_{11}(0) + \frac{n(\omega_0, \beta_E)}{2n(\omega_0, \beta_E) + 1}(1 - e^{-t/T_1}). \quad (2.10)$$

In other words, at long times, the state of the qubit becomes the thermal state at the temperature of the environment

$$\lim_{t \rightarrow \infty} \rho_S(t) = \frac{e^{-\beta_E H_S}}{\text{Tr} \{e^{-\beta_E H_S}\}}. \quad (2.11)$$

Qubit initialization and [P.1]

In practical situations, the temperature of the surroundings of the qubits employed in quantum computers has an associated thermal energy of at least one order of magnitude less than the qubit energy¹. This implies that $\beta\omega_0 \sim 10$ and effectively $n(\omega_0, \beta_E) \sim 0$ meaning that, in the long time limit, all the qubits in a quantum computer tend towards the state $|0\rangle$ in very good approximation. This fact can be employed for the initialization of solid-state qubits, the system is left to relax towards the ground state. Usually, not all components of a quantum computer are at those low cryogenic temperatures, but present a descending gradient of temperature as they are closer to the

¹Typical values for a superconducting qubit energy are around 5GHz and temperatures of 20mK

physical qubits. In [P.1], it was pointed out that when a qubit is in direct contact with an environment at a certain temperature, thermalization of the qubit to that temperature is only a quasi-stationary state. If the system is left untouched for a sufficiently long time, it may thermalize to a state with a different temperature. This phenomenon can have implications for the initialization of the qubit. If the initialization time is sufficiently long, the qubit may reach an unexpected initial state, which can decrease the fidelity of the initialization procedure. Hopefully, the thermal mass of the qubit surroundings is high enough, and continuously pumped, so that thermalization to a higher temperature is unlikely. More sophisticated initialization protocols exist, for instance qubits initialization with tunable environments [43], initialization by repetitive projective measurements [44], or external coherent drive [45] to cool down the qubit, whose initialization fidelity is not affected by thermal population limits.

2.4 Markovian pure dephasing

In the previous section, we noted that dissipative dynamics lead to both changes in energy and a decrease in coherence of the qubit. However, it is also possible to experience decoherence without energy dissipation. This phenomenon is known as phase damping or pure dephasing noise. By following the procedure outlined in the previous section, we can construct a Hamiltonian that induces this effect on the qubit as,

$$H = \frac{\omega_0}{2}\sigma_z + \sigma_z \otimes B + H_E , \quad (2.12)$$

where now qubit operators only act through σ_z . The Markovian ME describing this scenario, derived in Appendix A.2, is

$$\frac{d}{dt}\rho_S(t) = -i[H_S, \rho_S(t)] + \frac{\Gamma}{2}(\sigma_z\rho_S(t)\sigma_z - \rho_S(t)) , \quad (2.13)$$

where Γ encodes the action of the environment and represents the rate at which the qubit loses coherence. The solution of this master equation is

$$\begin{pmatrix} \rho_{00}(t) & \rho_{01}(t) \\ \rho_{10}(t) & \rho_{11}(t) \end{pmatrix} = \begin{pmatrix} \rho_{00}(0) & e^{i\omega'_0 t - \Gamma t} \rho_{01}(0) \\ e^{-i\omega'_0 t - \Gamma t} \rho_{10}(0) & \rho_{11}(0) \end{pmatrix}, \quad (2.14)$$

where the timescale of decoherence is now $T_2 = \Gamma^{-1}$. The timescale of pure dephasing is referred to as T_ϕ , but in this case it coincides with T_2 . If in the master equation of the previous section we included a pure dephasing term then the decoherence time would have two contributions

$$|\rho_{01}(t)| = e^{-t/T_2} |\rho_{01}(0)| = e^{-t/(2T_1)} e^{-t/T_\phi} |\rho_{01}(0)|, \quad (2.15)$$

where the total decoherence time T_2 is given by the relation

$$\frac{1}{T_2} = \frac{1}{T_\phi} + \frac{1}{2T_1}. \quad (2.16)$$

In general, the decoherence time obeys $2T_1 \geq T_2$ (if there is presence of dissipative dynamics), but usually, because of the presence of pure dephasing, the decoherence time is shorter than the relaxation time, i.e., $T_2 < T_1$.

While a Markovian ME is a good description of the dissipative dynamics, which mostly come from thermalizing processes, pure dephasing is not always well described by Markovian dynamics. It has been observed [46, 47, 48, 49, 50, 51, 52, 53] that qubit dephasing presents coherence revivals and has $1/f$ spectral distribution causing the appearance of slow oscillating contributions, indications of non-Markovianity in the evolution of qubit decoherences. A more realistic approach has to be considered to model pure dephasing noise. In the following sections, we explore coherent noise models that can reproduce the observed effects, and we also explore mitigation techniques on them. First, we present a semiclassical model where the noise is induced by classical fluctuators by introducing the Random Telegraph

Noise (RTN). In the last section, we introduce a full quantum model, that is physically motivated, and employ the techniques of open quantum systems to study the decoherence effects.

2.5 Non-Markovian pure dephasing: semiclassical model

It has been widely observed that the source of noise in solid-state implementations of quantum computing [54, 55, 56] is caused by the presence of two-level defects within amorphous materials at low temperatures [57, 58]. Surprisingly, this effect appears to be universal across different materials and compositions, and it is particularly prominent in amorphous materials at temperatures below the Kelvin scale. When these two-level defects, or two-level systems (TLS), are strongly coupled to their surrounding environment, their dynamics are described by incoherent fluctuations between their two states, giving rise to what is referred to as fluctuators. A semiclassical model can be introduced to describe the pure dephasing noise induced by these fluctuators. Notably, this noise model is non-Markovian, rendering the previous section's model too simplistic to capture its complexity.

The state of the fluctuators can be described by a classical random variable $b_k^i(t) \in \{+1, -1\}$, where k indicates individual fluctuators and the superindex i indicates one particular realization of the random process. These fluctuator independently fluctuate between their two possible states at the rate γ_k . The probability that a fluctuator switches n times after some time t follows a Poisson distribution

$$p_n(t) = \frac{(\gamma_k t)^n}{n!} e^{-\gamma_k t}, \quad (2.17)$$

so that the average number of switches of fluctuator k during an interval of length τ is $\gamma_k \tau$. The autocorrelation function of a single fluctuator follows

an exponential decay,

$$C(t - t') = \langle b_k^i(t) b_k^i(t') \rangle_i = e^{-2\gamma_k |t - t'|} , \quad (2.18)$$

which indicates that the spectrum (Fourier transform of the autocorrelation function) is Lorentzian

$$S_{\text{RTN}}(\gamma_k, \omega) = \int_{-\infty}^{\infty} d\tau C(\tau) e^{i\tau\omega} = \frac{4\gamma_k}{4\gamma_k^2 + \omega^2} . \quad (2.19)$$

Each of the fluctuators is coupled to the qubit with a coupling strength v_k . The stochastic variable

$$\chi^i(t) = \sum_{i=1}^{N_{\text{RTN}}} v_k b_k^i(t) , \quad (2.20)$$

captures the effect of the fluctuators on the qubit, where N_{RTN} is the number of fluctuators. The influence of the fluctuators is incorporated into the qubit's Hamiltonian through a interaction of the type

$$H^i(t) = \frac{\omega_0 + \chi^i(t)}{2} \sigma_z , \quad (2.21)$$

where ω_0 is the energy splitting of the two levels of the qubit.

The evolution of the qubit under one of the realizations of the Hamiltonian (2.21) is unitary, but we have to consider the averaged evolution after many of these realizations, which, in general, represents a non-unitary evolution. If $\rho^i(t)$ represents the evolution of realization i , to obtain the averaged evolution we have to consider the expectation value over realizations $\rho(t) = \langle \rho^i(t) \rangle_i$. In an experiment, the expectation value is obtained as

$$\langle \rho^i(t) \rangle_i = \frac{1}{N_{\text{traj}}} \sum_{i=1}^{N_{\text{traj}}} \rho^i(t) , \quad (2.22)$$

where N_{traj} is the number of realizations of the stochastic process. Ideally, this number should be big to achieve convergence to the expected value. The averaged evolution of a qubit under this model becomes

$$\rho(t) = \begin{pmatrix} \rho_{00}(0) & \rho_{01}(0)e^{-i\omega_0 t}W(t) \\ \rho_{10}(0)e^{i\omega_0 t}W(t) & \rho_{11}(0) \end{pmatrix}, \quad (2.23)$$

where $W(t) = \langle e^{i \int_0^t \chi^i(t') dt'} \rangle_i$ is the decoherence function.

In the following, we study this decoherence function in different scenarios. The decoherence function can be defined for a general pure dephased qubit as

$$W(t) = \frac{|\rho_{01}(t)|}{|\rho_{01}(0)|}. \quad (2.24)$$

Single fluctuator

Computing the decoherence function $W(t)$ requires knowing the probability distribution of the accumulated phase

$$\phi^i(t) = \int_0^t \chi^i(t') dt', \quad (2.25)$$

which for a single fluctuator, with coupling strength v_k and switching rate γ_k , was analytically obtained in [59, 60]. The decoherence function induced by a single fluctuator k can be obtained as

$$W_k(t) = \left\langle e^{i \int_0^t \chi^i(t') dt'} \right\rangle_i = \begin{cases} e^{-\gamma_k t} \left(\cos \delta_k t + \frac{\gamma_k}{\delta_k} \sin \delta_k t \right), & \gamma_k < v_k, \\ e^{-\gamma_k t} \left(\cosh \delta_k t + \frac{\gamma_k}{\delta_k} \sinh \delta_k t \right), & \gamma_k \geq v_k, \end{cases} \quad (2.26)$$

where $\delta_k = \sqrt{|\gamma_k^2 - v_k^2|}$. Depending on the relation between the coupling strength and the rate, the decoherence function can monotonously decay ($v_k < \gamma_k$) or can present revivals ($v_k > \gamma_k$), indicating the presence of

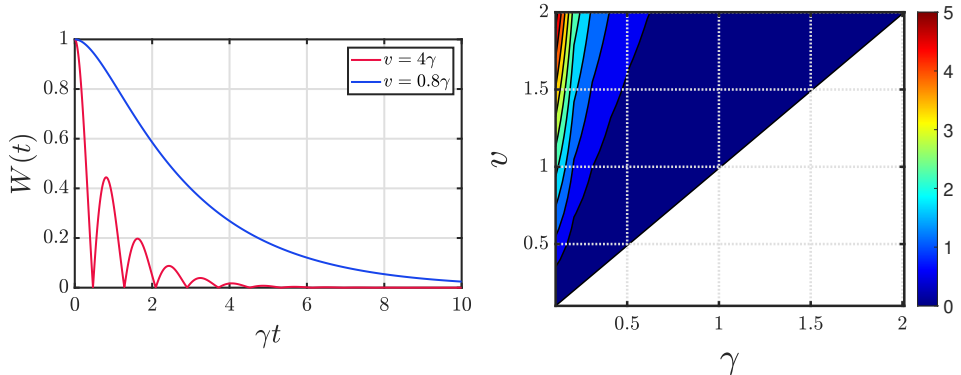


Figure 2.1: (Left) Evolution of the decoherence function for one evolution of each kind, i.e., one with weak coupling and one with strong coupling. (Right) Contour plot in the $\gamma - v$ plane of the non-Markovianity, where the white region indicates a null non-Markovianity.

non-Markovianity. The decoherence time is approximately given by $T_\phi = (\gamma_k - \sqrt{\gamma_k^2 - v_k^2})/2$ for the weak coupling regime and $T_\phi = \gamma_k/2$ for the strong coupling regime. In Fig. 2.1 we present the decoherence function of the two regimes, as well as the degree of non-Markovianity given by the BLP measure in terms of these parameters. On the one hand, we can see that when $v_k < \gamma_k$ the measure on non-Markovianity vanishes and the decoherence function presents a monotonous decay. On the other hand, when $v_k > \gamma_k$, the decoherence presents revivals and the non-Markovianity measure indicates presence of memory effects, a phenomenon that cannot be obtained with a Markovian ME as the one employed in the previous section.

Ensemble of fluctuators

In general, the qubit is coupled to an ensemble of fluctuators, but what is the probability distribution of its switching rates and couplings? It

has been experimentally observed that superconducting qubits exhibit $1/f$ flux noise [61, 62] with a weak dependence on the particular experimental implementation. In order to recover a $1/f$ spectrum in the model described in the previous section the following is required,

$$S(\omega) = \int_{\gamma_{\min}}^{\gamma_{\max}} S_{\text{RTN}}(\gamma, \omega) p(\gamma) d\gamma \propto \frac{1}{\omega}, \quad (2.27)$$

where $p(\gamma)$ is the probability distribution of the fluctuators frequencies. This requirement is fulfilled if the fluctuators switching rates are also distributed according to a $p(\gamma) \propto 1/\gamma$ distribution. The cutoff frequencies for the switching rates, γ_{\min} and γ_{\max} , can be set by experimental timescales. Very small switching rates are almost stationary during the whole experiment $\gamma_{\min} \approx 1/t_{\text{exp}}$, with t_{exp} the duration of the experiment, while very fast switching rates average out quickly, $\gamma_{\max} \approx 1/\Delta t$ with Δt the sampling timescale. The decoherence function of an ensemble of *independent* fluctuators is simply the product of the decoherence functions of each fluctuator

$$W_{1/f}(t) = \langle e^{i \sum_{k=1}^{N_{\text{RTN}}} v_k^i \int_0^t dt' p_k^i(t')} \rangle_i = \prod_{k=1}^{N_{\text{RTN}}} \langle e^{i v_k^i \int_0^t dt' p_k^i(t')} \rangle_i = \prod_{k=1}^{N_{\text{RTN}}} W_k(t). \quad (2.28)$$

Mitigation of RTN noise

To reduce the decoherence induced by RTN noise, induced by only one fluctuator throughout the rest of the section, mitigation techniques can be applied on the qubit. Let us consider the simple spin echo technique which consists on applying a σ_x pulse on the qubit in the intermediate time of the evolution, and another σ_x at the end. For an evolution of length $2\Delta t$, the application of a σ_x pulse at the intermediate time Δt and at the final time $2\Delta t$ has the following effect on the unitary evolution of a single trajectory

of the noise process

$$U^i(0, t) = \sigma_x e^{i\frac{\sigma_z}{2} \int_{\Delta t}^{2\Delta t} dt' \chi^i(t')} \sigma_x e^{i\frac{\sigma_z}{2} \int_0^{\Delta t} dt' \chi^i(t')} = e^{i\frac{\sigma_z}{2} (\int_0^{\Delta t} dt' \chi^i(t') - \int_{\Delta t}^{2\Delta t} dt' \chi^i(t'))}. \quad (2.29)$$

We use the convention to express times in terms of Δt , the time between pulse applications. This evolution changes the coherence of the qubit as

$$\rho_{01}^i(2\Delta t) = e^{i(\int_0^{\Delta t} dt' \chi^i(t') - \int_{\Delta t}^{2\Delta t} dt' \chi^i(t'))} \rho_{01}(0), \quad (2.30)$$

so that the averaged decoherence function can be written as

$$W(2\Delta t) = \left\langle \exp \left(i \int_0^{2\Delta t} \beta(t') \chi^i(t') dt' \right) \right\rangle_i, \quad (2.31)$$

with

$$\beta(t') = \begin{cases} 1 & \text{for } 0 < t' \leq \Delta t, \\ -1 & \text{for } \Delta t < t' < 2\Delta t. \end{cases} \quad (2.32)$$

The function $\beta(t)$ is referred to as the filter function of the mitigation technique, it takes values ± 1 and switches sign at definite time instants that depend on the mitigation technique. Below we present the filter function of the different mitigation techniques that we apply on RTN noise and the resulting decoherence function. The average performed in Eq. (2.31) can be computed using the method developed in [63]. The decoherence function between time instants at which a pulse is applied, where the filter function is constant, obeys the differential equation [63]

$$\frac{d^2}{dt^2} W(t) + \left[2\gamma - \frac{d \ln \beta(t)}{dt} \right] \frac{d}{dt} W(t) + v^2 W(t) = 0, \quad (2.33)$$

with initial conditions $W(0) = 1$ and $W'(0) = 0$. The derivative of $\ln \beta(t)$ introduces discontinuities in the derivative of $W(t)$ at times when $\beta(t)$ changes sign, which implies that $W'(t_s^+) = -W'(t_s^-)$, where t_s^+ (t_s^-) is the switch time from the right (left). In what follows, we present a derivation of

the decoherence function for spin echo sequence (2.29), periodic dynamical decoupling and for Pauli twirl, which all have a different filter function.

- i) **Free induced decay:** The free induced decay (FID) is the evolution of the qubit subject to the environment, but no manipulation of the noise is present. The filter function is a constant function of time $\beta(t) = 1$, and the solution of the differential equation (2.33) is the same as obtained with other methods in Eq. (2.26), which we rewrite here

$$W_{FID}(t) = e^{-\gamma t} \left(\cos(\delta t) + \frac{\gamma}{\delta} \sin(\delta t) \right), \quad (2.34)$$

with $\delta = \sqrt{v^2 - \gamma^2}$, and we dropped the index of the fluctuators since we are only considering one.

- ii) **Spin echo:** The spin echo sequence exemplified in Eq. (2.29) is the simplest mitigation technique. The differential equation (2.33) is solved for the time interval 1: $0 < t < \Delta t$ with initial condition $W_1(0) = 1$ and $W_1'(0) = 0$ and the time interval 2: $\Delta t < t < 2\Delta t$ with initial (boundary) conditions $W_2(\Delta t) = W_1(\Delta t)$ and $W_2'(\Delta t) = -W_1'(\Delta t)$, because of the discontinuity of $\beta(t)$. The subindex in $W_n(t)$ indicates at which time interval the function is calculated. The decoherence function at the end of the evolution is

$$W_{SE}(2\Delta t) = e^{-\gamma 2\Delta t} \left(1 + \frac{\gamma}{\delta} \sin(\delta 2\Delta t) + \frac{\gamma^2}{\delta^2} (1 - \cos(\delta 2\Delta t)) \right), \quad (2.35)$$

This decoherence function has higher value than the FID decoherence function (2.34) evaluated at time $2\Delta t$.

- iii) **Dynamical decoupling:** The periodic dynamical decoupling filter function $\beta(t)$ switches between $+1$ and -1 at regular time intervals Δt . With the continuity of $W(t)$ and the discontinuity of its derivative, we

can construct $W_n(t)$ for the time interval $t \in [(n-1)\Delta t, n\Delta t)$, which depends on the previous steps. The dependence is captured in the following set of equations

$$W''_{n+1}(t) + 2\gamma W'_{n+1}(t) + v^2 W_{n+1}(t) = 0, \quad (2.36)$$

$$W'_{n+1}(n\Delta t) = -W'_n(n\Delta t), \quad (2.37)$$

$$W_{n+1}(n\Delta t) = W_n(n\Delta t), \quad (2.38)$$

with initial conditions $W_0(0) = 1$ and $W'_0(0) = 0$. These equations can be reduced to the following recurrence relations

$$W_0(0) = 1, \quad (2.39)$$

$$W'_0(0) = 0, \quad (2.40)$$

$$W_{n+1}((n+1)\Delta t) = e^{-\gamma\Delta t} \left\{ \left(\cos(\delta\Delta t) + \frac{\gamma}{\delta} \sin(\delta\Delta t) \right) W_n(n\Delta t) \right. \\ \left. - \sin(\delta\Delta t) \frac{W'_n(n\Delta t)}{\delta} \right\}, \quad (2.41)$$

$$W'_{n+1}((n+1)\Delta t) = -e^{-\gamma\Delta t} \left\{ \left(\cos(\delta\Delta t) - \frac{\gamma}{\delta} \sin(\delta\Delta t) \right) W'_n(n\Delta t) \right. \\ \left. + \sin(\delta\Delta t) \frac{v^2}{\delta} W_n(n\Delta t) \right\}. \quad (2.42)$$

This recurrence relation can be written as a matrix system $\vec{W}_{n+1} = M\vec{W}_n$ where $\vec{W}_n = (W_n(n\Delta t), W'_n(n\Delta t))^T$. The general term can be obtained by recursive application of the matrix M to the initial condition $\vec{W}_0 = (1, 0)^T$, i.e. $\vec{W}_n = M^n \vec{W}_0$. The general term is

$$W_{DD}(n\Delta t) = e^{-n\gamma\Delta t} \left[\frac{\lambda_+^n + \lambda_-^n}{2} + \frac{\cos(\delta\Delta t)}{\sqrt{1+\alpha^2}} \frac{\lambda_+^n - \lambda_-^n}{2} \right] \quad (2.43)$$

where $\lambda_{\pm} = \alpha \pm \sqrt{1+\alpha^2}$ with $\alpha = \frac{\gamma}{\delta} \sin(\delta\Delta t)$. This result was obtained in [64, 65] employing a transfer matrix method.

iv) **Pauli twirling:** The effect of applying Pauli gates instead of just σ_x differs in that the set (\mathbb{I}, σ_z) does not change the sign of $\beta(t)$ while the set (σ_x, σ_y) has the effect of flipping the sign of $\beta(t)$. After each time step, we have a 50% chance of flipping the sign of the filter function. Since the action of the decoherence function is lineal, we have to average over all the possible decoherence functions. After the first step the decoherence function is simply given by

$$W_1(\Delta t) = e^{-\gamma\Delta t} \left(\cos(\delta\Delta t) + \frac{\gamma}{\delta} \sin(\delta\Delta t) \right). \quad (2.44)$$

In the next step, we have to consider the average over the two possibilities, $\beta(t)$ keeps a constant sign or $\beta(t)$ flips sign

$$\begin{aligned} W_{\text{twirl}}(2\Delta t) &= \frac{1}{2}W_1(2\Delta t) + \frac{1}{2}W_2(2\Delta t) \\ &= \frac{e^{-\gamma 2\Delta t}}{2} \left(\cos(\delta 2\Delta t) + 2\frac{\gamma}{\delta} \sin(\delta\Delta t) + 1 + \frac{\gamma^2}{\delta^2} (1 - \cos(\delta 2\Delta t)) \right) \\ &= e^{-\gamma 2\Delta t} \left(\cos(\delta\Delta t) + \frac{\gamma}{\delta} \sin(\delta\Delta t) \right)^2. \end{aligned} \quad (2.45)$$

In the third step, we have to consider 4 possibilities which starts to become a cumbersome computation

$$W_{\text{twirl}}(3\Delta t) = \frac{1}{4} (W_1(3\Delta t) + W_2(3\Delta t) + W_3(3\Delta t) + W_{2p}(3\Delta t)), \quad (2.46)$$

where $W_i(t)$ are the same functions obtained from the dynamical decoupling case, but $W_{2p}(t)$ is the function obtained from solving the differential equation (2.33) in the interval $[2\Delta t, 3\Delta t]$ with boundary conditions $W_{2p}(2\Delta t) = W_1(2\Delta t)$ and $W'_{2p}(2\Delta t) = -W'_1(2\Delta t)$. Luckily enough, this expression simplifies to

$$W_{\text{twirl}}(3\Delta t) = e^{-\gamma 3\Delta t} \left(\cos(\delta\Delta t) + \frac{\gamma}{\delta} \sin(\delta\Delta t) \right)^3. \quad (2.47)$$

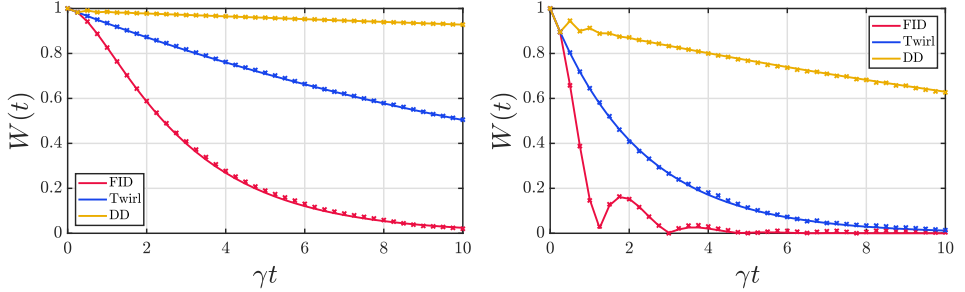


Figure 2.2: (Left) Evolution of the decoherence function induced by a weakly coupled fluctuator $v = 0.8\gamma$ for different mitigation techniques. The red lines correspond to a free evolution, where the qubit is only subject to RTN noise, the blue line corresponds to a qubit that is subject to Pauli twirling and the yellow line is a qubit subject to dynamical decoupling. (Right) Same comparison for a strongly coupled fluctuator with $v = 2\gamma$. The time step at which each pulse is applied is $\Delta t = 1/(4\gamma)$. The crosses represent numerical simulations of the decoherence functions with 10^4 realizations, while the continuous lines represent the derived analytical formulas.

To compute the following step this systematic procedure can be applied, and with the use of the inductive method, it can be shown that for a general number of steps

$$W_{\text{twirl}}(n\Delta t) = e^{-\gamma n\Delta t} \left(\cos(\delta\Delta t) + \frac{\gamma}{\delta} \sin(\delta\Delta t) \right)^n, \quad (2.48)$$

which is an original result, and was verified by a numerical simulation of multiple realizations of the noise process and random selection of twirl pulses.

In Fig. 2.2 we show the effectiveness of each mitigation technique on RTN noise of a single fluctuator and compare the analytical results with numerical simulations. It can be observed that dynamical decoupling is the

most effective at reducing the overall decay of the decoherence function, while the Pauli twirl is still better than doing nothing. As mentioned before, the Pauli twirl is better suited for mitigating noise during quantum algorithms, while dynamical decoupling can only be applied on idle qubits. Since the fluctuators are independent, the decoherence function for an ensemble of them can be obtained in the same fashion as before.

Unbalanced fluctuators

So far, we only considered fluctuators that have balanced transition rates between their two states, i.e., the rate of transition from the $-1 \rightarrow 1$ state γ_+ is the same as the transition rate from the $1 \rightarrow -1$ state γ_- . This assumption is valid if the energy difference of the fluctuator levels E_f is small compared to the thermal energy, i.e., $E_f \ll k_B T$. If that is not the case, the rates are related [66, 67] by $\gamma_-/\gamma_+ = e^{-E_f/k_B T}$, so that, for low temperature, the transition $1 \rightarrow -1$ is dominant (spontaneous emission).

The decoherence function for the unbalanced case is

$$W(t) = e^{-\gamma_u t} \left| \cosh(\delta_u t) + \frac{\gamma_u}{\delta_u} \sinh(\delta_u t) \right|, \quad (2.49)$$

where $\gamma_u = \frac{\gamma_+ + \gamma_-}{2}$ is the average decay rate and $\delta_u = \sqrt{\gamma_u^2 - v^2 + iv\Delta\gamma}$ with $\Delta\gamma = \gamma_+ - \gamma_- = 2\gamma_u \tanh(E_f/2k_B T)$. The effect of dynamical decoupling on this unbalanced RTN noise was analytically obtained in [65]. While this model gives reasonable predictions at temperatures near the energy of the fluctuator and above, it starts to fail at lower temperatures where quantum effects become relevant. Below this point, the TLS cannot be described as a classical state that incoherently flips between two states, and one needs to consider a model of a coherent TLS. In the next section, we propose a model that takes into account a coherent TLS coupled to an external environment that slowly reduces its coherence.

We can see that, at very low temperatures, this semiclassical model fails to fully describe the decoherence of the qubit. For instance, considering a common case [68] where $E_f \approx 10k_B T$ the rate difference approximately becomes $2\gamma_u$ and $\delta_u = \gamma_u + iv$, so that the decoherence function reads

$$W(t) = \frac{e^{-\gamma_u t}}{\sqrt{2(\gamma_u^2 + v^2)}} \left(v^2 \cos(2vt) + (2\gamma_u^2 + v^2) \cosh(2\gamma_u t) + 2\gamma_u (v \sin(2vt) + \gamma_u \sinh(2\gamma_u t)) \right)^{1/2}, \quad (2.50)$$

which in the long time limit reaches a constant value

$$\lim_{t \rightarrow \infty} W(t) = \sqrt{\frac{\gamma_u^2 + (\frac{v}{2})^2}{\gamma_u^2 + v^2}}, \quad (2.51)$$

contrary to what is expected. In a true quantum model, as a result of the interaction between qubit and TLS, there should be a transfer of coherence to the TLS that is destroyed by the environment. This semiclassical model is too simple and cannot capture the quantum nature of the qubit-TLS interaction. In the following section we introduce a full quantum model that describes this interaction.

2.6 Non-Markovian pure dephasing: quantum model

There have been some proposals [69, 70, 71, 72] of microscopic quantum models to describe the noise induced by coherent TLS, see [68] for a review of their physical motivation. In general, the TLS are modelled by an asymmetric double well potential, with ϵ the energy difference of the minima and Δ the tunneling rate. In this section, we construct a quantum model where the qubit is coupled to a coherent TLS, that is in turn coupled to

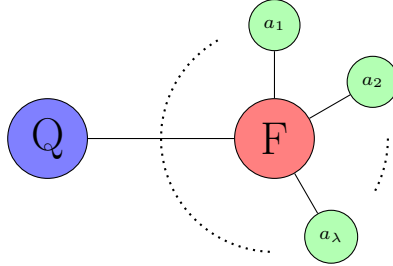


Figure 2.3: Schematic picture of the model. The qubit (Q) is coupled to the fluctuator (F), which in turn is coupled to its own bath of harmonic oscillators a_λ .

an external reservoir at a finite temperature. The total Hamiltonian reads $H = H_S + H_E + H_I$, where the system qubit-TLS Hamiltonian has three terms $H_S = H_Q + H_{TLS} + H_{QT}$,

$$H_Q = \frac{1}{2}\omega_q\tau_z, \quad H_{TLS} = \frac{\epsilon}{2}\sigma_z + \frac{\Delta}{2}\sigma_x, \quad H_{QT} = \frac{v}{2}\tau_z\sigma_z, \quad (2.52)$$

where τ_i are Pauli matrices acting on the qubit's Hilbert space and σ_i on the TLS's space. The TLS Hamiltonian is an effective description of the double well described before. The qubit-TLS interaction H_{QT} induces pure dephasing on the qubit. The energy difference of the TLS levels is $E_F = \sqrt{\Delta^2 + \epsilon^2}$.

The environment is a bosonic reservoir that couples directly to the TLS, but not to the qubit. The environment and interaction Hamiltonians are

$$H_B = \sum_k \omega_k b_k^\dagger b_k, \quad H_I = \sigma_+ \sum_k g_k b_k + \sigma_- \sum_k g_k^* b_k^\dagger. \quad (2.53)$$

In Fig. 2.3 we sketch a schematic picture of this composite environment.

Simplified evolution

Since the interaction Hamiltonian is the same as in the simple model of Section 2.3, one might be tempted to construct the same master equation as Eq. (2.6) with the system Hamiltonian $H_S = H_Q + H_{TLS} + H_{QT}$. That would not be correct, since the TLS does not only interact with the environment: it also interacts with the qubit, which modifies the evolution of the interaction operators σ_{\pm} . If we consider this simplified evolution model, the ME that describes the evolution of the qubit-TLS system is

$$\begin{aligned} \frac{d}{dt}\rho_{QT}(t) = & -i[H_Q + H_{TLS} + H_{QT}, \rho_{QT}(t)] \\ & + \Gamma n(E_f, \beta_E)(\sigma_+ \rho_S(t) \sigma_- - \frac{1}{2}\{\sigma_- \sigma_+, \rho_{QT}(t)\}) \\ & + \Gamma(n(E_f, \beta_E) + 1)(\sigma_- \rho_{QT}(t) \sigma_+ - \frac{1}{2}\{\sigma_+ \sigma_-, \rho_{QT}(t)\}) , \end{aligned} \quad (2.54)$$

where $\rho_{QT}(t)$ is the density matrix of the qubit-TLS state. This is a model that resembles the semiclassical model presented in Section 2.5, where the fluctuator is only affected by the environment and not by the qubit state. To obtain the reduced density matrix of the qubit, we need to take the partial trace with respect to the TLS, i.e., $\rho_Q(t) = \text{Tr}_{TLS}\{\rho_{QT}(t)\}$. The correspondence is incredibly similar with the RTN fluctuator model, with the parameter correspondence $\gamma_+ = \Gamma n(E_f, \beta_E)$, $\gamma_- = \Gamma(n(E_f, \beta_E) + 1)$, and being v the interaction strength between qubit and TLS in H_{QT} . Note that the relation $\gamma_-/\gamma_+ = e^{-E_f/k_B T}$ holds for this parameter correspondence. In Fig. 2.4, we present a comparison of the RTN decoherence function and the decoherence function given by this master equation for different temperatures. It can be observed that, for high temperatures, both models give the same evolution of the decoherence function, but when the temperatures get lower the solutions start to deviate from each other. We restricted ourselves to

2.6. NON-MARKOVIAN PURE DEPHASING: QUANTUM MODEL 61

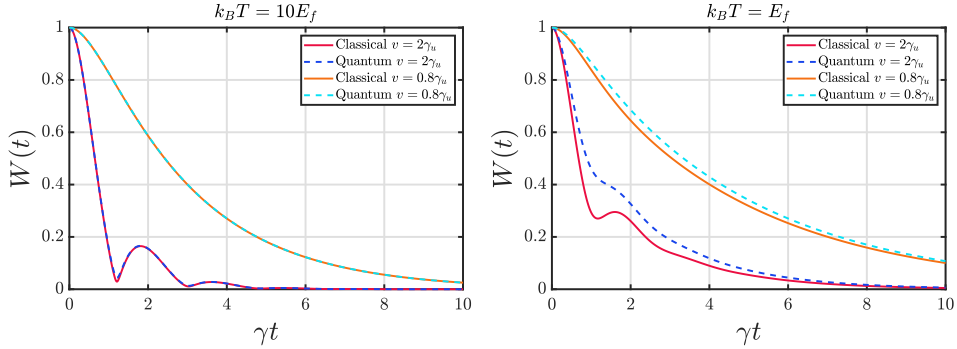


Figure 2.4: Comparison between the evolution of the decoherence function in the unbalanced fluctuator model and the simplified quantum model. In the panel on the left the temperature is much higher than the fluctuator energy and the two models produce the same decoherence function. In the right panel, the thermal energy is of the same order as the fluctuator energy, and a discrepancy between models starts to become apparent.

the case with a null tunneling rate of the TLS ($\Delta = 0$) to closely relate to the semiclassical model, which does not include any mechanism to describe the tunneling between TLS levels.

Correct evolution

To consider the correct dynamics of the quantum model, we first rewrite the interaction Hamiltonian in terms of Hermitian operators

$$H_I = \sigma_x \otimes \frac{1}{2} \sum_k g_k (a_k + a_k^\dagger) + \sigma_y \otimes \frac{i}{2} \sum_k g_k (a_k - a_k^\dagger), \quad (2.55)$$

so that we can directly employ the Redfield equation (1.66). The evolution of the TLS operators is given by

$$\sigma_x(t) = e^{i(H_Q + H_{TLS} + H_{QT})t} \sigma_x e^{-i(H_Q + H_{TLS} + H_{QT})t}, \quad (2.56)$$

which depends non-trivially on all the constituents of the qubit-TLS Hamiltonian. Similarly, we can obtain the evolution of σ_y . If the evolution of these operators was given solely by H_{TLS} the resulting ME would be the same as Eq. (2.54), which is equivalent to a weak coupling limit of the qubit-TLS interaction². We can write the evolution of these operators through the spectral decomposition of H_S as in Eq. (1.69)

$$\begin{aligned}\sigma_x(t) &= e^{-iD_+t}\Pi_2\sigma_x\Pi_1 + e^{iD_+t}\Pi_1\sigma_x\Pi_2 + e^{-iD_-t}\Pi_4\sigma_x\Pi_3 + e^{iD_-t}\Pi_3\sigma_x\Pi_4 \\ &\quad + \sum_{i=1}^4 \Pi_i\sigma_x\Pi_i , \\ \sigma_y(t) &= e^{-iD_+t}\Pi_2\sigma_y\Pi_1 + e^{iD_+t}\Pi_1\sigma_y\Pi_2 + e^{-iD_-t}\Pi_4\sigma_y\Pi_3 + e^{iD_-t}\Pi_3\sigma_y\Pi_4 ,\end{aligned}\tag{2.57}$$

where $D_{\pm} = \sqrt{\Delta^2 + (v \pm \epsilon)^2}$ are the energy transitions between eigenstates of the qubit-TLS Hamiltonian H_S , and $\Pi_i = |E_i\rangle\langle E_i|$ the projection operators onto these eigenstates $|E_i\rangle$, which are

$$|E_1\rangle = \frac{1}{\sqrt{2D_+^2 + 2D_+(\epsilon + v)}}((v + \epsilon) + D_+, \Delta, 0, 0)^T \equiv |\uparrow\nearrow\rangle , \tag{2.58}$$

$$|E_2\rangle = \frac{1}{\sqrt{2D_+^2 - 2D_+(\epsilon + v)}}((v + \epsilon) - D_+, \Delta, 0, 0)^T \equiv |\uparrow\searrow\rangle , \tag{2.59}$$

$$|E_3\rangle = \frac{1}{\sqrt{2D_-^2 + 2D_-(\epsilon - v)}}(0, 0, (\epsilon - v) + D_-, \Delta)^T \equiv |\downarrow\nearrow\rangle , \tag{2.60}$$

$$|E_4\rangle = \frac{1}{\sqrt{2D_-^2 - 2D_-(\epsilon - v)}}(0, 0, (\epsilon - v) - D_-, \Delta)^T \equiv |\downarrow\searrow\rangle , \tag{2.61}$$

$$(2.62)$$

²If $v = 0$, H_Q commutes with H_{TLS} and with σ_x so that it does not contribute to the evolution of the interaction operators with the environment.

2.6. NON-MARKOVIAN PURE DEPHASING: QUANTUM MODEL 63

expressed in the spin z component of qubit and TLS, with respective eigenvalues

$$\begin{aligned} E_1 &= \frac{1}{2}(\omega_0 + D_+) , & E_2 &= \frac{1}{2}(\omega_0 - D_+) , \\ E_3 &= \frac{1}{2}(-\omega_0 + D_-) , & E_4 &= \frac{1}{2}(-\omega_0 - D_-) . \end{aligned} \quad (2.63)$$

The correlation functions are given by

$$C_{xx}(t) = \frac{1}{4} \int d\omega J(\omega) n(\omega, \beta_E) e^{-i\omega t} + J(\omega) (n(\omega, \beta_E) + 1) e^{i\omega t} , \quad (2.64)$$

$$C_{xy}(t) = \frac{i}{4} \int d\omega J(\omega) n(\omega, \beta_E) e^{-i\omega t} - J(\omega) (n(\omega, \beta_E) + 1) e^{i\omega t} . \quad (2.65)$$

The remaining two are related to these ones as $C_{yy}(t) = C_{xx}(t)$ and $C_{yx}(t) = -C_{xy}(t)$. We have considered a continuum limit of the modes of the reservoir so that

$$J(\omega) = \sum_k |g_k|^2 \delta(\omega - \omega_k) = g\omega e^{-\omega/\omega_c} , \quad (2.66)$$

which is an ohmic spectral function [73, 2], where g is proportional to the coupling strength with the environment, and ω_c is a frequency cutoff for the modes. Since no easy expression can be obtained for the evolution operators, we implement numerically the operators into the Redfield equation to obtain the evolution of the qubit-TLS system.

We can obtain a more amenable master equation in Lindblad form considering the secular approximation, that is, removing the fast oscillating terms of the qubit-TLS system in the Bloch-Redfield ME (1.72). This approximation is only valid if the timescale of the removed terms is much faster than the relaxation time. In this system, the slowest system term defines the timescale

$$\tau_S = \frac{1}{|D_+ - D_-|} = \frac{1}{\sqrt{\Delta^2 + (v + \epsilon)^2} - \sqrt{\Delta^2 + (v - \epsilon)^2}} , \quad (2.67)$$

which becomes large if v goes to 0, but in this situation³ we could resort to the master equation of the previous subsection. This approximation also fails if $\Delta^2 \gg (\epsilon \pm v)^2$. The relaxation timescale is given by the coupling strength with the environment $\tau_R = g^{-1}$, and the approximation is valid in the regime $\tau_S \ll \tau_R$.

The ME after the secular approximation becomes

$$\begin{aligned} \frac{d}{dt}\rho_{QT}(t) = & -i[H_Q + H_{TLS} + H_{QT} + H_{LS}, \rho_{QT}(t)] \\ & + \sum_{i=1}^4 \gamma_i (L_i \rho_{QT}(t) L_i^\dagger - \frac{1}{2} \{L_i^\dagger L_i, \rho_{QT}(t)\}) , \end{aligned} \quad (2.68)$$

where the operators and corresponding rates are

$$\gamma_1 = J(D_+) (n(D_+, \beta_E) + 1) , \quad L_1 = \Pi_2 \sigma_- \Pi_1 , \quad (2.69)$$

$$\gamma_2 = J(D_+) n(D_+, \beta_E) , \quad L_2 = \Pi_1 \sigma_+ \Pi_2 , \quad (2.70)$$

$$\gamma_3 = J(D_-) (n(D_-, \beta_E) + 1) , \quad L_3 = \Pi_4 \sigma_- \Pi_3 , \quad (2.71)$$

$$\gamma_4 = J(D_-) n(D_-, \beta_E) , \quad L_4 = \Pi_3 \sigma_+ \Pi_4 . \quad (2.72)$$

$$(2.73)$$

and we do not explicitly write the Lamb shift Hamiltonian for the sake of space. If we take a close look at the rates and operators 1 and 3, they resemble the γ_- and σ_- operator in Eq. (2.54), but in this case, since the interaction of the TLS with the qubit is taken into account, the rates and operators take into account the correct level transitions of the qubit-TLS system. The same occurs for the rates 2 and 4.

This interpretation is more easily understood in the case of vanishing detuning $\Delta = 0$ of the TLS, in which case the transition energies simplify

³The case $v \rightarrow 0$ represent a mathematical singularity because the transition frequencies of H_S become degenerate and a different approach has to be followed. Fortunately, in this case, it is much simpler and is described in the previous subsection.

2.6. NON-MARKOVIAN PURE DEPHASING: QUANTUM MODEL 65

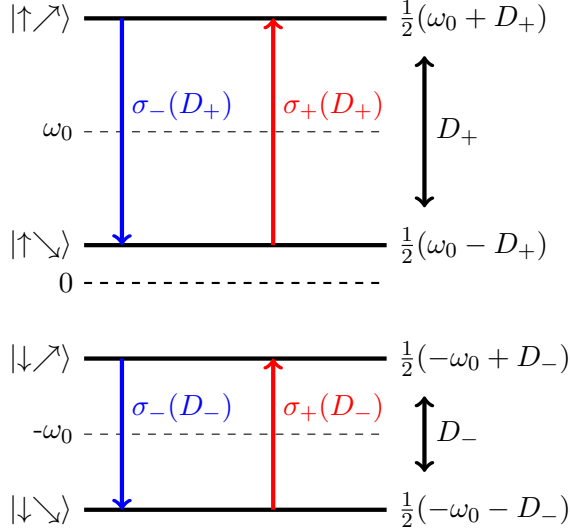


Figure 2.5: Sketch of the energy levels of the qubit-TLS system. The black horizontal lines represent the energy levels of the system. The blue and red lines represent the only allowed transitions with $\sigma_+(D_+) = \Pi_1\sigma_+\Pi_2$, $\sigma_-(D_+) = \Pi_2\sigma_-\Pi_1$, $\sigma_+(D_-) = \Pi_3\sigma_+\Pi_4$ and $\sigma_-(D_-) = \Pi_4\sigma_-\Pi_3$ the operators that drive them. The double arrowed thick lines indicate the energy difference of the levels with allowed transitions.

to $D_{\pm} = |\epsilon \pm v|$. In Fig. 2.5 we represent the energy levels of the qubit-TLS system, the transition energies, and corresponding operators. Depending on the state of the qubit the transitions of the TLS states happen with different energies. If the qubit is in the up state, the transitions between the TLS states occur with energy D_+ and the rates depend on it, while if the qubit is in the down state, they occur with energy D_- and the corresponding rates. In the simplified model of the last subsection, where the qubit interaction is not taken into account, the transitions between the TLS states occur with the same rate, only dependent on E_f .

If the fluctuator has detuning $\Delta \neq 0$ the model becomes richer. The energy structure is similar to the one sketched in Fig. 2.5; the transition rates depend on the original values of D_{\pm} but the transition operators are tilted, i.e., the eigenbasis of the qubit and the TLS are no longer parallel.

Conclusions and outlook

The quantum model presented in this section constitutes a good candidate to represent the noise processes that induce noise on solid-state qubit implementations of quantum computing, where the source of noise comes from two-level systems present in amorphous solids [68]. We showed that this model has rich dynamics, and that the RTN noise model only represents a very simplified case of the proposed noise model, and that it fails at low temperatures. The aim of the construction of this quantum model is to also assess the efficiency of mitigation techniques on the more realistic quantum model.

To consider a periodic dynamical decoupling sequence acting on this system, the qubit-TLS Hamiltonian would be modified as

$$H_S \rightarrow H_S + H_{DD}(t) \equiv H_S + \frac{\pi}{2} \sum_n \delta(t - n\Delta t) \tau_x, \quad (2.74)$$

where we considered ideal pulses, equally spaced by Δt , so that at times $n\Delta t$ the qubit state is flipped. This modification of the qubit-TLS Hamiltonian will cause a modification of the evolved interaction operators with the environment, whose free evolution is given by the unitary operator

$$U(t, 0) = e^{-iH_{QT}(t - \lfloor \frac{t}{\Delta t} \rfloor \Delta t)} (\sigma_x e^{-iH_{QT}\Delta t})^{\lfloor \frac{t}{\Delta t} \rfloor}, \quad (2.75)$$

where $\lfloor \cdot \rfloor$ is the floor function. This stepwise evolution operator makes considering the Markovian approximation done in Eq. (1.61) not doable, since the system operator $S(t - \tau)$ for $\tau > t$ is not well-defined with this

2.6. NON-MARKOVIAN PURE DEPHASING: QUANTUM MODEL 67

evolution operator. In this case, we have to resort to the ME (1.60), which has a time dependent generator, and, given the complexity, we have to employ numerical methods, which is a work in progress.

Part II

Quantum Walks

and their use in the simulation of physical theories

Chapter 3

Discrete Time Quantum Walks

3.1 Introduction

A random walk is a random process that describes the displacement of a walker following a succession of random steps on a graph. The most common random walk model is that of a walker on a regular lattice, where the jump probability of the walker to the adjacent locations is given by some probability distribution, but there are other possible scenarios. Random walks can be used, for instance, to model the random motion of molecules in liquids or gases (Brownian motion) and has applications in many scientific fields, such as biology, chemistry or computer science, to name a few. The expected position of the walker is described by a probability distribution, that is determined by the random jump probability and the specific graph. The basic example of a random walk is a walker on the integer number line \mathbb{Z} , which, after each step, jumps one position in the positive or negative direction conditioned to the outcome of a balanced coin toss.

An analogous quantum random walk (QW) was proposed in 1993 by Aharonov et al. [74], in which the walker is a quantum particle that cannot be localized due to quantum uncertainties. The state of the walker is described instead by a spinor wave function, and the jump probabilities are conditioned to an internal degree of freedom, which plays the role of a quantum coin. Due to the quantum character of the walker, its probability distribution is different from that of the classical one. Quantum walks can also be defined in continuous time. Childs et al. gave in [75] the general definition, which is based on a Hamiltonian formulation in which the internal degree of freedom of the walker is not needed. While continuous-time quantum walks have many important applications and properties, the works in this chapter are focused on discrete time quantum walks.

It was already pointed out in [74] that the dispersion of the quantum walker is quadratically faster than that of the classical walker. This fact allowed the discovery of more efficient search algorithms than their classical counterparts. For instance, Grover's algorithm [22] can be viewed as a quantum walk search algorithm [76]. Similar search algorithms based on quantum walks, such as the element distinctness problem [77], have also been shown to be more efficient than the classical counterparts. Finally, QWs also proved to be more efficient in probability distribution sampling problems [78, 79]. It has also been shown that QWs can be used as a universal computational model [80, 81].

There have been numerous experimental proposals to implement quantum walks. The first proposed platform for implementing the discrete time QW was using ion traps [82], where the discrete lattice was encoded in the vibrational modes of the ions, and the coin state was encoded in the internal electronic state of the ions. Many more platforms have been proposed such as QED cavities [83], or optical lattices [84], to name a few. See [85] for a comprehensive review of physical implementations.

In this chapter we introduce the basic definition of a classical random walk and a quantum walk, and describe their differences and their correspondence in Section 3.2. In Section 3.3 we review the properties of the QW in momentum space and its spectrum. Finally, in Section 3.4 we present the continuous limit of the discrete time quantum walk, and review the application of QW to the simulation of physical theories. The rest of the sections are devoted to summarizing the remaining publications.

3.2 The Random Walk on the line: Classical and Quantum

The classical random walk (CRW) on the integer number line describes a walker with definite position at each step of the evolution. The walker is displaced along the discrete positions of the line, and is only allowed to jump to adjacent locations, i.e., at each time step it only has two possible positions to move. The jump direction is determined by a balanced coin toss, but it can be generalized to different probabilities for each direction. In Fig. 3.1 we represent the location of 50 random walkers after 10 steps, where all walkers started in the location $j = 0$. Notice that no walker is present in odd position numbers; if we performed an odd number of steps, the walkers would be only located on odd positions. The probability of finding the walker at position j at the time step n is given by a binomial distribution

$$P_{n,j} = \frac{1}{2^n} \binom{n}{\frac{j+n}{2}}, \quad (3.1)$$

where $j \in \mathbb{Z}$ is the position in the integer line and n the time step of the evolution. This probability is null for $j + n$ odd, such that at even (odd) steps the walkers are only located in even (odd) positions. In Fig. 3.1 we plot the probability distribution multiplied by the number of walkers with

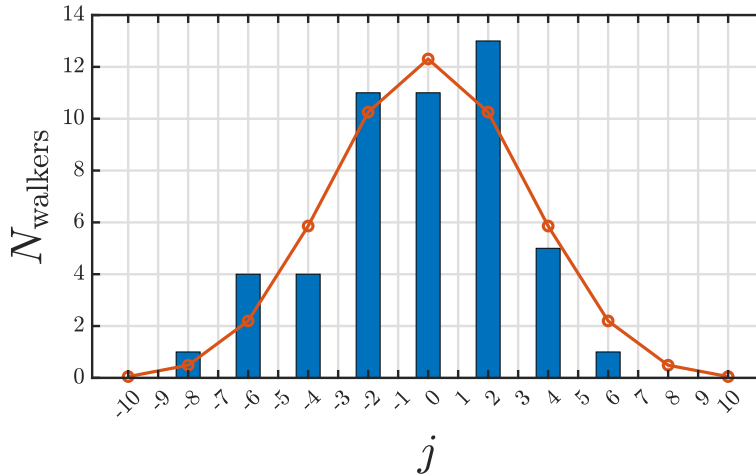


Figure 3.1: Number of walkers in each position of the integer number line after 10 steps. All walkers started in the position $j = 0$. The orange line represents the expected number of walkers at each position.

the zeros of the function removed for illustrative purposes. After many steps, the binomial distribution approaches a Gaussian distribution. The standard deviation of this binomial distribution is given by $\sigma_{\text{CRW}}(n) = \sqrt{\sum_j j^2 P_{n,j} - (\sum_j j P_{n,j})^2} = \sqrt{n}$, which is the typical standard deviation of diffusive processes.

The walker in the quantum random walk [86, 87, 88] on the line is represented by a two component spinor that contains two amplitudes, which, while in the initial condition might be localized in the central position, represents in general a superposition of the walker at different locations. The state of the walker, in addition to the spatial degree of freedom, is given by a two-dimensional internal degree of freedom, which is called the quantum coin. The Hilbert space of the spatial degree of freedom, \mathcal{H}_x , is of infinite dimension and is generated by the basis $\{|j\rangle; j \in \mathbb{Z}\}$. The Hilbert space

of the quantum coin, \mathcal{H}_C , is a 2-dimensional space generated by the basis $\{|\uparrow\rangle, |\downarrow\rangle\}$. The total Hilbert space is their tensor product $\mathcal{H} = \mathcal{H}_C \otimes \mathcal{H}_x$. The state of the walker in the defined basis at time $n \in \mathbb{Z}$ can be written as

$$|\psi_n\rangle = \sum_j (\psi_{n,j}^\uparrow |\uparrow\rangle + \psi_{n,j}^\downarrow |\downarrow\rangle) \otimes |j\rangle, \quad (3.2)$$

where $\psi_{n,j}^s$, with $s = \{\uparrow, \downarrow\}$, are the spinor components at step n and position j . We can project the state of the walker onto the spatial basis and represent the state of the walker as a spinor,

$$|\psi_{n,j}\rangle = \langle j|\psi_n\rangle = \begin{pmatrix} \psi_{n,j}^\uparrow \\ \psi_{n,j}^\downarrow \end{pmatrix}, \quad (3.3)$$

where we defined the canonical representation of the coin components as $|\uparrow\rangle = (1, 0)^T$ and $|\downarrow\rangle = (0, 1)^T$.

The one-step evolution of the quantum walker is composed of two operations: a quantum coin toss that mixes the walker coin components, followed by a conditional displacement operator that displaces the position of the walker depending on the internal degree of freedom. We can write this one-step operation as

$$|\psi_{n+1}\rangle = \hat{W} |\psi_n\rangle = \hat{S}(\hat{C} \otimes \mathbb{I}_x) |\psi_n\rangle, \quad (3.4)$$

where \hat{C} is a general unitary operation acting on the internal state of the walker and \hat{S} is the conditional shift operator defined as

$$\hat{S} = |\uparrow\rangle\langle\uparrow| \otimes \sum_j |j+1\rangle\langle j| + |\downarrow\rangle\langle\downarrow| \otimes \sum_j |j-1\rangle\langle j|. \quad (3.5)$$

The conditional shift operator transforms states of the form $|\uparrow\rangle|j\rangle$ to states $|\uparrow\rangle|j+1\rangle$ and states $|\downarrow\rangle|j\rangle$ to states $|\downarrow\rangle|j-1\rangle$, i.e., displaces states with the up (down) state to the right (left). The evolution from a given initial

condition $|\psi_0\rangle$ up to step $n = 1, 2, \dots$ is simply $|\psi_n\rangle = \hat{W}^n |\psi_0\rangle$. The walker does not have a definite position, only upon measurement of the position, the state of the walker collapses and its position becomes definite. The associated probability distribution of the walker at time n is given in terms of its state components as

$$P_{n,j} = \sum_{s=\uparrow\downarrow} |\langle s, j | \psi_n \rangle|^2 = |\psi_{n,j}^\uparrow|^2 + |\psi_{n,j}^\downarrow|^2. \quad (3.6)$$

If the probability of the quantum walker to move to the left and right are equal from an initially localized state, i.e., $P_{1,j+1} = P_{1,j-1}$, we say that the quantum coin is balanced. When the quantum walker position for a balanced coin is measured after each step, it reduces to the CRW. This procedure gives the quantum walker the same probability distribution as in the classical case. To illustrate this, let us consider the following balanced quantum coin operator

$$\hat{C} = e^{i\sigma_x\pi/4} = \frac{1}{\sqrt{2}} \begin{pmatrix} 1 & i \\ i & 1 \end{pmatrix}, \quad (3.7)$$

and a walker with initial coin state

$$|\psi_0\rangle = |\uparrow\rangle |0\rangle. \quad (3.8)$$

After the first step the state of the walker becomes

$$|\psi_1\rangle = \hat{S}(\hat{C} \otimes \mathbb{I}_x) |\psi_0\rangle = \hat{S} \frac{|\uparrow\rangle + i|\downarrow\rangle}{\sqrt{2}} |0\rangle = \frac{1}{\sqrt{2}} (|\uparrow\rangle |1\rangle + i|\downarrow\rangle |-1\rangle) \quad (3.9)$$

which, upon measurement, has a 50% chance of having moved one step to the left or to the right, and the walker state will either collapse to the state $|\uparrow\rangle |1\rangle$ or the state $|\downarrow\rangle |-1\rangle$, which after successive iterations of this process (unitary evolution and measurement) represents the same classical random walk.

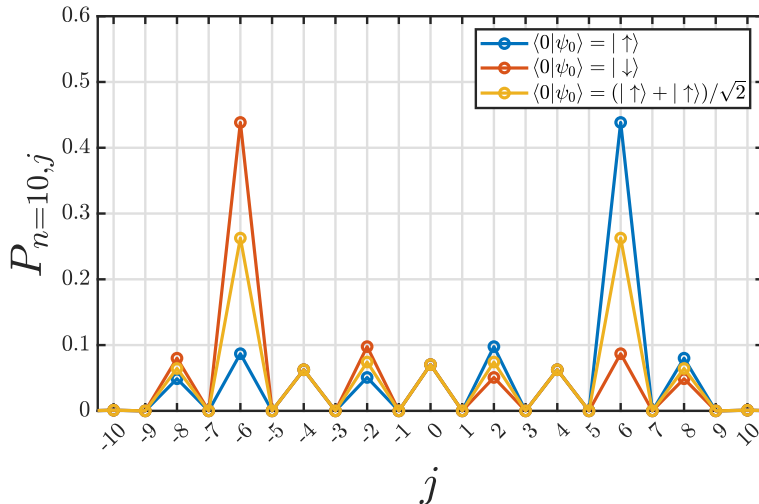


Figure 3.2: Probability distribution of the QW for different initial conditions (3.8) after $n = 10$ steps.

The power of the quantum walk lies in leaving it freely evolve (without intermediate measurements) through the unitary evolution (3.4). In Fig. 3.2 we represent the probability distribution (3.6) for different initially localized coin states of the form $|\psi_0\rangle = |s\rangle |0\rangle$, including the initial state (3.8), after 10 steps. We can see that, even though the QW is initially localized in the center, the final probability distribution depends on the initial state of the coin. In the left panel of Fig. 3.3 we show a contour plot of the probability density (3.6) of the initial coin state that produced the symmetric probability distribution of Fig. 3.2.

If we compare these probability distributions with the one for the CRW shown in Fig. 3.1 we can see that the highest probability of the QW is further away from the center than in the classical case. We can see in the left panel of Fig. 3.3 that the maximums of the probability density propagate

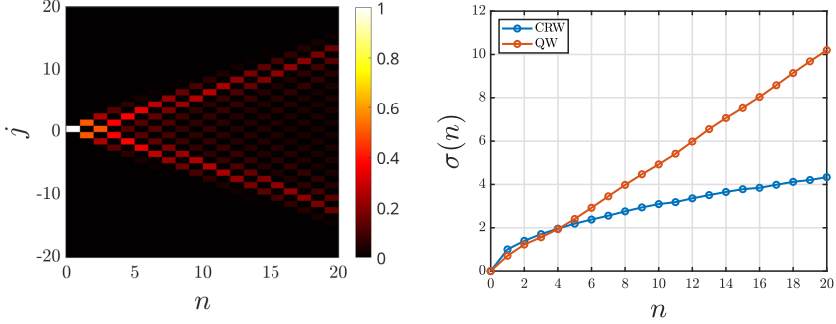


Figure 3.3: (Left) Probability distribution of the QW with initial coin state $|\psi_0\rangle = (|\uparrow\rangle + |\downarrow\rangle)/\sqrt{2}$ as a function of time. (Right) Standard deviation of the CRW and the QW as a function of time.

with constant velocity away from the center. The dispersion of the quantum walker is faster than that of the CRW and can be demonstrated [88] to be quadratically faster with time, i.e., $\sigma_{\text{QW}}(n) = \sqrt{\sum_j j^2 P_{n,j} - (\sum_j j P_{n,j})^2} \propto n$, which is the typical standard deviation of ballistic processes. The classical walker had a diffusive dispersion $\sigma_{\text{CRW}}(t) \propto \sqrt{n}$. In Fig. 3.3 we compare the standard deviation for the CRW and the QW with initial condition (3.8).

Quantum walks can also be extended to higher dimensions. A Hilbert space for an additional spatial coordinate can be similarly defined \mathcal{H}_y with basis $\{|l\rangle\}_{l \in \mathbb{Z}}$ so that the total Hilbert space $\mathcal{H} = \mathcal{H}_C \otimes \mathcal{H}_x \otimes \mathcal{H}_y$ is spanned by $\{|s\rangle |j, l\rangle\}$. The walker has components in both dimension $\psi_{n,j,l}^s$. The one-step evolution can be defined in different ways, for instance, the split-step QW [89] is given by

$$|\psi_{n+1}\rangle = \hat{S}_y(\hat{C}_y \otimes \mathbb{I}_x \otimes \mathbb{I}_y) \hat{S}_x(\hat{C}_x \otimes \mathbb{I}_x \otimes \mathbb{I}_y) |\psi_n\rangle, \quad (3.10)$$

where $\hat{S}_y = \sum_{j,l} |j, l+1\rangle \langle j, l| \otimes |\uparrow\rangle \langle \uparrow| + \sum_{j,l} |j, l-1\rangle \langle j, l| \otimes |\downarrow\rangle \langle \downarrow|$ is the conditional shift operator along the new dimension. There are two different

coin operators that act before applying the shift in each direction. B

3.3 QW in momentum space

To obtain the evolution of the QW one could simply compute the n -th power of the evolution operator \hat{W} , task that requires diagonalizing the \hat{W} operator if one wants to obtain a closed analytical form. The coin operator \hat{C} , which only acts on the coin space, is straightforward to diagonalize. The shift operator (3.5) is already diagonal in the coin basis, but it is not diagonal in the spatial basis, since we have terms of the form $|j \pm 1\rangle \langle j|$. To aid in this task, we consider the Fourier transform of the spatial basis. Since the spatial degree of freedom is discrete, the possible momenta are degenerate, so that its transformation is restricted to the first Brillouin zone and defined as

$$|k\rangle = \sum_{j \in \mathbb{Z}} |j\rangle e^{ikj}, \quad (3.11)$$

where $k \in [-\pi, \pi)$ is called the quasi-momentum. The inverse transformation is defined as

$$|j\rangle = \frac{1}{2\pi} \int_{-\pi}^{\pi} dk |k\rangle e^{-ikj}, \quad (3.12)$$

and the mathematical relations

$$\sum_j e^{i(k-k')j} = 2\pi\delta(k - k'), \quad \frac{1}{2\pi} \int_{-\pi}^{\pi} dk e^{ik(j-j')} = \delta_{jj'}, \quad (3.13)$$

guarantee the orthonormality condition of basis elements. The state of the walker can be expressed in both basis as

$$|\psi_n\rangle = \sum_{s=\uparrow,\downarrow} \sum_j \psi_{n,j}^s |s\rangle |j\rangle = \sum_{s=\uparrow,\downarrow} \frac{1}{2\pi} \int_{-\pi}^{\pi} dk \tilde{\psi}_n^s(k) |s\rangle |k\rangle, \quad (3.14)$$

so that the spinor components in both bases are related as

$$\tilde{\psi}_n^s(k) = \sum_{j \in \mathbb{Z}} e^{-ikj} \psi_{n,j}^s, \quad (3.15)$$

or with the inverse relation as

$$\psi_{n,j}^s = \frac{1}{2\pi} \int_{-\pi}^{\pi} dk \tilde{\psi}_n^s(k) e^{ikj}. \quad (3.16)$$

We can define the quasi-momentum operator

$$\hat{K} = \frac{1}{2\pi} \int_{-\pi}^{\pi} dk k |k\rangle \langle k|, \quad (3.17)$$

whose action on the quasi-momentum basis is $\hat{K} |k\rangle = k |k\rangle$. We define the translation operator

$$\begin{aligned} \hat{T} = e^{-i\hat{K}} &= \frac{1}{2\pi} \int_{-\pi}^{\pi} dk e^{-ik} |k\rangle \langle k| \\ &= \frac{1}{2\pi} \int_{-\pi}^{\pi} dk e^{-ik} \sum_{j,j'} |j'\rangle \langle j| e^{ik(j'-j)} = \sum_j |j+1\rangle \langle j|, \end{aligned} \quad (3.18)$$

where in the last step we made use of the relation (3.13). The operator T translates spatial basis elements one position to the right $\hat{T} |j\rangle = |j+1\rangle$, and its adjoint $\hat{T}^\dagger = e^{i\hat{K}}$, displaces them to the left $\hat{T}^\dagger |j\rangle = |j-1\rangle$. The operator \hat{K} is the generator of translations in the discrete lattice. The condition shift operator can be rewritten as

$$\hat{S} = e^{-i\sigma_z \hat{K}}, \quad (3.19)$$

which is diagonal in the quasi-momentum basis.

The evolution of the walker up to step n can be easily computed in the momentum basis (in which \hat{S} is already diagonal) through the diagonalization

of \hat{W} . To obtain the solution in the position basis, the inverse Fourier transform of the spinor components has to be performed. See [88, 86] for examples where the analytical solution of the walker components at an arbitrary step are obtained.

3.4 The continuum limit of the discrete time Quantum Walk

One can associate a physical space to the space spanned by the discrete lattice of the QW. A lattice spacing ϵ_x can be introduced to connect both spaces as $|x\rangle = |\epsilon_x j\rangle$ where $|x\rangle$ is the basis of a position Hilbert space that is discretized, by a spacing ϵ_x . A similar procedure can be done for the temporal coordinate $t = \epsilon_t n$ with a spacing ϵ_t . The shift operator produces a conditional shift in the discretized physical space by an amount ϵ_x , such that, $e^{-i\hat{K}} |x\rangle = |x + \epsilon_x\rangle$. We can relate the quasi-momentum with the physical momentum, in the limit of small ϵ_x , as $\hat{K} = \epsilon_x \hat{p}$.

Let us consider a coin operator of the form $C(\theta) = e^{i\theta\sigma_x}$. We can now write the time step in physical units as

$$|\psi_{t+\epsilon_t}\rangle = e^{-i\sigma_z\epsilon_x\hat{p}} e^{i\theta\sigma_x} |\psi_t\rangle . \quad (3.20)$$

If we let the angle of rotation to have a small variation with respect to a fixed angle $\theta = \theta_0 + \epsilon_m \bar{\theta}$, we can write a series expansion in the small parameters of this time step as

$$|\psi_t\rangle + \epsilon_t \partial_t |\psi_t\rangle = (1 - i\epsilon_x \sigma_z \hat{p})(1 + i\epsilon_m \bar{\theta} \sigma_x) e^{i\theta_0 \sigma_x} |\psi_t\rangle , \quad (3.21)$$

where we employed the infinitesimal definition of the time derivative

$$\partial_t |\psi_t\rangle \approx \frac{|\psi_{t+\epsilon_t}\rangle - |\psi_t\rangle}{\epsilon_t} , \quad (3.22)$$

and the series expansion of the exponential up to first order in the small parameters ϵ_x and ϵ_m . To obtain a consistent continuum limit of this equation, it is required that $\epsilon_x = \epsilon_t = \epsilon_m = \epsilon$. We assume that the walker components coincide with continuous functions of position $x = \epsilon j$ and time $t = \epsilon n$, that is, $\psi_{n,j}^s \rightarrow \Psi^s(t, x)$, which are the components of a state in continuous space-time

$$|\Psi(t)\rangle = \int dx \Psi^\uparrow(t, x) |x\rangle |\uparrow\rangle + \int dx \Psi^\downarrow(t, x) |x\rangle |\downarrow\rangle . \quad (3.23)$$

Taking Eq. (3.21) up to zeroth order in ϵ yields

$$|\Psi(t)\rangle = e^{i\theta_0 \sigma_x} |\Psi(t)\rangle , \quad (3.24)$$

which, in order to be satisfied, requires $\theta_0 = 0$. Up to first order in ϵ , $O(\epsilon)$, equation (3.21) satisfies

$$\partial_t |\Psi(t)\rangle = -i\sigma_z \hat{p} |\Psi(t)\rangle + i\bar{\theta} \sigma_x |\Psi(t)\rangle . \quad (3.25)$$

We can project this equation to the position basis and, recalling that $\langle x | \hat{p} | \Psi(t) \rangle = -i\partial_x \langle x | \Psi(t) \rangle = -i\partial_x \Psi(t, x)$, it can be rewritten as

$$(i\gamma^\mu \partial_\mu - m)\Psi(t, x) = 0 , \quad (3.26)$$

with $\mu = t, x$, where $\gamma^t = \sigma_x$, $\gamma^x = -i\sigma_y$ and $m = -\bar{\theta}$. Equation (3.26) is the Dirac equation of continuous space-time. This means that, if the quantum walk parameters are taken such that ϵ is small, one can recover the probability distribution of a relativistic fermionic particle in one dimension.

In Fig. 3.4 we plot a comparison obtained from the continuous Dirac equation (3.26) and the quantum walk defined in Eq. (3.20) with the parameter correspondence $\bar{\theta} = -\epsilon m$, and the scaled coordinates $t = \epsilon n$ and $x = \epsilon j$. The initial condition used in the Dirac equation was

$$\Psi^\uparrow(x, 0) = \left(\frac{2}{\pi}\right)^{1/4} e^{-x^2} , \quad \Psi^\downarrow(x, 0) = 0 , \quad (3.27)$$

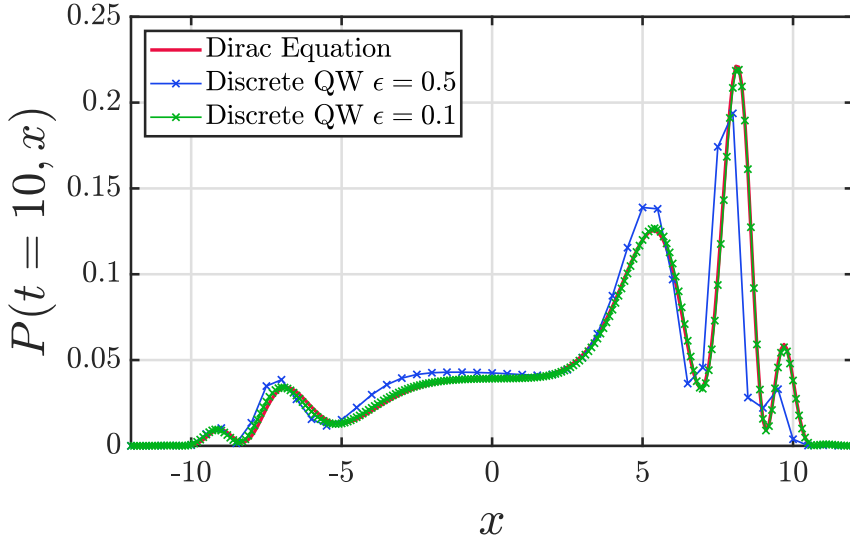


Figure 3.4: Comparison of the solution obtained from the Dirac equation and a discrete QW for different values of the parameter ϵ . The initial conditions are defined in Eqs. (3.28,3.29), and we have chosen a mass $m = 1$.

which corresponds to an initial condition of the walker

$$\psi_{0,j}^{\uparrow} = N e^{-(\epsilon j)^2}, \quad \psi_{0,j}^{\downarrow} = 0, \quad (3.28)$$

where N is a normalization factor that has to be chosen such that the normalization in the $x = \epsilon j$ coordinate is the same for both initial conditions, i.e.,

$$\epsilon \sum_j \left(|\psi_{0,j}^{\uparrow}|^2 + |\psi_{0,j}^{\downarrow}|^2 \right) = 1. \quad (3.29)$$

It can be seen that, as the parameter ϵ decreases, the quantum walk probability distribution approaches that of the spinor obtained from the continuous Dirac equation.

While we considered a coin operator of the form $C(\theta) = e^{i\theta\sigma_x}$, other choices can lead to the same continuum limit with a different representation of the gamma matrices γ^μ .

Quantum Walk Hamiltonian

One can formally define a Hermitian operator \hat{H} that generates the unitary time step of the QW as

$$\hat{W} = e^{-i\hat{H}} . \quad (3.30)$$

Let us consider that in a small time step this operator is also small, i.e., $\hat{H} = \epsilon\bar{H}$, so that the infinitesimal time step is

$$|\psi_{t+\epsilon}\rangle = e^{-i\epsilon\bar{H}} |\psi_t\rangle , \quad (3.31)$$

which can be expanded up to first order, following the same procedure as before, as

$$|\Psi(t)\rangle + \epsilon\partial_t |\Psi(t)\rangle = (\mathbb{I} - i\epsilon\bar{H}) |\Psi(t)\rangle . \quad (3.32)$$

At first order in ϵ the state obeys a Hamiltonian equation

$$i\partial_t |\Psi(t)\rangle = \bar{H} |\Psi(t)\rangle , \quad (3.33)$$

where, for the previous continuum limit, \bar{H} coincides with the Dirac Hamiltonian

$$\bar{H} = -\gamma^t\gamma^x\hat{p} + m , \quad (3.34)$$

where we recall that $m = -\bar{\theta}$. This definition will be useful when considering the continuum limit in [P.3].

3.5 Inhomogeneous coin operator

Up until now, we assumed that the coin operator is independent of the step and position of the walker. More general coin operators with both spatial

and temporal dependence can be considered, and whose continuum limits lead to a diverse phenomenology. Let us consider, as a simple example, a modification of the coin considered in the previous section

$$C(\theta, \alpha_j) = e^{i\theta\sigma_x} e^{i\alpha_j} , \quad (3.35)$$

where we allow the parameter α_j to have a dependence on the position of the walker. We can perform a similar parametrization of $\alpha_j = \epsilon\bar{\alpha}_j$ as before, where ϵ is the same small parameter as before. The new QW one step is approximated as

$$|\psi_t\rangle + \epsilon_t \partial_t |\psi_t\rangle = (1 - i\epsilon_x \sigma_z \hat{p})(1 + i\epsilon_m \bar{\theta} \sigma_x)(1 + i\epsilon\bar{\alpha}_j) |\psi_t\rangle , \quad (3.36)$$

which, when projected into the spatial basis, leads to the continuum limit

$$(i\gamma^\mu D_\mu - m)\Psi(t, x) = 0 , \quad (3.37)$$

where $D_\mu = \partial_\mu - iA_\mu$ is the covariant derivative. The function A_μ is the electromagnetic potential with components $A_t = \bar{\alpha}(x)$ of the associated continuous function of $\bar{\alpha}_j$, and $A_x = 0$. This electromagnetic potential is associated with an electric field $E = \partial_x \bar{\alpha}(x)$. If one considers a global phase with a linear dependence in the position, $\alpha_j = \epsilon\phi j$, the quantum walk with coin operator (3.35) can be used to simulate a Dirac equation with constant electric field $E = \phi$. An equivalent quantum walk has been studied in [90] where long time properties were explored. In [91] the same walker was observed to undergo Bloch oscillations under weak electric fields. Similarly, the coin can be modified to obtain a continuum limit of the Dirac equation with magnetic fields, for instance, it was shown in [92] the existence of Landau level of the discrete QW in the presence of a constant magnetic field. See [93, 94] for the obtention of the continuum limit of general gauge theories of 2D QWs and numerical demonstrations of the electromagnetic phenomena of Bloch oscillations and $\vec{E} \times \vec{B}$ drift. A modification of the

coin operator was also studied in [95, 96] to obtain, in the continuum limit, a Dirac equation in curved space-times, where a Schwarzschild space-time was simulated by a quantum walk. In [97] the method was extended to two-dimensional quantum walks, which allowed the study of a fermion under the metric induced by gravitational waves. A continuum limit that matched the Dirac equation in curved space-time was also obtained in [98] where the QW was instead constructed in a triangular and in a hexagonal lattice.

3.6 QW simulation of warped geometry in high energy theories (Publication [P.2])

The existence of a continuum limit of different quantum walks that match Dirac like equations allowed the simulation of a plethora of physical systems. Apart from the simulation of fermions in curved space-times and electromagnetic fields, described in the previous section, quantum walks can be constructed to simulate neutrino oscillations [99], charged fluid dynamics [100], topological phenomena [101] or relativistic diffusion [P.3], to name a few examples. In [P.2] we investigate the properties of a quantum walk that, in the continuum limit, simulates the Randall-Sundrum (RS) model of extra dimensions [102]. The RS model was introduced to explain the hierarchy problem of high energy physics (HEP) theories, by the addition of an extra warped dimension, which had a 4-dimensional brane in each end. Gravity is present along the whole space-time, but the matter fields of the Standard Model of particles become confined in one of the branes, the matter brane. We define a 2-dimensional QW with one warped spatial dimension and an ordinary spatial dimension. We derive the Dirac equation that arises in this reduced curved space-time and establish the boundary conditions that the fermionic fields have to obey. The symmetry conditions on this lower dimension space-time restricted the study to massless fermions,

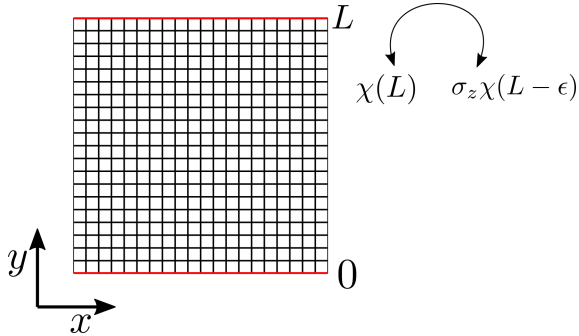


Figure 3.5: Spatial lattice of the 2D QW of the RS model. The lattice is infinite along the x direction, but is finite in the y direction, of length L .

which may acquire an effective mass when restricted to the matter brane. We also study the spectrum of the solutions of the continuum model, where one can already see that the eigenfunctions of the Dirac equation present confinement towards the matter brane.

We constructed a quantum walk that, in the continuum limit, recovers the derived Dirac equation following the method introduced in [97]. The grid created for the quantum walk is represented in Fig. 3.5. The ordinary spatial dimension is infinite, and a sufficiently large lattice is taken in that direction so that the walker does not reach the lattice ends. The warped dimension is finite, and appropriate boundary conditions are set at the extremes, where the walker is reflected with a phase flip. This is the same boundary condition that the Dirac fermions have to obey in the continuum model. The construction of the QW was consistent with this condition at all times.

Firstly, we observed that the QW model reproduces the phenomenology expected from the RS model, that is, a walker initially localized in the center of the warped dimension will become localized in the extreme of the warped

dimension where matter fields are confined. The confining property of the model is controlled by the warp coefficient, and we confirmed that, when this parameter is increased, the localization of the walker towards the matter brane is stronger. Since we were restricted to massless fermions, most part of the probability density of the walker propagates at the speed of light, and the direction of propagation is chirality dependent, that is, the upper (lower) components propagates to the right (left) in the ordinary dimension. These fronts are located at position $x = t$ and we defined the probability distribution along the y direction as the freely propagating distribution (FPD). We performed a decomposition of the walker components in terms of the eigenfunctions obtained from the continuum Dirac equation and studied the mode composition of the FPDs. We observed that, while initially the FPD can be composed of high energy modes, in the long time limit the FPD is mostly composed by the lowest energy mode. This effect is indicative of some type of dissipation during the propagation to the regions inside the light cone. Finally, we investigated the entanglement entropy between the coin and the spatial degree of freedom. The QW step generates entanglement between these degrees of freedom and becomes smaller for higher values of the warp coefficient. We attributed this effect to the lower dispersion of the walker probability distribution with increasing warp coefficient.

While QWs have proven successful at reproducing some effects of HEP theories, they lack the power to simulate multiple particle interactions. However, the formalism can be modified to include particle interactions. There have been some efforts [103, 104] to describe two and three particle states, but more work has to be done to have a simulation framework for HEP. We also mention that quantum walks are not free of defects present in lattice theories, such as the fermion doubling problem. Quantum cellular automata [18, 105, 106] is a lattice theory similar to QWs, where in each location the quantum system can be of any finite dimension. The evolution

is also discrete in time and have been shown to simulate simple quantum field theory models, for instance, the Schwinger model [107].

3.7 Relativistic diffusion as the continuum limit of a stochastic QW (Publication [P.3])

In the previous section, we studied a QW that had a spatial inhomogeneous coin. In [P.3] we study a coin that is inhomogeneous in time, and where the temporal dependence is stochastic, this type of evolution can be viewed as a type of temporal noise on the coin operator. We studied two ways to generate a temporal stochastic coin, but here we briefly explain the one that closely connects with the first part of the thesis. We can define a noise process on a walker in the operator sum representation as

$$\rho_{n+1} = (1 - p_1 - p_2)\hat{W}\rho_n\hat{W}^\dagger + p_1\sigma_z\rho_n\sigma_z + p_2\sigma_x\rho_n\sigma_x, \quad (3.38)$$

where ρ_n is the density matrix at time step n , p_1 is the probability that the walker suffers a phase flip error, p_2 is the probability to suffer a bit flip error, and with probability $1 - p_1 - p_2$ it undergoes the usual unitary evolution of the QW. We can define $p_i = \epsilon\gamma_i$, where ϵ is the same as the infinitesimal time step, and follow in a similar fashion as in Section 1.3 to obtain a continuous ME

$$\partial_t\rho = -i[\overline{H}, \rho] + \gamma_1(\sigma_z\rho\sigma_z - \rho) + \gamma_2(\sigma_x\rho\sigma_x - \rho), \quad (3.39)$$

where \overline{H} is the infinitesimal generator of the unitary dynamics of the QW $\hat{W} = e^{-i\epsilon\overline{H}}$, and coincides with the Hamiltonian obtained in the continuum limit from the unitary evolution of the QW, which is in general the Dirac Hamiltonian. The other way to construct a stochastic QW that leads to the same continuum limit, consists on applying a unitary composed of a general $SU(2)$ coin operator and the conditional shift operator (3.5). The coin

operator can be parametrized with 4 constant parameters that are randomly sampled from independent probability distributions. The correspondence between this implementation and the previous one is obtained if the standard deviations of these parameters coincide with the rates γ_i .

This continuous equation represents a model of quantum relativistic diffusion. We represent the density matrix of the spinor in the Pauli basis, and the dynamical equation becomes a system of four partial differential equations that are numerically solved using an operator splitting method. This method allowed us to study the phenomenology of the continuous model, which can be summarized into two regimes: A ballistic propagation regime, in which the initial wave-packet propagates at a constant velocity, and after some time, which depends on the strength of the noise, transitions into a diffusive regime. This latter regime is characterized by a constant expected value of the position and by an increase of the standard deviation proportional to \sqrt{t} , characteristic of diffusive processes. Finally, a model that also adds spatial noise on top of the temporal noise is studied, and similar Lindbladian dynamics are obtained in the continuum limit.

3.8 Non-linear coin operator and solitons (Publication [P.4])

Another variant of the coin operator that introduces non-linearities on the phases of the coin components was introduced in [108]. The phases were dependent on the probability density of the walker at each position. The model was inspired by the non-linear optical Galton board, where the non-linearities were caused by a non-linear Kerr medium. The main result of the work was the formation of soliton-like structures, that is, the walker probability distribution was extended and stable. In the language of

optical systems, the non-linear effects of the medium counteract the natural dispersion of the light.

In [P.4] we consider a similar model, together with an experimental proposal, where the non-linearities are introduced in the angle of the coin operator, that is, the angle of rotation at each position of the walker depends on the probability density at that position. The continuum limit of this quantum walk gives a non-linear Dirac equation where there is a non-linear term similar to the one appearing in the Nambu-Jona-Lasinio model [109]. We do an in-depth study of the continuum limit equation. First, we explore the stability of homogeneous stationary solutions and identify the regimes in which soliton-like solutions can appear. Secondly we find, under reasonable assumptions, a stationary solution of the continuous model that has the usual characteristics of a soliton.

The insight obtained from the continuum equation is checked in the discrete model numerically. We find the existence of soliton-like structures with the same solution as the continuum equation. We also investigate initial conditions that propagate at a constant speed and observe a typical characteristic of solitons, which is that during a collision the solitary wave-packets are not disturbed. The stability analysis of the continuum equation indicated that other type of stationary solutions should exist, the dark solitons, which were observed in the discrete model. A dark soliton is generated in the domain wall between two stable solutions, where the probability of finding the walker vanishes in the transition. This valley of probability density is found to be stationary.

We have also studied the stability of solitons when they are subject to an additional phase that simulates an external electric field. For electric field intensities that are irrational the solitons remained localized but their smooth characterized structure is lost. For rational fractions of 2π electric

field intensities we characterized two regimes: For strong electric fields, an initial soliton becomes slowly disrupted and the walker disperses and an increase of the non-linearity parameter slows down the dispersion produced by the strong electric field. For weak electric fields, oscillations of the soliton central position are present. Finally, we also explored a 2D version of these model, where no evidence of soliton formation was found.

Appendices

A.1 Derivation ME dissipative noise model

To obtain a master equation for the evolution of the qubit described in Eq. (2.4) we can employ the Redfield ME [73] for interaction Hamiltonians of the form $H_I = L \otimes B^\dagger + L^\dagger \otimes B$ as

$$\frac{d\rho_S(t)}{dt} = -i[H_S, \rho_S(t)] + \left(\int_0^t d\tau \alpha^+(\tau) [L^\dagger(-\tau)\rho_S(t), L] + \int_0^t d\tau \alpha^-(\tau) [L(-\tau)\rho_S(t), L^\dagger] + h.c. \right), \quad (\text{A.1})$$

where $L(t) = e^{iH_S t} L e^{-iH_S t}$ which in our case $H_S = \omega_0 \sigma_z / 2$ and $L(t) = e^{i\omega_0 t} \sigma_+$. The correlation functions are $\alpha^+(\tau) = \text{Tr}_E \{ B^\dagger(\tau) B \rho_E \}$ and $\alpha^-(\tau) = \text{Tr}_E \{ B(\tau) B^\dagger \rho_E \}$, which for a general bosonic or fermionic reservoir [2, 73] become

$$\alpha^+(\tau) = \int d\omega J(\omega) n(\omega, \beta) e^{i\omega\tau}, \quad (\text{A.2})$$

$$\alpha^-(\tau) = \int d\omega J(\omega) (n(\omega, \beta) + 1) e^{-i\omega\tau}, \quad (\text{A.3})$$

$$(\text{A.4})$$

where $J(\omega)$ is the spectral density of the reservoir, and $n(\omega, \beta) = [e^{\beta\omega} \mp 1]^{-1}$ is the average number of quanta of the bosonic (fermionic) reservoir modes at an inverse temperature β . We can define $\gamma = J(\omega_0)$ and the rates

$$\gamma^+ = \int_0^\infty d\tau \alpha^+(\tau) e^{-i\omega_0\tau} = \gamma n(\omega_0, \beta) + i\Delta^+, \quad (\text{A.5})$$

$$\gamma^- = \int_0^\infty d\tau \alpha^-(\tau) e^{i\omega_0\tau} = \gamma (n(\omega_0, \beta) + 1) + i\Delta^-, \quad (\text{A.6})$$

where we made use of the property

$$\int_0^\infty e^{i\omega t} dt = \pi\delta(\omega) + i\mathcal{P}\left(\frac{1}{\omega}\right). \quad (\text{A.7})$$

We can rewrite the ME as

$$\begin{aligned} \frac{d\rho_S(t)}{dt} = & -i[H_S, \rho_S(t)] + \gamma_+(\sigma_+\rho_S(t)\sigma_- - \sigma_-\sigma_+\rho_S(t)) \\ & + \gamma_+^*(\sigma_+\rho_S(t)\sigma_- - \rho_S(t)\sigma_-\sigma_+) \\ & + \gamma_-(\sigma_-\rho_S(t)\sigma_+ - \sigma_+\sigma_-\rho_S(t)) \\ & + \gamma_-^*(\sigma_+\rho_S(t)\sigma_+ - \rho_S(t)\sigma_+\sigma_-) \end{aligned} \quad (\text{A.8})$$

this equation can be brought into the canonical Lindblad form in Eq. (2.6) without the need of a secular approximation. This is true since the interaction operators σ_+ and σ_- connect the eigenstates of H_S , i.e., in their spectral decomposition they only have one component of frequency ω_0 . This fact implies that the Bloch-Redfield equation of this system does not have oscillatory terms (which are the ones discarded in the secular approximation). The system Hamiltonian gets modified as

$$H'_S = H_S + \Delta^+\sigma_-\sigma_+ + \Delta^-\sigma_+\sigma_-, \quad (\text{A.9})$$

where the operators $\sigma_-\sigma_+$ and $\sigma_+\sigma_-$ are equivalent to σ_z and only produce a change in the frequency of the system and the ground state energy.

A.2 Derivation ME pure dephasing noise model

The Hamiltonian model described in Eq. (2.12) can be solved employing the Redfield Eq. (1.64). This case is very simple since the interaction operators commuted with the Hamiltonian of the systems so that $\sigma_z(t) = e^{iH_S t} \sigma_z e^{-iH_S t} = \sigma_z$. The Redfield equation can simply be operated to obtain

$$\frac{d\rho_S(t)}{dt} = -i[H_S, \rho_S(t)] + \Gamma(\sigma_z \rho_S(t) \sigma_z - \rho_S(t)) , \quad (\text{A.10})$$

where we defined

$$\int_0^t d\tau C(\tau) = \int_0^\tau \text{Tr}_E \{B(t)B\rho_E\} = \Gamma/2 + i\Delta . \quad (\text{A.11})$$

The real part of this quantity give the decay rate and the imaginary part gets cancelled by the hermitian conjugate part of the Redfield equation.

Resum en valencià

Prefaci

Em vaig sorprendre per primera vegada amb la mecànica quàntica quan vaig entendre¹ el teorema de Bell i el paper que té l'entrellaçament en la teoria. Des d'aquell moment, vaig quedar fascinat per la teoria i per totes les preguntes fonamentals que queden obertes, no sols des del punt de vista científic, sinó també filosòfic.

Aquesta fascinació per la mecànica quàntica em va incitar a buscar un projecte de tesi de màster relacionat amb aquest camp. Així vaig trobar els meus tutors de tesi i vaig dur a terme el meu primer treball científic en el camp dels sistemes quàntics oberts. Durant el període predoctoral, gràcies a la col·laboració amb un investigador postdoctoral, vaig adintrar-me en el camp dels caminants quàntics. Aquests dos camps han compostat els principals continguts de la meua tesi, que s'ha dividit en dues parts dedicades a cadascun d'aquests temes.

Per altra banda, durant l'etapa predoctoral, he tingut l'oportunitat de donar classes en el grau de física. He estat professor de les assignatures de

¹"If quantum mechanics hasn't profoundly shocked you, you haven't understood it yet." Niels Bohr.

física quàntica, fet que m'ha permès revisitar els conceptes més bàsics de la mecànica quàntica i plantejar-me noves qüestions que durant el grau no havia considerat. Finalment, també he tingut l'oportunitat d'estudiar per compte propi qüestions més filosòfiques, com ara les interpretacions de la mecànica quàntica, la història del debat Einstein-Bohr sobre la completitud de la teoria i els models ontològics sobre la realitat de l'estat quàntic. Aquestes exploracions han donat lloc a discussions molt interessants.

Part I: Sistemes quàntics oberts

Introducció

La Mecànica Quàntica (MQ) és la teoria més fonamental de la naturalesa que coneixem actualment. Des de la seua concepció en la dècada de 1920, ha demostrat ser una teoria d'èxit a diferents nivells de complexitat, des de descriure correctament els nivells d'energia de l'àtom d'hidrogen fins a predir l'existència de les partícules elementals que constitueixen els blocs constructors de la matèria. Tot i que la teoria ha demostrat ser exitosa, quan hi ha un nivell de complexitat cada vegada més alt, cal emprar mètodes aproximats o perturbatius.

Els sistemes quàntics gairebé mai estan completament aïllats, ens referim a ells com a sistemes oberts, i s'han de considerar en interacció amb un entorn circumdant, que probablement afectarà la dinàmica del sistema obert. El nombre de graus de llibertat de l'entorn és generalment molt més alt que els del sistema obert. Podríem recórrer a mètodes exactes per resoldre l'evolució de tot el sistema aïllat, format pel sistema obert i el seu entorn. En la pràctica, aquesta tasca ràpidament esdevé inviable.

La teoria dels sistemes quàntics oberts (SQO) ha desenvolupat les eines per descriure el sistema obert sense la necessitat de donar una descripció

exacta dels graus de llibertat ambientals. L'ús de la teoria dels sistemes quàntics oberts ha tingut èxit en el camp de l'òptica quàntica, on, per exemple, una cavitat amb pèrdues pot modificar les taxes de les transicions i modificar l'estat estacionari del sistema. La teoria dels SQO ha experimentat un augment de popularitat gràcies a la seua aplicabilitat en escenaris tecnològics quàntics, on els fenòmens de decoherència i dissipació estan ben capturats pel formalisme, i constitueix un banc de proves per a l'estudi de tècniques de mitigació i control.

Evolució i equacions mestres

Considerem la situació general en què el sistema obert S està acoblat a un entorn E . L'espai de Hilbert total és el producte tensorial de l'espai de Hilbert de cada subsistema $\mathcal{H} = \mathcal{H}_S \otimes \mathcal{H}_E$. El sistema complet es descriu pels hamiltonians lliures de cada subsistema, H_S per al sistema obert i H_E per a l'entorn, més el hamiltonià d'interacció H_I entre ambdós. L'evolució tant del sistema com de l'entorn ve donada pel hamiltonià total $H = H_S + H_E + H_I$, de manera que l'estat de tot el sistema en el temps t és

$$|\psi(t)\rangle = e^{-iH(t-t_0)} |\psi(t_0)\rangle , \quad (\text{R.1})$$

on $|\psi(t_0)\rangle$ és l'estat inicial del sistema compost i definim $U(t, t_0) = \exp[-iH(t-t_0)]$, l'operador d'evolució unitària. Aquesta evolució unitària ve donada per l'equació de Schrödinger²

$$i \frac{d}{dt} |\psi(t)\rangle = H |\psi(t)\rangle . \quad (\text{R.2})$$

Finalment, el sistema obert es descriu completament traient la tràcia parcial respecte a l'entorn de l'estat final

$$\rho_S(t) = \text{Tr}_E \{ \rho_{SE}(t) \} = \text{Tr}_E \left\{ U(t, t_0) \rho_{SE}(t_0) U^\dagger(t, t_0) \right\} , \quad (\text{R.3})$$

²En unitats naturals on $\hbar = 1$.

$$\begin{array}{ccc}
 \rho_{SE}(t_0) & \xrightarrow{\text{unitary evolution}} & \rho(t) = U(t, t_0)\rho_{SE}(t_0)U^\dagger(t, t_0) \\
 \text{Tr}_E \downarrow & & \downarrow \text{Tr}_E \\
 \rho_S(t_0) & \xrightarrow{\text{dynamical map}} & \rho_S(t) = \phi_{(t, t_0)}[\rho_S(t_0)]
 \end{array}$$

Figure R.1: Diagrama que mostra l'acció del mapa dinàmic $\phi(t)$. És possible evolucionar tot el sistema i traçar l'entorn per obtenir la dinàmica del SQO, o alternativament, l'evolució del SQO pot ser descrita pel mapa dinàmic.

on $\rho_{SE}(t_0) = |\psi(t_0)\rangle\langle\psi(t_0)|$.

En la pràctica, aquest procediment, descrit pel camí superior dret de la Fig. R.1, no és factible i cal recórrer a una representació de l'evolució reduïda a S . L'objecte matemàtic $\phi_{(t, t_0)}$ que descriu l'evolució de l'estat inicial del sistema obert S fins al temps t s'anomena mapa dinàmic i codifica l'efecte de l'entorn sobre el sistema obert, un procediment que es descriu pel camí inferior esquerra del diagrama de la Fig. R.1.

En general, quan l'evolució del sistema obert està donada per un mapa dinàmic, la seua dinàmica esdevé irreversible, amb l'excepció del mapa dinàmic que representa una dinàmica unitària. Aquest fenomen està estretament relacionat amb la generació d'entrellaçament entre el sistema i l'entorn al llarg de l'evolució. Quan dos sistemes s'entrellacen, la informació ja no està continguda en els sistemes individuals, sinó codificada en l'estat global del sistema compost. L'obtenció de la traça parcial de l'entorn equival a realitzar una mitjana sobre els graus de llibertat de l'entorn. Aleshores, la matriu de densitat reduïda dona una mescla probabilística clàssica d'estats quàntics compatibles del sistema, ja que l'estat quàntic real només es descriu correctament globalment. Si l'entrellaçament entre el

sistema i l'entorn és màxim, la matriu de densitat reduïda del sistema esdevé l'estat màximament mesclat, i no es pot extreure informació sobre el sistema o l'entorn simplement mesurant el sistema. Aquesta situació es compren més fàcilment seguint el camí superior dret de la Fig. R.1: la dinàmica unitària entrellaça el sistema amb l'entorn, i quan s'aplica la traça parcial sobre un d'ells, l'estat resultant només conserva part de la informació. És possible que existeixi un mapa invers d'aquesta evolució $\phi^{-1}(t, t_0)$, tal que $\phi^{-1}(t, t_0)[\phi_{(t,t_0)}[\rho]] = \phi_{(t,t_0)}[\phi_{(t,t_0)}^{-1}[\rho]] = \rho$, però en general no serà un mapa dinàmic que preserve les propietats dels estats quàntics.

El mapa dinàmic pot ser matemàticament representat de diferents formes. Una d'elles és mitjançant operadors de Kraus

$$\rho_S(t) = \sum_{\mu} K_{\mu}(t, 0) \rho_S(0) K_{\mu}^{\dagger}(t, 0) , \quad (\text{R.4})$$

on cada operador K_{μ} representa un canal de decaïment del sistema obert. Aquesta representació, junt amb la seua condició de normalització, preserva la traça (probabilitats) del estat quàntic, és lineal i preserva la positivitats dels operadors. Aquestes son propietat necessàries per a que els mapes dinàmics evolucionen estats quàntics a altres estats quàntics, i no resulten en matrius densitats que no representen estats quàntics. Una altra forma de representar el mapa dinàmic és mitjançant una equació diferencial per a la matriu reduïda del sistema. Si la dinàmica del sistema es Markoviana, es a dir, es pot representar com una cadena de Markov de mapes dinàmics, l'equació diferencial que descriu l'evolució es pot escriure com

$$\frac{d}{dt} \rho(t) = -i[H, \rho(t)] + \sum_k \gamma_k \left(L_k \rho(t) L_k^{\dagger} - \frac{1}{2} \{L_k^{\dagger} L_k, \rho(t)\} \right) , \quad (\text{R.5})$$

on γ_k son constants positives, H es un operador hermític i L_k són els anomenats operadors de Lindblad.

Si la interacció entre sistema i ambient es feble es pot derivar un equació diferencial pertorbativa en la intensitat de l'acoblament. Per a obtindre una equació diferencial tancada per a la matriu reduïda del sistema cal considerar l'aproximació de Born, que consisteix en assumir que, com la interacció entre sistema i ambient es tant feble, el sistema i ambient estan en un estat separable durant l'evolució. Una segona aproximació usualment considerada és l'aproximació Markoviana, que assumeix que la relaxació del ambient és molt més ràpida que la dinàmica de relaxació del sistema. L'equació diferencial que descriu la dinàmica del sistema baix aquestes suposicions és

$$\frac{d\rho_S(t)}{dt} = -i[H_S, \rho_S(t)] - \sum_{\mu} [S_{\mu}, \Lambda_{\mu} \rho_S(t) - \rho_S(t) \Lambda_{\mu}^{\dagger}] , \quad (\text{R.6})$$

on S_{μ} són els operadors d'interacció del sistema i

$$\Lambda_{\mu} = \sum_{\nu} \int_0^{\infty} d\tau C_{\mu,\nu}(\tau) S_{\nu}(-\tau) , \quad (\text{R.7})$$

on $C_{\mu,\nu}(\tau)$ són les funcions de correlació del ambient. Aquesta equació diferencial és clau per a l'estudi de l'evolució dels sistemes quàntics oberts considerats en la publicació [P.1] i en el Capítol 2 de la tesi.

Ambients fora de l'equilibri i pretermalització (Publicació [P.1])

En la publicació [P.1] estudiem un ambient que es troba fora de l'equilibri. L'ambient està compost per dos sistemes bosònics que es troben a diferents temperatures, però sols un d'ells està en contacte directe amb el sistema obert, que el considerem com un sistema de dos nivells. El Hamiltonià total ve donat per

$$H = H_S + H_E + H_{\text{int}} , \quad (\text{R.8})$$

on H_S i H_E són els Hamiltonians lliures del sistema i de l'entorn, respectivament, i H_{int} és el Hamiltonià d'interacció entre el sistema i l'entorn. Com havíem dit, modelitzem el sistema com un sistema de dos nivells amb el Hamiltonià lliure:

$$H_S = \frac{1}{2}\omega_0\sigma_z, \quad (\text{R.9})$$

on ω_0 és l'energia del salt d'energia entre els dos nivells. Modelitzem l'entorn al qual està acoblat el sistema com un conjunt d'oscil·ladors harmònics oberts, on cada mode en el primer reservori (RI) està acoblat a un reservori independent d'oscil·ladors que nomenem RII. El Hamiltonià que descriu aquest entorn és:

$$H_E = H_{\text{RI}} + H_{\text{RII}} + H_{\text{int},2}, \quad (\text{R.10})$$

on

$$H_{\text{RI}} = \sum_{\lambda} \omega_{\lambda} a_{\lambda}^{\dagger} a_{\lambda} \quad \text{and} \quad H_{\text{RII}} = \sum_{\lambda,k} \omega_{\lambda,k} b_{\lambda,k}^{\dagger} b_{\lambda,k}, \quad (\text{R.11})$$

són els Hamiltonians lliures de RI i RII, respectivament. Els operadors d'aquests Hamiltonians compleixen les relacions de commutació canòniques. La interacció entre RI i RII es descriu amb el Hamiltonià:

$$H_{\text{int},2} = \sum_{\lambda} \left(a_{\lambda}^{\dagger} \otimes \sum_k \tilde{g}_{\lambda,k} b_{\lambda,k} + a_{\lambda} \otimes \sum_k \tilde{g}_{\lambda,k}^* b_{\lambda,k}^{\dagger} \right), \quad (\text{R.12})$$

on $\tilde{g}_{\lambda,k}$ representa la força d'acoblament entre l'oscil·lador λ en RI i l'oscil·lador k en RII. El sistema es troba en una *configuració d'estrella*, és a dir, el SQO està acoblat a tots els operadors bosònics λ de RI, i a la seua vegada, cadascun d'aquests està acoblat a un reservori d'oscil·ladors harmònics que forma part de RII, com es mostra a la Fig. R.2. Només RI s'acobla directament al SQO, amb el Hamiltonià d'interacció:

$$H_{\text{int}} = \sigma_- \otimes \sum_{\lambda} g_{\lambda}^* a_{\lambda}^{\dagger} + \sigma_+ \otimes \sum_{\lambda} g_{\lambda} a_{\lambda}, \quad (\text{R.13})$$

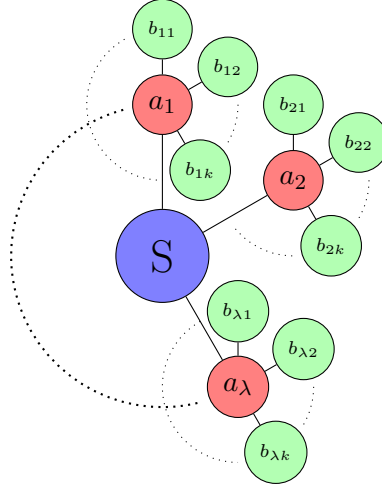


Figure R.2: Imatge esquemàtica del model. El SQO està acoblat en una configuració d'estrela a un conjunt d'oscil·ladors harmònics a_λ , que estan acoblats als seus propis banys individuals d'oscil·ladors harmònics $b_{\lambda,k}$.

que només considera interaccions que conserven el nombre de partícules. Considerem com a estat inicial un producte tensorial:

$$\rho(0) = \rho_S(0) \otimes \rho_E(0) = \rho_S(0) \otimes \rho_I^{\text{th}}(\beta_I) \otimes \rho_{II}^{\text{th}}(\beta_{II}) . \quad (\text{R.14})$$

L'estat inicial del sistema pot ser arbitrari, mentre que els estats inicials dels reservoris s'assumeix que són tèrmics, possiblement a diferents temperatures:

$$\rho_i^{\text{th}}(\beta_i) = \frac{e^{-\beta_i H_{Ri}}}{Z_i(\beta_i)} , \quad (\text{R.15})$$

on $Z(\beta_i) = \text{Tr}\{e^{-\beta_i H_{Ri}}\}$ és la funció de partició i $\beta_i = 1/T_i$ és la temperatura inversa de cada reservori, $i = \{I, II\}$.

Amb l'ús d'aproximacions d'acoblament dèbil i Markovianes, hem derivat una equació mestra per descriure l'evolució de la matriu de densitat

reduïda del sistema, traçant l'evolució de l'entorn. Malgrat aquestes aproximacions, hem pogut observar una dinàmica rica del sistema obert, amb l'existència d'un estat transitori, anomenat estat pretèrmic, abans de la termalització final, la qual es troba determinada únicament pel reservori més gran. Hem investigat sota quines condicions es presenta la pretermalització i hem conclòs que aquest estat té una vida més llarga quan RI, acoblatat directament al SQO, té major temperatura i RII està més fred, així com quan l'acoblement entre els reservoris és el més petit possible. Hem presentat una manera de caracteritzar la pretermalització que és independent de la condició inicial del SQO, mitjançant l'evolució del volum d'estats accessibles.

També hem demostrat que hi ha dinàmiques no trivials i competició de diferents escales de temps quan considerem dos entorns fora de l'equilibri acoblats a través sistema. És ben conegut que, en la situació estàndard on els entorns estan en equilibri, s'estableix i preval un flux de calor amb una direcció determinada (des del reservori més càlid cap al més fred) en temps llargs. Curiosament, quan considerem entorns fora de l'equilibri, observem que els temps induïts pels diferents entorns poden fer que el flux de calor canviï de direcció, fins i tot més d'una vegada.

La dinàmica del SQO i els seus corrents no evolucionen segons una única escala de temps, sinó que presenten una dinàmica més rica que pot ser evident en experiments i processos d'informació quàntica, particularment en temps llargs. La presència d'un estat pretèrmic transitori pot ser aprofitada en aplicacions tecnològiques quàntiques, per exemple, considerant els protocols d'inicialització d'un qubit acoblat a un ambient. El reservori RII pot ser potencialment controlat segons el nostre esquema, per optimitzar encara més el protocol. En altres paraules, el nostre treball descriu la possibilitat de manipular i controlar un sistema obert mitjançant la modificació i el control extern del ambient al qual està acoblat directament.

Aquest esquema pot adaptar-se per incloure més reserves externes a diferents temperatures. Es poden trobar entorns de diverses capes, per exemple, en ordinadors quàntics superconductors, on els qubits es veuen afectats no només per capes circumdants refredades criogènicament, sinó també per capes exteriors amb temperatures cada vegada més altes. Considerar aquesta estructura de reservoris ens permetria trobar estats transitoris i estacionaris addicionals del qubit, que potencialment es podrien aprofitar i controlar. Un tema interessant per a investigacions futures seria considerar la dinàmica més enllà de l'aproximació de dèbil acoblament i la inclusió d'efectes no Markovians.

Computació quàntica

La afirmació que la informació quàntica d'un sistema es perd quan aquest s'entrellaça amb el seu entorn és un tret distintiu entre la informació clàssica i quàntica. Dit d'una altra manera, la informació d'un sistema quàntic compost no és la suma de les seves parts. Aquesta característica profunda de la mecànica quàntica va ser posada de manifest per primer cop per John Bell en 1964, el treball de qui va portar a la comprensió que la informació quàntica està codificada en correlacions no locals entre les diferents parts d'un sistema físic.

Una altra diferència clau entre la informació quàntica i clàssica és que l'adquisició d'informació en un sistema quàntic pateix de dos problemes: i) el procés de mesura en la mecànica quàntica és un procediment probabilístic; ii) també provoca la pertorbació del sistema que s'està mesurant, deguda al col·lapse de la funció d'ona durant el procés de mesura.

Algú temps després d'aquests descobriments, es va assenyalar en 1982 de manera independent per Feynman i Benioff, i per l'obra inadvertida de Yuri Manin, que els sistemes quàntics podrien realitzar càlculs. La

motivació més remarcable va ser la complexitat de simular sistemes quàntics clàssicament. No hi ha restricció fonamental perquè les màquines clàssiques simulen sistemes quàntics; al cap i a la fi, consisteix a calcular una matriu de rotació i aplicar-la a un vector en un espai de Hilbert, però el problema es torna exponencialment més complicat per a sistemes més grans. Aquesta limitació va motivar l'ús de sistemes quàntics per simular sistemes quàntics analògics. Un simulador quàntic no seria res més que un sistema quàntic que pot ser manipulat molt precisament per simular altres sistemes quàntics.

Les característiques peculiars de la informació quàntica, que la distingeixen de la seva contrapartida clàssica, van indicar que els sistemes quàntics podrien tenir un impacte profund no només en la simulació de sistemes quàntics sinó en els fonaments de la computació. Això es va fer evident amb l'aparició de l'algorisme de factorització de Shor el 1994, que va mostrar que un ordinador quàntic podia factoritzar un nombre gran més eficientment que els algorismes coneguts fins aleshores, i l'algorisme de cerca de Grover, que és un algorisme de cerca quàntica amb un augment quadràtic d'eficiència en comparació amb els millors algorismes clàssics possibles.

El paradigma més emprat per al processament de la informació quàntica es realitza amb col·leccions de sistemes de dos nivells anomenats qubits, en analogia amb el bit clàssic. El qubit és el portador més bàsic de la informació quàntica. Una computació segueix generalment tres passos: (i) inicialització del qubit a un estat conegut, (ii) manipulació del qubit, que consisteix en aplicar operacions a qubits individuals o operacions que involucren (entrellacen) diversos qubits, i (iii) mesura. Com que els resultats de la mesura són probabilístics, pot ser necessari repetir els passos anteriors diverses vegades.

El marc més comú per descriure les manipulacions dels qubits és el model de circuits quàntics. En aquest model, els qubits es representen com

fil, i les manipulacions sobre ells es representen amb portes que actuen sobre aquests fil. Aquestes portes tenen una implementació física corresponent que es realitza sobre el qubit físic, però aquesta abstracció permet eliminar tots els detalls físics i centrar-se únicament en el processament de la informació quàntica o en els algorismes quàntics. Si les combinacions d'aquestes portes permeten realitzar qualsevol operació quàntica possible, es diu que és un conjunt universal de portes. Es pot demostrar que un conjunt de portes de qubit individuals i una porta de dos qubits que entrellaça són universals. Per exemple, un d'aquests conjunts està compost per les tres rotacions del qubit l voltant de tres eixos ortogonals i la porta CNOT, que, condicionada a l'estat d'un qubit de control, inverteix l'estat del qubit objectiu.

La primera proposta per implementar físicament els qubits, que va poder realitzar un conjunt universal de portes, es va fer el 1994 quan Peter Zoller i Ignacio Cirac van proposar en el seu treball seminal un sistema d'ions refredats. Després d'aquesta proposta inicial, s'han proposat molts sistemes quàntics que poden ser més controlables o tenir millor escalabilitat. Una de les implementacions més populars i prometedores és la dels anomenats qubits superconductors, que es realitzen amb un circuit tancat que, quan es refreda a temperatures criogèniques, mostra propietats superconductores. La corrent en els circuits es fa de parelles de Cooper que poden mostrar les propietats quàntiques de superposició i entrellaçament. Les operacions en aquests sistemes es poden realitzar amb l'ús d'impulsos de microones.

Tot i que els sistemes quàntics dissenyats per portar i processar informació quàntica es poden construir, no estan lliures de la interacció amb altres sistemes externs. L'entrellaçament entre els diferents components d'un ordinador quàntic ha de ser mantingut i protegit, però l'entrellaçament amb sistemes externs indesitjats, que no participen en la computació, s'ha d'evitar. A continuació, ens preocupem per aquest últim aspecte i fem ús de la teoria dels sistemes quàntics oberts, introduïda al capítol anterior, per

estudiar els efectes de la termalització i decoherència dels qubits.

Soroll sobre qubits

Els dos principals processos que pateix un qubit en interacció amb l'ambient són la dissipació i la decoherència. La dissipació produeix intercanvis energètics entre qubit i ambient, procés que canvia les probabilitats de mesurar el qubit en la base computacional. La dissipació sempre va acompanyada d'una pèrdua de coherència, és a dir, es perd la superposició quàntica entre els estats del qubit. El principal efecte que produeix la dissipació és el procés de termalització, l'ambient es troba en un estat tèrmic a una temperatura finita i desplaça el qubit cap a un estat tèrmic a la mateixa temperatura per tal d'assolir l'equilibri. Per altra banda, un qubit pot estar subjecte únicament a decoherència, sense patir pèrdues energètiques, en aquest cas el procés s'anomena de desfasament pur. Un qubit pot sofrir decoherència degut tant a dissipació com a desfasament pur alhora.

No hi ha evidències de que la dissipació siga un procés no-Markovià, la dinàmica d'un qubit amb dissipació pot ser descrita amb una equació mestra com la Eq. (R.5). En canvi, el desfasament pur s'ha observat amb característiques no-Markovianes. És àmpliament reconegut que la font de soroll en les implementacions d'estat sòlids de la computació quàntica [54, 55, 56] es deu a la presència de defectes de dos nivells en materials amorfs a temperatures baixes [57, 58]. Sorprenentment, aquest efecte sembla ser universal en diferents materials i composicions, i es fa particularment evident en materials amorfs a temperatures per sota de l'escala Kelvin.

Model semiclàssic. Quan aquests defectes de dos nivells, o sistemes de dos nivells (SDN), estan fortament acoblats al seu entorn, la seva dinàmica es descriu per mitjà de fluctuacions incoherents entre els seus dos estats,

donant lloc al que es coneix com fluctuadors. Un model semiclàssic pot ser introduït per descriure el soroll de desfasament pur induït per aquests fluctuadors. L'estat dels fluctuadors pot ser descrit per una variable aleatòria clàssica $b_k^i(t) \in \{+1, -1\}$, on k indica fluctuadors individuals i el superíndex i indica una realització particular del procés aleatori. Aquests fluctuadors fluctuen independentment entre els seus dos possibles estats a una taxa γ_k . La probabilitat que un fluctuador canviï n vegades després d'un temps t segueix una distribució de Poisson

$$p_n(t) = \frac{(\gamma_k t)^n}{n!} e^{-\gamma_k t}, \quad (\text{R.16})$$

de manera que el nombre mitjà de canvis del fluctuador k durant un interval de longitud τ és $\gamma_k \tau$. La funció d'autocorrelació d'un únic fluctuador segueix una decaïment exponencial,

$$C(t - t') = \langle b_k^i(t) b_k^i(t') \rangle_i = e^{-2\gamma_k |t - t'|}, \quad (\text{R.17})$$

la qual cosa indica que l'espectre (transformada de Fourier de la funció d'autocorrelació) és lorentzià

$$S_{\text{RTN}}(\gamma_k, \omega) = \int_{-\infty}^{\infty} d\tau C(\tau) e^{i\tau\omega} = \frac{4\gamma_k}{4\gamma_k^2 + \omega^2}. \quad (\text{R.18})$$

Cada un dels fluctuadors està acoblat al qubit amb una intensitat d'acoblament v_k . La variable estocàstica

$$\chi^i(t) = \sum_{i=1}^{N_{\text{RTN}}} v_k b_k^i(t), \quad (\text{R.19})$$

captura l'efecte dels fluctuadors sobre el qubit, on N_{RTN} és el nombre de fluctuadors. La influència dels fluctuadors s'incorpora al hamiltonià del qubit a través d'una interacció del tipus

$$H^i(t) = \frac{\omega_0 + \chi^i(t)}{2} \sigma_z, \quad (\text{R.20})$$

on ω_0 és la separació d'energia entre els dos nivells del qubit. Cal destacar que aquest model de soroll pot presentar dinàmica no-Markoviana. El text principal he estudiat diferents hem deduït la formula de la decoherència dels qubit sota aquest model de soroll sotmès a diferents tècniques de mitigació que intenten reduir l'efecte negatiu del soroll.

Model quàntic. S'han proposat diferents models quàntics microscòpics per descriure el soroll induït per SDN coherents [69, 70, 71, 72], consulteu [68] per una revisió de la seva motivació física. En general, els SDN es modelen mitjançant un potencial de doble pou asimètric, amb ϵ com la diferència d'energia dels mínims i Δ descriu l'intensitat del efecte túnel entre els dos mínims. Construïm un model quàntic on el qubit està acoblat a un SDN coherent, que al seu torn està acoblat a un reservori extern a una temperatura finita. El hamiltonià total és $H = H_S + H_E + H_I$, on el hamiltonià del sistema qubit-SDN té tres termes $H_S = H_Q + H_{TLS} + H_{QT}$,

$$H_Q = \frac{1}{2}\omega_q\tau_z, \quad H_{TLS} = \frac{\epsilon}{2}\sigma_z + \frac{\Delta}{2}\sigma_x, \quad H_{QT} = \frac{v}{2}\tau_z\sigma_z, \quad (\text{R.21})$$

on τ_i són les matrius de Pauli que actuen a l'espai de Hilbert del qubit i σ_i a l'espai del TLS. El hamiltonià del TLS és una descripció efectiva del doble pou descrit anteriorment. La interacció qubit-TLS H_{QT} indueix un enfosquiment pur al qubit. La diferència d'energia dels nivells del TLS és $E_F = \sqrt{\Delta^2 + \epsilon^2}$.

L'entorn és un reservori bosònic que s'acopla directament al TLS, però no al qubit. Els hamiltonians de l'entorn i de la interacció són

$$H_B = \sum_k \omega_k b_k^\dagger b_k, \quad H_I = \sigma_+ \sum_k g_k b_k + \sigma_- \sum_k g_k^* b_k^\dagger. \quad (\text{R.22})$$

A la Fig. R.3 es presenta un esbós d'aquest entorn compost. La dinàmica d'aquest model pot ser descrita mitjançant l'equació de Redfield (R.6) on

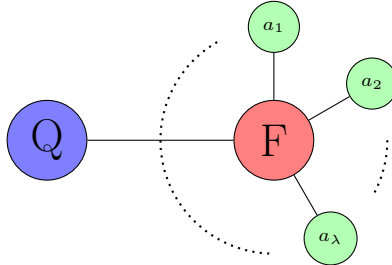


Figure R.3: Schematic picture of the model. The qubit (Q) is coupled to the fluctuator (F), which in turn is coupled to its own bath of harmonic oscillators a_λ .

el Hamiltonià del sistema obert ve donat per H_S i sols es traça el ambient d'oscil·ladors bosònics. Per tal d'obtindre la funció de decoherència del qubit cal traçar el SDN. En el text principal duem a terme una aproximació secular per tal de tindre una visió física general dels nivells energètics del sistema i les energies d'interacció. També hem comprovat que el model semiclàssic reproduïx la dinàmica d'aquest model en el límit d'altres temperatures, on les suposicions fetes per al model semiclàssic són correctes. L'objectiu final de l'estudi d'aquest model és comprovar l'efectivitat de les tècniques de mitigació sobre un model purament quàntic.

Part II: Caminants quàntics

Introducció

Un passeig aleatori és un procés aleatori que descriu el desplaçament d'un caminant seguint una successió de passos aleatoris en un graf. El model de passeig aleatori més comú és el d'un caminant en una xarxa regular, on la probabilitat de salt del caminant a les ubicacions adjacents es dona per

alguna distribució de probabilitat, però hi ha altres escenaris possibles. Els passejos aleatoris es poden utilitzar, per exemple, per modelar el moviment aleatori de molècules en líquids o gasos (moviment brownià) i té aplicacions en molts camps científics, com la biologia, la química o la informàtica, per nomenar-ne alguns. El valor esperat de la posició del caminant es descriu mitjançant una distribució de probabilitat, que està determinada per la probabilitat del salt aleatori i el graf específic. L'exemple bàsic d'un passeig aleatori és un caminant a la recta numèrica \mathbb{Z} , que, després de cada pas, salta una posició en la direcció positiva o negativa condicionada al resultat d'un llançament de moneda equilibrat.

Es va proposar un passeig aleatori quàntic anàleg (QW) el 1993 per Aharonov et al. [74], en el qual el caminant és una partícula quàntica que no es pot localitzar a causa de les incerteses quàntiques. En canvi, l'estat del caminant es descriu mitjançant una funció d'ona d'espínor, i les probabilitats de salt estan condicionades a un grau de llibertat intern, que juga el paper d'una moneda quàntica. A causa del caràcter quàntic del caminant, la seva distribució de probabilitat és diferent de la del cas clàssic. Els passejos quàntics també es poden definir en temps continu. Childs et al. van donar en [75] la definició general, que es basa en una formulació hamiltoniana en la qual no és necessària la moneda interna del caminant. Tot i que els passejos quàntics en temps continu tenen moltes aplicacions i propietats importants, els treballs d'aquesta tesi es centren en els passejos quàntics a temps discret.

Ja es va assenyalar en [74] que la dispersió del caminant quàntic és quadràticament més ràpida que la del caminant clàssic. Aquest fet va permetre descobrir algorismes de cerca més eficients que els seus equivalents clàssics. Per exemple, l'algoritme de Grover [22] es pot veure com un algoritme de cerca de passeig quàntic [76]. També s'ha demostrat que algorismes de cerca similars basats en passejos quàntics, com el problema de la distinció d'elements [77], són més eficients que els equivalents clàssics.

Finalment, els passejos quàntics també es van demostrar més eficients en problemes d'obtenció de mostres de distribució de probabilitat [78, 79]. També s'ha demostrat que els passejos quàntics es poden utilitzar com a model de computació universal [80, 81].

Existeixen nombroses propostes experimentals per implementar passejos quàntics. La primera plataforma proposada per implementar el passeig quàntic en temps discret utilitzava trampes d'ions [82], on la malla discreta es codificava en els modes vibracionals dels ions, i l'estat de la moneda es codificava en l'estat electrònic intern dels ions. S'han proposat moltes altres plataformes, com ara les cavitats de QED [83] o les retícules òptiques [84], per citar-ne algunes. Consulteu [85] per obtenir una revisió exhaustiva de les implementacions físiques.

El caminant en el passeig quàntic aleatori [86, 87, 88] a la recta es representa mitjançant un espinor, que, tot i que en la condició inicial pot estar localitzat en la posició central, representa en general una superposició del caminant en diferents localitzacions. L'estat del caminant, a més del grau de llibertat espacial, es dona per un grau de llibertat intern de dues dimensions, que s'anomena moneda quàntica. L'espai de Hilbert del grau de llibertat espacial, \mathcal{H}_x , és d'infinita dimensió i està generat per la base $\{|j\rangle; j \in \mathbb{Z}\}$. L'espai de Hilbert de la moneda quàntica, \mathcal{H}_C , és un espai de 2 dimensions generat per la base $\{|\uparrow\rangle, |\downarrow\rangle\}$. L'espai de Hilbert total és el seu producte tensorial $\mathcal{H} = \mathcal{H}_C \otimes \mathcal{H}_x$. L'estat del caminant en aquesta base a temps $n \in \mathbb{Z}$ es pot escriure com

$$|\psi_n\rangle = \sum_j (\psi_{n,j}^\uparrow |\uparrow\rangle + \psi_{n,j}^\downarrow |\downarrow\rangle) \otimes |j\rangle, \quad (\text{R.23})$$

on $\psi_{n,j}^s$, amb $s = \{\uparrow, \downarrow\}$, són les components del spinor al pas n i la posició j . Podem projectar l'estat del caminant sobre la base espacial i representar

l'estat del caminant com un espinor,

$$|\psi_{n,j}\rangle = \langle j|\psi_n\rangle = \begin{pmatrix} \psi_{n,j}^\uparrow \\ \psi_{n,j}^\downarrow \end{pmatrix}, \quad (\text{R.24})$$

on hem definit la representació canònica de les components de la moneda com $|\uparrow\rangle = (1, 0)^T$ i $|\downarrow\rangle = (0, 1)^T$.

L'evolució d'un pas del caminant quàntic es compon de dues operacions: un llançament de moneda quàntica que barreja les components de la moneda del caminant, seguit d'un operador de desplaçament condicional que desplaça la posició del caminant segons el grau de llibertat intern. Podem escriure aquesta operació d'un pas com

$$|\psi_{n+1}\rangle = \hat{W} |\psi_n\rangle = \hat{S}(\hat{C} \otimes \mathbb{I}_x) |\psi_n\rangle, \quad (\text{R.25})$$

on \hat{C} és una operació unitària general que actua sobre l'estat intern del caminant i \hat{S} és l'operador de desplaçament condicional definit com

$$\hat{S} = |\uparrow\rangle\langle\uparrow| \otimes \sum_j |j+1\rangle\langle j| + |\downarrow\rangle\langle\downarrow| \otimes \sum_j |j-1\rangle\langle j|. \quad (\text{R.26})$$

L'operador de desplaçament condicional transforma els estats de la forma $|\uparrow\rangle|j\rangle$ en estats $|\uparrow\rangle|j+1\rangle$ i els estats $|\downarrow\rangle|j\rangle$ en estats $|\downarrow\rangle|j-1\rangle$, és a dir, desplaça els estats amb l'estat cap amunt (cap avall) cap a la dreta (esquerra). L'evolució des d'una condició inicial donada $|\psi_0\rangle$ fins al pas $n = 1, 2, \dots$ és simplement $|\psi_n\rangle = \hat{W}^n |\psi_0\rangle$. El caminant no té una posició definitiva, només en mesurar la posició, l'estat del caminant es col·lapsa i la seva posició es torna definitiva. La distribució de probabilitat associada del caminant al temps n es dona en termes de les seves components d'estat com

$$P_{n,j} = \sum_{s=\uparrow\downarrow} |\langle s, j|\psi_n\rangle|^2 = |\psi_{n,j}^\uparrow|^2 + |\psi_{n,j}^\downarrow|^2. \quad (\text{R.27})$$

Es pot associar un espai físic a l'espai generat per la xarxa discreta del QW. Es pot introduir un espaiat de la xarxa discreta, ϵ_x , per connectar ambdós espais com $|x\rangle = |\epsilon_x j\rangle$ on $|x\rangle$ és la base d'un espai de Hilbert de posició que està discretitzat per un espaiat ϵ_x . Un procediment similar es pot fer per a la coordenada temporal $t = \epsilon_t n$ amb un espaiat ϵ_t . L'operador de desplaçament produeix un desplaçament condicional a l'espai físic discretitzat per una quantitat ϵ_x , de manera que $e^{-i\hat{K}} |x\rangle = |x + \epsilon_x\rangle$, on \hat{K} és l'operador quasi-moment, el generador de translacions de la xarxa discreta. Podem relacionar el quasi-moment amb el moment físic, en el límit de ϵ_x xicotet, com $\hat{K} = \epsilon_x \hat{p}$. Finalment, si considerem l'operador moneda com una rotació d'angle $\theta = \epsilon_m \hat{\theta}$, es pot demostrar que l'equació d'evolució del QW es pot escriure com una equació diferencial per a un espinor, i que aquesta correspon a l'equació de Dirac

$$(i\gamma^\mu \partial_\mu - m)\Psi(t, x) = 0 \ , \quad (\text{R.28})$$

on γ^μ són les matrius de Dirac. Si l'angle del operador moneda es deixa dependre de la posició de QW en la xarxa i del pas de temps de l'evolució es poden obtenir límits al continu més interessants. Per exemple, si al pas de temps del QW s'afegeix una fase global que depèn linealment de la posició, el límit al continu d'aquest QW correspon a l'equació de Dirac amb un camp elèctric constant. Diferents eleccions de moneda poden donar lloc a qualsevol configuració de camp electromagnètic [93, 94], o a equacions de Dirac en espai-temps corbats. L'estudi del límit al continu també pot ser emprat per entendre la dinàmica del model discret, pot donar informació sobre les solucions estacionàries [P.4].

Simulació de geometria plegada en teories d'altres energies mitjançant QW (Publicació [P.2])

L'existència d'un límit continu de diferents QWs que coincideixen amb equacions similars a les de Dirac ha permès la simulació d'una gran varietat de sistemes físics mitjançant QWs. A més de la simulació de fermions en espais-temps corbats i camps electromagnètics els QWs poden ser construïts per simular oscil·lacions de neutrins [99], dinàmica de fluids carregats [100], fenòmens topològics [101] o difusió relativista [P.3], per nomenar-ne alguns exemples. En [P.2] investiguem les propietats d'un QW que, en el límit contínu, simula el model de dimensions extra de Randall-Sundrum (RS) [102]. El model RS es va introduir per explicar el problema de jerarquia de les teories d'altres energies (HEP), mitjançant l'addició d'una dimensió extra corbada, que tenia una brana de 4 dimensions en cada extrem. La gravetat està present en tot l'espai-temps, però els camps de matèria del Model Estàndard de partícules es troben confinats en una de les branques, la brana de matèria. Definim un QW de 2 dimensions amb una dimensió espacial corbada i una dimensió espacial ordinària. Derivem l'equació de Dirac que sorgeix en aquest espai-temps corbat reduït i establim les condicions de contorn que els camps fermiònics han de satisfer. Les condicions de simetria en aquest espai-temps de dimensions més baixes restringeixen l'estudi a fermions sense massa, que poden adquirir una massa efectiva quan es restringeixen a la brana de matèria. També estudiem l'espectre de les solucions del model continu, on ja es pot observar que les autofuncions de l'equació de Dirac presenten confinament cap a la brana de matèria.

Hem construït una QW que, en el límit contínu, recupera l'equació de Dirac derivada seguint el mètode introduït a [97]. La xarxa creada per al QW es representa a la Fig. R.4. La dimensió espacial ordinària és infinita, i es pren una xarxa prou gran en aquesta direcció perquè el caminant no

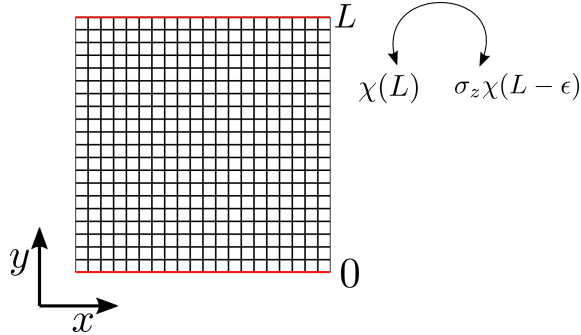


Figure R.4: Xarxa espacial del QW del model RS. La xarxa és infinita en la direcció x , però és finita en la direcció y , amb una longitud de L .

arribe als extrems de la xarxa. La dimensió corbada és finita, i es defineixen condicions de contorn adequades als extrems, on el caminant és reflectit amb una inversió de fase. Aquesta és la mateixa condició de contorn que els fermions de Dirac han de satisfer en el model continu. La construcció del QW és coherent amb aquesta condició en tot moment.

En primer lloc vam observar que el QW reproduïx la fenomenologia esperada pel model RS, és a dir, un caminant inicialment localitzat en el centre de la dimensió corbada es localitzarà a l'extrem de la dimensió corbada on els camps de matèria estan confinats. La propietat de confinament del model està controlada pel coeficient de curvatura, i vam confirmar que, quan aquest paràmetre augmenta, la localització del caminant cap a la brana de matèria és més intensa. Com aquest model està restringit a fermions sense massa, la major part de la densitat de probabilitat del caminant es propaga a la velocitat de la llum, i la direcció de propagació depèn de la quiralitat, és a dir, les components superiors (inferiors) es propaguen cap a la dreta (esquerra) en la dimensió ordinària. Aquests fronts de probabilitat, que es desplacen a la velocitat de la llum, estan situats a la posició $x = t$, i

definim aquesta distribució de probabilitat al llarg de la direcció y com la distribució de propagació lliure (DPL). Vam realitzar una descomposició de les components del caminant en termes de les autofuncions obtingudes de l'equació de Dirac contínua i vam estudiar la composició de modes de les DPL. Vam observar que, tot i que inicialment les DPL poden estar compostes per modes d'alta energia, a la llarga, les DPL estan principalment compostes pel mode d'energia més baixa. Aquest efecte indica alguna mena de dissipació, durant la propagació, cap a les regions interiors del con del llum.

Finalment, vam investigar l'entropia d'entrellat entre la moneda i el grau de llibertat espacial. El pas del QW genera entrellaçament entre aquests graus de llibertat i es redueix per a valors més alts del coeficient de curvatura. Vam atribuir aquest efecte a la menor dispersió de la distribució de probabilitat del caminant amb l'augment del coeficient de curvatura.

Tot i que els QW han demostrat ser exitosos en reproduir alguns efectes de les teories de física d'altres energies, manquen la capacitat de simular interaccions entre múltiples partícules. No obstant això, el formalisme es pot modificar per incloure interaccions entre partícules. S'han realitzat alguns esforços [103, 104] per descriure estats de dues i tres partícules, però cal fer més treball per tenir un marc de simulació per a HEP. També cal esmentar que les caminades quàntiques no estan lliures de defectes presents en les teories de discretes, com pot ser el problema del doblament de fermions. Els autòmats cel·lulars quàntics [18, 105, 106] són una teoria de xarxa discreta similar als QW, on en cada ubicació el sistema quàntic pot tenir qualsevol dimensió finita. L'evolució també és discreta en el temps i s'ha demostrat que poden simular models senzills de teoria quàntica de camps, per exemple, el model de Schwinger [107].

Simulació de difusió relativista mitjançant un QW estocàstic (Publicació [P.3])

A la publicació anterior, hem estudiat un (QW) que tenia una moneda espacial inhomogènia. En [P.3] estudiem una moneda que és inhomogènia en el temps, i on la dependència temporal és estocàstica; aquest tipus d'evolució es pot veure com un tipus de soroll temporal a l'operador de la moneda. Hem estudiat dues maneres de generar una moneda temporal estocàstica, però ací expliquem breument la que es connecta més estretament amb la primera part de la tesi. Podem definir un procés de soroll en un caminant en la representació de suma d'operadors com

$$\rho_{n+1} = (1 - p_1 - p_2)\hat{W}\rho_n\hat{W}^\dagger + p_1\sigma_z\rho_n\sigma_z + p_2\sigma_x\rho_n\sigma_x, \quad (\text{R.29})$$

on ρ_n és la matriu de densitat en el pas de temps n , p_1 és la probabilitat que el caminant pateixi un error de gir de fase, p_2 és la probabilitat de patir un error de intercanvi de bit, i amb probabilitat $1 - p_1 - p_2$ es sotmet a l'evolució usual unitària del QW. Podem definir $p_i = \epsilon\gamma_i$, on ϵ és el mateix que el pas de temps infinitesimal, i seguir de manera similar a la derivació infinitesimal de l'equació de Lindblad a partir de la representació dels operadors de Kraus, per obtenir una equació mestra contínua

$$\partial_t\rho = -i[\overline{H}, \rho] + \gamma_1(\sigma_z\rho\sigma_z - \rho) + \gamma_2(\sigma_x\rho\sigma_x - \rho), \quad (\text{R.30})$$

on \overline{H} és el generador infinitesimal de la dinàmica unitària del QW $\hat{W} = e^{-i\epsilon\overline{H}}$, i coincideix amb el hamiltonià obtingut en el límit continu de l'evolució unitària del QW, que és en general el hamiltonià de Dirac. L'altra manera de construir un QW estocàstic, que condueix al mateix límit continu, consisteix en aplicar una unitària composta per un operador de moneda $SU(2)$ general i l'operador de desplaçament condicional (3.5). L'operador de moneda es pot parametritzar amb 4 paràmetres constants que es mostregen aleatòriament de distribucions de probabilitat independents. La correspondència entre

aquesta implementació i la anterior s'obté si les desviacions estàndard d'aquests paràmetres coincideixen amb les taxes γ_i .

Aquesta equació contínua representa un model de difusió quàntica relativista. Representem la matriu de densitat del espinor en la base de Pauli, i l'equació dinàmica esdevé un sistema de quatre equacions amb derivades parcials que es resolen numèricament mitjançant un mètode de descomposició d'operadors. Aquest mètode ens va permetre estudiar la fenomenologia del model continu, que es pot resumir en dos règims: un règim de propagació balística, en què el paquet d'ona inicial es propaga a una velocitat constant, i després d'un temps, que depèn de la intensitat del soroll, fa la transició a un règim difusiu. Aquest darrer règim es caracteritza per un valor esperat constant de la posició i per un augment de la desviació estàndard proporcional a \sqrt{t} , característica dels processos difusius. Finalment, es va estudiar un model que afegeix soroll espacial a sobre del soroll temporal, i es van obtenir dinàmiques Lindbladianes similars en el límit continu.

Formació de solitons en un QW no-lineal (Publicació [P.4])

Una altra variant de l'operador de moneda que introdueix no linealitats en les fases de les components del caminant va ser introduïda a [108]. Les fases depenien de la densitat de probabilitat del caminant en cada posició. El model està pel tauler de Galton òptic no lineal, on les no linealitats són causades per un medi no lineal de Kerr. El resultat principal del treball va ser la formació d'estructures similars a solitons, és a dir, la distribució de probabilitat del caminant es extensa i estable. En el llenguatge dels sistemes òptics, els efectes no lineals del medi contraresten la dispersió natural de la llum.

En [P.4] considerem un model similar, juntament amb una proposta

experimental, on les no linealitats s'introdueixen en l'angle de l'operador de moneda, és a dir, l'angle de rotació en cada posició del caminant depèn de les components del caminant en aquesta posició:

$$C(\theta_{t,x}) = e^{-i\theta_{t,x}\sigma_y} = \begin{pmatrix} \cos \theta_{t,x} & -\sin \theta_{t,x} \\ \sin \theta_{t,x} & \cos \theta_{t,x} \end{pmatrix}, \quad (\text{R.31})$$

on l'angle de rotació ve donat per

$$\theta_{t,x} = \theta_0 + \alpha |u_{t,x}| |d_{t,x}| \sin \delta_{t,x}, \quad (\text{R.32})$$

on em expressat explícitament les components del caminant en funció del seu mòdul i fase $u_{t,x} = |u_{t,x}| e^{i\varphi_{t,x}^u}$, $d_{t,x} = |d_{t,x}| e^{i\varphi_{t,x}^d}$ i $\delta_{t,x} = \varphi_{t,x}^u - \varphi_{t,x}^d$ és la diferència de fases. Les components del caminant evolucionen explícitament a cada pas com

$$\begin{aligned} u_{t+1,x} &= \cos(\theta_{t,x-1})u_{t,x-1} - \sin(\theta_{t,x-1})d_{t,x-1}, \\ d_{t+1,x} &= \sin(\theta_{t,x+1})u_{t,x+1} + \cos(\theta_{t,x+1})d_{t,x+1}. \end{aligned} \quad (\text{R.33})$$

El límit contínu d'aquest QW proporciona una equació de Dirac no lineal on hi ha un terme no lineal similar al que apareix en el model de Nambu-Jona-Lasinio [109]. Fem un estudi detallat de l'equació diferencial contínua. En primer lloc, explorem la estabilitat de solucions estacionàries homogènies i identifiquem els règims en què poden aparèixer solucions similars a solitons. En segon lloc, trobem, sota suposicions raonables, una solució estacionària del model continu que té les característiques usals d'un solitó.

Els resultats obtinguts de l'equació contínua es verifica en el model discret numèricament. Trobem l'existència d'estructures similars a solitons amb la mateixa solució que l'equació contínua. També investiguem condicions inicials que es propaguen a una velocitat constant i observem una

característica típica dels solitons, que és que durant una col·lisió els paquets d'ones no es pertorben. L'anàlisi d'estabilitat de l'equació contínua indica que haurien de existir altres tipus de solucions estacionàries, els solitons foscos, els quals observem en el model discret. Un solitó fosc es genera a la paret de domini entre dues solucions estables, on la probabilitat de trobar el caminant desapareix en la transició. Aquesta vall de densitat de probabilitat és estacionària.

També hem estudiat l'estabilitat dels solitons quan estan sotmesos a una fase addicional que simula un camp elèctric extern. Per a intensitats de camp elèctric irracionals, els solitons continuen localitzats però la seua estructura característica suau es perd. Per a fraccions racionals de 2π d'intensitats de camp elèctric, hem caracteritzat dos règims: per a camps elèctrics forts, un solitó inicial es desfà lentament i el caminant es dispersa, i un augment del paràmetre de no linealitat redueix la dispersió produïda pel camp elèctric fort. Per a camps elèctrics febles, hi ha oscil·lacions de la posició central del solitó. Finalment, també hem explorat una versió bidimensional d'aquest model, on no hem trobat cap evidència de formació de solitons.

Bibliography

- [1] Rivas A, Huelga S F. *Open Quantum Systems*. Springer Berlin Heidelberg, 2012.
- [2] Breuer H P, Petruccione F. *The theory of open quantum systems*. Great Clarendon Street: Oxford University Press, 2002.
- [3] Kossakowski A. *On quantum statistical mechanics of non-Hamiltonian systems*. *Reports on Mathematical Physics*, 3(4):247–274, 1972. [https://doi.org/10.1016/0034-4877\(72\)90010-9](https://doi.org/10.1016/0034-4877(72)90010-9).
- [4] Ingarden R, Kossakowski A. *On the connection of nonequilibrium information thermodynamics with non-hamiltonian quantum mechanics of open systems*. *Annals of Physics*, 89(2):451–485, 1975. [https://doi.org/10.1016/0003-4916\(75\)90190-6](https://doi.org/10.1016/0003-4916(75)90190-6).
- [5] Breuer H P, Laine E M, Piilo J. *Measure for the Degree of Non-Markovian Behavior of Quantum Processes in Open Systems*. *Phys. Rev. Lett.*, 103:210401, 2009. [10.1103/PhysRevLett.103.210401](https://doi.org/10.1103/PhysRevLett.103.210401).
- [6] Gorini V. *Completely positive dynamical semigroups of N-level systems*. *J. Math. Phys.*, 17(5):821, 1976. [10.1063/1.522979](https://doi.org/10.1063/1.522979).

- [7] Lindblad G. *On the generators of quantum dynamical semigroups*. Commun.Math. Phys., 48(2):119–130, 1976. [10.1007/bf01608499](https://doi.org/10.1007/bf01608499).
- [8] Preskill J. Lecture notes in Quantum Computation. Caltech Particle Theory Group, Spring, 2022.
- [9] Alicki R, Lendi K. Quantum Dynamical Semigroups and Applications. Springer Berlin Heidelberg, 2007.
- [10] Rivas, Huelga S F, Plenio M B. *Quantum non-Markovianity: characterization, quantification and detection*. Reports on Progress in Physics, 77(9):094001, 2014. [10.1088/0034-4885/77/9/094001](https://doi.org/10.1088/0034-4885/77/9/094001).
- [11] Lorenzo S, Plastina F, Paternostro M. *Geometrical characterization of non-Markovianity*. Phys. Rev. A, 88:020102, 2013. [10.1103/PhysRevA.88.020102](https://doi.org/10.1103/PhysRevA.88.020102).
- [12] Laine E M, Piilo J, Breuer H P. *Measure for the non-Markovianity of quantum processes*. Phys. Rev. A, 81:062115, 2010. [10.1103/PhysRevA.81.062115](https://doi.org/10.1103/PhysRevA.81.062115).
- [13] Hall M J W, Cresser J D, Li L, et al. *Canonical form of master equations and characterization of non-Markovianity*. Phys. Rev. A, 89:042120, 2014. [10.1103/PhysRevA.89.042120](https://doi.org/10.1103/PhysRevA.89.042120).
- [14] Cattaneo M, Giorgi G L, Maniscalco S, et al. *Local versus global master equation with common and separate baths: superiority of the global approach in partial secular approximation*. New J. Phys., 21(11):113045, 2019. [10.1088/1367-2630/ab54ac](https://doi.org/10.1088/1367-2630/ab54ac).
- [15] Vinjanampathy S, Anders J. *Quantum thermodynamics*. Contemporary Physics, 57(4):545–579, 2016.

- [16] Kosloff R, Levy A. *Quantum Heat Engines and Refrigerators: Continuous Devices*. Annual Review of Physical Chemistry, 65(1):365–393, 2014.
- [17] Bell J S. *On the Einstein Podolsky Rosen paradox*. Physics Physique Fizika, 1(3):195–200, 1964. [10.1103/physicsphysiquefizika.1.195](https://doi.org/10.1103/physicsphysiquefizika.1.195).
- [18] Feynman R P. *Simulating physics with computers*. Int J Theor Phys, 21(6-7):467–488, 1982. [10.1007/bf02650179](https://doi.org/10.1007/bf02650179).
- [19] Benioff P. *Quantum mechanical hamiltonian models of turing machines*. J Stat Phys, 29(3):515–546, 1982. [10.1007/bf01342185](https://doi.org/10.1007/bf01342185).
- [20] Manin Y. *Computable and Uncomputable*. 1980.
- [21] Shor P. Algorithms for quantum computation: discrete logarithms and factoring. in: Proceedings of Proceedings 35th Annual Symposium on Foundations of Computer Science. IEEE Comput. Soc. Press, 1994.
- [22] Grover L K. A fast quantum mechanical algorithm for database search. in: Proceedings of Proceedings of the twenty-eighth annual ACM symposium on Theory of computing - STOC '96. ACM Press, 1996.
- [23] Deutsch D E. *Quantum computational networks*. Proc. R. Soc. Lond. A, 425(1868):73–90, 1989. [10.1098/rspa.1989.0099](https://doi.org/10.1098/rspa.1989.0099).
- [24] Sleator T, Weinfurter H. *Realizable Universal Quantum Logic Gates*. Phys. Rev. Lett., 74:4087–4090, 1995. [10.1103/PhysRevLett.74.4087](https://doi.org/10.1103/PhysRevLett.74.4087).
- [25] Nielsen M A, Chuang I L. *Quantum Computation and Quantum Information: 10th Anniversary Edition*. Cambridge University Press, 2010.

- [26] Cirac J I, Zoller P. *Quantum Computations with Cold Trapped Ions*. Phys. Rev. Lett., 74:4091–4094, 1995. [10.1103/PhysRevLett.74.4091](https://doi.org/10.1103/PhysRevLett.74.4091).
- [27] Peres A. *Reversible logic and quantum computers*. Phys. Rev. A, 32:3266–3276, 1985. [10.1103/PhysRevA.32.3266](https://doi.org/10.1103/PhysRevA.32.3266).
- [28] Dieks D. *Communication by EPR devices*. Physics Letters A, 92(6):271–272, 1982. [https://doi.org/10.1016/0375-9601\(82\)90084-6](https://doi.org/10.1016/0375-9601(82)90084-6).
- [29] Wootters W K, Zurek W H. *A single quantum cannot be cloned*. Nature, 299(5886):802–803, 1982. [10.1038/299802a0](https://doi.org/10.1038/299802a0).
- [30] Shor P W. *Scheme for reducing decoherence in quantum computer memory*. Phys. Rev. A, 52:R2493–R2496, 1995. [10.1103/PhysRevA.52.R2493](https://doi.org/10.1103/PhysRevA.52.R2493).
- [31] Fowler A G, Mariantoni M, Martinis J M, et al. *Surface codes: Towards practical large-scale quantum computation*. Phys. Rev. A, 86:032324, 2012. [10.1103/PhysRevA.86.032324](https://doi.org/10.1103/PhysRevA.86.032324).
- [32] Raussendorf R, Harrington J. *Fault-Tolerant Quantum Computation with High Threshold in Two Dimensions*. Phys. Rev. Lett., 98:190504, 2007. [10.1103/PhysRevLett.98.190504](https://doi.org/10.1103/PhysRevLett.98.190504).
- [33] Dennis E, Kitaev A, Landahl A, et al. *Topological quantum memory*. Journal of Mathematical Physics, 43(9):4452–4505, 2002. [10.1063/1.1499754](https://doi.org/10.1063/1.1499754).
- [34] Kitaev A. *Fault-tolerant quantum computation by anyons*. Annals of Physics, 303(1):2–30, 2003. [https://doi.org/10.1016/S0003-4916\(02\)00018-0](https://doi.org/10.1016/S0003-4916(02)00018-0).

- [35] Viola L, Lloyd S. *Dynamical suppression of decoherence in two-state quantum systems*. Phys. Rev. A, 58:2733–2744, 1998. [10.1103/PhysRevA.58.2733](https://doi.org/10.1103/PhysRevA.58.2733).
- [36] Viola L, Knill E, Lloyd S. *Dynamical Decoupling of Open Quantum Systems*. Phys. Rev. Lett., 82:2417–2421, 1999. [10.1103/PhysRevLett.82.2417](https://doi.org/10.1103/PhysRevLett.82.2417).
- [37] Khodjasteh K, Lidar D A. *Fault-Tolerant Quantum Dynamical Decoupling*. Phys. Rev. Lett., 95:180501, 2005. [10.1103/PhysRevLett.95.180501](https://doi.org/10.1103/PhysRevLett.95.180501).
- [38] Uhrig G S. *Keeping a Quantum Bit Alive by Optimized π -Pulse Sequences*. Phys. Rev. Lett., 98:100504, 2007. [10.1103/PhysRevLett.98.100504](https://doi.org/10.1103/PhysRevLett.98.100504).
- [39] Cywiński L, Lutchyn R M, Nave C P, et al. *How to enhance dephasing time in superconducting qubits*. Phys. Rev. B, 77:174509, 2008. [10.1103/PhysRevB.77.174509](https://doi.org/10.1103/PhysRevB.77.174509).
- [40] Wallman J J, Emerson J. *Noise tailoring for scalable quantum computation via randomized compiling*. Phys. Rev. A, 94:052325, 2016. [10.1103/PhysRevA.94.052325](https://doi.org/10.1103/PhysRevA.94.052325).
- [41] Hashim A, Naik R K, Morvan A, et al. *Randomized Compiling for Scalable Quantum Computing on a Noisy Superconducting Quantum Processor*. Phys. Rev. X, 11:041039, 2021. [10.1103/PhysRevX.11.041039](https://doi.org/10.1103/PhysRevX.11.041039).
- [42] Temme K, Bravyi S, Gambetta J M. *Error Mitigation for Short-Depth Quantum Circuits*. Phys. Rev. Lett., 119:180509, 2017. [10.1103/PhysRevLett.119.180509](https://doi.org/10.1103/PhysRevLett.119.180509).

- [43] Johnson M A I, Madzik M T, Hudson F E, et al. *Beating the Thermal Limit of Qubit Initialization with a Bayesian Maxwell's Demon*. Phys. Rev. X, 12:041008, 2022. [10.1103/PhysRevX.12.041008](https://doi.org/10.1103/PhysRevX.12.041008).
- [44] Ristè D, Leeuwen J G, Ku H S, et al. *Initialization by Measurement of a Superconducting Quantum Bit Circuit*. Phys. Rev. Lett., 109:050507, 2012. [10.1103/PhysRevLett.109.050507](https://doi.org/10.1103/PhysRevLett.109.050507).
- [45] Valenzuela S O, Oliver W D, Berns D M, et al. *Microwave-Induced Cooling of a Superconducting Qubit*. Science, 314(5805):1589–1592, 2006.
- [46] Rower D A, Ateshian L, Li L H, et al. *Evolution of $1/f$ Flux Noise in Superconducting Qubits with Weak Magnetic Fields*. Phys. Rev. Lett., 130:220602, 2023. [10.1103/PhysRevLett.130.220602](https://doi.org/10.1103/PhysRevLett.130.220602).
- [47] Szczesniak D, Kais S. *Magnetic flux noise in superconducting qubits and the gap states continuum*. Sci Rep, 11(1), 2021. [10.1038/s41598-021-81450-x](https://doi.org/10.1038/s41598-021-81450-x).
- [48] Rower D A, Ateshian L, Li L H, et al. *Evolution of $1/f$ Flux Noise in Superconducting Qubits with Weak Magnetic Fields*. Phys. Rev. Lett., 130(22), 2023. [10.1103/physrevlett.130.220602](https://doi.org/10.1103/physrevlett.130.220602).
- [49] Bialczak R C, McDermott R, Ansmann M, et al. *$1/f$ Flux Noise in Josephson Phase Qubits*. Phys. Rev. Lett., 99:187006, 2007. [10.1103/PhysRevLett.99.187006](https://doi.org/10.1103/PhysRevLett.99.187006).
- [50] Heide C, Eckstein T, Boolakee T, et al. *Electronic Coherence and Coherent Dephasing in the Optical Control of Electrons in Graphene*. Nano Letters, 21(22):9403–9409, 2021.

- [51] Anton S M, Müller C, Birenbaum J S, et al. *Pure dephasing in flux qubits due to flux noise with spectral density scaling as $1/f^\alpha$* . Phys. Rev. B, 85:224505, 2012. [10.1103/PhysRevB.85.224505](https://doi.org/10.1103/PhysRevB.85.224505).
- [52] Burnett J J, Bengtsson A, Scigliuzzo M, et al. *Decoherence benchmarking of superconducting qubits*. npj Quantum Inf, 5(1), 2019. [10.1038/s41534-019-0168-5](https://doi.org/10.1038/s41534-019-0168-5).
- [53] Catelani G, Nigg S E, Girvin S M, et al. *Decoherence of superconducting qubits caused by quasiparticle tunneling*. Phys. Rev. B, 86:184514, 2012. [10.1103/PhysRevB.86.184514](https://doi.org/10.1103/PhysRevB.86.184514).
- [54] Nakamura Y, Pashkin Y A, Tsai J S. *Coherent control of macroscopic quantum states in a single-Cooper-pair box*. Nature, 398(6730):786–788, 1999. [10.1038/19718](https://doi.org/10.1038/19718).
- [55] Barends R, Kelly J, Megrant A, et al. *Superconducting quantum circuits at the surface code threshold for fault tolerance*. Nature, 508(7497):500–503, 2014. [10.1038/nature13171](https://doi.org/10.1038/nature13171).
- [56] Mohseni M, Read P, Neven H, et al. *Commercialize quantum technologies in five years*. Nature, 543(7644):171–174, 2017. [10.1038/543171a](https://doi.org/10.1038/543171a).
- [57] Enss C, Hunklinger S. *Low-Temperature Physics*. Springer-Verlag, 2005.
- [58] Esquinazi P. *Tunneling Systems in Amorphous and Crystalline Solids*. Springer Berlin Heidelberg, 1998.
- [59] Bergli J, Galperin Y M, Altshuler B L. *Decoherence in qubits due to low-frequency noise*. New Journal of Physics, 11(2):025002, 2009. [10.1088/1367-2630/11/2/025002](https://doi.org/10.1088/1367-2630/11/2/025002).

- [60] Bergli J, Galperin Y M, Altshuler B L. *Decoherence of a qubit by non-Gaussian noise at an arbitrary working point*. Phys. Rev. B, 74:024509, 2006. [10.1103/PhysRevB.74.024509](https://doi.org/10.1103/PhysRevB.74.024509).
- [61] Kakuyanagi K, Meno T, Saito S, et al. *Dephasing of a Superconducting Flux Qubit*. Phys. Rev. Lett., 98:047004, 2007. [10.1103/PhysRevLett.98.047004](https://doi.org/10.1103/PhysRevLett.98.047004).
- [62] Yoshihara F, Harrabi K, Niskanen A O, et al. *Decoherence of Flux Qubits due to $1/f$ Flux Noise*. Phys. Rev. Lett., 97:167001, 2006. [10.1103/PhysRevLett.97.167001](https://doi.org/10.1103/PhysRevLett.97.167001).
- [63] Galperin Y M, Altshuler B L, Bergli J, et al. *Non-Gaussian Low-Frequency Noise as a Source of Qubit Decoherence*. Phys. Rev. Lett., 96:097009, 2006. [10.1103/PhysRevLett.96.097009](https://doi.org/10.1103/PhysRevLett.96.097009).
- [64] Bergli J, Faoro L. *Exact solution for the dynamical decoupling of a qubit with telegraph noise*. Phys. Rev. B, 75:054515, 2007. [10.1103/PhysRevB.75.054515](https://doi.org/10.1103/PhysRevB.75.054515).
- [65] Ramon G. *Non-Gaussian signatures and collective effects in charge noise affecting a dynamically decoupled qubit*. Phys. Rev. B, 92:155422, 2015. [10.1103/PhysRevB.92.155422](https://doi.org/10.1103/PhysRevB.92.155422).
- [66] Ramon G, Hu X. *Decoherence of spin qubits due to a nearby charge fluctuator in gate-defined double dots*. Phys. Rev. B, 81:045304, 2010. [10.1103/PhysRevB.81.045304](https://doi.org/10.1103/PhysRevB.81.045304).
- [67] Ramon G. *Dynamical decoupling of a singlet-triplet qubit afflicted by a charge fluctuator*. Phys. Rev. B, 86:125317, 2012. [10.1103/PhysRevB.86.125317](https://doi.org/10.1103/PhysRevB.86.125317).

- [68] Müller C, Cole J H, Lisenfeld J. *Towards understanding two-level-systems in amorphous solids: insights from quantum circuits*. Reports on Progress in Physics, 82(12):124501, 2019. [10.1088/1361-6633/ab3a7e](https://doi.org/10.1088/1361-6633/ab3a7e).
- [69] Wold H J, Brox H, Galperin Y M, et al. *Decoherence of a qubit due to either a quantum fluctuator, or classical telegraph noise*. Phys. Rev. B, 86:205404, 2012. [10.1103/PhysRevB.86.205404](https://doi.org/10.1103/PhysRevB.86.205404).
- [70] Beaudoin F, Coish W A. *Microscopic models for charge-noise-induced dephasing of solid-state qubits*. Phys. Rev. B, 91:165432, 2015. [10.1103/PhysRevB.91.165432](https://doi.org/10.1103/PhysRevB.91.165432).
- [71] Paladino E, Faoro L, Falci G, et al. *Decoherence and $1/f$ Noise in Josephson Qubits*. Phys. Rev. Lett., 88:228304, 2002. [10.1103/PhysRevLett.88.228304](https://doi.org/10.1103/PhysRevLett.88.228304).
- [72] Abel B, Marquardt F. *Decoherence by quantum telegraph noise: A numerical evaluation*. Phys. Rev. B, 78:201302, 2008. [10.1103/PhysRevB.78.201302](https://doi.org/10.1103/PhysRevB.78.201302).
- [73] Vega I, Alonso D. *Dynamics of non-Markovian open quantum systems*. Rev. Mod. Phys., 89:015001, 2017. [10.1103/RevModPhys.89.015001](https://doi.org/10.1103/RevModPhys.89.015001).
- [74] Aharonov Y, Davidovich L, Zagury N. *Quantum random walks*. Phys. Rev. A, 48:1687–1690, 1993. [10.1103/PhysRevA.48.1687](https://doi.org/10.1103/PhysRevA.48.1687).
- [75] Childs A M, Farhi E, Gutmann S. *An Example of the Difference Between Quantum and Classical Random Walks*. Quantum Information Processing, 1(1/2):35–43, 2002. [10.1023/a:1019609420309](https://doi.org/10.1023/a:1019609420309).
- [76] Ambainis A, Kempe J, Rivosh A. *Coins make quantum walks faster*. in: Proceedings of ACM-SIAM Symposium on Discrete Algorithms, 2004.

- [77] Ambainis A. *Quantum Walk Algorithm for Element Distinctness*. SIAM Journal on Computing, 37(1):210–239, 2007.
- [78] Wocjan P, Abeyesinghe A. *Speedup via quantum sampling*. Phys. Rev. A, 78:042336, 2008. [10.1103/PhysRevA.78.042336](https://doi.org/10.1103/PhysRevA.78.042336).
- [79] Orsucci D, Briegel H J, Dunjko V. *Faster quantum mixing for slowly evolving sequences of Markov chains*. Quantum, 2:105, 2018. [10.22331/q-2018-11-09-105](https://arxiv.org/abs/1809.10501).
- [80] Childs A M. *Universal Computation by Quantum Walk*. Phys. Rev. Lett., 102:180501, 2009. [10.1103/PhysRevLett.102.180501](https://doi.org/10.1103/PhysRevLett.102.180501).
- [81] Lovett N B, Cooper S, Everitt M, et al. *Universal quantum computation using the discrete-time quantum walk*. Phys. Rev. A, 81:042330, 2010. [10.1103/PhysRevA.81.042330](https://doi.org/10.1103/PhysRevA.81.042330).
- [82] Travaglione B C, Milburn G J. *Implementing the quantum random walk*. Phys. Rev. A, 65:032310, 2002. [10.1103/PhysRevA.65.032310](https://doi.org/10.1103/PhysRevA.65.032310).
- [83] Sanders B C, Bartlett S D, Tregenna B, et al. *Quantum quincunx in cavity quantum electrodynamics*. Phys. Rev. A, 67:042305, 2003. [10.1103/PhysRevA.67.042305](https://doi.org/10.1103/PhysRevA.67.042305).
- [84] Dür W, Raussendorf R, Kendon V M, et al. *Quantum walks in optical lattices*. Phys. Rev. A, 66:052319, 2002. [10.1103/PhysRevA.66.052319](https://doi.org/10.1103/PhysRevA.66.052319).
- [85] Manouchehri K, Wang J. *Physical Implementation of Quantum Walks*. Springer Berlin Heidelberg, 2014.
- [86] Venegas-Andraca S E. *Quantum walks: a comprehensive review*. Quantum Inf Process, 11(5):1015–1106, 2012. [10.1007/s11128-012-0432-5](https://doi.org/10.1007/s11128-012-0432-5).

- [87] Arnault P. Discrete-time quantum walks and gauge theories, 2021.
- [88] Portugal R. Quantum Walks and Search Algorithms. Springer New York, 2013.
- [89] Kitagawa T, Rudner M S, Berg E, et al. *Exploring topological phases with quantum walks*. Phys. Rev. A, 82:033429, 2010. [10.1103/PhysRevA.82.033429](https://doi.org/10.1103/PhysRevA.82.033429).
- [90] Cedzich C, Rybár T, Werner A H, et al. *Propagation of Quantum Walks in Electric Fields*. Phys. Rev. Lett., 111:160601, 2013. [10.1103/PhysRevLett.111.160601](https://doi.org/10.1103/PhysRevLett.111.160601).
- [91] Arnault P, Pepper B, Pérez A. *Quantum walks in weak electric fields and Bloch oscillations*. Phys. Rev. A, 101:062324, 2020. [10.1103/PhysRevA.101.062324](https://doi.org/10.1103/PhysRevA.101.062324).
- [92] Arnault P, Debbasch F. *Landau levels for discrete-time quantum walks in artificial magnetic fields*. Physica A: Statistical Mechanics and its Applications, 443:179–191, 2016. [10.1016/j.physa.2015.08.011](https://doi.org/10.1016/j.physa.2015.08.011).
- [93] Arnault P, Debbasch F. *Quantum walks and discrete gauge theories*. Phys. Rev. A, 93:052301, 2016. [10.1103/PhysRevA.93.052301](https://doi.org/10.1103/PhysRevA.93.052301).
- [94] Cedzich C, Geib T, Werner A H, et al. *Quantum walks in external gauge fields*. Journal of Mathematical Physics, 60(1), 2019. [10.1063/1.5054894](https://doi.org/10.1063/1.5054894).
- [95] Di Molfetta G, Brachet M, Debbasch F. *Quantum walks in artificial electric and gravitational fields*. Physica A: Statistical Mechanics and its Applications, 397:157–168, 2014. <https://doi.org/10.1016/j.physa.2013.11.036>.

- [96] Arrighi P, Di Molfetta G, Facchini S. *Quantum walking in curved spacetime: discrete metric*. Quantum, 2:84, 2018. [10.22331/q-2018-08-22-84](https://arxiv.org/abs/10.22331/q-2018-08-22-84).
- [97] Arnault P, Debbasch F. *Quantum walks and gravitational waves*. Annals of Physics, 383:645–661, 2017. [10.1016/j.aop.2017.04.003](https://arxiv.org/abs/10.1016/j.aop.2017.04.003).
- [98] Arrighi P, Molfetta G D, Marquez-Martin I, et al. *From curved spacetime to spacetime-dependent local unitaries over the honeycomb and triangular Quantum Walks*. Sci Rep, 9(1), 2019. [10.1038/s41598-019-47535-4](https://arxiv.org/abs/10.1038/s41598-019-47535-4).
- [99] Molfetta G D, Pérez A. *Quantum walks as simulators of neutrino oscillations in a vacuum and matter*. New J. Phys., 18(10):103038, 2016. [10.1088/1367-2630/18/10/103038](https://arxiv.org/abs/10.1088/1367-2630/18/10/103038).
- [100] Zylberman J, Di Molfetta G, Brachet M, et al. *Quantum simulations of hydrodynamics via the Madelung transformation*. Phys. Rev. A, 106:032408, 2022. [10.1103/PhysRevA.106.032408](https://arxiv.org/abs/10.1103/PhysRevA.106.032408).
- [101] Panahiyan S, Fritzsche S. *Toward simulation of topological phenomena with one-, two-, and three-dimensional quantum walks*. Phys. Rev. A, 103:012201, 2021. [10.1103/PhysRevA.103.012201](https://arxiv.org/abs/10.1103/PhysRevA.103.012201).
- [102] Randall L, Sundrum R. *Large Mass Hierarchy from a Small Extra Dimension*. Phys. Rev. Lett., 83:3370–3373, 1999. [10.1103/PhysRevLett.83.3370](https://arxiv.org/abs/10.1103/PhysRevLett.83.3370).
- [103] Cai X, Yang H, Shi H L, et al. *Multiparticle Quantum Walks and Fisher Information in One-Dimensional Lattices*. Phys. Rev. Lett., 127:100406, 2021. [10.1103/PhysRevLett.127.100406](https://arxiv.org/abs/10.1103/PhysRevLett.127.100406).

- [104] Bisio A, D’Ariano G M, Mosco N, et al. *Solutions of a Two-Particle Interacting Quantum Walk*. Entropy, 20(6), 2018. [10.3390/e20060435](https://doi.org/10.3390/e20060435).
- [105] Deutsch D, Penrose R. *Quantum theory, the Church–Turing principle and the universal quantum computer*. Proceedings of the Royal Society of London. A. Mathematical and Physical Sciences, 400(1818):97–117, 1985. [10.1098/rspa.1985.0070](https://doi.org/10.1098/rspa.1985.0070).
- [106] Arrighi P. *An overview of quantum cellular automata*. Nat Comput, 18(4):885–899, 2019. [10.1007/s11047-019-09762-6](https://doi.org/10.1007/s11047-019-09762-6).
- [107] Arrighi P, Bény C, Farrelly T. *A quantum cellular automaton for one-dimensional QED*. Quantum Inf Process, 19(3), 2020. [10.1007/s11128-019-2555-4](https://doi.org/10.1007/s11128-019-2555-4).
- [108] Navarrete-Benlloch C, Pérez A, Roldán E. *Nonlinear optical Galton board*. Phys. Rev. A, 75:062333, 2007. [10.1103/PhysRevA.75.062333](https://doi.org/10.1103/PhysRevA.75.062333).
- [109] Nambu Y, Jona-Lasinio G. *Dynamical Model of Elementary Particles Based on an Analogy with Superconductivity. I*. Phys. Rev., 122:345–358, 1961. [10.1103/PhysRev.122.345](https://doi.org/10.1103/PhysRev.122.345).

Publications



PAPER

Prethermalization of quantum systems interacting with non-equilibrium environments

OPEN ACCESS

RECEIVED
21 May 2020REVISED
15 July 2020ACCEPTED FOR PUBLICATION
21 July 2020PUBLISHED
24 August 2020Andreu Anglés-Castillo¹, Mari Carmen Bañuls^{2,3,5}, Armando Pérez¹ and Inés De Vega⁴¹ Departamento de Física Teórica & IFIC, Universidad de Valencia-CSIC, 46100 Burjassot (Valencia) Spain² Max-Planck-Institut für Quantenoptik, Hans-Kopfermann-Str. 1, 85748 Garching, Germany³ Munich Center for Quantum Science and Technology (MCQST), Schellingstr. 4, D-80799 München, Germany⁴ Department of Physics and Arnold Sommerfeld Center for Theoretical Physics, Ludwig-Maximilians-University Munich, Germany⁵ Author to whom any correspondence should be addressed.E-mail: banulsm@mpq.mpg.de

Keywords: open quantum systems, prethermalization, master equations

Original content from
this work may be used
under the terms of the
[Creative Commons
Attribution 4.0 licence](https://creativecommons.org/licenses/by/4.0/).Any further distribution
of this work must
maintain attribution to
the author(s) and the
title of the work, journal
citation and DOI.

Abstract

The usual paradigm of open quantum systems falls short when the environment is actually coupled to additional fields or components that drive it out of equilibrium. Here we explore the simplest such scenario, by considering a two level system coupled to a first thermal reservoir that in turn couples to a second thermal bath at a different temperature. We derive a master equation description for the system and show that, in this situation, the dynamics can be especially rich. In particular, we observe prethermalization, a transitory phenomenon in which the system initially approaches thermal equilibrium with respect to the first reservoir, but after a longer time converges to the thermal state dictated by the temperature of the second environment. Using analytical arguments and numerical simulations, we analyze the occurrence of this phenomenon, and how it depends on temperatures and coupling strengths. The phenomenology gets even richer if the system is placed between two such non-equilibrium environments. In this case, the energy current through the system may exhibit transient features and even switch direction, before the system eventually reaches a non-equilibrium steady state.

1. Introduction

The standard theory of open quantum systems (OQS) typically considers that the system is coupled to a single reservoir in equilibrium to analyse properties such as decoherence, dissipation and non-Markovianity [1–4]. A richer situation emerges in the frame of quantum thermodynamics and thermal machines, in which the system is coupled to two or more reservoirs, each of them equilibrated at a different temperature and/or chemical potential [5–8]. Once the coupling is activated, the open system evolves towards a non-equilibrium steady state that may contain persistent heat, particle or spin currents. An even more involved scenario occurs when the system is coupled to one or more reservoirs that are each of them out of equilibrium and therefore evolve in time. As a consequence, the action of the environment into the system dynamics is no longer encoded in a correlation function that is time-translational invariant, such that $\alpha(t, \tau) = \alpha(t - \tau)$, but rather on a correlation function that depends on both the current time of evolution t and the past times τ .

The motivation to analyze complex environments beyond the standard OQS paradigm of single and multiple equilibrium reservoirs is strong. From an application perspective, out of equilibrium environments that present a temperature gradient can be encountered in electron transfer processes in quantum chemistry and biology [9], in cellular media [10] and even in the thermosynthesis processes that use the solar energy to create chemical compounds [11], to name just a few examples. These types of environments may indeed be driven by an external source, corresponding to other molecular or biological structures or even to the electromagnetic field. Non-equilibrium environments are also present in quantum technological devices,

where the quantum system of interest may be directly coupled to an environment that is itself coupled to a second reservoir, thermalized at a different temperature. Such temperature gradient of the different components and subsystems surrounding the quantum system of interest is particularly present in quantum computers [12, 13]. Superconducting qubits, for instance, are cooled down to cryostatic temperatures, while their surrounding components, including amplifiers and processing units, as well as the cables and waveguides that connect them to each other and to the qubit, are at higher temperatures the further they are from the circuit.

Describing these situations is of fundamental and timely interest, but it also represents a significant challenge, as the effects of indirect reservoirs on the OQS dynamics cannot be captured with a simple Markovian approximation. To this aim, one possibility is to compute the full dynamics, including the system and the environments, and then trace out the environmental degrees of freedom to obtain the OQS reduced dynamics. However, the dimension of the full Hilbert space grows exponentially fast with the number of degrees of freedom, and further, the relevant states may be largely entangled as well, which makes inefficient a direct use of state of the art numerical methods like Monte Carlo [14–16] and matrix product states [17–21].

While several approaches can be found in the literature to describe the full dynamics of the system coupled to a single bath [22–25], much fewer works can be found that treat the presence of a second environment driving the first one out of equilibrium. In this context, reference [26] considers an effective (surrogate) Hamiltonian to describe the system and its direct coupling to a primary environment (represented by a finite number of modes), while a second and larger environment is introduced and coupled to the first. This second environment is treated stochastically. Here we propose an alternative approach, which extends the standard tools of the OQS theory, namely the weak coupling approximation and the master equation approach, to consistently tackle the problem in at least a limit of interest.

To be specific, we consider a two-level quantum system coupled to a first reservoir (RI) that is in turn coupled to a second reservoir (RII). Initially, each reservoir is in a thermal state at a different temperature, respectively T_I and T_{II} . We additionally consider that RII induces a Markovian evolution on the modes of RI so that they thermalize efficiently. Therefore, even if RI is initially in thermal equilibrium, the coupling to a second reservoir at a different temperature will drive it away from it, and enforce its evolution towards a new equilibrium state with respect to RII. Thus, the dissipation of the open system will display very rich features reflecting the interplay between two different timescales: thermalization of the system at a temperature T_I , and the thermalization to its final equilibrium state with T_{II} . If the conditions of the environment are suitable, and these two timescales are temporally separated, prethermalization [27] of the OQS is observed, which is a stage in which the system remains thermalized at T_I .

The plan of the paper is the following: We present the details of our model in section 2, while in section 3 we discuss the master equation that is used to describe the reduced dynamics of the open system. This master equation depends on a set of correlation functions that encode the effects of both reservoirs in the open system, and which are discussed in section 4. Sections 5 and 6 describe the effects of prethermalization when considering a single and two out of equilibrium reservoirs, respectively. Finally, we draw some conclusions in section 7.

2. Model with two interacting environments

As is standard in the theory of OQS [3, 28, 29] we consider that the total evolution of system plus the environment is unitary and described by the Hamiltonian,

$$H = H_S + H_E + H_{\text{int}}, \quad (1)$$

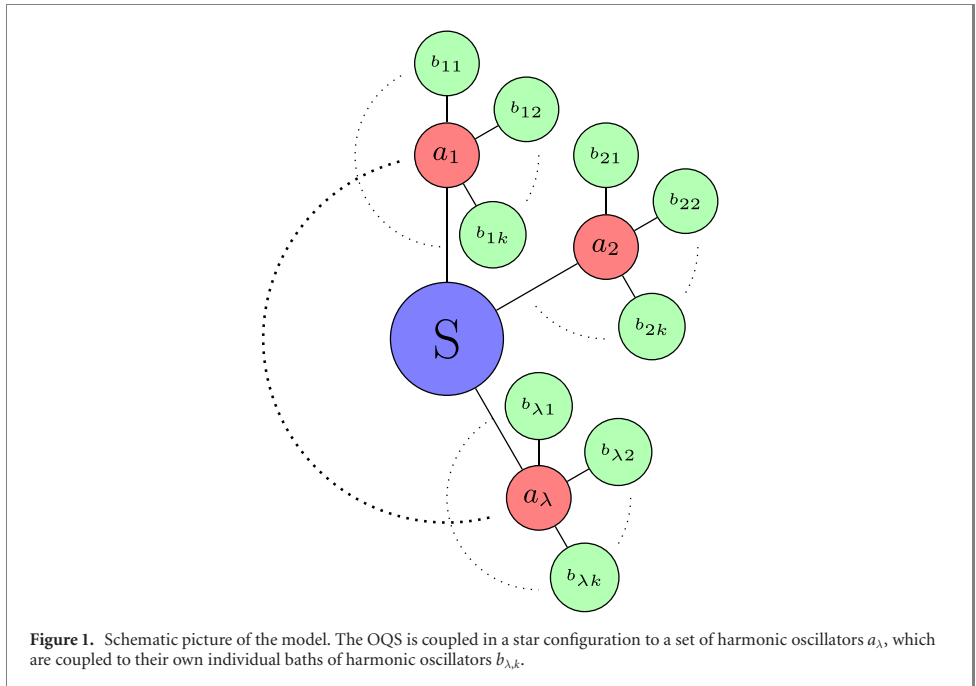
where H_S and H_E are the free Hamiltonians of the system and environment, respectively, and H_{int} is the interaction Hamiltonian between system and environment. We model the system as a two level system with the free Hamiltonian

$$H_S = \frac{1}{2}\omega_0\sigma_z, \quad (2)$$

where ω_0 is the energy⁶ gap between levels. We model the environment to which the system is coupled as a set of open harmonic oscillators that is a first reservoir (RI) of harmonic oscillators where each mode in RI is coupled to a independent reservoir, included in the second reservoir (RII). The Hamiltonian describing this environment is

$$H_E = H_{RI} + H_{RII} + H_{\text{int},2}, \quad (3)$$

⁶ Throughout this article we consider natural units in which the reduced Plank constant and the Boltzmann constant $\hbar = k_B = 1$.



where

$$H_{\text{RI}} = \sum_{\lambda} \omega_{\lambda} a_{\lambda}^{\dagger} a_{\lambda} \quad \text{and} \quad H_{\text{RII}} = \sum_{\lambda,k} \omega_{\lambda,k} b_{\lambda,k}^{\dagger} b_{\lambda,k}, \quad (4)$$

are the free Hamiltonians of RI and RII, respectively, with operators that obey the commutation relations

$$[a_{\lambda}, a_{\lambda'}^{\dagger}] = \delta_{\lambda,\lambda'}, \quad \text{and} \quad [b_{\lambda,k}, b_{\lambda',k'}^{\dagger}] = \delta_{\lambda,\lambda'} \delta_{k,k'}, \quad (5)$$

and whose interaction

$$H_{\text{int},2} = \sum_{\lambda} \left(a_{\lambda}^{\dagger} \otimes \sum_k \tilde{g}_{\lambda,k} b_{\lambda,k} + a_{\lambda} \otimes \sum_k \tilde{g}_{\lambda,k}^* b_{\lambda,k}^{\dagger} \right), \quad (6)$$

conserves the boson number. The coupling strength between the λ -th oscillator in RI and the k th oscillator in RII is $\tilde{g}_{\lambda,k}$. The system is in a *star configuration*, i.e. the QOS is coupled to all the λ bosonic operators of RI, and in turn each of these is coupled to a reservoir of harmonic oscillators that is a part of RII, as depicted in figure 1. Only the first reservoir couples directly to the QOS, with the interaction Hamiltonian

$$H_{\text{int}} = \sigma_{-} \otimes \sum_{\lambda} g_{\lambda}^* a_{\lambda}^{\dagger} + \sigma_{+} \otimes \sum_{\lambda} g_{\lambda} a_{\lambda}, \quad (7)$$

which only considers interactions that conserve the particle number. We take as initial state a tensor product,

$$\rho(0) = \rho_{\text{S}}(0) \otimes \rho_{\text{E}}(0) = \rho_{\text{S}}(0) \otimes \rho_{\text{I}}^{\text{th}}(\beta_{\text{I}}) \otimes \rho_{\text{II}}^{\text{th}}(\beta_{\text{II}}). \quad (8)$$

The initial state of the system can be arbitrary, while the initial states of the reservoirs are assumed to be thermal, possibly at different temperatures,

$$\rho_i^{\text{th}}(\beta_i) = \frac{e^{-\beta_i H_{\text{R}i}}}{Z_i(\beta_i)}, \quad (9)$$

where $Z(\beta_i) = \text{Tr}\{e^{-\beta_i H_{\text{R}i}}\}$ is the partition function and $\beta_i = 1/T_i$ is the inverse temperature of each reservoir, $i = \{\text{I}, \text{II}\}$.

Each reservoir may have a different spectral function depending on their microscopic properties and the problem considered. In our analysis, we consider the Caldeira–Leggett phenomenological model of spectral functions [30], which reads

$$J_i(\omega) = g_i \omega_{ci}^{1-s_i} \omega^{s_i} e^{-\omega/\omega_{ci}}, \quad (10)$$

where g_i is the strength of the coupling, s_i is a factor that takes different values depending on the particular environment that needs to be modelled, and ω_{ci} determines a smooth frequency cut off for the modes of the reservoir.

3. Study of the system evolution

To obtain a closed equation for the dynamics of the open quantum system, we consider that it is weakly coupled to its environment, which makes it evolve slowly. Thus we can derive a second order weak coupling master equation (ME) for the reduced density matrix of the open quantum system. The derivation of the ME is standard and can be found in numerous works [28, 31],

$$\frac{d}{dt} \rho_S(t) = -i[H_S, \rho_S(t)] + \left(\int_0^t d\tau \alpha^+(t, \tau) [V_{\tau-t} \sigma_+ \rho_S(t), \sigma_-] + \int_0^t d\tau \alpha^-(t, \tau) [V_{\tau-t} \sigma_- \rho_S(t), \sigma_+] + \text{h.c.} \right), \tag{11}$$

where $V_t \mathcal{O} = e^{iH_S t} \mathcal{O} e^{-iH_S t}$ is the free evolution of the operator $\mathcal{O} = \{\sigma_+, \sigma_-\}$, and the correlation functions are defined by

$$\alpha^+(t, \tau) = \text{Tr}\{B(t)^\dagger B(\tau) \rho_E(0)\}, \quad \alpha^-(t, \tau) = \text{Tr}\{B(t) B(\tau)^\dagger \rho_E(0)\}, \tag{12}$$

with $B(t) = e^{iH_E t} B e^{-iH_E t}$ the free evolution of the environment operator $B = \sum_\lambda g_\lambda a_\lambda$. Notice that this equation is second order in the interaction operator B , and that no first order term is present, since it is proportional to $\text{Tr}_E\{H_{\text{int}}(t) \rho_E(0)\}$, which is null for the initial state defined in equations (8) and (9). This equation is a time-local ME, since its evolution can be recast in the form

$$\dot{\rho}_S(t) = \Lambda_t[\rho_S(t)], \tag{13}$$

where Λ_t is a linear map, such that $\Lambda_t[\rho(t)]$ is Hermitian and traceless for any ρ . To fully describe the OQS through the differential equation (11), the correlation functions (12) have to be computed for the initial states $\rho_E(0)$ defined in equations (8) and (9). The following section is devoted to this derivation, but first we rewrite the ME in equation (11) under its canonical form.

3.1. Canonical form of the ME

Any time-local ME equation of the form (13) can be recast into a canonical ME [32], of the form

$$\frac{d}{dt} \rho_S(t) = -i[H(t), \rho_S(t)] + \sum_{k=1}^{d^2-1} \gamma_k(t) \left(L_k(t) \rho_S(t) L_k^\dagger(t) - \frac{1}{2} \{L_k^\dagger(t) L_k(t), \rho_S(t)\} \right), \tag{14}$$

where $\gamma_k(t)$ are the canonical decay rates corresponding to the canonical decoherence channels $L_k(t)$, with $k = 1, \dots, d^2 - 1$, and d the dimension of the Hilbert space of the OQS. $H(t)$ is, in general, not identical to the free Hamiltonian of the system, since the interaction with the environment modifies it. The most common effect is a shift of the natural frequency of the OQS, the so-called Lamb shift. The equation is often written in a more compact form as

$$\frac{d}{dt} \rho_S(t) = -i[H(t), \rho_S(t)] + \mathcal{D}(t, \rho_S(t)). \tag{15}$$

where the first term represents the unitary evolution of the OQS. The second term in (15) encompasses the dissipative part of the evolution.

Recasting the time-local ME in this form allows us to easily evaluate whether, despite being an approximated equation, it still preserves complete positivity of the evolution. In detail, if the decay rates $\gamma_k(t)$ are non-negative we can ensure that this is the case and that the dynamical map of the OQS is Markovian [32]. The canonical decay rates, and the Lamb shift for our model, are discussed in the next section and in appendix A.

4. Out-of-equilibrium correlation functions and decay rates

Obtaining the correlation functions (12) requires to compute the time evolution of $a_\lambda(t)$ in the operator $B(t) = \sum_\lambda g_\lambda a_\lambda(t)$. We can simplify this calculation by assuming a large separation of timescales between the second and the first reservoir. Specifically, we consider that the modes of the first reservoir, $a_\lambda(t)$ slowly evolve towards an equilibrium state with respect to the second reservoir, and that this evolution is well

described with the Markov approximation. This is discussed in appendix B, while the computation of the correlation functions is treated in appendix C. Thus, the correlation functions are given by

$$\begin{aligned} \alpha^+(t, t') &= \frac{1}{\pi} \int d\omega J_I(\omega) n_I(\omega) e^{i\omega t'} e^{-\frac{J_{II}(\omega)}{2}(2t-t')} + \frac{1}{\pi^2} \iint d\omega d\omega' J_I(\omega) n_{II}(\omega') K(\omega, \omega') C(\omega, \omega', t, t'), \\ \alpha^-(t, t') &= \frac{1}{\pi} \int d\omega J_I(\omega) (n_I(\omega) + 1) e^{-i\omega t'} e^{-\frac{J_{II}(\omega)}{2}(2t-t')} + \frac{1}{\pi^2} \iint d\omega d\omega' J_I(\omega) (n_{II}(\omega') + 1) K(\omega, \omega') \\ &\quad \times C^*(\omega, \omega', t, t'), \end{aligned} \quad (16)$$

where $J_i(\omega)$, with $i = \{I, II\}$, are the spectral functions of each reservoir, which have the general form (10), and $n_i(\omega) = [\exp(\beta_i \omega) - 1]^{-1}$ is the average thermal number of quanta in mode ω at inverse temperature β_i . We have defined the function

$$K(\omega, \omega') = \frac{J_{II}(\omega')}{\left(\frac{J_{II}(\omega)}{2}\right)^2 + (\omega - \omega')^2}, \quad (17)$$

which is proportional to a Lorentzian kernel of width $J_{II}(\omega)/2$, and the function

$$C(\omega, \omega', t, t') = \left[e^{-i\omega' t} - e^{(-i\omega - \frac{J_{II}(\omega)}{2})t} \right] \left[e^{i\omega'(t-t')} - e^{(i\omega - \frac{J_{II}(\omega)}{2})(t-t')} \right]. \quad (18)$$

Notice that, even though we can consider that the open system is weakly coupled to RI, and thus its master equation is obtained within a second order perturbation theory, a Markov approximation cannot be taken in a straightforward way. The reason is that the correlation functions (16) are no longer dependent on the time difference $t - \tau$, but on both times t and τ such that one can not simply extend the integration limits in equation (11) by assuming that the integral kernel decays much faster than the system evolution time-scale, as it is done in the Markov approximation.

We observe that the second term of the correlation functions contains the resonant term $K(\omega, \omega')$ (see equation (17)) with a width proportional to the coupling strength between environments, and centered at $\omega = \omega'$. Approximating this term by a delta function is consistent with the weak coupling approximation already considered between RI and RII. Using this approach, we obtain an analytical approximation for the canonical decay rates $\gamma_{\pm}(t)$, which correspond to the decoherence channels $L_{\pm} = \sigma^{\pm}$ (see appendix A), and which can be split into two contributions, $\gamma_{\pm}(t) = \gamma_{\pm}^{ST}(t) + \gamma_{\pm}^{LT}(t)$, where the terms are labelled in reference to their short time (ST) or long time (LT) dominance. The ST terms are

$$\begin{aligned} \gamma_+^{ST}(t) &= J_I(\omega_0) n_I(\omega_0) e^{-J_{II}(\omega_0)t} \\ \gamma_-^{ST}(t) &= J_I(\omega_0) (n_I(\omega_0) + 1) e^{-J_{II}(\omega_0)t}, \end{aligned} \quad (19)$$

and the LT terms read

$$\begin{aligned} \gamma_+^{LT}(t) &= J_I(\omega_0) n_{II}(\omega_0) (1 - e^{-J_{II}(\omega_0)t}), \\ \gamma_-^{LT}(t) &= J_I(\omega_0) (n_{II}(\omega_0) + 1) (1 - e^{-J_{II}(\omega_0)t}). \end{aligned} \quad (20)$$

The validity of approximating equation (17) by a delta function is discussed in D. These decay rates present a very suggestive form: at short times, the LT terms of each decay rate is negligible, while at later times it dominates (see appendix D for a visual reference). The strength of the decay rates is governed by the spectral function of the first environment, while the second environment spectral function is responsible for the timescales at which each term dominates.

With this approximate expression for the decay rates it is possible to prove analytically that indeed the OQS evolves, at long times, to a thermal state at the inverse temperature of the second reservoir β_{II} (see appendix E). Furthermore, since they are non-negative at all times, we can ensure that the ME preserves complete positivity.

5. Prethermalization

The decay rates obtained in the previous section already suggest that the evolution of the OQS may exhibit two different timescales. However, as it will soon become apparent, how well defined these two scales are will be strongly determined not only by the value of g_{II} , but also by other factors, such as the temperature of each reservoir. Depending on these factors, there may be a transitory state in which the OQS remains close to a thermal state corresponding to the initial temperature of RI, but after some longer time it finally relaxes to a thermal state with the temperature of RII.

This transient effect is an instance of *prethermalization*, a phenomenon in which the system, after a short time, seems to relax to a state different from the true thermal equilibrium, which is eventually reached after a much longer timescale [27, 33–35]. The most studied scenario of prethermalization concerns weakly non-integrable systems, in which an eigenstate of an integrable model is evolved under a quenched Hamiltonian that weakly breaks integrability. The short time dynamics is still determined by almost conserved quantities, and the system arrives to a prethermalized state, but at long times the breaking of the integrability dominates and the system finally thermalizes [36]. The phenomenon has also been studied in the context of OQS in [37, 38] and observed experimentally in ultra-cold bosonic atoms [39–41].

In our setup, a small coupling to the second reservoir ($g_{II} \neq 0$) can play a similar role to the integrability breaking, as it perturbs the thermal equilibrium of the environment RI (which would otherwise remain stable). In this way, the initial temperature of RI may determine the short time evolution and the arrival to a prethermal state, while the final equilibrium is determined by RII. We will thus consider that prethermalization has occurred when the system reaches a state, independent of its initial conditions, close to the thermal equilibrium at β_I , and this state is maintained for a finite time, before the evolution definitely drives the system to the equilibrium with RII.

In order to verify the occurrence of the effect, we analyse the evolution of all possible initial states. We conveniently express the density matrix in terms of the polarization vector, $\rho(t) = (I + \vec{p}(t) \cdot \vec{\sigma})/2$ and integrate the time evolution equations (see appendix A). The formal solution for the polarization vector is

$$\vec{p}(t) = r(t)R(t)\vec{p}(0) + \vec{d}(t), \tag{21}$$

where

$$R(t) = \begin{pmatrix} \cos(\tilde{\Omega}(t)) & -\sin(\tilde{\Omega}(t)) & 0 \\ \sin(\tilde{\Omega}(t)) & \cos(\tilde{\Omega}(t)) & 0 \\ 0 & 0 & 1 \end{pmatrix}, \tag{22}$$

is a rotation matrix, that performs a rotation about the z axis with angular frequency $\tilde{\Omega}(t) = \int_0^t dt' \Omega(t')$, where $\Omega(t)$ is the shifted frequency of the OQS due to the action of the environment (see appendix A), $r(t) = e^{-\tilde{\Gamma}(t)}$ is a scaling factor that affects equally all components, with $\tilde{\Gamma}(t) = \int_0^t dt' (\gamma_+(t') + \gamma_-(t'))$, where $\gamma_+(t)$ and $\gamma_-(t)$ are the canonical decay rates, and $\vec{d}(t) = (0, 0, c(t))$ is a displacement vector in the z direction, with

$$c(t) = e^{-\tilde{\Gamma}(t)} \int_0^t dt' e^{\tilde{\Gamma}(t')} (\gamma_+(t') - \gamma_-(t')). \tag{23}$$

From this result, it is apparent that the effect of the dynamical map on any state is to rotate the polarization vector around the z axis, rescale it by $r(t)$ and add a displacement $c(t)$ along the vertical direction. These transformations are independent of the initial state, hence the space of accessible states, initially described by the volume limited by the Bloch sphere, is isotropically contracted and shifted, and can be characterized by its time dependent radius and center.

We would like to emphasize that the Lamb shift does not play any role in the evolution of the diagonal elements of the reduced density matrix, which ultimately means that it does not affect either the long time thermalization or the prethermalization dynamics. It is encoded in the angular frequency of equation (22) and thus it has the effect of rotating the ball of accessible states with an angular velocity different from ω_0 , but does not affect the rescaling and displacement of the whole space.

This representation allows us to understand how fast the memory of the initial state is lost, and in which state the OQS is. For the approximate decay rates equations (19) and (20) we obtain the following expression for the radius of the ball of accessible states

$$r(t) = e^{-(2n_{II}(\omega_0)+1)J_I(\omega_0)t} \exp\left(2(n_{II}(\omega_0) - n_I(\omega_0)) \frac{J_I(\omega_0)}{J_{II}(\omega_0)} (1 - e^{-J_{II}(\omega_0)t})\right), \tag{24}$$

which in the limit $J_{II}(\omega_0)t \rightarrow 0$ becomes

$$r(t) = e^{-(2n_{II}(\omega_0)+1)J_I(\omega_0)t}, \tag{25}$$

that is the expression that we would obtain if only RI was considered. This means that the rate at which the volume of the accessible states reduces is mainly governed by RI. A smaller coupling between OQS and RI would cause a slower reduction of the accessible states space. The center of the ball of accessible states is given by the evolved polarization vector of the maximally mixed state, namely the origin of the Bloch sphere, and is thus at $\vec{c}(t) = (0, 0, c(t))$ with

$$c(t) = -J_I(\omega_0) \int_0^t dt' e^{-(2n_{II}(\omega_0)+1)J_I(\omega_0)(t-t')} \exp\left(2(n_I(\omega_0) - n_{II}(\omega_0)) J_I(\omega_0) \frac{e^{-J_{II}(\omega_0)t} - e^{-J_{II}(\omega_0)t'}}{J_{II}(\omega_0)}\right). \tag{26}$$

This expression has no analytic solution, but can be solved in the short time limit (ST), $J_{II}(\omega_0)t \ll 1$. If the exponentials inside the second factor are Taylor expanded in terms of $J_{II}(\omega_0)t$ and $J_{II}(\omega_0)t' \leq J_{II}(\omega_0)t$ up to first order, the resulting integral is solvable and yields

$$c_{ST}(t) = \frac{e^{-J_I(2n_I(\omega_0)+1)t} - 1}{2n_I(\omega_0) + 1}. \tag{27}$$

Within this regime, we distinguish two limiting cases

- When $J_I(\omega_0)(2n_I(\omega_0) + 1)t \ll 1$, equation (27) approximately reduces to

$$c_{ST}(t) \approx \frac{-J_I(2n_I(\omega_0) + 1)}{2n_I(\omega_0) + 1}t, \tag{28}$$

which at time $t = 0$ corresponds to the center of the Bloch sphere.

- When $J_I(\omega_0)(2n_I(\omega_0) + 1)t \gg 1$, the exponential in equation (27) vanishes, and this expression becomes

$$c_{ST} = \frac{-1}{2n_I(\omega_0) + 1}, \tag{29}$$

such that $(0, 0, c_{ST})$ corresponds to the thermal state $\rho_S^{th}(\beta_I)$. This expression holds when

$$J_I(\omega_0)(2n_I(\omega_0) + 1) \gg J_{II}(\omega_0), \tag{30}$$

in which case the ball of accessible states is centred around the point corresponding to the thermal state of the OQS at β_I as long as $J_{II}(\omega_0)t \ll 1$. Moreover, in this limit the radius of the ball of accessible states equations (24) and (25) is close to 0, meaning that the state of the OQS is independent of the initial condition and close to the state $\rho_S^{th}(\beta_I)$, which shows that the system thermalizes to β_I .

Equation (30), shows that the condition for the OQS to prethermalize to β_I , depends on the relationship of this temperature and the coupling strengths, but is independent of β_{II} . In the next section we analyse how β_{II} affects the prethermalization.

The long time (LT) limit ($J_{II}(\omega_0)t \rightarrow \infty$) of equation (26), studied analytically in appendix F, yields

$$c_{LT} = \frac{-1}{2n_{II}(\omega_0) + 1}, \tag{31}$$

where the point $(0, 0, c_{LT})$ corresponds to the thermal state $\rho_S^{th}(\beta_{II})$ as the asymptotic state. This asymptotic state was also checked analytically using the approximate decay rates in appendix E.

To illustrate the above discussion, we display in figures 2 and 3 the evolution of the system in two different scenarios. In both cases, the time dependence of the $\rho_{++}(t) = \langle +|\rho_S(t)|+ \rangle$ component⁷ of the state of the system is shown for several initial pure states, which allows us to visualize the evolution of the ball of accessible states. In the first case, for $\beta_I = 1, \beta_{II} = 0.1$ and $g_{II} = 10^{-5}$ we observe prethermalization (figure 2), but when the coupling is increased to $g_{II} = 10^{-2}$ (figure 3), the phenomenon does not appear.

Following our previous considerations, we identify two relevant timescales that govern the OQS evolution in the prethermalization regime of figure 2. First, the time t_1 after which the OQS has evolved to the thermal state at β_I . At this time, the space of accessible states has already contracted to a point, so that the state reached is independent of the initial condition. The second timescale t_{II} determines the time required for thermalization to the asymptotic state $\rho_S^{th}(\beta_{II})$. If t_1 is sufficiently smaller than t_{II} , as in figure 2, the system first evolves to $\rho_S^{th}(\beta_I)$ (red dot), and stays close to it for a certain time t_{pr} , which we call prethermalization time. After this time, it smoothly evolves to $\rho_S^{th}(\beta_{II})$ (green dot). As shown in figure 3, when the conditions of the problem do not allow for prethermalization, we observe the thermalization of any initial condition directly to the state $\rho_S^{th}(\beta_{II})$, without any transitory approach to $\rho_S^{th}(\beta_I)$.

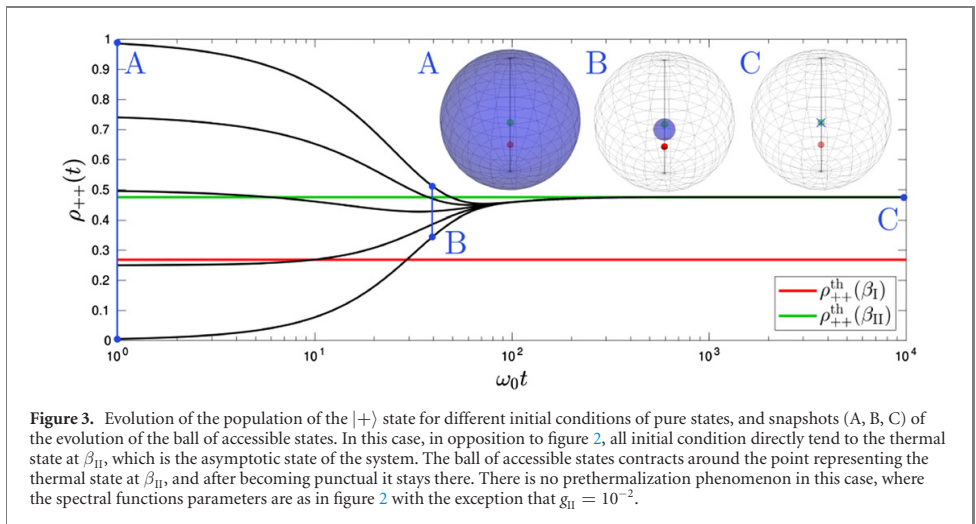
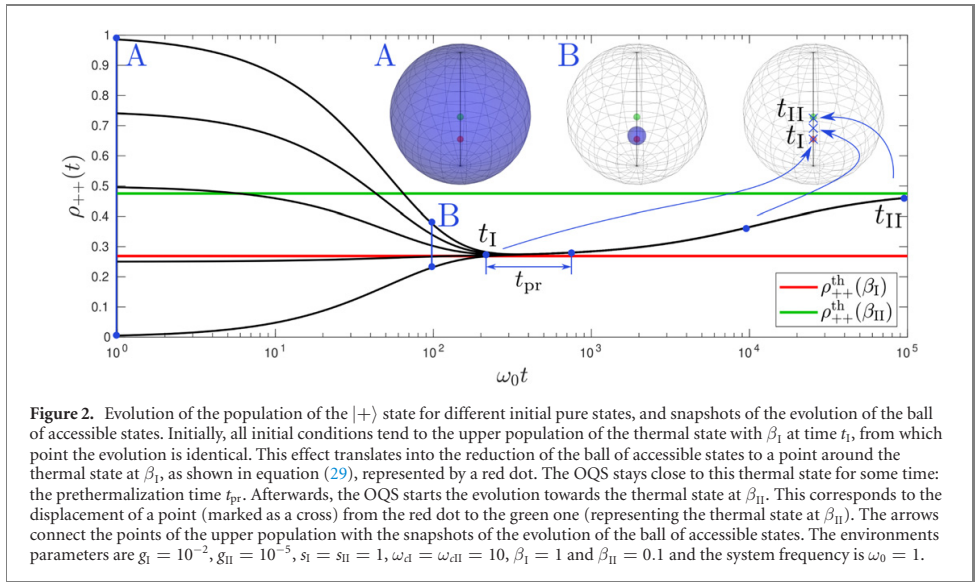
5.1. Prethermalization time

To give a more quantitative estimation of the time during which the OQS remains approximately thermalized at the temperature β_I , i.e. the prethermalization time t_{pr} , we make use of the trace distance

$$T(\rho_1, \rho_2) = \frac{1}{2} \text{Tr} \left\{ \sqrt{(\rho_1 - \rho_2)^2} \right\}, \tag{32}$$

between the evolved state of the OQS, with initial condition $\rho_S(0) = \rho_S^{th}(\beta_I)$, and the thermal state $\rho_S^{th}(\beta_{II})$. We define t_{pr} as the time elapsed between the time at which the radius of the ball of accessible states has

⁷ Where $|\pm\rangle$ is the eigenbasis defined by H_S in equation (2) with eigenvalues $\pm\omega_0/2$.



reduced below 10%, and the time at which the above trace becomes bigger than a fixed trace distance d_{pr} . This represents a threshold distance below which two states could not be distinguished. If the order in which these events happen is the opposite, it means that no prethermalization is present.

We can visualize this by looking at the dynamics of the polarization vector corresponding to the density matrix of the system, starting from $\rho_{th}(\beta_I)$. If that point has been significantly displaced before the ball of accessible states has contracted, then no prethermalization is present: see figures 2 and 3 for a visual reference of this criterion. If the trace distance between the thermal state of the system at β_I and β_{II} is smaller than d_{pr} , the prethermalization time is not defined, as these two states would not be distinguishable.

With this definition we studied how t_{pr} varies as a function of the initial temperatures of both reservoirs, as well as for different values of the coupling strength between them, i.e. g_{II} . In figure 4 we show the prethermalization time as a function of the trace distance for fixed β_I varying β_{II} . We observe the prethermalization time to be longer, the closer the two states are. The same can be appreciated in figure 5, which shows the calculation of t_{pr} for different separations of the thermal states at β_I and β_{II} : When they are closer (orange line) t_{pr} is higher and when they are further apart (blue and green lines) t_{pr} decreases.

We realized that the prethermalization scale for fixed temperatures of both reservoirs depends inversely with g_{II} , i.e., $t_{pr} \sim g_{II}^{-1}$, for small values of g_{II} . This can be clearly seen, for small coupling strenghts, in

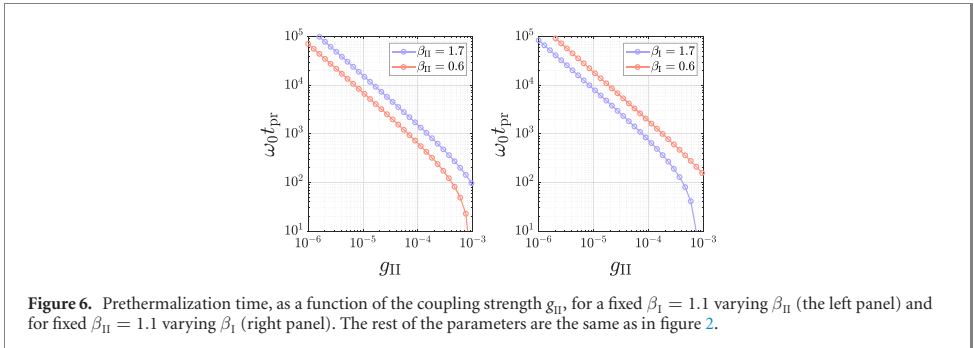
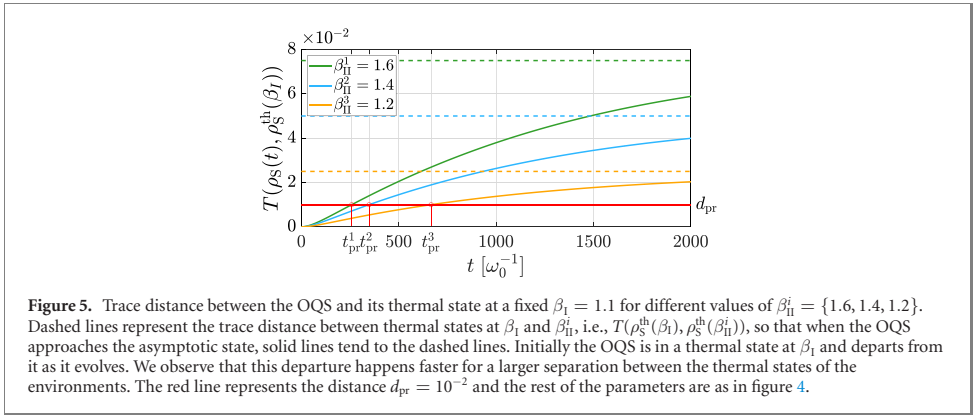
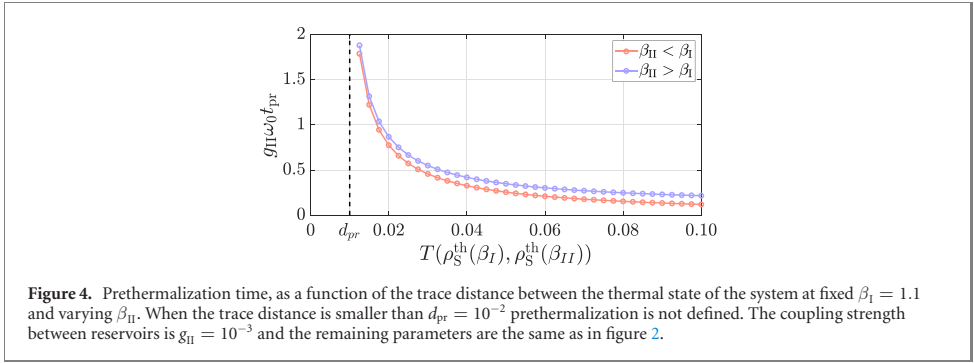
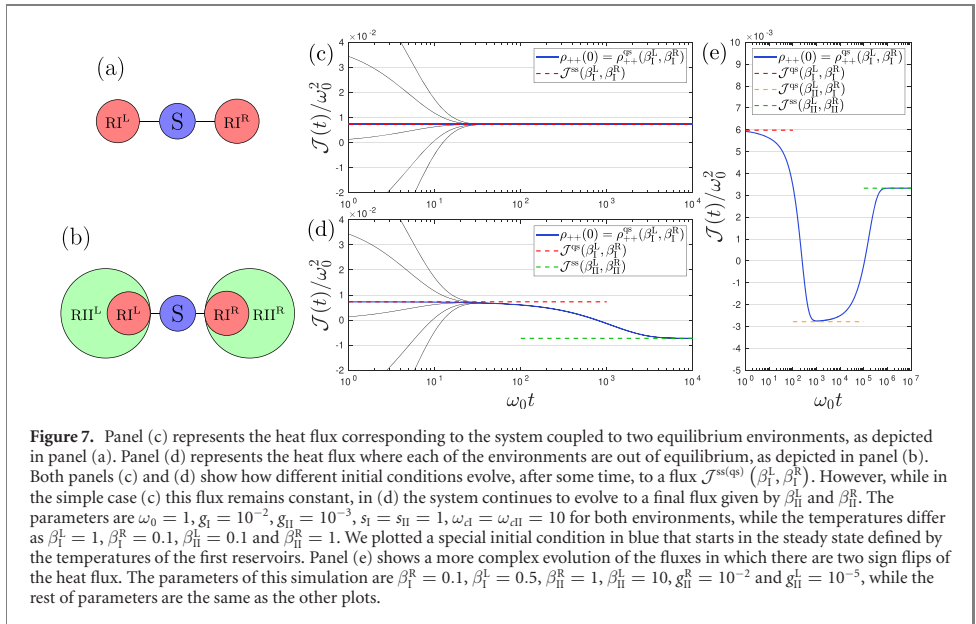


figure 6. In this figure we checked that condition (30) is fulfilled for all points. It was pointed out in [33] that the thermalization time t_{II} scales as g_{II}^{-1} similarly as t_{pr} , and we checked that this is true for our case⁸ as well.

From figures 4 and 6 we also observe that the time the OQS stays in the prethermal state is shorter for a higher temperature of RII (lower β_{II}), while the duration of the prethermalized state increases with β_{II} . A similar qualitative behaviour is observed for varying β_I (see right panel of figure 6), but the overall prethermalization scale is smaller in case of a larger β_I .

⁸ In [33] the thermalization timescales with g^{-2} , where the weakly perturbed Hamiltonian is proportional to g . In our case the perturbation is proportional to $g_{\lambda,k}$ and $g_{II} \propto |g_{\lambda,k}|^2$.



6. Composite non-equilibrium environments

In the scenario discussed in the previous sections, the OQS is expected to reach a steady state at thermal equilibrium, consistent with the temperature of the largest reservoir RII. However, using the same ME formalism it is also possible to construct more complex scenarios in which the steady state of the open system is out of equilibrium, for instance when the system is coupled to two independent environments, as depicted in the left column of figure 7. The additional environment gives rise to a new dissipative term in the master equation (15) and a new term in the environment corrected Hamiltonian $H(t)$. The corresponding rates and Lamb shift corrections are computed identically as before. The heat flow between environments produces a change in the energy of the system $E_S = \text{Tr}\{H_S \rho_S(t)\}$, where H_S is the system Hamiltonian. The evolution of this quantity can be expressed by the canonical ME (15) as

$$\frac{dE_S}{dt} = -i \text{Tr} \{H_S [\tilde{H}(t), \rho_S(t)]\} + \sum_{\nu=L,R} \text{Tr} \{H_S \mathcal{D}^{(\nu)}(t, \rho_S(t))\}, \quad (33)$$

where the superindex $(\nu) = \{L, R\}$ refers to the left and right environments and $\tilde{H}(t) = H_S + \sum_{\nu} \frac{1}{2} \Delta \omega^{(\nu)}(t) \sigma_z$. Since $\tilde{H}(t)$ and H_S are both proportional to σ_z , the first term vanishes, and the second one defines the heat fluxes

$$\mathcal{J}^{(\nu)}(t) = \text{Tr} \{H_S \mathcal{D}^{(\nu)}(t, \rho_S(t))\}, \quad (34)$$

from environment (ν) to the OQS. By convention, we consider the heat flux from the right reservoir to be positive, and the one from the left to be negative. Thus, a positive total heat flux indicates a flow of energy from right to left, and vice versa. In the following subsections we first analyze the heat fluxes when the left and right reservoirs are each in a thermal equilibrium state, and then when each of them are out of equilibrium.

6.1. Heat flux between environments in equilibrium

In the case of equilibrium environments of figure 7(a), which we depict as single reservoirs on each side of the OQS, any initial state reaches a non equilibrium steady state that depends on the initial state of both environments under our model assumptions. In figure 7(c) we plot the total heat flux $\mathcal{J}^L(t) + \mathcal{J}^R(t)$ calculated using equation (34) with $\gamma_+^{(\nu)} = J_1^{(\nu)}(\omega_0) n_1^{(\nu)}(\omega_0)$ and $\gamma_-^{(\nu)} = J_1^{(\nu)}(\omega_0) (n_1^{(\nu)}(\omega_0) + 1)$ the decay rates of the spin boson model with one reservoir. We observe that initially, the heat flux depends on the initial condition, but after some time it always converges to the value in the steady state,

$$\mathcal{J}^{\text{ss}(\nu)} = \omega_0 \left[\gamma_+^{(\nu)} - \rho_{++}^{\text{qs}}(\beta_1^L, \beta_1^R) \left(\gamma_+^{(\nu)} + \gamma_-^{(\nu)} \right) \right], \quad (35)$$

where $\rho_{+++}^{qs}(\beta_1^L, \beta_1^R)$ is given in appendix G. When the OQS reaches the asymptotic state there is a constant heat flux from the environment with the higher temperature. In figure 7(c), which corresponds to $\beta_1^R < \beta_1^L$, this is observed by a positive steady state flux.

6.2. Heat flux between environments that are out of equilibrium

We now consider the case where the OQS is coupled to two out of equilibrium reservoirs, as schematically depicted in figure 7(b). Figure 7(d) shows that the heat flux, independently of the initial condition, is dominated by the temperature gradient between β_1^R and β_1^L , while the gradient for $\beta_{II}^{(R,L)}$ becomes relevant at longer times. The timescale in which each gradient is dominant is determined by $g_{II}^{(\nu)}$. Interestingly, we observe that the interplay between these gradients may even produce a change of sign in the current. This is because we have chosen $\beta_1^R < \beta_1^L$, but $\beta_{II}^R > \beta_{II}^L$, such that the quasi-stationary flux is positive (the right RI is hotter than the left RI), while at long times is negative (since the right RII is colder than the left RII).

Moreover, one can tune these gradients and the couplings $g_{II}^{(\nu)}$ to be such that there are two changes of sign in the heat current. This is observed in figure 7(e), where $\beta_1^R < \beta_1^L < \beta_{II}^R < \beta_{II}^L$ and $g_{II}^R > g_{II}^L$, which leads to an initial and final positive flux ($\beta_1^R < \beta_1^L$). But as $g_{II}^R > g_{II}^L$ there is some time that the quasi-stationary flux is determined by $\beta_1^L < \beta_{II}^L$, such that the flux during that time is negative.

The stationary and quasi-stationary states for the setup figure 7(b) can be explicitly derived, and are shown in appendix G.

7. Conclusions

We have presented a model to describe an OQS which is coupled to a hierarchy of environments at different temperatures, a situation that can be found in complex environments and interfaces that are present in both natural and quantum technological scenarios. Although these situations are in principle very complex to analyse, we have shown here that, under certain constraints, one can extract a well-behaved master equation that allows such a description in relevant limits.

In detail, we have considered an open system directly coupled to a reservoir RI, at an inverse temperature β_1 , that is driven out of equilibrium because of its coupling to a second reservoir RII at β_{II} . With the use of weak coupling and Markovian approximations, we have derived a master equation to describe the evolution of the reduced density matrix of the system, by tracing out the evolution of the environment. Even with these approximations, we were able to observe a rich dynamics of the open system, with the existence of a transitory state, called prethermal state, before the final thermalization, which was found to be determined by the larger reservoir solely. We investigated under which conditions prethermalization is present, and concluded that this state is longer lived when the reservoir RI, directly coupled to the OQS, is hotter and RII colder, as well as when the coupling between reservoirs is the smallest possible. We presented a way to characterize prethermalization that is independent of the initial condition of the OQS, through the evolution of the volume of accessible states.

We have also shown that non-trivial dynamics and competing timescales are also present when we consider two out of equilibrium environments coupled to the system. It is well-known that, in the standard situation where the environments are in equilibrium, a heat flux with a given direction (from the hot to the cold reservoir) is established and prevails at long times. Interestingly, when considering out of equilibrium environments we observe that the timescales induced by different environments may induce that the heat flux switches direction, even more than once.

As shown, the OQS dynamics and its currents do not evolve according to a single timescale, but present a richer dynamics that may be evident in experiments and quantum information processes, particularly at long times. The presence of a prethermalization transitory may be harnessed in quantum technological applications, for instance by considering the initialization protocols of a qubit based on coupling it to a reservoir [42, 43]. The added reservoir can potentially be controlled by a second one, according to our scheme, in order to optimize further the protocol. In other words, our work describes the possibility of manipulating and controlling an open system by externally modifying and controlling the reservoir to which it is directly coupled.

Our scheme can be adapted to include more external reservoirs at different temperatures. Multiple layer environments can be found, for instance, in superconducting quantum computers, where qubits are affected not only by surrounding layers cryogenically cooled, but also by outer layers at increasingly higher temperatures. Considering this reservoir structure would allow us to find additional transitory and steady states of the OQS, which can potentially be harnessed and controlled. An interesting subject for further investigation would also be the consideration of the dynamics beyond the weak-coupling approximation, and the inclusion of non-Markovian effects.

Acknowledgments

This work has been partly funded by the CNRS PEPs Spain-France PIC2017FR6, the Spanish FEDER/MCIyU-AEI grant FPA2017-84543-P, SEV-2014-0398, Generalitat Valenciana grant PROMETEO/2019/087 and the Deutsche Forschungsgemeinschaft (DFG, German Research Foundation) under Germany's Excellence Strategy – EXC-2111 – 390814868. We also acknowledge support from CSIC Research Platform PTI-001. IDV acknowledges financial support by DFG-grant GZ: VE 993/1-1.

Appendix A. Canonical master equation, decay rates and frequency shift

For the interaction Hamiltonian considered in equation (7), the canonical decay rates and decoherence channels of the master equation (11) are

$$\begin{aligned}\gamma_1(t) &= P(t) + P^*(t) \equiv \gamma_+(t), & L_1(t) &= \sigma^+ \equiv L_+, \\ \gamma_2(t) &= M(t) + M^*(t) \equiv \gamma_-(t), & L_2(t) &= \sigma^- \equiv L_-, \\ \gamma_3(t) &= 0, & L_3(t) &= \frac{1}{\sqrt{2}}\sigma_z,\end{aligned}\quad (A1)$$

where we defined

$$P(t) = \int_0^t dt' \alpha^+(t, t') e^{-i\omega_0 t'}, \quad (A2)$$

and

$$M(t) = \int_0^t dt' \alpha^-(t, t') e^{i\omega_0 t'}. \quad (A3)$$

The operator $H(t)$ is a modification of the free Hamiltonian of the OQS

$$H(t) = H_S + \frac{1}{2}\Delta\omega(t)\sigma_z, \quad (A4)$$

which, in this case, represents a shift of the natural frequency of the system, given by

$$\Delta\omega(t) = \frac{i}{2}(P(t) - P^*(t)) - \frac{i}{2}(M(t) - M^*(t)). \quad (A5)$$

Therefore, this Hamiltonian can be rewritten as

$$H(t) = \frac{1}{2}\Omega(t)\sigma_z, \quad (A6)$$

where $\Omega(t) = \omega_0 + \Delta\omega(t)$, is the shifted frequency of the OQS due to the action of the environment. The ME for the different matrix elements of the reduced density matrix reads

$$\begin{aligned}\dot{\rho}_{++}(t) &= \gamma_+(t) - \rho_{++}(t)[\gamma_+(t) + \gamma_-(t)], \\ \dot{\rho}_{+-}(t) &= \{-i\Omega(t) - [\gamma_+(t) + \gamma_-(t)]\} \rho_{+-}(t),\end{aligned}\quad (A7)$$

where $\rho_{++}(t) = \langle +|\rho_S(t)|+ \rangle$ is the upper population and $\rho_{+-}(t) = \langle +|\rho_S(t)|- \rangle$ is the coherence, in the $|\pm\rangle$ eigenbasis of H_S . We made use of the trace preservation of the dynamical map.

Appendix B. Evolution of RI operators

The time evolution of the operator $a_\lambda(t)$ is given by the Heisenberg equation

$$\frac{d}{dt}a_\lambda(t) = i[H_E, a_\lambda(t)] = -i\omega_\lambda a_\lambda(t) - i\sum_k \tilde{g}_{\lambda k} b_{\lambda k}(t), \quad (B1)$$

where $b_{\lambda k}(t)$ is, in turn, given by its corresponding equation

$$\frac{d}{dt}b_{\lambda k}(t) = i[H_E, b_{\lambda k}(t)] = -i\omega_{\lambda, k} b_{\lambda k}(t) - i\tilde{g}_{\lambda k} a_\lambda(t). \quad (B2)$$

Formal integration of the latter and substitution on the former yields

$$\frac{d}{dt}\tilde{a}_\lambda(t) = -i\sum_k \tilde{g}_{\lambda k} b_{\lambda k}(0) e^{-i(\omega_{\lambda, k} - \omega_\lambda)t} - \sum_k \tilde{g}_{\lambda k}^2 \int_0^t dt' e^{-i(\omega_{\lambda, k} - \omega_\lambda)(t-t')} \tilde{a}_\lambda(t'), \quad (B3)$$

where we also performed the change of variable $\tilde{a}_\lambda(t) = e^{i\omega_\lambda t} a_\lambda(t)$ in order to separate the free evolution part of this operator for a better implementation of the following approximation. The first term on the rhs is the quantum noise originated by RII. The second term can be simplified under the Weisskopf–Wigner approximation [44, 45], where the operator $\tilde{a}_\lambda(t)$ is assumed to vary with a rate slower than ω_λ . This allows us to move the operator $\tilde{a}_\lambda(t)$ outside the integral and, since the exponential inside the integral evolves faster than $\tilde{a}_\lambda(t)$, to extend the integration limit to infinity, i.e.

$$\int_0^t dt' e^{i(\omega_\lambda - \omega_{\lambda,k})(t-t')} \tilde{a}_\lambda(t') \approx \tilde{a}_\lambda(t) \int_0^\infty d\tau e^{i(\omega_\lambda - \omega_{\lambda,k})\tau}, \tag{B4}$$

where the change of variable $\tau = t - t'$ has been performed. The above approximation is, in fact, a Markovian approximation for the interaction with RII, since the operator $\tilde{a}_\lambda(t)$ only depends on t , so that we have neglected its past evolution. This integral can be solved via the Sokhotski–Plemelj theorem by rewriting the second term in the rhs of equation (B3) as $\gamma_\lambda \tilde{a}_\lambda(t)$, where we defined the damping constant

$$\gamma_\lambda = \pi \sum_k |\tilde{g}_{\lambda k}|^2 \delta(\omega_{\lambda,k} - \omega_\lambda) - i \sum_k |\tilde{g}_{\lambda k}|^2 \mathcal{P} \left(\frac{1}{\omega_{\lambda,k} - \omega_\lambda} \right). \tag{B5}$$

This approximation allows for an exact solution of equation (B3), which after undoing the change of variable introduced above leads to

$$a_\lambda(t) = a_\lambda(0) e^{-(i\omega_\lambda + \gamma_\lambda)t} + \int_0^t dt' e^{-(i\omega_\lambda + \gamma_\lambda)(t-t')} f_\lambda(t'), \tag{B6}$$

where we introduced

$$f_\lambda(t) = -i \sum_k \tilde{g}_{\lambda k} b_{\lambda k}(0) e^{-i\omega_{\lambda,k} t}. \tag{B7}$$

Appendix C. Correlation function of the ME

Once the time dependence of the operator $B(t) = \sum_\lambda g_\lambda a_\lambda(t)$ is explicitly known, we can compute the correlation functions (12). First notice that the first (second) term of equation (B6) is lineal in operators acting on RI (RII), so that the traces, which are linear in these operators, will be null, and only the quadratic ones will yield non vanishing terms. In this way $\alpha^+(t, \tau)$ becomes

$$\begin{aligned} \alpha^+(t, \tau) &= \sum_{\lambda, \lambda'} g_\lambda^* g_{\lambda'} e^{(i\omega_\lambda - \gamma_\lambda)t} e^{(-i\omega_{\lambda'} - \gamma_{\lambda'})\tau} T_{\lambda, \lambda'}^I + \sum_{\lambda, \lambda'} g_\lambda^* g_{\lambda'} \int_0^t dt' \int_0^\tau dt'' T_{\lambda, \lambda'}^{II}(t', t') \\ &\times e^{(i\omega_\lambda - \gamma_\lambda)(t-t')} e^{(-i\omega_{\lambda'} - \gamma_{\lambda'})(\tau-t'')}, \end{aligned} \tag{C1}$$

where the first trace is

$$T_{\lambda, \lambda'}^I = \text{Tr}_I \{ a_\lambda^\dagger a_{\lambda'} \rho_I(0) \} \text{Tr}_{II} \{ \rho_{II}(0) \} = \delta_{\lambda, \lambda'} n_I(\omega_\lambda), \tag{C2}$$

and similarly the second one gives

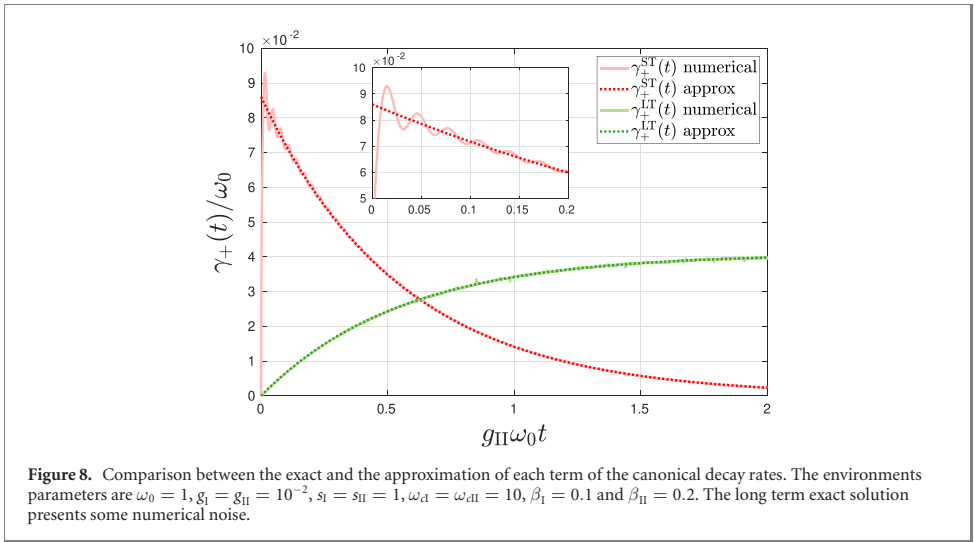
$$\begin{aligned} T_{\lambda, \lambda'}^{II}(t', t') &= \text{Tr}_{I, II} \{ f_\lambda^\dagger(t') f_{\lambda'}(t'') (\rho_I(0) \otimes \rho_{II}(0)) \} \\ &= \sum_{k, k'} \tilde{g}_{\lambda k}^* \tilde{g}_{\lambda' k'} e^{i\omega_{\lambda,k} t'} e^{-i\omega_{\lambda',k'} t''} n_{II}(\omega_{\lambda,k}) \delta_{\lambda, \lambda'} \delta_{k, k'}, \end{aligned} \tag{C3}$$

where the commutation relations (5) have been used, and $n_i(\omega) = [\exp(\beta_i \omega) - 1]^{-1}$ is the average thermal number of quanta in the mode ω at an inverse temperature β_i , for the $i = \{I, II\}$ environment. After these results, it remains to perform the sums in λ' and k' , and the integrals of the second term to yield

$$\alpha^+(t, \tau) = \sum_\lambda |g_\lambda|^2 n_I(\omega_\lambda) e^{i\omega_\lambda(t-\tau)} e^{-\gamma_\lambda(t+\tau)} + \sum_{\lambda, k} |g_\lambda|^2 |\tilde{g}_{\lambda k}|^2 n_{II}(\omega_{\lambda,k}) C_{\lambda,k}(t, \tau), \tag{C4}$$

where we defined

$$C_{\lambda,k}(t, \tau) = \frac{e^{i\omega_{\lambda,k} t} - e^{(i\omega_\lambda - \gamma_\lambda)t}}{-i(\omega_\lambda - \omega_{\lambda,k}) + \gamma_\lambda} \frac{e^{-i\omega_{\lambda,k} \tau} - e^{(-i\omega_\lambda - \gamma_\lambda)\tau}}{i(\omega_\lambda - \omega_{\lambda,k}) + \gamma_\lambda}. \tag{C5}$$



By following similar steps one arrives, for $\alpha^-(t, \tau)$, to

$$\alpha^-(t, \tau) = \sum_{\lambda} |g_{\lambda}|^2 (n_1(\omega_{\lambda}) + 1) e^{-i\omega_{\lambda}(t-\tau)} e^{-\gamma_{\lambda}(t+\tau)} + \sum_{\lambda,k} |g_{\lambda}|^2 |\tilde{g}_{\lambda,k}|^2 (n_{II}(\omega_{\lambda,k}) + 1) C_{\lambda,k}^*(t, \tau). \quad (C6)$$

The spectral function is related to the couplings in equations (C4) and (C6) in the following way

$$J_1(\omega) = 2\pi \sum_{\lambda} |g_{\lambda}|^2 \delta(\omega_{\lambda} - \omega), \quad (C7)$$

for RI and

$$J_{II}^{\lambda}(\omega) = 2\pi \sum_k |\tilde{g}_{\lambda,k}|^2 \delta(\omega_{\lambda,k} - \omega), \quad (C8)$$

for RII, where the λ index in $J_{II}^{\lambda}(\omega)$ corresponds to the reservoir to which mode a_{λ} is coupled to. We will assume that all the reservoirs that surround any a_{λ} are identical, so that we drop the λ dependence on the spectral function of RII. These definitions allow us to reformulate the problem in integral form.

Since in the master equation (11) the system operators evolve with $\tau - t$, it is suitable to introduce the change of variable $t' = t - \tau$. With these considerations one obtains the correlation functions in equation (16) in integral form. We also comment that we have neglected the imaginary part of (B5) such that $\gamma_{\lambda} = J_{II}(\omega_{\lambda})/2$. It is well-known that the contribution of the imaginary part of equation (B5) can be re-casted as a Lamb shift Hamiltonian of the form $H_{RI}^{LS} = \sum_{\lambda} \gamma_{\lambda}^{imag} a_{\lambda}^{\dagger} a_{\lambda}$, where $\gamma_{\lambda}^{imag} = \Im\{\gamma_{\lambda}\}$. This Hamiltonian is diagonal with H_{RI} , and therefore only contributes as a shift to the energies ω_{λ} that is not relevant for our analysis.

Appendix D. Validity of approximate decay rates

The validity of the approximation of the Lorentzian kernel $K(\omega, \omega')$ in equation (17) by a delta function in order to obtain an analytical expression for the canonical decay rates, depends on the parameters of the spectral functions (10) for both environments. We have numerically checked the accuracy of the approximation for a broad range of parameters that is relevant for our study. This is illustrated in figure 8, where we compare both terms of $\gamma_+(t)$ with the exact result (numerical integration of equation (A2)). The ST term does not reproduce the oscillations of the exact solution, while the LT term perfectly matches the exact result.

We also considered a more accurate approximation, which consists in taking $J_{II}(\omega)$ independent of ω , instead of approximating $K(\omega, \omega_0)$ by a delta function. This allowed to resolve the oscillatory nature of γ_{\pm}^{ST} , which is of frequency ω_0 , but the result is not as intuitive as the decay rates (19) and (20).

Appendix E. Equilibrium asymptotic state

With the help of the approximation (19) and (20) we are able to compute the asymptotic state, and prove that the OQS thermalizes to a thermal state with the temperature of RII. Consider the differential equation for the upper population in equation (A7), and the asymptotic limit

$$\rho^{ss} = \lim_{t \rightarrow \infty} \rho_S(t), \tag{E1}$$

where the density matrix becomes independent of time, then

$$\rho_{+++}^{ss} = \lim_{t \rightarrow \infty} \frac{\gamma_+(t)}{\gamma_+(t) + \gamma_-(t)} = \frac{e^{-\beta_{II}\omega_0/2}}{e^{\beta_{II}\omega_0/2} + e^{-\beta_{II}\omega_0/2}}. \tag{E2}$$

The coherence matrix element obeys an oscillatory decay equation, encoding the decoherence of the OQS. Trace preservation and hermiticity of the density matrix can be used to obtain the remaining matrix elements, so as to check that, indeed

$$\rho^{ss} = \frac{e^{-H_S \beta_{II}}}{Z(\beta_{II})}, \tag{E3}$$

i.e., the OQS asymptotic state is a thermal state at temperature β_{II} .

Appendix F. Asymptotic limit of the center of the ball of accessible states

To consider the limit $J_{II}(\omega_0)t \rightarrow \infty$ of equation (26), we first introduce the following change of variables

$$x = Ae^{-J_{II}(\omega_0)t'}, \tag{F1}$$

with

$$A = 2(n_I(\omega_0) - n_{II}(\omega_0)) \frac{J_I(\omega_0)}{J_{II}(\omega_0)}, \tag{F2}$$

$$B = (2n_{II}(\omega_0) + 1) \frac{J_I(\omega_0)}{J_{II}(\omega_0)}, \tag{F3}$$

and

$$\epsilon = e^{-J_{II}(\omega_0)t}. \tag{F4}$$

Then equation (26) becomes

$$c(\epsilon) = \frac{J_I(\omega_0)}{J_{II}(\omega_0)} (A\epsilon)^B e^{A\epsilon} \int_A^{A\epsilon} x^{-B-1} e^{-x} dx \tag{F5}$$

which can be rewritten as a difference of two incomplete gamma functions

$$c(\epsilon) = \frac{J_I(\omega_0)}{J_{II}(\omega_0)} (A\epsilon)^B e^{A\epsilon} [\Gamma(-B, A) - \Gamma(-B, A\epsilon)], \tag{F6}$$

where we made use of the definition

$$\Gamma(a, z) = \int_z^\infty t^{a-1} e^{-t} dt. \tag{F7}$$

The first term of equation (F6) is null in the limit $\epsilon \rightarrow 0$ ($J_{II}(\omega_0)t \rightarrow \infty$), while the second one becomes equation (31) after taking the limit

$$\lim_{\epsilon \rightarrow 0} \frac{\Gamma(-B, A\epsilon)}{(A\epsilon)^{-B}} = \frac{1}{B}. \tag{F8}$$

Appendix G. Non-equilibrium asymptotic state

The addition of a new environment is encoded, in the ME for the upper population, as

$$\dot{\rho}_{+++}(t) = \sum_{\nu=\{L,R\}} \left(\gamma_+^{(\nu)}(t) - \rho_{+++}(t) [\gamma_+^{(\nu)}(t) + \gamma_-^{(\nu)}(t)] \right), \tag{G1}$$

which in the steady state limit allows us to obtain

$$\rho_{+++}^{ss} = \lim_{t \rightarrow \infty} \frac{\gamma_+^L(t) + \gamma_+^R(t)}{\gamma_+^L(t) + \gamma_-^L(t) + \gamma_+^R(t) + \gamma_-^R(t)}. \tag{G2}$$

By taking the limit, one obtains the following matrix element of the non-equilibrium steady state

$$\rho_{++}^{\text{ss}} = \frac{J_I^L(\omega_0)n_{II}^L(\omega_0) + J_I^R(\omega_0)n_{II}^R(\omega_0)}{J_I^L(\omega_0)(2n_{II}^L(\omega_0) + 1) + J_I^R(\omega_0)(2n_{II}^R(\omega_0) + 1)}, \quad (\text{G3})$$

while the coherence matrix element in the steady state is null. The rest of the matrix elements can be obtained from the trace preserving property of the evolution. Even though this steady state does not directly represent a thermal state, one can obtain an effective temperature for the OQS, since it is a diagonal state in the basis of H_S . The effective temperature of the OQS in the steady state is defined as

$$\beta_{\text{eff}} = \frac{1}{\omega_0} \ln \left(\frac{1 - \rho_{++}^{\text{ss}}}{\rho_{++}^{\text{ss}}} \right), \quad (\text{G4})$$

which is a function of both temperatures β_{II} of the environments. A very similar expression is obtained for the quasi-stationary states $\rho_{++}^{\text{qs}}(\beta_I^L, \beta_I^R)$

$$\frac{J_I^L(\omega_0)n_i^L(\omega_0) + J_I^R(\omega_0)n_j^R(\omega_0)}{J_I^L(\omega_0)(2n_i^L(\omega_0) + 1) + J_I^R(\omega_0)(2n_j^R(\omega_0) + 1)}, \quad (\text{G5})$$

where the indices i, j refer to whether the corresponding environment is in the prethermal state ($i = I$) or in the asymptotic state ($i = II$). This allows us to obtain the quasi-stationary state of the OQS when both environments are prethermalizing ($i = j = I$), or the state when one has thermalized while the other remains in the prethermalization stage ($i = I, j = II$, or interchanged). When $i = j = II$ it corresponds to the asymptotic state of equation (G3).

ORCID iDs

Andreu Anglés-Castillo  <https://orcid.org/0000-0003-2883-4851>

Mari Carmen Bañuls  <https://orcid.org/0000-0001-6419-6610>

Armando Pérez  <https://orcid.org/0000-0002-6713-9483>

Inés De Vega  <https://orcid.org/0000-0002-1873-9503>

References

- [1] Rivas A, Huelga S F and Plenio M B 2014 *Rep. Prog. Phys.* **77** 094001
- [2] Breuer H-P, Laine E-M, Piilo J and Vacchini B 2016 *Rev. Mod. Phys.* **88** 021002
- [3] de Vega I and Alonso D 2017 *Rev. Mod. Phys.* **89** 015001
- [4] Li L, Hall M J and Wiseman H M 2018 *Phys. Rep.* **759** 1
- [5] Geva E and Kosloff R 1992 *J. Chem. Phys.* **96** 3054
- [6] Kosloff R 2013 *Entropy* **15** 2100
- [7] Schaller G 2014 *Open Quantum Systems Far from Equilibrium* (Berlin: Springer)
- [8] Goold J, Huber M, Riera A, del Rio L and Skrzypczyk P 2016 *J. Phys. A: Math. Theor.* **49** 143001
- [9] Craven G T and Nitzan A 2016 *Proc. Natl. Acad. Sci.* **113** 9421
- [10] Yang J-M, Yang H and Lin L 2011 *ACS Nano* **5** 5067
- [11] Muller A W J and Schulze-Makuch D 2006 *Origins Life Evol. Biospheres* **36** 177
- [12] Krinner S, Storz S, Kurpiers P, Magnard P, Heinsoo J, Keller R, Lütolf J, Eichler C and Wallraff A 2019 *EPJ Quantum Technol.* **6** 2
- [13] Lekitsch B, Weidt S, Fowler A G, Mølmer K, Devitt S J, Wunderlich C and Hensinger W K 2017 *Sci. Adv.* **3** e1601540
- [14] Metropolis N, Rosenbluth A W, Rosenbluth M N, Teller A H and Teller E 1953 *J. Chem. Phys.* **21** 1087
- [15] Troyer M and Werner P 2009 *ALP Conf. Proc.* **1162** 98
- [16] Bauer B et al 2011 *J. Stat. Mech.* **2011** P05001
- [17] Cirac J I and Verstraete F 2009 *J. Phys. A: Math. Theor.* **42** 504004
- [18] Verstraete F, Murg V and Cirac J 2008 *Adv. Phys.* **57** 143
- [19] Schollwöck U 2011 *Ann. Phys.* **326** 96
- [20] Orús R 2014 *Ann. Phys.* **349** 117
- [21] Silvi P, Tschirsich F, Gerster M, Jünemann J, Jaschke D, Rizzi M and Montangero S 2019 *SciPost Phys. Lect. Notes* **8** 1
- [22] Hughes K H, Christ C D and Burghardt I 2009 *J. Chem. Phys.* **131** 024109
- [23] Prior J, Chin A W, Huelga S F and Plenio M B 2010 *Phys. Rev. Lett.* **105** 050404
- [24] Chin A W, Rivas n., Huelga S F and Plenio M B 2010 *J. Math. Phys.* **51** 092109
- [25] de Vega I and Bañuls M C 2015 *Phys. Rev. A* **92** 052116
- [26] Katz G, Gelman D, Ratner M A and Kosloff R 2008 *J. Chem. Phys.* **129** 034108
- [27] Berges J, Borsányi S and Wetterich C 2004 *Phys. Rev. Lett.* **93** 142002
- [28] Breuer H P and Petruccione F 2002 *The Theory of Open Quantum Systems* (Oxford: Oxford University Press)
- [29] Rivas A and Huelga S F 2012 *Open Quantum Systems* (Berlin: Springer)
- [30] Leggett A J, Chakravarty S, Dorsey A T, Fisher M P A, Garg A and Zwerger W 1987 *Rev. Mod. Phys.* **59** 1
- [31] Halimeh J C and de Vega I 2017 *Phys. Rev. A* **95** 052108
- [32] Hall M J W, Cresser J D, Li L and Andersson E 2014 *Phys. Rev. A* **89** 042120

- [33] Mallayya K, Rigol M and De Roeck W 2019 *Phys. Rev. X* **9** 021027
- [34] Mori T, Ikeda T N, Kaminishi E and Ueda M 2018 *J. Phys. B: At. Mol. Opt. Phys.* **51** 112001
- [35] Kollar M, Wolf F A and Eckstein M 2011 *Phys. Rev. B* **84** 054304
- [36] Bertini B, Essler F H L, Groha S and Robinson N J 2015 *Phys. Rev. Lett.* **115** 180601
- [37] Lange F, Lenarčič Z and Rosch A 2018 *Phys. Rev. B* **97** 165138
- [38] Lenarčič Z, Lange F and Rosch A 2018 *Phys. Rev. B* **97** 024302
- [39] Gring M et al 2012 *Science* **337** 1318
- [40] Smith D A et al 2013 *New J. Phys.* **15** 075011
- [41] Langen T, Gring M, Kuhnert M, Rauer B, Geiger R, Smith D A, Mazets I E and Schmiedmayer J 2013 *Eur. Phys. J. Spec. Top.* **217** 43
- [42] Tuorila J, Partanen M, Ala-Nissila T and Möttönen M 2017 *npj Quantum Inf.* **3** 27
- [43] Tuorila J, Stockburger J, Ala-Nissila T, Ankerhold J and Möttönen M 2019 *Phys. Rev. Res.* **1** 013004
- [44] Weisskopf V and Wigner E P 1997 Berechnung der natürlichen linienbreite auf grund der diracschen lichttheorie *Part I: Particles and Fields. Part II: Foundations of Quantum Mechanics* (Berlin: Springer) pp 30–49
- [45] Scully M O and Zubairy M S 1997 *Quantum Optics* (Cambridge: Cambridge University Press)



OPEN

A quantum walk simulation of extra dimensions with warped geometry

Andreu Anglés-Castillo[✉] & Armando Pérez

We investigate the properties of a quantum walk which can simulate the behavior of a spin 1/2 particle in a model with an ordinary spatial dimension, and one extra dimension with warped geometry between two branes. Such a setup constitutes a $1 + 1$ dimensional version of the Randall–Sundrum model, which plays an important role in high energy physics. In the continuum spacetime limit, the quantum walk reproduces the Dirac equation corresponding to the model, which allows to anticipate some of the properties that can be reproduced by the quantum walk. In particular, we observe that the probability distribution becomes, at large time steps, concentrated near the “low energy” brane, and can be approximated as the lowest eigenstate of the continuum Hamiltonian that is compatible with the symmetries of the model. In this way, we obtain a localization effect whose strength is controlled by a warp coefficient. In other words, here localization arises from the geometry of the model, at variance with the usual effect that is originated from random irregularities, as in Anderson localization. In summary, we establish an interesting correspondence between a high energy physics model and localization in quantum walks.

Quantum walks (QWs) constitute an interesting possibility for simulating physical phenomena from many fields. The discrete time version describes the motion of a spin 1/2 particle on a lattice. For instance, by simply incorporating suitable position-dependent phases on the unitary operator that implements the time evolution, one can mimic the effects of an external electromagnetic field^{1–8}. In the continuum limit (when both the time step and the lattice spacing tend to zero), the Dirac equation in presence of such fields is recovered. In an analogous way, the motion of a Dirac particle in presence of a gravitational field can be simulated by an appropriate choice of the operator that drives the evolution, either on a rectangular or other types of lattices^{3,9,10}. Other scenarios include vacuum or matter neutrino oscillations^{11–13}, and one can even establish some connections to lattice field theories¹⁴.

There is also a different connection of QWs with quantum field theories, namely the possibility to explore some models which include extra dimensions, which are only manifested at very high energies. The possibility of extra dimensions of space was first suggested by Theodor Kaluza and Oscar Klein^{15,16} seeking an unified theory of electromagnetic and gravitational fields into a higher dimensional field, with one of the dimensions compactified. Experimental data from particle colliders restrict the compactification radius to such small scales that it becomes virtually impossible to explore these extra dimensions. Different ideas have been proposed to overcome this difficulty, for example the domain wall model introduced by Rubakov and Shaposhnikov¹⁷, in which the particle couples to an external scalar field. The motion of a spin 1/2 particle moving inside such a geometry was analyzed in Ref.¹⁸. In addition to recovering the corresponding Dirac equation in the continuum limit, the QW shows, at finite spacetime spacing, localization of the particle within the brane due to the coupling to the field.

Spatial localization is an important phenomenon in physics, which appears within the context of diffusion processes in lattices. It can arise from random noise on the lattice sites, giving rise to Anderson localization¹⁹ and causing a metal–insulator transition, but it can also be the consequence of the action of an external periodic potential (see e.g. Refs.^{20–22}). Similarly, one obtains localization for the 1-dimensional QW when spatial disorder is included^{23–25}, non-linear effects²⁶, or by the use of a spatially periodic coin²⁷. The results in Ref.¹⁸ show, however, that localization can also appear as a consequence of the interaction with a *smooth* external potential, instead of a random, or even periodic, perturbation.

In this paper, we investigate localization effects that arise within a different context, which is also inspired on high energy physics, and was originally proposed to address the *hierarchy problem* (the observed difference between the Higgs mass, and the Planck scale, in many orders of magnitude), and is commonly referred to as

Departament de Física Teòrica & IFIC, Universitat de València-CSIC, 46100 Burjassot, València, Spain. ✉email: andreu.angles@ific.uv.es

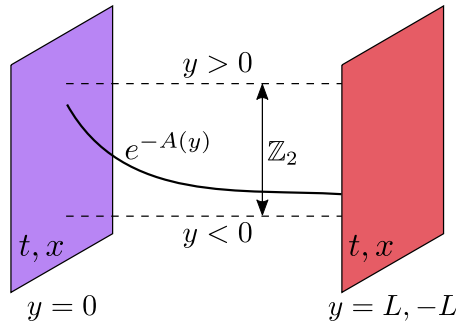


Figure 1. Schematic representation of the extra dimension in the Randall–Sundrum model.

the Randall–Sundrum model²⁸. This model assumes an extra dimension which extends between two branes (with a topology that will be discussed later). Here we consider a simplified version with one ordinary spatial dimension and one extra dimension, and define a QW that reproduces the dynamics of a spin 1/2 particle in the continuum spacetime limit.

Unlike the Rubakov and Shaposhnikov model, there is no coupling to an external scalar field. Instead, this model presents a warped geometry along the extra dimension. As we will show, this curvature is at the root of a localization effect of the QW towards the second (low energy) brane. The stationary states of the model in the continuum limit become concentrated close to the low energy brane for high values of the warp coefficient, which quantifies the strength of the localization. The localization of the QW can be analyzed by quantifying its overlap with these stationary states. This allows us to tailor the dynamics of the QW, showing a different behavior as the value of the warp coefficient is changed. In this way, we arrive at a QW model with a rich phenomenology, where some properties are inherited from the continuum field theoretic model. There is, in this sense, a mutual multidisciplinary benefit: one can design a QW which simulates an important high energy physics model. In exchange, the knowledge of the continuum properties is useful to understand, and to control, the dynamics of the QW in different regimes.

This paper is organized as follows. We first define the Randall–Sundrum model in 1 + 1 spatial dimensions, along with its main properties. We pay special attention to the stationary states of the Hamiltonian, which play a crucial role in understanding the dynamics of the proposed QW. Next, we define a QW which allows to recover the dynamics of the Randall–Sundrum model for a spin 1/2 particle, and we study its phenomenology. Namely, we show that the distribution probability, as well as the expected value of the position along the extra dimension, approaches the lower brane at large time, and that this approaching proceeds more slowly for larger values of the warp coefficient, which turns out to be the main parameter in controlling the dynamics. We also analyze the entanglement entropy between spatial and internal degrees of freedom, exhibiting a complex behavior as a function of that parameter, which can be attributed to the different sharpness of the probability distribution. We finally conclude by collecting and discussing our main results.

The model

Orbifold S^1/\mathbb{Z}_2 and background geometry. As described in the “Introduction”, we consider the Randall–Sundrum model (RSM)²⁸ with a single extra dimension y , together with a 2-dimensional ordinary spacetime, whose coordinates are denoted by $x^\mu = \{t, x\}$. The total spacetime possesses $D = 3$ dimensions. The extra dimension y is compactified on a circle of radius R , and subject to a \mathbb{Z}_2 symmetry. These features are captured by the equivalences

$$S^1 : y \sim y + 2\pi R, \tag{1}$$

$$\mathbb{Z}_2 : y \sim -y, \tag{2}$$

which define the orbifold S^1/\mathbb{Z}_2 describing this extra dimension. Along the y dimension, the orbifold is a finite segment with two fixed points at $y = 0$ and $y = \pi R \equiv L$. The RSM assumes that there is a $(D - 1)$ -brane of ordinary dimensions at each fixed point, see Fig. 1 for a sketch of the space configuration and the orbifold symmetries.

The matter fields are supposed to reside on the brane at $y = L$, which is referred to as the “visible brane”, while the brane at $y = 0$ is the “hidden brane”. Both branes contribute to the bulk background geometry through their tensions, or vacuum energies, T_{vis} and T_{hid} respectively^{28,29}. The total background action is

$$S = \int_{-L}^L dy \int dx^\mu \sqrt{|g|} (2\alpha \mathcal{R} - \Lambda) + S_{\text{vis}} + S_{\text{hid}}, \tag{3}$$

where the first term is the usual Einstein–Hilbert action of the total space, with Λ the bulk cosmological constant, α a constant and $|g|$ the absolute value of the metric determinant, while

$$S_{\text{vis}} = - \int dx^\mu \sqrt{|g_{\text{vis}}|} T_{\text{vis}}, \tag{4}$$

$$S_{\text{hid}} = - \int dx^\mu \sqrt{|g_{\text{hid}}|} T_{\text{hid}}, \tag{5}$$

are the action contributions of the branes tensions, with the induced metrics $g_{\text{vis}}(x^\mu) = g(x^\mu, y = L)$ and $g_{\text{hid}}(x^\mu) = g(x^\mu, y = 0)$. To address the hierarchy problem, the following metric was proposed

$$ds^2 = e^{-2A(y)} \eta_{\mu\nu} dx^\mu dx^\nu - dy^2, \tag{6}$$

where $e^{-2A(y)}$ is a *warp factor*, a rapidly changing function along the additional dimension, and $\eta_{\mu\nu}$ is the Minkowski metric with signature $(+, -)$. The metric in Eq. (6) obeys Einstein's equations that are obtained from the action (3). We refer the reader to the Supplementary Information for the standard computation particularized to this lower-dimensional spacetime. We also show that, as a consequence of these equations, the function in the exponent is given by

$$A(y) = k|y|, \tag{7}$$

where k is the so called *warp coefficient*.

Fermions in the Randall–Sundrum model. We now focus on the study of spin 1/2 fermions, whose evolution equation is the Dirac equation in curved spacetime

$$(i\gamma^a e_a^\mu D_\mu - m)\Psi = 0. \tag{8}$$

The γ^a are the Dirac gamma matrices in a local rest frame, and the covariant derivative is

$$D_\mu = \partial_\mu - \frac{i}{4} \omega_\mu^{ab} \sigma_{ab}, \quad \text{with} \quad \sigma_{ab} = \frac{i}{2} [\gamma_a, \gamma_b], \tag{9}$$

where ω_μ^{ab} is the spin connection. The *vierbeins* e_a^μ allow to express the Dirac matrices in a rest frame, that is, they perform a change of basis to a non-coordinate system in which the metric becomes the Minkowski metric

$$g_{\mu\nu} e_a^\mu e_b^\nu = \eta_{ab}. \tag{10}$$

Equation (8) defines the vector current

$$j^\mu = \sqrt{|g|} e_a^\mu \bar{\Psi} \gamma_a \Psi, \tag{11}$$

whose conservation $\partial_\mu j^\mu = 0$ imposes the normalization condition

$$\int dx^\mu \sqrt{|g|} e_0^\mu \Psi^\dagger \Psi = 1. \tag{12}$$

In the case of 2 spatial dimensions, the Dirac equation (8) can be reduced, after some algebra, to

$$i\gamma^a \left[e_a^\mu \partial_\mu \Psi + \frac{1}{2\sqrt{|g|}} \partial_\mu (e_a^\mu \sqrt{|g|}) \Psi \right] - m\Psi = 0, \tag{13}$$

where the γ_a matrices become Pauli matrices. A simple choice of the vierbein obeying relation (10) is

$$e_0 = (e^{A(y)}, 0, 0), \quad e_1 = (0, e^{A(y)}, 0), \quad e_2 = (0, 0, 1), \tag{14}$$

which yields the following expression for the Dirac equation

$$i\partial_t \Psi = -i\gamma^0 \gamma^1 \partial_x \Psi - i\gamma^0 \gamma^2 \partial_y (e^{-A(y)} \Psi) + \gamma_0 e^{-A(y)} m \Psi. \tag{15}$$

This expression can be rewritten in Hamiltonian form as

$$i\partial_t \chi = \mathcal{H} \chi, \tag{16}$$

with

$$\mathcal{H} = -\frac{i}{2} \{B^x, \partial_x\} - \frac{i}{2} \{B^y, \partial_y\} + \gamma_0 e^{-A(y)} m, \tag{17}$$

where the change of variable $\chi = e^{-A(y)/2} \Psi$ was performed, and we defined

$$B^x = \gamma^0 \gamma^1, \quad B^y = e^{-A(y)} \gamma^0 \gamma^2. \tag{18}$$

The symbol $\{.,.\}$ represents the anticommutator of two operators. There is some freedom in the choice of the gamma matrices. For convenience, we choose

$$\gamma^0 = \sigma_x, \quad \gamma^1 = i\sigma_y, \quad \gamma^2 = i\sigma_z. \tag{19}$$

Boundary conditions for fermionic fields. The periodic condition (1) simply implies that the fermionic fields need also to be periodic

$$\chi(x^\mu, y + 2L) = \chi(x^\mu, y), \tag{20}$$

but the \mathbb{Z}_2 needs a deeper consideration, since it has to leave the fermionic action invariant. We can write the fermionic action as

$$S_F = \int dx^\mu \int_{-L}^L dy \bar{\chi}(x^\mu, y) \left(i\gamma^\mu \partial_\mu + i\gamma^2 \partial_y e^{-A(y)} - e^{-A(y)} m \right) \chi(x^\mu, y). \tag{21}$$

which is extremized by the Dirac equation (15). Under \mathbb{Z}_2 , the fermionic action becomes

$$S_F = \int dx^\mu \int_{-L}^L dy \bar{\chi}(x^\mu, -y) \left(i\gamma^\mu \partial_\mu - i\gamma^2 \partial_y e^{-A(-y)} - e^{-A(-y)} m \right) \chi(x^\mu, -y). \tag{22}$$

The general boundary condition for a fermionic field under \mathbb{Z}_2 is given by $\chi(x^\mu, -y) = T_\chi[\mathbb{Z}_2] \chi(x^\mu, y)$ ^{30,31}, where $T_\chi[\mathbb{Z}_2]$ is the matrix representation for the action of \mathbb{Z}_2 . We rename it to $T_\chi[\mathbb{Z}_2] = M$ to alleviate the notation. We then need to find an operator M that keeps the action invariant. The action (22) is therefore transformed as

$$S_F = \int dx^\mu \int_{-L}^L dy \bar{\chi}(x^\mu, y) \gamma^0 M^\dagger \gamma^0 \left(i\gamma^\mu \partial_\mu - i\gamma^2 \partial_y e^{-A(y)} - e^{-A(y)} m \right) M \chi(x^\mu, y), \tag{23}$$

and establishes the following restrictions for M to keep the action (21) invariant,

$$\gamma^0 M^\dagger \gamma^0 \gamma^\mu M = \gamma^\mu, \tag{24}$$

$$\gamma^0 M^\dagger \gamma^0 \gamma^2 M = -\gamma^2, \tag{25}$$

$$\gamma^0 M^\dagger \gamma^0 M = \mathbb{I}, \tag{26}$$

where the first 2 conditions come from the kinetic terms of the action, and the last one arises from the mass term. There does not exist a solution for M that solves all conditions simultaneously, although $M = \eta\sigma_z$ is a solution for the first 2, with $\eta = \pm 1$ (since $M^2 = \mathbb{I}$). This means that a constant mass term is forbidden. In the following we restrict ourselves to the case where the “bulk mass” m vanishes. The action of the fermionic field is therefore

$$S_F = \int dx^\mu \int_{-L}^L dy \bar{\chi}(x^\mu, y) \left(i\gamma^\mu \partial_\mu + i\gamma^2 \partial_y e^{-A(y)} \right) \chi(x^\mu, y), \tag{27}$$

and the fermionic field has to obey the boundary condition

$$\chi(x^\mu, -y) = \eta\sigma_z \chi(x^\mu, y), \tag{28}$$

with $\eta = \pm 1$.

Stationary solutions. In this model, the Dirac field satisfies a complicated equation, Eq. (15), which is difficult to address even numerically. In order to obtain some insight, we first look for stationary solutions, which are defined as the eigenstates of the Hamiltonian. For $m = 0$, and with our choice of the gamma matrices, the Hamiltonian takes the form

$$\mathcal{H} = -\sigma_z \hat{p}_x + \frac{\sigma_y}{2} \left(e^{-A(y)} \hat{p}_y + \hat{p}_y e^{-A(y)} \right), \tag{29}$$

where $\hat{p}_k = -i\partial_k$ is the momentum operator along the k direction ($k = x, y$). The stationary states $\phi_n(x, y)$ corresponding to energy E_n satisfy

$$\mathcal{H} \phi_n(x, y) = E_n \phi_n(x, y). \tag{30}$$

It is convenient to introduce a Fourier transform on the ordinary dimension x :

$$\tilde{\phi}_n(q, y) = \int dx e^{-iqx} \phi_n(x, y), \tag{31}$$

since the field is free to move along this direction. We found the energies

$$E_n = \pm \sqrt{q^2 + (k\alpha_n)^2}, \tag{32}$$

where

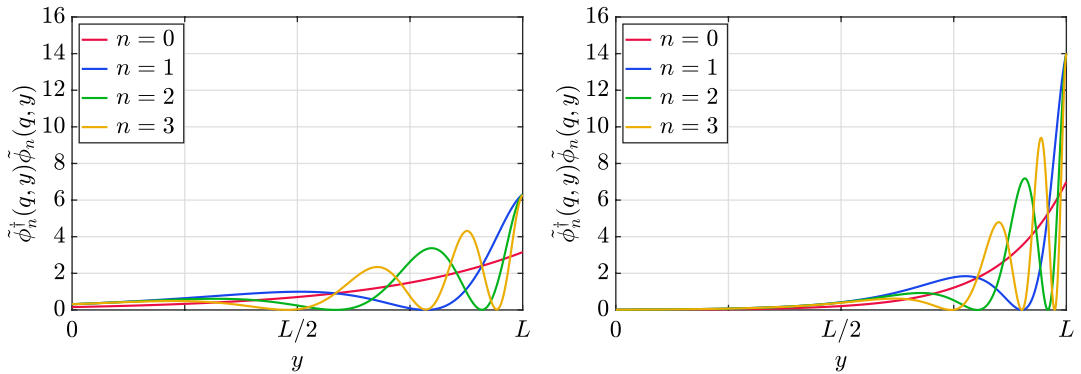


Figure 2. Plots of the probability distribution for the first four stationary states, with positive energy and a value of $q = 10$, for $kL = 3$ on the left and for $kL = 7$ on the right.

$$\alpha_n = \frac{n\pi}{e^{kL} - 1}, \quad n = 0, 1, \dots \tag{33}$$

The eigenfunctions associated with this spectrum that satisfy the boundary condition (28), for the particular case with $\eta = 1$, are

$$\tilde{\phi}_n^\uparrow(q, y) = \sqrt{\frac{2k}{e^{kL} - 1}} \frac{E_n + q}{\sqrt{(E_n + q)^2 + (k\alpha_n)^2}} e^{\frac{k|y|}{2}} \cos\left[\alpha_n(e^{k|y|} - 1)\right], \tag{34}$$

$$\tilde{\phi}_n^\downarrow(q, y) = \sqrt{\frac{2k}{e^{kL} - 1}} \frac{k\alpha_n}{\sqrt{(E_n + q)^2 + (k\alpha_n)^2}} e^{\frac{k|y|}{2}} \sin\left[\alpha_n(e^{k|y|} - 1)\right] \text{sign}(y), \tag{35}$$

where the components of the spinor field are $\tilde{\phi}_n = (\tilde{\phi}_n^\uparrow, \tilde{\phi}_n^\downarrow)^T$. The particular case $n = 0$ only has an upper component, which is given by

$$\tilde{\phi}_0^\uparrow(q, y) = \sqrt{\frac{k}{e^{kL} - 1}} e^{\frac{k|y|}{2}} \text{sign}(E_n + q), \tag{36}$$

and is undefined for energy and momentum with different sign. The procedure to obtain the eigenfunctions is detailed in the Supplementary Information, as well as the solution for $\eta = -1$. The probability distribution associated to these wavefunctions is concentrated around $y = L$ for high values of the warp coefficient k . We illustrate this behavior in Fig. 2, where we have plotted the probability density for the first modes with positive energy, and momentum $q = 10$, for a value of the warp coefficient $kL = 3$ and $kL = 7$, respectively.

A quantum walk for the Randall–Sundrum model

Once we have discussed the main properties of the RSM in the continuum spacetime, we focus on the main goal of our work, which consists in constructing a QW that is able to simulate the dynamics of a spin 1/2 particle subject to the geometric effects and symmetries of the model. To incorporate the metric, we adapt the scheme introduced in Ref.⁹, which allows to reproduce (in the continuum limit) a Dirac equation of the form Eq. (16).

The QW is defined on a 2-dimensional discrete grid with x and y axis, with discrete positions labeled by r and s , respectively. The grid points are equally spaced by ε , so that the spatial coordinates can be related to the grid points by $x = \varepsilon r$ and $y = \varepsilon s$. The Hilbert space that corresponds to these spatial degrees of freedom, $\mathcal{H}_{\text{spatial}}$ is spanned by the basis $\{|x = \varepsilon r, y = \varepsilon s\rangle\}/r, s \in \mathbb{Z}$. Time steps are labeled by $j \in \mathbb{N}$, and are also equally spaced by ε . The coin (or internal) space is a 2 dimensional Hilbert space $\mathcal{H}_{\text{coin}}$, so that the total Hilbert space is $\mathcal{H}_{\text{tot}} = \mathcal{H}_{\text{spatial}} \otimes \mathcal{H}_{\text{coin}}$. At a given time step, the state of the walker will be represented by a two component spinor $|\chi_j\rangle \in \mathcal{H}_{\text{tot}}$. The one step evolution of the QW is given by

$$|\chi_{j+1}\rangle = U|\chi_j\rangle, \tag{37}$$

where we made use of the general operator introduced in Ref.⁹. The structure of U consists on alternating displacement operators along each direction, together with unitary operators which are functions of some angle that is allowed to be spacetime dependent. Since the displacement operator and the position-dependent unitaries do not commute in general, a term containing the spatial derivative of those unitaries appears in the continuum limit, which is needed for a construction that takes the form of Eq. (17). The angles appearing in this general expression have to be chosen to reproduce the appropriate operators B^x and B^y given by Eq. (18) that correspond

to the metric (or vierbein) of the model. Some of these angles are trivial in our case, so that one arrives to a simplified expression, given by (details are given in the Supplementary Information):

$$U = R^{-1}(y) [\Theta(y) S_y(-\varepsilon/2)]^2 R(y) S_x(-\varepsilon), \tag{38}$$

where $S_k(\varepsilon) = \exp(-i\sigma_z p_k \varepsilon)$ are spin-dependent shift operators in the direction $\pm k$ (with $k = x, y$),

$$\Theta(y) = \begin{pmatrix} -c(y) & is(y) \\ -is(y) & c(y) \end{pmatrix}, \tag{39}$$

with $c(y) = e^{-A(y)}$, $s(y) = \sqrt{1 - e^{-2A(y)}}$, and

$$R(y) = \frac{1}{\sqrt{2}} \begin{pmatrix} f^*(y) & if(y) \\ -f^*(y) & if(y) \end{pmatrix}, \tag{40}$$

where $f(y) = \sqrt{\frac{1+c(y)}{2}} + i\sqrt{\frac{1-c(y)}{2}}$. At each position (r, s) we introduce

$$\chi_{j,r,s} \equiv (x = \varepsilon r, y = \varepsilon s | \chi_j) = \begin{pmatrix} \chi_{j,r,s}^\uparrow \\ \chi_{j,r,s}^\downarrow \end{pmatrix}, \tag{41}$$

which represents the amplitude (given a component of the spin) for the particle to be localized at the position labeled by (r, s) and time step j . In this way, the time step defined by (37) can be recast as a recursive formula for $\chi_{j,r,s}$, which is provided in the Supplementary Information. In order to implement this QW to simulate fermions in the RSM, appropriate conditions have to be set to comply with the boundary conditions (20) and (28). It can be explicitly shown, from the recursive formula for $\chi_{j,r,s}$, that this QW dynamics respects (28), in the sense that, if the walker obeys the condition

$$\chi_{j,r,-s} = \eta \sigma_z \chi_{j,r,s}, \tag{42}$$

at time j , it is also obeyed at time $j + 1$. For the simulations, we discretize the y coordinate along the segment $[-L, L]$ with a spacing ε , and impose an initial condition which satisfies Eq. (42). We use the same lattice spacing in the x direction, together with a strategy that adapts its effective extension to the time step. We also impose periodic boundary conditions on the grid to respect condition (20), taking into account that functions evaluated at $y = L + \varepsilon$ should be identified with functions at $y = -L + \varepsilon$ to respect the periodicity in the range $[-L, L]$.

As discussed above, the parameter that governs the amount of warp in the extra dimension is given by the product kL . One can wonder how the ordinary spacetime limit (corresponding, in our case, to just one spatial dimension x) can be recovered. To this end, we consider two different lattice spacing ε_x and ε_y along the x and y directions, respectively. We first impose the limit $kL \rightarrow 0$, so that the vierbein becomes trivial (or, in other words, the metric $g_{\mu\nu}$ becomes the Minkowski metric). Still, U will contain the displacement operator $S_y(-\varepsilon_y/2)$ along a hidden closed dimension y . To get rid of it, we just need to further take the limit $\varepsilon_y \rightarrow 0$, which yields

$$U \rightarrow S_x(-\varepsilon_x). \tag{43}$$

The above unitary operator can be interpreted as a QW which describes, in the continuum limit, the one-dimensional Dirac equation of a massless particle, as a special case of the model.

Results

The QW defined in the previous section is guaranteed to reproduce (in the continuum limit) a Dirac equation of the form (16), such as the one corresponding to the RSM. The question that arises concerns the dynamics appearing at a finite lattice and time step spacing. Of course, one does not expect the QW to behave exactly as the continuum field but, to what extent do they differ? Are there any new features that appear in the discrete case? In particular, we are interested in looking for some kind of probability concentration towards the visible brane, for a given initial condition. In this Section we explore all these features.

Stationarity of the eigenstates solutions on the quantum walk. As an initial comparison, we start by considering the discretized version of the eigenstates corresponding to the continuum limit Hamiltonian, obtained before. Such states remain stationary within this limit (i.e. they just evolve by adopting a trivial phase). How do they evolve under the action of the QW? We consider an initial state which corresponds to an eigenstate of the continuum, with fixed momentum q , and check whether the QW evolution of this state is stationary. The initial condition of the walker is therefore

$$\chi_{0,r,s} = \tilde{\phi}_n(q, \varepsilon s) e^{iq\varepsilon r}, \tag{44}$$

which represents a constant probability density along the ordinary dimension x . As expected, the QW evolution does not remain stationary, although it keeps a close resemblance to the initial state. This can be observed from Fig. 3, where we represented the normalized marginal probability along the y direction of the walker (after summing over x) at different time steps, for an initial stationary state solution with $n = 2$, and warp coefficient $kL = 3$.

Localization in the QW. We now investigate the localization capability of the above defined QW, i.e., whether it shows a tendency to concentrate the walker towards the visible brane at $y = L$. We consider an initial walker which is fully localized

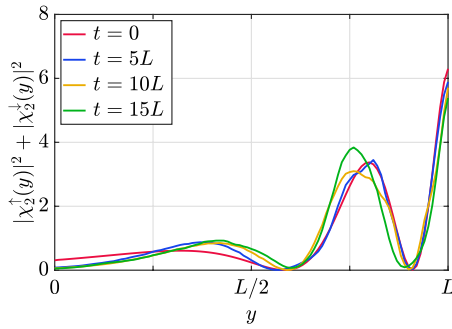


Figure 3. Snapshots of the probability density starting from an initial eigenstate with $n = 2$ and positive energy, for a value of $kL = 3$, and $q = 10$. The simulation grid has 100 points along the y direction, and enough points have been taken in the x direction to ensure that the total probability density does not leak outside the boundaries.

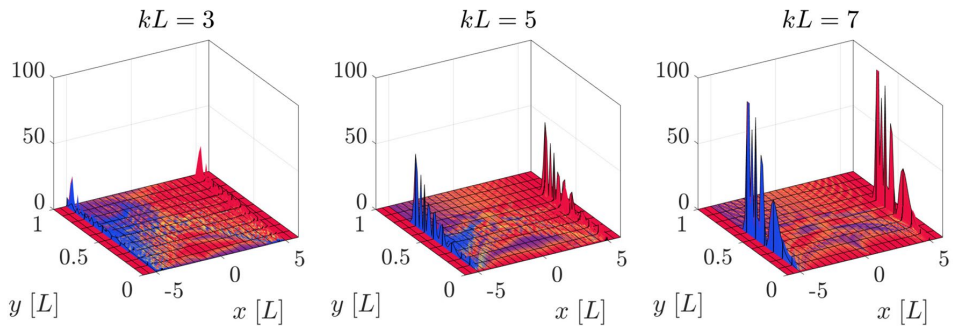


Figure 4. Probability density distribution, at $t = 5L$, of an initial localized walker centred at $(x_0, y_0) = (0, L/2)$ for different values of kL with initial coin components $C_0 = \frac{1}{\sqrt{2}}(1, i)^T$. The height of the curve represents the probability of finding the walker in that position, and the colors indicate the coin state. The red (blue) color indicates a predominance of the upper (lower) component, while yellow stands for a superposition of both components. The simulation grid has 100 points along the y direction, and enough points have been taken in the x direction to ensure that the total probability density does not leak outside the boundaries.

$$\chi_{0,r,s} = \delta_{x,0} \delta_{y,y_0} C_0, \tag{45}$$

where C_0 is the initial coin state, and we recall that $x = \varepsilon r$ and $y = \varepsilon s$. We explore the evolution of a walker which is initially localized at the center of the extra dimension, that is at $y_0 = \frac{L}{2}$, and we study the probability distribution for different values of the warp coefficient, at a given time step. In Fig. 4 we show the surface plot of the probability density with the above initial conditions, and $C_0 = \frac{1}{\sqrt{2}}(1, i)^T$, which induces a symmetric evolution in the ordinary dimension. The blue (red) color of the surface represents dominance of the upper (lower) coin component, while yellow stands for a superposition of both components.

We notice that most of the probability distribution in the x direction is concentrated along a freely propagating front which moves at the maximum speed ($x = \pm t$), consistently with the fact that the QW simulates massless fermions. We also notice that most of the right propagating distribution (positive values of x) is dominated by the upper coin component, while the part propagating to the left (negative values of x) mainly contains the lower coin component, a fact that can also be inferred from the explicit evolution of the QW (see Supplementary Information for details). The propagation of the walker along the extra dimension y strongly depends on the value of the warp coefficient. At $t = 5L$, the distribution with the lowest value of kL possesses non-zero values on the visible brane $y = L$, while the other two do not. In fact, the displacement of the probability distribution towards $y = L$ is slower for the highest kL . In other words, a larger value of the warp coefficient dramatically increases the time scale of the dynamics along the extra dimension, and makes it prohibitively expensive (in terms of computational cost) to explore larger values of kL than those considered here.

In order to investigate whether the QW exhibits the same behavior as the stationary states, in the sense that a higher value of the warp coefficient induces a stronger localization near the visible brane, we study the distribution of the freely propagated parts of the walker (the regions around $x = \pm t$), where most of the probability density is concentrated, as can be readily seen in Fig. 4. The probability distribution associated to these two zones

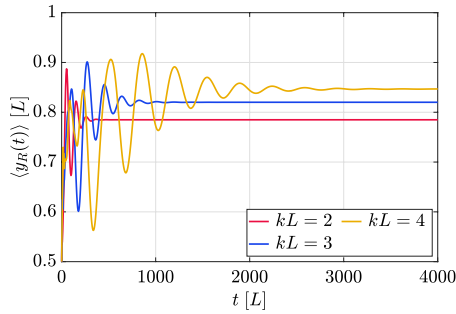


Figure 5. Expected value of the probability distribution along the extra dimension y , as calculated from the FPD, for different values of the warp coefficient kL . The initial condition is the same as in Fig. 4.

will be referred to as the “freely propagating distribution” (FPD). In terms of the spinor components, these are the probability density distributions obtained from $\chi_{j,s}^R \equiv \chi_{j,j,s}$ and $\chi_{j,s}^L \equiv \chi_{j,-j,s}$, where $r = \pm j$ restricts the wavefunction to the two freely propagating peaks. In Fig. 5 we represent the expected value for these distributions along the y dimension, which can be defined as

$$\langle y_{R(L)}(t) \rangle = \sum_s \varepsilon s \chi_{j,s}^{R(L)\dagger} \chi_{j,s}^{R(L)}, \tag{46}$$

where $t = \varepsilon j$, for different values of kL . First of all we notice that this quantity reaches an asymptotic value, which is closer to L for higher warp coefficients. Secondly, as discussed above, the warp coefficient induces a change in the time scale of the dynamics, so that lower values of the warp coefficient show a faster convergence towards the asymptotic state, consistently with the features already observed in Fig. 4.

Mode decomposition of the freely propagating distribution. Our simulations indicate that the FPD reaches a steady state along the extra dimension, in a similar fashion as the expected value (46). This evolution can be appreciated from the plots of Fig. 6. At late times (lower row), the probability distribution resembles the probability density of a stationary state with positive energy and momentum in one of the lowest modes: $n = 0$ for the right FPD, and $n = 1$ for the left FPD. It is important to recall that, as discussed above, the right (left) FPD is predominantly composed by the upper (lower) component of the spinor, and that $n = 0$ has no lower component: see Eq. (36). This causes a fundamental difference when comparing the left and right contributions. In order to investigate these features on the time evolution, we introduce a decomposition on the wavefunction of the walker as a combination of the stationary states basis. This allows us to write

$$\chi_{j,r,s} = \int_{-\pi/\varepsilon}^{\pi/\varepsilon} \frac{dq}{2\pi} \sum_n \beta_n(q, t) \tilde{\phi}_n(q, \varepsilon s) e^{-iq\varepsilon t}, \tag{47}$$

where the temporal dependence is included on the $\beta_n(q, t)$ coefficients. In the Supplementary Information we detail how these factors can be computed, and define their normalization conditions. In particular, we are interested on the contribution of each value n , therefore we integrate out the dependence in the quasi-momentum q . In other words, we are interested on the following (time-dependent) coefficients:

$$B_n(t) = \int_{-\pi/\varepsilon}^{\pi/\varepsilon} \frac{dq}{2\pi} |\beta_n(q, t)|^2. \tag{48}$$

The different mode components $B_n(t)$ of Fig. 6 have been included as an inset in those plots. On the one hand, it can be observed that, at long times, when a steady state has been reached, the FPDs are mostly composed by the lowest possible mode ($n = 0$ or $n = 1$, as discussed above). On the other hand, at short times, the FPDs contain additional higher modes.

Entanglement entropy. Finally, we study the entanglement properties that the QW exhibits between the coin and position degrees of freedom for the already considered, initially localized state. The entanglement can be quantified using the von Neumann entropy of the reduced density matrix in the coin space

$$S(t) = -\text{Tr}\{\rho_c(t) \log_2 \rho_c(t)\}, \tag{49}$$

where $\rho_c(t = \varepsilon j) = \sum_{r,s} \chi_{j,r,s} \chi_{j,r,s}^\dagger$ is the reduced density matrix in the coin space, i.e. after tracing out the spatial degrees of freedom. In the simple case of a QW on a line with a constant coin operator, the entanglement primarily arises as a consequence of the presence of the spin-dependent displacement operator S in the unitary U , although it can be modulated by both the angle of the coin operator and by the initial state^{32,33}. For the same

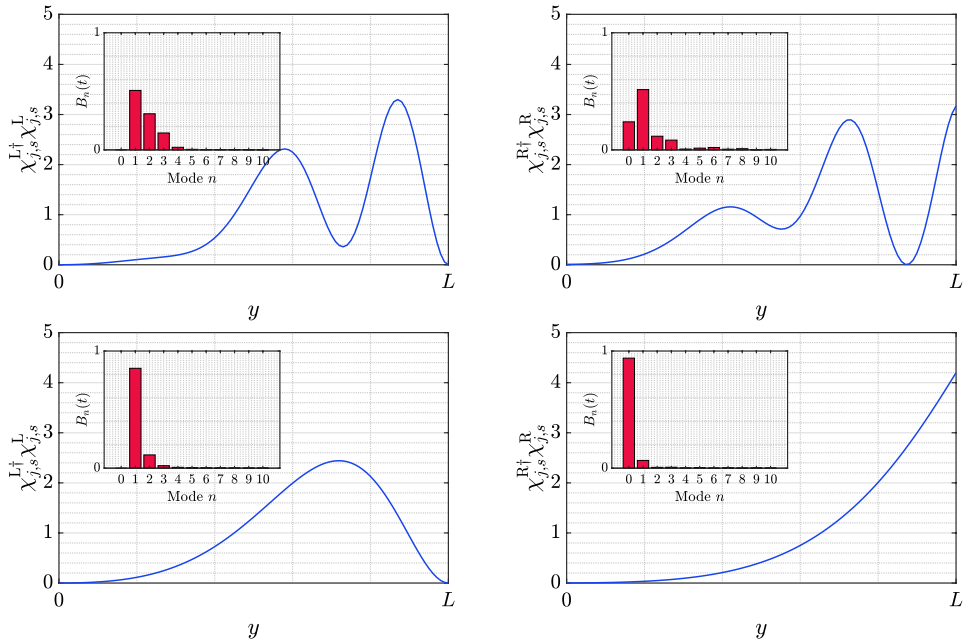


Figure 6. Probability distributions of the FPDs along the extra dimension y , for the value $kL = 3$. The inset is a histogram showing the value of the $B_n(t)$ coefficients, as defined by Eq. (48): see the text for an explanation. The left (right) panels show the left (right) FPD. The top panels are calculated at a shorter time $t = 50L$ and the bottom ones at a longer time $t = 1000L$. The initial condition is the same as in Fig. 5, and the simulation grid has 200 points along the y direction.

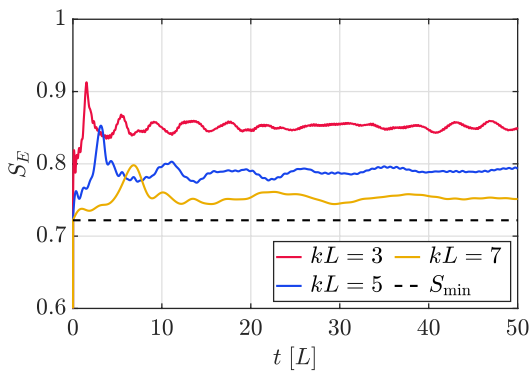


Figure 7. Evolution of the entanglement entropy with the initial condition Eq. (45) centred at $y_0 = L/2$ for different values of the warp coefficient and initial coin components $C_0 = \frac{1}{\sqrt{5}}(1, 2i)$. The dotted line represent the minimum value the entropy can reach for very high values of kL , which is computed in the Supplementary Information. This simulation grid has 50 points along the y direction.

reason, we also expect entanglement to be produced in our model, although an analytical calculation, similar to previous references, is probably unfeasible for a 2D spatial case which, moreover, includes position-dependent unitaries, as in Eq. (38).

In Fig. 7 we plot the evolution of the entanglement entropy of a fully localized initial state for different values of the warp coefficient, with a coin state $C_0 = \frac{1}{\sqrt{5}}(1, 2i)^T$. Notice that this choice is different from that one used in the previous section, for reasons that are explained below. It can be seen that the entanglement entropy reaches lower values as kL increases, an effect that can probably be due to the fact that the probability density in between

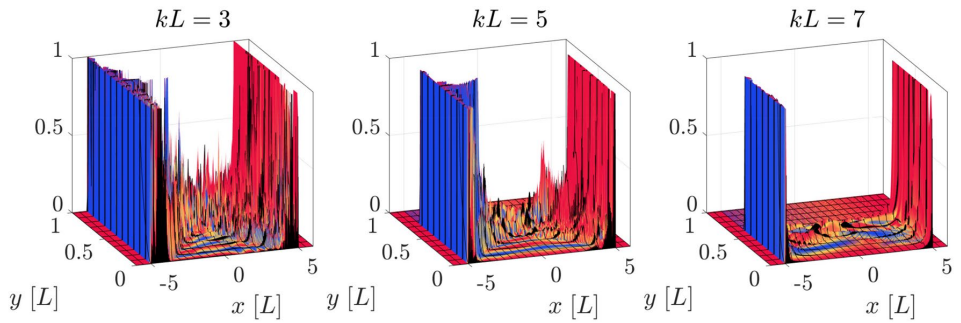


Figure 8. Probability density distribution, at $t = 5L$, for an initially localized walker centered at $(x_0, y_0) = (0, L/2)$, and different values of kL , with initial coin components $C_0 = \frac{1}{\sqrt{5}}(1, 2i)^T$. The vertical axis has been zoomed in to show that the probability density between the two regions of the FPD is more scrambled for lower values of the warp coefficient. The colors and grid parameters are the same as in Fig. 4.

the FPDs becomes more spread (and therefore “less ordered”) at lower values of kL . This can be observed in Fig. 8, where we plotted a zoomed version of Fig. 4, but obtained with the above initial coin components $C_0 = \frac{1}{\sqrt{5}}(1, 2i)^T$. One can see that, for lower values of the warp coefficient, a significant part of the probability distribution is scrambled in the intermediate region between both parts of the FPD. This diffusion effect can be totally mitigated for extreme values of the warp coefficient, leading to a minimum value of the entropy which is completely dominated by the FPD, and can be obtained from the initial coin components. In the Supplementary Material we show this limiting situation, and how the corresponding entropy can be computed. The initial coin state $C_0 = \frac{1}{\sqrt{2}}(1, i)^T$ previously used produces values of the entropy which are very close to unity in all cases, making it difficult to appreciate the effects that are discussed above.

Conclusions

We have investigated a quantum walk which allows to simulate the Randall–Sundrum model of extra dimensions, while satisfying the constraints imposed by the symmetries of that model. This model has played an important role in high energy physics, aiming to solve the hierarchy problem, by introducing one finite extra dimension that possesses two branes at its extremes. The matter fields are confined in the visible brane, while gravity is allowed to span along this whole dimension. We worked it out for the case of spin 1/2 fermions in a two dimensional space, composed by an ordinary dimension and an orbifolded one, apart from time, and obtained the Dirac equation in this spacetime configuration. The boundary conditions of the orbifold on the fermionic field forced it to be massless on the bulk. In this lower dimensional space we were able to obtain the eigenenergies of the fermionic field, as well as the corresponding eigenstates, showing a probability density which is concentrated near the visible brane, a phenomenon that bears an analogy with the localization effect that can be found in many scenarios^{19–21,23,24,26,27}.

This analogy motivated us to seek localization effects on the QW that we introduced to simulate the RSM. The QW is defined in such a way that, in the continuum limit, the Dirac equation of the fermionic field for the RSM metric is recovered. We investigated the confining capabilities of the QW, by considering an initially localized walker away from the visible brane. We concluded that the freely propagating parts of the probability distribution, where the probability is mostly concentrated, reach an asymptotic value of the expected position along the extra dimension. Moreover, the asymptotic value gets closer to the visible brane for higher values of the warp coefficient, which therefore drives the strength of localization, and also noticed that it had an effect on the timescale of the dynamics, by delaying them for higher values of the coefficient.

At long time steps, the probability densities show an asymptotic shape, with a resemblance with the eigenstates that were obtained in the continuous model, which suggested a study based on the decomposition of the wavefunction in terms of these stationary states. We found that the freely propagating parts of the QW are dominated, in the asymptotic regime, by the lowest possible (i.e., compatible with the symmetries of the model) modes. At intermediate time steps, the same decomposition manifests a combination of multiple modes with higher energy.

Finally, we found that the entanglement between coin and spatial degrees of freedom is reduced for stronger warp coefficients. We associated this result to the higher spreading of the density distribution for the lower values of the warp coefficient.

We conclude that quantum walks are suitable candidates for simulating models of field theories with extra dimensions that rely on the curvature of the spacetime. Not only the model is interesting from the point of view of the field theory: It allows to design a quantum process that can be tailored to exhibit very rich dynamics, showing free propagation in one dimension, and an asymptotic confining behavior on the other one, with rates that can be tuned by an appropriate choice of the parameters. In this way, the interplay between high energy physics and quantum simulations can be of mutual benefit.

Received: 12 May 2021; Accepted: 5 January 2022
Published online: 04 February 2022

References

- Cedzich, C. *et al.* Propagation of quantum walks in electric fields. *Phys. Rev. Lett.* **111**, 160601. <https://doi.org/10.1103/PhysRevLett.111.160601> (2013).
- Arnault, P. & Debbasch, F. Landau levels for discrete-time quantum walks in artificial magnetic fields. *Phys. A Stat. Mech. Appl.* **443**, 179–191 (2016).
- Di Molfetta, G., Brachet, M. & Debbasch, F. Quantum walks in artificial electric and gravitational fields. *Phys. A Stat. Mech. Appl.* **397**, 157–168 (2014).
- Yalçınkaya, idl. & Gedik, Z. Two-dimensional quantum walk under artificial magnetic field. *Phys. Rev. A* **92**, 042324. <https://doi.org/10.1103/PhysRevA.92.042324> (2015).
- Bru, L. A., Hinarejos, M., Silva, F., de Valcárcel, G. J. & Roldán, E. Electric quantum walks in two dimensions. *Phys. Rev. A* **93**, 032333. <https://doi.org/10.1103/PhysRevA.93.032333> (2016).
- Arnault, P. & Debbasch, F. Quantum walks and discrete gauge theories. *Phys. Rev. A* **93**, 052301. <https://doi.org/10.1103/PhysRevA.93.052301> (2016).
- Márquez-Martín, I., Arnault, P., Di Molfetta, G. & Pérez, A. Electromagnetic lattice gauge invariance in two-dimensional discrete-time quantum walks. *Phys. Rev. A* **98**, 032333. <https://doi.org/10.1103/PhysRevA.98.032333> (2018).
- Cedzich, C., Geib, T., Werner, A. H. & Werner, R. F. Quantum walks in external gauge fields. *J. Math. Phys.* **60**(1), 2019 (2019) [arXiv:1808.10850v1](https://arxiv.org/abs/1808.10850v1).
- Arnault, P. & Debbasch, F. Quantum walks and gravitational waves. *Ann. Phys.* **383**, 645–661 (2017).
- Arrighi, P., Di Molfetta, G., Marquez-Martín, I. & Pérez, A. From curved spacetime to spacetime-dependent local unitaries over the honeycomb and triangular quantum walks. *Sci. Rep.* **9**, 10904. <https://doi.org/10.1038/s41598-019-47535-4> (2019).
- Molfetta, G. D. & Pérez, A. Quantum walks as simulators of neutrino oscillations in a vacuum and matter. *N. J. Phys.* **18**, 103038 (2016).
- Mallick, A., Mandal, S. & Chandrashekar, C. M. Neutrino oscillations in discrete-time quantum walk framework. *Eur. Phys. J. C* **77**, 85. <https://doi.org/10.1140/epjc/s10052-017-4636-9> (2017).
- Jha, A. K., Chatla, A. & Bambah, B. A. Quantum simulation of oscillating neutrinos. In *5th International Conference on Particle Physics and Astrophysics* (2020). [arXiv:2010.06458v2](https://arxiv.org/abs/2010.06458v2).
- Arnault, P., Perez, A., Arrighi, P. & Farrelly, T. Discrete-time quantum walks as fermions of lattice gauge theory. *Phys. Rev. A* **99**, 032110. <https://doi.org/10.1103/PhysRevA.99.032110> (2019).
- Kaluza, T. Zum unitätsproblem der physik. *Sitzungsber. Preuss. Akad. Wiss. Berlin (Math. Phys.)* **K1**, 966 (1921).
- Klein, O. Quantentheorie und fünfdimensionale relativitätstheorie. *Zeitschrift für Physik* **37**, 895–906. <https://doi.org/10.1007/BF01397481> (1926).
- Rubakov, V. & Shaposhnikov, M. Do we live inside a domain wall?. *Phys. Lett. B* **125**, 136–138 (1983).
- Márquez-Martín, I., Di Molfetta, G. & Pérez, A. Fermion confinement via quantum walks in (2+1)-dimensional and (3+1)-dimensional space-time. *Phys. Rev. A* **95**, 042112. <https://doi.org/10.1103/PhysRevA.95.042112> (2017).
- Anderson, P. W. Absence of diffusion in certain random lattices. *Phys. Rev.* **109**, 1492 (1956).
- Aubry, S. & André, G. Analyticity breaking and Anderson localization in incommensurate lattices. *Ann. Israel Phys. Soc.* **3**, 18 (1980).
- Grepel, D. R., Fishman, S. & Prange, R. E. Localization in an incommensurate potential: An exactly solvable model. *Phys. Rev. Lett.* **49**, 833–836. <https://doi.org/10.1103/PhysRevLett.49.833> (1982).
- Lahini, Y. *et al.* Observation of a localization transition in quasiperiodic photonic lattices. *Phys. Rev. Lett.* **103**, 013901. <https://doi.org/10.1103/PhysRevLett.103.013901> (2009).
- Joye, A. & Merkli, M. Dynamical localization of quantum walks in random environments. *J. Stat. Phys.* **140**, 1025–1053. <https://doi.org/10.1007/s10955-010-0047-0> (2010).
- Schreiber, A. *et al.* Decoherence and disorder in quantum walks: From ballistic spread to localization. *Phys. Rev. Lett.* **106**, 180403. <https://doi.org/10.1103/PhysRevLett.106.180403> (2011).
- Crespi, A. *et al.* Anderson localization of entangled photons in an integrated quantum walk. *Nat. Photon.* **7**, 322–328 (2013) [arXiv:1304.1012v1](https://arxiv.org/abs/1304.1012v1).
- Navarrete-Benlloch, C., Pérez, A. & Roldán, E. Nonlinear optical Galton board. *Phys. Rev. A At. Mol. Opt. Phys.* **75**, 1–7 (2007) [arXiv:0604084](https://arxiv.org/abs/0604084).
- Shikano, Y. & Katsura, H. Localization and fractality in inhomogeneous quantum walks with self-duality. *Phys. Rev. E* **82**, 031122. <https://doi.org/10.1103/PhysRevE.82.031122> (2010).
- Randall, L. & Sundrum, R. Large mass hierarchy from a small extra dimension. *Phys. Rev. Lett.* **83**, 3370–3373. <https://doi.org/10.1103/PhysRevLett.83.3370> (1999).
- Arkani-Hamed, N., Dimopoulos, S. & Dvali, G. Phenomenology, astrophysics, and cosmology of theories with submillimeter dimensions and TEV scale quantum gravity. *Phys. Rev. D* **59**, 086004. <https://doi.org/10.1103/PhysRevD.59.086004> (1999).
- Haba, N., Hosotani, Y. & Kawamura, Y. Classification and dynamics of equivalence classes in SU(N) gauge theory on the Orbifold S¹/Z₂. *Prog. Theor. Phys.* **111**, 265–289. <https://doi.org/10.1143/PTP.111.265> (2004).
- Choi, K.-S. & E. Kim, J. Quarks and leptons from orbifolded superstring. *Lect. Notes Phys.* pp. 78–80 (2006).
- Romanelli, A. Distribution of chirality in the quantum walk: Markov process and entanglement. *Phys. Rev. A* **81**, 062349. <https://doi.org/10.1103/PhysRevA.81.062349> (2010).
- Hinarejos, M., Di Franco, C., Romanelli, A. & Pérez, A. Chirality asymptotic behavior and non-markovianity in quantum walks on a line. *Phys. Rev. A* **89**, 052330. <https://doi.org/10.1103/PhysRevA.89.052330> (2014).

Acknowledgements

This work has been funded by the Spanish Grant AEI-MICINN, PID2020-113334GB-I00/AEI/10.13039/501100011033, SEV-2014-0398 and Generalitat Valenciana grant PROMETEO/2019/087. We also acknowledge support from CSIC Research Platform PTI-001.

Author contributions

A.A.C. and A.P. contributed equally to the results of this paper. All authors reviewed the manuscript.

Competing interests

The authors declare no competing interests.

Additional information

Supplementary Information The online version contains supplementary material available at <https://doi.org/10.1038/s41598-022-05673-2>.

Correspondence and requests for materials should be addressed to A.A.-C.

Reprints and permissions information is available at www.nature.com/reprints.


Publisher's note Springer Nature remains neutral with regard to jurisdictional claims in published maps and institutional affiliations.



Open Access This article is licensed under a Creative Commons Attribution 4.0 International License, which permits use, sharing, adaptation, distribution and reproduction in any medium or format, as long as you give appropriate credit to the original author(s) and the source, provide a link to the Creative Commons licence, and indicate if changes were made. The images or other third party material in this article are included in the article's Creative Commons licence, unless indicated otherwise in a credit line to the material. If material is not included in the article's Creative Commons licence and your intended use is not permitted by statutory regulation or exceeds the permitted use, you will need to obtain permission directly from the copyright holder. To view a copy of this licence, visit <http://creativecommons.org/licenses/by/4.0/>.

© The Author(s) 2022

Quantum simulation of quantum relativistic diffusion via quantum walks

Pablo Arnault^{1,8} , Adrian Macquet², Andreu Anglés-Castillo¹ , Iván Márquez-Martín^{1,3}, Vicente Pina-Canelles¹, Armando Pérez¹, Giuseppe Di Molfetta^{1,4,5} , Pablo Arrighi⁶ and Fabrice Debbasch⁷

¹ Departamento de Física Teórica and IFIC, Universidad de Valencia and CSIC, Dr. Moliner 50, 46100 Burjassot, Spain

² Univ. Côte d'Azur and Obs. Côte d'Azur, Lab. ARTEMIS, 35150 Janzé, France

³ Aix-Marseille Univ., Université de Toulon, CNRS, LIS, Marseille, France

⁴ Université publique, CNRS, LIS, Marseille, France

⁵ Quantum Computing Center, Keio University, 3-14-1 Hiyoshi, Kohoku-ku, Yokohama, Kanagawa 223-8522, Japan

⁶ Aix-Marseille Univ., Université de Toulon, CNRS, LIS, Marseille and IXXI, Lyon, France

⁷ Sorbonne Université, Observatoire de Paris, Université PSL, CNRS, LERMA, F-75005, Paris, France

E-mail: pablo.arnault@ific.uv.es

Received 20 March 2020

Accepted for publication 23 March 2020

Published 30 April 2020



Abstract

Two models are first presented, of a one-dimensional discrete-time quantum walk (DTQW) with temporal noise on the internal degree of freedom (i.e., the coin): (i) a model with both a coin-flip and a phase-flip channel, and (ii) a model with random coin unitaries. It is then shown that both these models admit a common limit in the spacetime continuum, namely, a Lindblad equation with Dirac-fermion Hamiltonian part and, as Lindblad jumps, a chirality flip and a chirality-dependent phase flip, which are two of the three standard error channels for a two-level quantum system. This, as one may call it, Dirac Lindblad equation, provides a model of quantum relativistic spatial diffusion, which is evidenced both analytically and numerically. This model of spatial diffusion has the intriguing specificity of making sense only with original unitary models which are relativistic in the sense that they have chirality, on which the noise is introduced: the diffusion arises via the by-construction (quantum) coupling of chirality to the position. For a particle with vanishing mass, the model of quantum relativistic diffusion introduced in the present work, reduces to the

⁸Author to whom any correspondence should be addressed.

well-known telegraph equation, which yields propagation at short times, diffusion at long times, and exhibits no quantumness. Finally, the results are extended to temporal noises which depend smoothly on position.

Keywords: noisy quantum walks, noisy quantum systems, decoherence, Lindblad equation, quantum simulation, relativistic diffusions, telegraph equation

(Some figures may appear in colour only in the online journal)

1. Introduction

In classical continuous media theory, diffusion in the absence of force field designates irreversible evolutions which are induced by and compensate for inhomogeneous repartitions of certain extensive quantities (charge, particle number, momentum and energy density). Under diffusions, the medium relaxes toward an equilibrium state where these quantities have time- and space-independent concentrations. On the microscopic scale, diffusion is always associated with random motions. The simplest example is Brownian motion, which was first observed by Brown in 1827, revisited theoretically by Einstein in 1905 [1] and is now the cornerstone of modern stochastic process theory. Diffusion also occurs in quantum and/or relativistic systems. The first attempts to describe quantum non-relativistic diffusion processes were made in the 1970s (see reference [2]). Quantum diffusion [3–5] occurs in open quantum systems interacting with their environment and is usually described through a deterministic differential transport equation of the Lindblad form [6] obeyed by the so-called reduced density operator of the system. The problem of finding macroscopic models of relativistic non-quantum diffusion was first considered in the 1940s by Landau and Eckhart [7, 8]. It was first revisited by Cattaneo [9], who suggested to model relativistic diffusion through the telegraph equation, and whose work, coupled with the Grad expansion technique [10] (see also reference [52] in reference [11]), laid the basis of the so-called extended thermodynamics theories [12]. All models produced by these efforts present serious difficulties, which range from non-causality and instability (see references [6, 7, 49] in reference [11]) to experimental refutation⁹ (see references [58, 59] in reference [11]). Also, all implementations of the extended thermodynamics philosophy are based on truncating the Grad expansion, which usually diverges. It therefore comes as no surprise that some experimental predictions of extended thermodynamics seem to diverge with the supposed precision of the implementation, thus making extended thermodynamics void of any real predictive power, at least for some phenomena like second sound (see the last chapter of [12]). The problem of finding microscopic models of relativistic non-quantum diffusion was in theory entirely solved by writing down a relativistic version of Boltzmann equation [13, 14], but practical computations and conceptual issues necessitated also extending stochastic process theory to the relativistic realm. The first relativistic stochastic process was considered by Dudley [15]. Though well-defined mathematically, this process is not of obvious physical usefulness and fails to predict important phenomena like thermalization. The first relativistic process of physical relevance is the relativistic Ornstein Uhlenbeck process (ROUP) and was presented in 1997 by Debbasch, Mallick and Rivet [16–18]. Franchi and Le Jan then revisited the Dudley process taking into account the physics of the ROUP, both in flat

⁹This experimental refutation has been obtained, in the references cited, in the non-relativistic regime, the relativistic regime being more difficult to access. That being said, because this non-relativistic regime can be derived as a limit of relativistic extended-thermodynamics models, the abovementioned experiments refute at least the kind of limit which has been taken and at most these relativistic extended-thermodynamics models themselves.

and curved spacetimes [19, 20]. A process mixing aspects of the Dudley process and of the ROUP was later introduced by Dunkel and Hänggi [21, 22]. Finally, the ROUP served as a basis for the construction of the first macroscopic model of bounded velocity diffusion free of any physical and mathematical pathology [2, 23–25]. Models of this type can be used for relativistic and non-relativistic bounded velocity diffusions [26]. Let us eventually mention two historical references on this topic of relativistic stochastic processes, references [27, 28].

In this paper, we develop a novel quantum-simulation scheme which models relativistic diffusive transport in the quantum regime, by mimicking an appropriate Lindblad equation via the continuum limit of a noisy discrete-time quantum walk (DTQW). Quantum simulation is a flourishing field, thanks to its advantages with respect to classical simulation: classical computers are especially inefficient at simulating quantum dynamics of highly entangled systems.

The advantage of some quantum algorithms with respect to their classical counterparts is already known, as with Grover’s algorithm [29], which can solve the task of searching an element in a database quadratically faster than known classical algorithms. Grover’s algorithm can be written in terms of a DTQW, whose spatial probability distribution spreads quadratically faster than that of a random walk. One more example is the proposal of using quantum walks for ranking nodes on a network [30]. Another application of DTQWs is the direct simulation of physical dynamics: if the set-up for them is chosen appropriately, they can be used to model several physical phenomena, e.g., the dynamics of fermions in the free case [31] or in an external Abelian (i.e., electromagnetic) [31–33] or non-Abelian [34] Yang–Mills gauge field, neutrino flavor oscillations [35], and fermion confinement [36]. These DTQW schemes are not limited to square-lattices backgrounds, but can also be designed on triangle and honeycomb lattices [37, 38]. Moreover, the (classical) field dynamics that DTQWs can mimic is not limited to flat-spacetime backgrounds, can be extended to curved spacetimes [39–43]. Action principles for DTQWs have been suggested, and the space-time covariance of the latter has been investigated, both in flat [44, 45] and in curved [46] spacetime.

The connections between DTQWs and lattice gauge theories have also been explored [47–50], and Wigner functions for DTQWs have been proposed in references [51–53]. A crucial feature of DTQWs is that they are intrinsically causal, i.e., information propagates, at most, at a finite velocity $c = 1$, which is why DTQWs are *a priori* especially suited to model quantum relativistic diffusions.

This article is organized as follows. Basics about DTQWs are reviewed in section 2, while section 3 introduces two models with temporal noise and a common continuous limit of the Lindblad form. Section 4 explores the phenomenology of this limit. Section 5 extends the previous results to temporal noises which depend smoothly on space. All results are summarized and discussed in the final section, while technicalities are dealt with in the appendices.

2. The unitary model: discrete-time quantum walk on the line

2.1. Presentation

Consider a series of quantum states, $|\Psi_t\rangle$, indexed by the discrete time $t \in \mathbb{N}\epsilon$, where $\epsilon > 0$ is the time step, and belonging to a Hilbert space $\mathcal{H}_c \otimes \mathcal{H}_p$, where (i) \mathcal{H}_c is the so-called *coin (Hilbert) space*, which is two dimensional and accounts for an internal, two-state degree of freedom (hereafter d.o.f.) we call coin (hence the index ‘c’), and (ii) \mathcal{H}_p is the *position (Hilbert) space* (hence the index ‘p’). The probability amplitudes of this state on the position basis,

$\{|x\rangle, x \in \mathbb{Z}a\}$, where $a > 0$ is the lattice spacing, are thus described by a two-component wave function, $\Psi_{t,x} \equiv \langle x|\Psi_t\rangle \equiv (\psi_{t,x}^L, \psi_{t,x}^R)^\top$, where \top denotes the transposition.

Consider that $|\Psi_t\rangle$ evolves according to the following standard model of discrete-time quantum walk on the line,

$$|\Psi_{t+\epsilon}\rangle = \hat{U}_{\xi_t^0, \xi_t^1, \hat{\theta}_t, \hat{\chi}_t} |\Psi_t\rangle, \tag{1}$$

where the one-step evolution operator, called *walk operator*, is

$$\hat{U}_{\xi_t^0, \xi_t^1, \hat{\theta}_t, \hat{\chi}_t} \equiv C_{\xi_t^0, \xi_t^1, \hat{\theta}_t, \hat{\chi}_t} S(\hat{p}). \tag{2}$$

This evolution operator is the succession of two unitary operators.

The first one is a coin-dependent *shift operator*,

$$S(\hat{p}) \equiv \begin{bmatrix} e^{ia\hat{p}} & 0 \\ 0 & e^{-ia\hat{p}} \end{bmatrix} = e^{ia\hat{p}\sigma^3}, \tag{3}$$

where σ^i is the i th Pauli matrix, and \hat{p} is the quasimomentum operator, which is Hermitian (this ensures that $S(\hat{p})$ is unitary) and satisfies $e^{ia\hat{p}} = \sum_x |x\rangle \langle x+a|$, so that the upper (resp. lower) component, ψ_t^L (ψ_t^R), is shifted left (resp. right), hence the superscript L (resp. R). Notice that we have implicitly introduced the LR basis of the coin space, namely, ($|L\rangle, |R\rangle$), which we have identified with $((1, 0)^\top, (0, 1)^\top)$.

The second operator is a so-called *coin operator*,

$$C_{\xi_t^0, \xi_t^1, \hat{\theta}_t, \hat{\chi}_t} \equiv e^{i\xi_t^0} \begin{bmatrix} e^{i\xi_t^1} \cos \hat{\theta}_t & ie^{i\hat{\chi}_t} \sin \hat{\theta}_t \\ ie^{-i\hat{\chi}_t} \sin \hat{\theta}_t & e^{-i\xi_t^1} \cos \hat{\theta}_t \end{bmatrix}, \tag{4}$$

which is nothing but an arbitrary 2×2 unitary matrix with 4 operator-valued entries,

$$\hat{f}_t \equiv \left(\hat{f}_t^l\right)_{l=0,\dots,3} \equiv \left(\xi_t^0, \xi_t^1, \hat{\theta}_t, \hat{\chi}_t\right), \tag{5}$$

acting on the position space. To endow the \hat{f}_t^l s (varying l and t), with the highest degree of arbitrariness, one must consider them (i) Hermitian, to ensure the *unitarity* of the coin operator, and (ii) *diagonal in the position basis*, that is,

$$\hat{f}_t^l |x\rangle \equiv f_{t,x}^l |x\rangle, \tag{6}$$

(which defines the sequences $f^l : (t, x) \mapsto f_{t,x}^l$, which are real-valued because of hermiticity), so as to ensure the *locality* of the walk operator in position space.

The \hat{f}_t^l s being diagonal in the position basis, they commute between each other, so that we can write the coin operator as

$$C_{\xi_t^0, \xi_t^1, \hat{\theta}_t, \hat{\chi}_t} = e^{i\xi_t^0} e^{i\frac{\hat{\chi}_t}{2}\sigma^3} e^{i\frac{\xi_t^1}{2}\sigma^3} e^{i\hat{\theta}_t\sigma^1} e^{i\frac{\xi_t^1}{2}\sigma^3} e^{-i\frac{\hat{\chi}_t}{2}\sigma^3}. \tag{7}$$

This readily shows that, if χ is space independent, it simply codes for a global change of coin basis at time t , which, in addition, commutes with the coin-dependent shift operator, so that, if χ is moreover time independent, it does not affect the dynamics. In appendix A, we explain the reasons for choosing this parametrization, equation (4) (or (7)), for the unitary group.

When the entries of the coin operator are time and space independent, the behavior of this dynamical system, equation (1), is well know. It yields, whatever the values of the

entries, two propagation fronts, one to the left, and the other to the right, and thus exhibits, in particular, ballistic spread, i.e., $O(t)$ spread. In the long-time limit, the spread is exactly $\sigma_\infty(t) = (a/\epsilon)t\sqrt{1 - \sin\theta}$ [54, 55]. Notice in particular that this spread¹⁰ is independent of ξ^0 , ξ^1 and χ .

Notice that we use hats for operators acting on the position space, the reason for this being that we do not identify them with their matrix representation. In contrast, we do not use hats for operators acting on the coin space, the reason for this being that we do identify them with their matrix representation.

2.2. Continuum limit

It is well known [39] (i) that the above lattice model, equation (1), possesses a continuum limit, $\epsilon \rightarrow 0$ and $a \rightarrow 0$, for the ballistic scaling¹¹,

$$a = \epsilon, \tag{8}$$

(which we assume from now on when taking continuum limits), provided, essentially, that ξ^0 , ξ^1 and θ , also go to zero with ϵ , and (ii) that the richest situation [39] is obtained when they scale as ϵ , i.e.,

$$\xi^0 \equiv \epsilon \bar{\xi}^0 \tag{9a}$$

$$\xi^1 \equiv \epsilon \bar{\xi}^1 \tag{9b}$$

$$\theta \equiv \epsilon \bar{\theta}, \tag{9c}$$

which we assume from now on when taking continuum limits (it will be recalled), where $\bar{\xi}^0$, $\bar{\xi}^1$ and $\bar{\theta}$, are arbitrary functions of time and space. Indeed, when these conditions are satisfied¹², the evolution operator reads

$$\hat{U}_{\epsilon \bar{\xi}^0, \epsilon \bar{\xi}^1, \epsilon \bar{\theta}, \hat{\chi}} = \mathbb{1} - i\epsilon H_{\bar{\xi}^0, \bar{\xi}^1, \bar{\theta}, \hat{\chi}}(\hat{p}) + O(\epsilon^2), \tag{10}$$

so that it has a valid continuum limit—i.e., the walk operator tends to the identity when ϵ tends to zero—which is generated by the following Hamiltonian,

$$H_{\bar{\xi}^0, \bar{\xi}^1, \bar{\theta}, \hat{\chi}}(\hat{p}) \equiv \alpha^1 \left(\hat{p} + \hat{\xi}^1 \right) + M_{\bar{\theta}, \hat{\chi}} \alpha^0 - \bar{\xi}^0 \mathbf{1}_2, \tag{11}$$

which is a generalization of the 1D Dirac Hamiltonian for a particle with mass matrix

$$M_{\bar{\theta}, \hat{\chi}} \equiv -\bar{\theta} D(\hat{\chi}), \tag{12}$$

where

$$D(\hat{\chi}) \equiv \text{diag} \left(e^{i\hat{\chi}}, e^{-i\hat{\chi}} \right), \tag{13}$$

and charge $q = -1$, coupled to an electromagnetic potential with covariant components

¹⁰ In reference [55], the spread is computed for $\xi^0 = \xi^1 = 0$ and $\chi = \pi/2$, but one can adapt the demonstration to arbitrary values for these angles. In short: (i) a constant χ does not even intervene in the dispersion relation of the DTQW, (ii) a constant ξ^0 does not intervene in the group velocity of the DTQW, and (iii) a constant ξ^1 is just a constant shift in the Brillouin zone, which is irrelevant when performing integrals of functions which are periodic with period the size of the Brillouin zone. For a rigorous mathematical proof of the long-time probability distribution of the DTQW (from which one can of course compute, in particular, the variance), see [56].

¹¹ Ballistic scaling means $\epsilon \propto a$, and we can choose $\epsilon = a$ without loss of generality, i.e., setting a/ϵ as the speed unit.

¹² Together with regularity conditions for the quantities that we Taylor expand in ϵ [39].

$$A_0 \equiv \bar{\xi}^0 \tag{14a}$$

$$A_1 \equiv -\bar{\xi}^1, \tag{14b}$$

and with the following representation of the alpha matrices,

$$\alpha^0 \equiv \sigma^1 \tag{15a}$$

$$\alpha^1 \equiv -\sigma^3. \tag{15b}$$

We have also introduced $\mathbf{1}_2$, the 2×2 identity matrix.

Assume $\chi \neq 0$: even if χ is spacetime independent, $D(\hat{\chi})$ cannot be absorbed in α^1 because $D(\hat{\chi})^2 \neq \mathbf{1}_2$, so that the Clifford algebra is not satisfied, and so the resulting Dirac equation does not square to the Klein–Gordon equation. When $\chi = 0$, we recover, of course, a standard Dirac Hamiltonian with real (though possibly spacetime-dependent) mass,

$$m \equiv -\bar{\theta}, \tag{16}$$

namely,

$$H_{\hat{A}_0, -\hat{A}_1, \hat{m}, \hat{\chi}=0}(\hat{p}) = H_{\hat{m}, \hat{A}_0}^{\text{Dirac}}(\hat{p} - \hat{A}_1) \tag{17a}$$

$$\equiv \alpha^1(\hat{p} - \hat{A}_1) + \hat{m}\alpha^0 - \hat{A}_0\mathbf{1}_2. \tag{17b}$$

For this reason, we assume from now on that $\chi = 0$, and introduce, for the purpose of compactness of notations in the continuum-limits sections to come, $\bar{\chi} \equiv \chi/\epsilon$, so that,

$$\chi \equiv \epsilon\bar{\chi} = 0. \tag{18}$$

Notice that we choose $\chi = 0$ solely for the sake of simplicity, — i.e., to match with the standard Dirac Hamiltonian with *real* (though possibly spacetime-dependent) mass, equation (17b)—, that is, one could perfectly consider an arbitrary spacetime dependence for χ in the computations to come, without any change in the results but that one¹³.

3. Two models of temporal coin noise with a common continuum limit

3.1. Discrete-time quantum walk with coin-flip and phase-flip channels

3.1.1. Lattice model. A simple and well-known model of temporal coin noise for the DTQW introduced in equation (1), is to consider that, for each evolution $t \rightarrow t + \epsilon$, the walker follows the unitary evolution with some probability $1 - \pi_+$, with π_+ independent on time, and that, with probability $\pi_+ = \pi_1 + \pi_2$, it undergoes either a phase-flip channel, that is, a coin-dependent phase flip¹⁴, i.e., evolves through the unitary σ^3 , with probability π_1 , or a

¹³ Regarding the role played by a spacetime-independent χ for the above Dirac Hamiltonian, equation (17), the reader may be interested in reference [57]. Regarding the role played by a spacetime-dependent χ in another class of continuum limits, the reader may be interested in reference [69]. Regarding the role played by the four spacetime-dependent angles in the original, spacetime-lattice model, equation (1), the reader may consult, for ξ^0 and ξ^1 , references [33, 39, 47–49, 58],—which show, among other results and in various, related settings, that these two angles correspond to lattice versions of the electromagnetic potential, having lattice U(1) gauge invariance —, and, for θ and χ , reference [58], which shows that these two angles encode the curvature of a discrete spacetime.

¹⁴ This phase flip is coin dependent, but the specification ‘coin dependent’ (i.e., in general, ‘internal-state dependent’) can be omitted, since a coin-independent phase flip leads to a trivial, identity channel, which is rarely of interest.

bit-flip channel, that is, a bit flip, i.e., evolves through the unitary σ^1 , with probability π_2 [59, 60].

To describe the behavior of a quantum noisy system statistically, i.e., its average behavior over a large number of realizations of the noisy dynamics, one needs the density-operator formalism. In the present case, the evolution equation for the density operator, $\hat{\rho}_t$, is simply,

$$\hat{\rho}_{t+\epsilon} = (1 - \pi_1 - \pi_2)\hat{U}_{\hat{f}_t}\hat{\rho}_t\hat{U}_{\hat{f}_t}^\dagger + \pi_1\sigma^3\hat{\rho}_t\sigma^3 + \pi_2\sigma^1\hat{\rho}_t\sigma^1. \quad (19)$$

3.1.2. Continuum limit. A simple condition for equation (19) taken for $\hat{f}_t = \epsilon\hat{f}_t$ to have a formal continuum limit as $\epsilon \rightarrow 0$ is to assume that $\pi_l \rightarrow_{\epsilon \rightarrow 0} 0$, $l = 1, 2$. For simplicity, we assume that they scale as ϵ ,

$$\pi_l \equiv \epsilon\tilde{\pi}_l, \quad l = 1, 2, \quad (20)$$

where $\tilde{\pi}_l$ is an arbitrary real number corresponding to a probability per unit time. After Taylor expanding equation (19) at first order in ϵ , canceling out the zeroth-order terms, and letting $\epsilon \rightarrow 0$, we are lead to the following equation,

$$\partial_t\hat{\rho} = -i[\hat{H}^o, \hat{\rho}] + \mathcal{L}_{\tilde{\Pi}}(\hat{\rho}), \quad (21)$$

where the Hamiltonian part is the Dirac one, see section 2.2,

$$\hat{H}_t^o \equiv H_{\hat{m}, \hat{A}_0|_t}^{\text{Dirac}}(\hat{p} - i\hat{A}_1|_t), \quad (22)$$

and the non-Hamiltonian, but still trace-preserving one, reads,

$$\mathcal{L}_{\tilde{\Pi}}(\hat{\rho}_t) \equiv \tilde{\pi}_1 [\sigma^3\hat{\rho}_t\sigma^3 - \hat{\rho}_t] + \tilde{\pi}_2 [\sigma^1\hat{\rho}_t\sigma^1 - \hat{\rho}_t], \quad (23)$$

and can be recast in a Lindblad form, whose most general writing is

$$\mathcal{L}_X(\hat{\rho}_t) \equiv \sum_{i \in I} X_i \left[L_i\hat{\rho}_tL_i^\dagger - \frac{1}{2}\{L_i^\dagger L_i, \hat{\rho}_t\} \right], \quad (24)$$

where $X \equiv (X_i)_{i \in I}$ is an arbitrary family of non-negative real numbers indexed by the label i belonging to some indexing space I , and the L_i s are the so-called Lindblad or jump operators, which act on the Hilbert space of the system and can be non-Hermitian. In the present case, i.e., in equation (23), we have $X = \tilde{\Pi} \equiv (\tilde{\pi}_1, \tilde{\pi}_2)$, $i = l = 1, 2$, and two Lindblad operators,

$$L_1 \equiv \sigma^3 \quad (25a)$$

$$L_2 \equiv \sigma^1, \quad (25b)$$

which are Hermitian, act solely on the coin space, and whose square is proportional to $\mathbf{1}_2$.

3.2. Discrete-time quantum walk with random coin unitaries

3.2.1. Lattice model. Another simple and well-known model of temporal coin noise for the DTQW introduced in equation (1), is to consider that, for each evolution $t \rightarrow t + \epsilon$, the values of the coin-operator parameters are not fixed numbers but sampled from respective probability distributions [61], so that we denote them with a prime, $\xi_{t,x}^{0'}$, $\xi_{t,x}^{1'}$, $\theta_{t,x}'$, and $\chi_{t,x}'$. For simplicity, we assume that these random values can depend on space only through their mean value, i.e.,

they have space-independent fluctuations and thus respective centered probability distributions (that is why we speak of *temporal* noise), that we denote p_t^l . This means that

$$f_{t,x}^l \equiv \epsilon \bar{f}_{t,x}^l + \omega_t^l \quad \text{for } l = 0, \dots, 3, \tag{26}$$

where (i) for $l = 0, \dots, 2$ (resp. $l = 3$), $\epsilon \bar{f}_{t,x}^l$ (resp. 0) is the mean value, which we have assumed scaling as ϵ (resp, vanishing), in order to recover, in the noiseless case, the previous Hamiltonian evolution, equation (17), and (ii) $\omega_t^l \in \mathbb{R}$ is the space-independent fluctuation, newly sampled from the probability distribution p_t^l at each time, and associated to a random variable Ω_t^l . Giving oneself a function p_t^l of $\omega_t \in \mathbb{R}$ for each t means assuming that the noise has *temporal independence*, i.e., the random variables Ω_t and $\Omega_{t'}$ are independent¹⁵ for $t' \neq t$. Now, in addition to temporal independence, we assume *stationarity*, i.e., that the p_t^l s do not depend explicitly on time: $p_t^l = p^l$. The four time-indexed random variables Ω_t^l associated to the possible values ω_t^l , are considered statistically independent, so that the probability density of getting ω_t^0 and ω_t^1 and ω_t^2 and ω_t^3 is given by the product $\prod_{l=0}^3 p^l(\omega_t^l)$.

The above model translates into the following evolution for the density operator, $\hat{\rho}_t$,

$$\hat{\rho}_{t+\epsilon} = \int d\mu \mathcal{U}_{\epsilon \hat{f}_t + \omega_t}(\hat{\rho}_t), \tag{27}$$

where the integration measure is

$$d\mu \equiv \prod_{l=0}^3 d\omega_t^l p^l(\omega_t^l), \tag{28}$$

with the normalization condition,

$$\int d\mu = 1, \tag{29}$$

and where each random unitary is given by

$$\mathcal{U}_{\epsilon \hat{f}_t + \omega_t}(\hat{\rho}_t) \equiv \hat{U}_{\epsilon \hat{f}_t + \omega_t} \hat{\rho}_t \hat{U}_{\epsilon \hat{f}_t + \omega_t}^\dagger. \tag{30}$$

We have omitted, for the sake of simplicity, the multiplication of ω_t by the identity operator acting on the position space, and will do so from now on unless otherwise mentioned. As expected (since we impose the linearity of the theory and the Hermiticity of $\hat{\rho}_t$ [62]), this evolution, equation (27), has the form of a Kraus decomposition, the densities of the Kraus operators being simply the random unitaries $\hat{U}_{\epsilon \hat{f}_t + \omega_t}$ (for simplicity, we have left the probability density in the integration measure $d\mu$, i.e., we have not included it in the definition of the Kraus operators).

3.2.2. Continuum limit. As in previous sections, we assume that the random variables introduced above, Ω_t^l , actually result from the product $\Omega_t^l \equiv \phi^l(\epsilon) \tilde{\Omega}_t^l$, where $\phi^l(\epsilon)$ is a function going to zero with ϵ , and $\tilde{\Omega}_t^l$ is *new random variable that we introduce*. This assumption ensures that $\hat{U}_{\epsilon \hat{f}_t + \Omega_t} \rightarrow \mathbb{1}$ as $\epsilon \rightarrow 0$, which, in turn, ensures that equation (27) remains consistent in that limit. For a large class of functions ϕ^l , we have that $\phi^l(\epsilon)$ is dominated, for $\epsilon \rightarrow 0$, by a term

¹⁵ This implies, in particular, that the noise is classically Markovian, since one can give, for any t and any $\omega_t \in \mathbb{R}$, the probability that $\Omega_t = \omega_t$, without the need to know the past history, i.e., the values $(\omega_{t'})_{\{t' < t\}}$, and hence (sufficient condition for Markovianity), without the need to know $(\omega_{t'})_{\{t' < t-\epsilon\}}$.

which scales as ϵ to some power $\nu_l > 0$. One can show that only $\nu_l = 1/2$ for all l s, delivers a non-trivial, non-unitary, trace-preserving limit for equation (27). We thus assume, in the end,

$$\Omega_t^l \equiv \sqrt{\epsilon} \tilde{\Omega}_t^l, \quad l = 0, \dots, 3, \tag{31}$$

with $\tilde{\Omega}_t^l$ independent from ϵ , i.e., with \tilde{p}^l independent from ϵ^{16} . This assumption is crucial for the upcoming derivation to be valid, because for the Taylor expansion of equation (33) to hold. In other words, this means that we have modified our model: indeed, for, e.g., one realization of this random-unitaries model, one samples, at each time, the 4 values $\tilde{\omega}_t^l$ from their respective probability distributions \tilde{p}^l , and *multiplies them* by $\sqrt{\epsilon}$ before taking the resulting products as arguments of the evolution operator¹⁷. This implies that the probability measure is not anymore that of equation (28), but that associated to the new random variable $\tilde{\Omega}_t^l$, namely,

$$d\tilde{\mu} \equiv \prod_{l=0}^3 d\tilde{\omega}_t^l \tilde{p}^l(\tilde{\omega}_t^l). \tag{32}$$

The Taylor expansion of $\hat{U}_{\epsilon \hat{f}_t + \sqrt{\epsilon} \tilde{\omega}_t}$ at order ϵ is not completely trivial, but can be derived from equation (7), and be cast as

$$\begin{aligned} \hat{U}_{\epsilon \hat{f}_t + \sqrt{\epsilon} \tilde{\omega}_t} &= 1 - i\epsilon \hat{H}_t^o + i\sqrt{\epsilon} \sum_{l=0}^2 \tilde{\omega}_t^l L_l - \frac{1}{2} (\sqrt{\epsilon})^2 \sum_{l=0}^2 (\tilde{\omega}_t^l)^2 (L_l)^2 \\ &\quad - (\sqrt{\epsilon})^2 [\tilde{\omega}_t^0 (\tilde{\omega}_t^1 \sigma^3 + \tilde{\omega}_t^2 \sigma^1) + \tilde{\omega}_t^2 \tilde{\omega}_t^3 (i\sigma^2)] + O(\epsilon^{3/2}). \end{aligned} \tag{33}$$

In this Taylor expansion, we recover a known, Hamiltonian part, \hat{H}_t^o , given by equation (22), and the L_l s, $l = 0, 1, 2$, are defined by equation (25) with $L_0 \equiv \mathbf{1}_2$. Notice that the variable $\tilde{\omega}_t^3 \equiv \tilde{\chi}_t$ only appears in the crossed terms, which are those just before the $O(\epsilon^{3/2})$.

Inserting the above Taylor expansion, equation (33), in the evolution equation, equation (27), and taking into account that the $\tilde{\Omega}_t^l$ s, varying l , are *independent* random variables (which is visible in the integration measure, equation (32)), and all have *vanishing mean*, yields

$$\hat{\rho} + \epsilon \partial_t \hat{\rho} = \hat{\rho} + \epsilon [-i[\hat{H}^o, \hat{\rho}] + \mathcal{L}_{\tilde{\Delta}^2}(\hat{\rho})] + O(\epsilon^{3/2}), \tag{34}$$

the non-Hamiltonian term being given by equation (23), notice the absence of L_0 , with

$$\tilde{\Delta}^2 \equiv (\tilde{\delta}_t^2)_{l=0, \dots, 3} \tag{35}$$

instead of $\tilde{\Pi} \equiv (\tilde{\pi}_1, \tilde{\pi}_2)$, where $\tilde{\delta}_t^l$ is by definition the standard deviation of $\tilde{\Omega}_t^l$ for any t . Because \tilde{p}^l is time independent, all its moments are, and in particular $\tilde{\delta}_t^2$. Canceling out, in the previous equation, the zeroth-order terms in ϵ , dividing then by ϵ , and letting $\epsilon \rightarrow 0$, yields equation (21)

¹⁶ Notice that \tilde{p}^l cannot depend on time since p^l does not.

¹⁷ That being said, maybe one can show that, though this condition (i.e., equation (31) with $\tilde{\Omega}_t^l$ independent of ϵ), is sufficient to derive the results to come, namely, equation (34), it is not necessary. Indeed, maybe one can show that the following, *milder* condition is sufficient to obtain equation (34), namely, that the random variables Ω_t^l scale as $\sqrt{\epsilon}$ only *on average*, i.e., that their standard deviation does. While the assumption made for the road we are going to follow, i.e., equation (31) with $\tilde{\Omega}_t^l$ independent of ϵ , implies the previous condition, the converse does not hold: indeed, although we can for sure always define $W_t^l \equiv \Omega_t^l / \sqrt{\epsilon}$, there is no reason, in the general case, that W_t^l does not depend on ϵ . In the case of uniform or Gaussian distributions, the two conditions are equivalent, but their are *a priori* not in the general case.

with $\tilde{\Delta}^2$ instead of $\tilde{\Pi}$. Notice that neither the noise on ξ^0 , nor that on χ , have any effect in this continuum limit.

Notice that the present random-unitaries-model formal continuum limit is for a DTQW that accepts a 1-step continuum limit [63]. The random-unitaries-model formal continuum limit has started to be explored for DTQWs accepting, not a 1-step continuum limit, but a 2-step one, in reference [61].

4. Dirac Lindblad equation with chirality-flip channel: a model of quantum relativistic diffusion

4.1. Description of the problem

4.1.1. Presentation. In the previous section, we have presented two spacetime-lattice models of quantum transport with temporal noise, equations (19) and (27), that deliver, in the continuum limit, the same (1 + 1)D Lindblad equation with Dirac Hamiltonian part and two standard error channels on the chirality: (i) a phase-flip channel with rate (probability per unit time) $\gamma_1/2 = \tilde{\pi}_1 = \tilde{\delta}_1^2$, and (ii) a bit-flip channel with rate $\gamma_2/2 = \tilde{\pi}_2 = \tilde{\delta}_2^2$. This Lindblad equation reads

$$\partial_t \hat{\rho} = -i[\hat{H}^o, \hat{\rho}] + \mathcal{L}_{\Gamma/2}(\hat{\rho}), \tag{36}$$

where \hat{H}^o is given by equation (22), $\mathcal{L}_X(\hat{\rho})$ by equation (24), and

$$\Gamma \equiv (\gamma_1, \gamma_2). \tag{37}$$

For the sake of simplicity, we choose a vanishing electric potential,

$$(A_0, A_1) = 0, \tag{38}$$

and a mass term

$$m \text{ independent of both space and time.} \tag{39}$$

How does the noise, $\mathcal{L}_{\Gamma/2}(\hat{\rho})$, on the chirality d.o.f. of the Dirac fermion, affect the dynamics of the spatial d.o.f.? A coupling between these two d.o.f.s is indeed expected, at a quantum level, because the mass entangles them¹⁸. We will see in section 4.2 that, although a vanishing mass indeed destroys the *purely quantum* coupling (i.e., the entanglement) between the internal and external d.o.f.s, the relativistic nature of the equation still introduces a certain coupling between the internal and external d.o.f.s, but which can be seen as *purely classical*, i.e., the intrinsic quantum nature of the chirality d.o.f. has no purely quantum phenomenal consequence, and this chirality could, in this massless case, be described in a non-quantum manner.

4.1.2. Equations on the Pauli basis. We decompose, for convenience, $\hat{\rho}_t$ on the Pauli basis,

$$\hat{\rho}_t = \frac{1}{2} \sum_{\mu=0}^3 \hat{\tau}_t^\mu \sigma^\mu, \tag{40}$$

¹⁸ This does not hold in a non-relativistic setting, i.e., the massive, free dynamics, does not entangle the internal and external d.o.f.s. The presence of a *non-uniform* magnetic field does always produce, be the model relativistic or not, such an entanglement, which is exemplified by the historical Stern–Gerlach experiment [64], which can be accounted for by a non-relativistic model.

where $\sigma^0 \equiv \mathbf{1}_2$. The \hat{r}_t^μ s are observables acting solely on the position space, which can be obtained from $\hat{\rho}_t$ by the following partial trace, denoted Tr_c , on the internal d.o.f.,

$$\hat{r}_t^\mu = \text{Tr}_c(\hat{\rho}_t \sigma^\mu). \tag{41}$$

In appendix B, we briefly comment on \hat{r}_t^0 and \hat{r}_t^3 .

Equation (36) can be rewritten as the following equation (\hat{p} is the momentum operator),

$$\partial_t \vec{\hat{r}} = \mathbf{P} \hat{p} \vec{\hat{r}} + \mathbf{P}^\dagger \vec{\hat{r}} \hat{p} + \mathbf{Q} \vec{\hat{r}}, \tag{42}$$

on the 4-component vector (of operators)

$$\vec{\hat{r}} \equiv (\hat{r}^0, \hat{r}^1, \hat{r}^2, \hat{r}^3)^\top, \tag{43}$$

where we have introduced two 4×4 matrices,

$$\mathbf{P} \equiv \begin{bmatrix} \cdot & \cdot & \cdot & \mathbf{i} \\ \cdot & \cdot & 1 & \cdot \\ \cdot & -1 & \cdot & \cdot \\ \mathbf{i} & \cdot & \cdot & \cdot \end{bmatrix}, \quad \mathbf{Q}_{\Gamma,m} \equiv \begin{bmatrix} \cdot & \cdot & \cdot & \cdot \\ \cdot & -\gamma_1 & \cdot & \cdot \\ \cdot & \cdot & -(\gamma_1 + \gamma_2) & -2m \\ \cdot & \cdot & 2m & -\gamma_2 \end{bmatrix}, \tag{44}$$

where we have denoted, in the matrices, the zeros by dots to make the writing less cumbersome. The matrices \mathbf{P} and $\mathbf{Q}_{\Gamma=0,m}$ are anti-Hermitian, because they correspond to the Hamiltonian part of the original equation on $\hat{\rho}$, equation (36), while $\mathbf{Q}_{\Gamma,m=0}$ is Hermitian (more precisely, diagonal and real), and corresponds to the non-Hamiltonian part of the original equation.

4.1.3. Explicit solution via Fourier transform. Since we have chosen a vanishing electromagnetic potential, equation (38), a spacetime-independent mass term, equation (39), and a space-independent noise, equation (42) is diagonal in momentum space. We introduce the momentum basis, $\{|p\rangle, p \in \mathbb{R}\}$. Applying $\langle p|$ on the left of equation (42), and $|q\rangle$ on its right, we obtain

$$\partial_t \vec{\tilde{r}}_{pq} = \mathbf{G}_{pq} \vec{\tilde{r}}_{pq}, \tag{45}$$

where

$$\tilde{r}_{pq}^\mu \equiv \langle p| \hat{r}^\mu |q\rangle, \tag{46}$$

and where we have introduced the following generator of the transport,

$$\mathbf{G}_{pq} \equiv \begin{bmatrix} \cdot & \cdot & \cdot & \mathbf{i}(p - q) \\ \cdot & -\gamma_1 & p + q & \cdot \\ \cdot & -(p + q) & -(\gamma_1 + \gamma_2) & -2m \\ \mathbf{i}(p - q) & \cdot & 2m & -\gamma_2 \end{bmatrix}. \tag{47}$$

The solution of equation (45) is well-known, and reads (we reintroduce the time label),

$$\vec{\tilde{r}}_{t,pq} = \mathbf{M}_{pq}(t - t_0) \vec{\tilde{r}}_{t_0,pq}, \tag{48}$$

where

$$\mathbf{M}_{pq}(t - t_0) \equiv e^{(t-t_0)\mathbf{G}_{pq}}. \tag{49}$$

In position space, the solution of our problem can thus be written explicitly as a two-dimensional Fourier transform, namely,

$$r_{t,xy}^\mu = \frac{1}{2\pi} \int \int_{\mathbb{R}^2} dp dq (\mathbf{M}_\nu^\mu)_{pq}(t - t_0) \tilde{r}_{t_0,pq}^\nu e^{i(px - qy)}, \tag{50}$$

where we sum over $\nu = 0, \dots, 3$. Since the matrix \mathbf{G}_{pq} is diagonalizable and can therefore be exponentiated, equation (50) provides a formal solution to the dynamics of $r_{t,xy}^\mu$. However, the diagonal form (and thus the exponential) is very cumbersome in the massive case, so that the explicit solution does not give insight on the phenomena it describes. Of course, one can always compute these integrals numerically and plot all desired observables. In what follows, we have used this expression only in the massless case, to check that it gives the same result as our numerical integration. The matrix exponential can in this case be performed directly using a symbolic mathematics software, without prior diagonalization. In the following sections, we shall get insight on the different regimes of the dynamics, first by viewing the equations directly in position space, just below.

4.1.4. System of equations in position space, and remarks. Let us rewrite our system of equations, equation (42), not in momentum space as above in equation (45), but in position space, by applying $\langle x|$ on the left of equation (42), and $|x'\rangle$ on its right, which yields

$$\partial_t r_{xx'}^0 = (\partial_x + \partial_{x'}) r_{xx'}^3 \tag{51a}$$

$$\partial_t r_{xx'}^3 = (\partial_x + \partial_{x'}) r_{xx'}^0 - \gamma_2 r_{xx'}^3 + 2 m r_{xx'}^2 \tag{51b}$$

$$\partial_t r_{xx'}^1 = -i(\partial_x - \partial_{x'}) r_{xx'}^2 - \gamma_1 r_{xx'}^1 \tag{52a}$$

$$\partial_t r_{xx'}^2 = i(\partial_x - \partial_{x'}) r_{xx'}^1 - (\gamma_1 + \gamma_2) r_{xx'}^2 - 2 m r_{xx'}^3, \tag{52b}$$

with

$$r_{xx'}^\mu \equiv \langle x| \hat{r}^\mu |x'\rangle. \tag{53}$$

One immediately sees that the mass couples equations (51) and (52). The case of a non-vanishing mass, $m \neq 0$, and no noise, $\Gamma = 0$, simply corresponds to standard, Dirac propagation [65, 66], and is recalled in appendix C.

Using the definition provided in equation (53), one can prove that

$$(\partial_x + \partial_{x'}) r_{xx'}^\mu |_{x=x'} = \partial_x R_x^\mu, \tag{54}$$

where

$$R_x^\mu \equiv r_{xx}^\mu, \tag{55}$$

so that the above system of four equations (51) and (52), considered for $x = x'$, yields

$$\partial_t R_x^0 = \partial_x R_x^3 \tag{56a}$$

$$\partial_t R_x^3 = \partial_x R_x^0 - \gamma_2 R_x^3 + 2 m R_x^2 \tag{56b}$$

$$\partial_t R_x^1 = -i(\partial_x - \partial_{x'}) r_{xx'}^2 |_{x=x'} - \gamma_1 R_x^1 \tag{57a}$$

$$\partial_t R_x^2 = i(\partial_x - \partial_{x'}) r_{xx'}^1 |_{x=x'} - (\gamma_1 + \gamma_2) R_x^2 - 2 m R_x^3. \tag{57b}$$

Notice that the R^μ s are real since the \hat{r}^μ s are Hermitian.

Decomposing $r_{xx'}^\mu$ in its real and imaginary parts,

$$r_{xx'}^\mu \equiv a_{xx'}^\mu + ib_{xx'}^\mu, \tag{58}$$

and recalling that the \hat{r}^μ s are Hermitian, equation (57) can be written as equation (60) below, which show that the reality of R^1 and R^2 is consistent with their evolution equations, since the latter only involve real coefficients and unknowns.

Now, notice that in the two first equations above, (56), only the densities, i.e., the quantities taken for $x = x'$, are involved. It also turns out that one can decouple R_x^0 from R_x^3 in equation (56), by increasing the order of the equations from 1 to 2 in time: after a few manipulations, one indeed realizes that R_x^0 and R_x^3 follow the same, following equation, equation (59),

$$\partial_t^2 R_x^d + \gamma_2 \partial_t R_x^d = \partial_x^2 R_x^d + 2m \partial_x R_x^2, \quad d = 0 \text{ or } 3, \tag{59}$$

$$\partial_t R_x^1 = 2\partial_x b_{xx'}^2|_{x=x'} - \gamma_1 R_x^1 \tag{60a}$$

$$\partial_t R_x^2 = -2\partial_x b_{xx'}^1|_{x=x'} - (\gamma_1 + \gamma_2)R_x^2 - 2mR_x^3. \tag{60b}$$

4.2. $m = 0, \Gamma \neq 0$: a chirality-flip noise on massless Dirac fermions yields the telegraph equation

If $m = 0$, equations (59) and (60) become

$$\partial_t^2 R_x^d + \gamma_2 \partial_t R_x^d = \partial_x^2 R_x^d, \quad d = 0 \text{ or } 3, \tag{61}$$

$$\partial_t R_x^1 = 2\partial_x b_{xx'}^2|_{x=x'} - \gamma_1 R_x^1 \tag{62a}$$

$$\partial_t R_x^2 = -2\partial_x b_{xx'}^1|_{x=x'} - (\gamma_1 + \gamma_2)R_x^2, \tag{62b}$$

which, as mentioned early in section 4.1.4, decouples equation (61) from equation (62).

4.2.1. Dynamics of the spatial degree of freedom: no quantumness. R^0 and R^3 are, respectively, the probability density and the left-current density. They code, together, for the diagonal coefficients of the density matrix in the full Hilbert space. They follow the same telegraph equation, equation (61), with characteristic speed and diffusion coefficients $c = 1$ and

$$D \equiv \frac{1}{\gamma_2}, \tag{63}$$

respectively: the chirality-flip noise causes the massless Dirac fermion to diffuse, in addition to its unitary propagating behavior. Notice that the phase-flip noise, characterized by γ_1 , has no effect on the dynamics of R^0 , nor on that of R^3 , in this massless case; this is commented in appendix D.

Consider equation (61) alone: because of the vanishing mass, it contains no quantum feature. If one can write down a dynamical equation for the density and current density, and needs no quantum amplitude of probability¹⁹, this means that the essence of the quantumness of the system, that is, coherence and entanglement, is, if any, limited to the internal off-diagonal space, described by \hat{r}^1 and \hat{r}^2 , coupled to each other through the system of equation (52), which is autonomous (i.e., independent of (51)) because m vanishes. That

¹⁹ So that no purely quantum phenomena can arise from the coherences $r_{xx'}^d, d = 0, 3$.

equation (61) contains no quantum feature is to be understood as the fact that the chirality-flip noise affects the spatial dynamics in a *purely classical manner*, i.e., *not* via *entanglement*.

In other words, the telegraph equation can be derived from a purely non-quantum modeling of the system. In particular, if viewed as a continuum limit of some discrete-spacetime dynamics, our system corresponds to a *persistent classical random walk* [67]. This is in contrast with the simpler, well-known *classical random walk*, which (i) is the one that is usually considered when the transport has no relativistic feature, and which (ii) leads to diffusion in the continuum²⁰ [17]. The telegraph equation can model the propagation of classical waves of light/electricity with dissipation (in wires, for example, hence its name) [67]. At short (long) times, propagation (diffusion) dominates over diffusion (propagation) [67]. Notice that the telegraph equation was proposed by Cattaneo to model relativistic diffusions and can be viewed as a precursor of extended thermodynamics models.

In the light of the comments of the previous paragraph, the massive noisy quantum model of the present work, equation (36), can be seen as a quantum model of relativistic diffusion. Other models which could be qualified as such for the same reasons, have been considered in the literature, but apparently mostly with a noise introduced *directly on the spatial d.o.f.* [71–74]. A particularity of the present work is thus to *introduce the noise on the internal d.o.f. only*. The solution of the telegraph equation, equation (61), is given by equation (70) for $\gamma_1 = 0$, so that $b = 0$ and $\kappa = \gamma_2$ in equation (69).

4.2.2. Dynamics of the internal d.o.f.: standard bit-flip decohering dynamics, classically coupled to the spatial degree of freedom. Without the external d.o.f. (i.e., replace $S(\hat{p})$ by $\mathbb{1}$ in equation (2)), we are left with the two standard error channels [60, 75] that we have introduced on the coin (see equations (51) and (52)): the populations’ difference r^3 decays exponentially with a rate γ_2 , and the real (resp. imaginary) part of the coherences, r^1 (resp. r^2), also decays exponentially, with a rate γ_1 (resp. $\gamma_1 + \gamma_2$). These two coin error channels²¹ are *purely* and *fully* decohering, i.e. (this is our terminology), they make the coherences decrease, as time increases, *monotonically* and *down to zero*, respectively, and in any basis of the internal space; that the populations’ difference go to zero is also independent of the basis²².

Let us now reconsider the external d.o.f.. Similarly to equation (54), one can prove the following identity,

$$(\partial_x - \partial_{x'})r_{xx'}^\mu|_{x=-x'} = \partial_x T_x^\mu, \tag{64}$$

where

$$T_x^\mu \equiv r_{x,-x}^\mu, \tag{65}$$

measures the coherence between the states $|x\rangle$ and $|-x\rangle$, and inserting equation (64) for $\mu = 1, 2$ into equation (52) yields, for $m = 0$,

$$\partial_t T^1 = -i\partial_x T^2 - \gamma_1 T^1 \tag{66a}$$

$$\partial_t T^2 = i\partial_x T^1 - (\gamma_1 + \gamma_2) T^2. \tag{66b}$$

²⁰ The *mathematical* connection, via analytical continuation, between the standard, unitary, i.e., non-noisy DTQW, and the telegraph equation, is well-known [68–70]. In the present work, the connection is not merely mathematical, but *physical*, via the introduction of noise in the unitary dynamics. More generally, whether the existence of such a type of connection via analytic continuation implies a physical connection when introducing a noise is an interesting question to be investigated.

²¹ By definition, a qubit error channel maps a pure state to a mixed state.

²² These results can be checked by a simple, direct computation.

Analogously to the manipulation performed to go from equations (56)–(59), one can actually decouple T^1 and T^2 : they follow the same telegraph equation as R^0 and R^3 but with a modified diffusion coefficient,

$$D' \equiv \frac{1}{2\gamma_1 + \gamma_2}, \tag{67}$$

and an additional self source of decoherence induced by γ_1 ,

$$\partial_t^2 T^i + \kappa \partial_t T^i = \partial_x^2 T^i + b T^i, \quad i = 1 \text{ or } 2, \tag{68}$$

with

$$\kappa \equiv 2\gamma_1 + \gamma_2 \geq 0 \tag{69a}$$

$$b \equiv -\gamma_1(\gamma_1 + \gamma_2) \leq 0. \tag{69b}$$

The solution of this equation, provided on page 217 of reference [76], reads

$$\begin{aligned} F_{t,x} = & \frac{1}{2} e^{-\frac{\kappa}{2}t} [f_{x+t} + f_{x-t}] + \frac{\gamma_2}{2} \frac{t}{2} e^{-\frac{\kappa}{2}t} \int_{x-t}^{x+t} dy \frac{I_1\left(\frac{\gamma_2}{2}z_y\right)}{z_y} f_y \\ & + \frac{1}{2} e^{-\frac{\kappa}{2}t} \int_{x-t}^{x+t} dy I_0\left(\frac{\gamma_2}{2}z_y\right) \left[g_y + \frac{\kappa}{2}f_y\right], \end{aligned} \tag{70}$$

where

$$z_y \equiv (t^2 - (x - y)^2)^{1/2}, \tag{71}$$

$$I_\nu(X) \equiv \sum_{n=0}^{+\infty} \frac{(X/2)^{\nu+2n}}{n! \Gamma(\nu + n + 1)}, \tag{72}$$

is the modified Bessel function of the first kind, and where we need two initial conditions because the equation is of order 2 in time,

$$f_x \equiv F_{0,x} \tag{73a}$$

$$g_x \equiv \partial_t F|_{0,x}. \tag{73b}$$

The first thing to mention is that, if both the initial function, $T^i_{t=0}$, and the initial time derivative, $\partial_t T^i|_{t=0}$, both vanish, then $T^i_t = 0$ for any t , i.e., *the dynamics generates no coherence between x and x'* . This is a consequence of choosing both a vanishing mass and a purely decohering noise. If γ_1 vanishes, no decoherence comes from self sources anymore (phase-flip channel); the remaining decoherence only comes from the chirality-flip channel, and, as already mentioned, the dynamics followed by both T^1 and T^2 is exactly the same as that followed by R^0 and R^3 , and can be viewed as the consequence of a purely classical coupling between the internal and the external d.o.f.s. In summary: the initial amount of coherence between the two internal states which is initially introduced in the system, is, as coherence between x and $-x$, spatially transported classically exactly as the probability density.

4.3. $m \neq 0, \Gamma \neq 0$: *chirality-flip noise on massive Dirac fermions (in the low-dispersion, that is, semi-classical regime)*

In appendix C, we recall the case, ($m \neq 0, \Gamma = 0$), of standard, Dirac propagation [65, 76]. Now, we want to investigate how the (sole) chirality-flip noise influences a *massive* Dirac fermion.

Already in the noiseless case, one can distinguish two regimes: (i) a *low-dispersion* regime, in which the global propagation, i.e., the average speed of the distribution, dominates over dispersion, i.e., over the average speed at which the distribution spreads with respect to the mean position, and (ii) its counterpart, the *dispersive* regime. Let us, for simplicity, focus on the first regime, that is, the non-quantum, or, rather, as we have called it, low-dispersion one, that can be approximately described as the propagation of a classical wave (in vacuum, a classical wave does not disperse)²³. That is, let us study the classical features of our dynamics, equation (56). As induced from the former, massless case, in section 4.2, it should be meaningful to qualify this classical dynamics as a *massive relativistic diffusion*.

4.3.1. *Validity of the low-dispersion regime (noiseless study)*. Let us consider the noiseless case, detailed in appendix C. If σ , the momentum spread of the initial (Gaussian) positive-energy wavepacket, equation (C10) for $t = 0$, is much smaller than the initial average momentum p_0 , that is, if

$$\frac{\sigma}{p_0} \ll 1, \tag{74}$$

then, intuitively, dispersion should be negligible with respect to propagation during some time. Let us evaluate this more precisely. One can prove (not shown) that, if condition (74) is satisfied, then one can approximate the dispersion relation $E_p = \sqrt{p^2 + m^2}$ by a quadratic function of $p - p_0$ by Taylor expanding it around p_0 , that is, one can make what we call the quadratic-dispersion-relation (QDR) approximation, which, conveniently, enables to do analytical computations (Gaussian integrals). In the QDR approximation, the mean position and spread are respectively given by

$$v_g \equiv \left. \frac{\partial E_p}{\partial p} \right|_{p=p_0} = \frac{p_0}{\sqrt{p_0^2 + m^2}} \tag{75}$$

and by equation (C15b). One can then prove (not shown) by an explicit computation that condition (74) actually ensures

$$\frac{v_d}{v_g} \ll 1, \tag{76}$$

that is, that we are in the low-dispersion regime.

²³ We say ‘low-dipersion’ rather than ‘non-quantum’ because we consider here no potential energy, so that the counterpart, dispersive regime is not ‘that quantum’ either, in the following sense. Consider first the non-relativistic regime: it is well-known that, without a potential energy, the Schrödinger equation can be seen as a classical wave equation in a dispersive medium, with dispersion relation $p^2/2m$. Now, if we are not in the non-relativistic regime, the only quantum feature is Zitterbewegung; apart from it, free Dirac propagation could be described by a scalar amplitude propagating classically in a dispersive medium, with dispersion relation $\sqrt{p^2 + m^2}$.

4.3.2. Physical quantities to be studied. Let us introduce the first moment of the probability distribution, i.e., the mean position,

$$\langle x \rangle_t \equiv \int_{\mathbb{R}} dx x P_{t,x}, \tag{77}$$

where $P_{t,x} \equiv R_{t,x}^0$ is the presence density, or probability distribution, defined in equation (55).

Let us also introduce the second, *non-centered* moment of the probability distribution, that is,

$$\langle x^2 \rangle_t \equiv \int_{\mathbb{R}} dx x^2 P_{t,x}. \tag{78}$$

Finally, let us introduce the exponent,

$$\eta_t \equiv \frac{d \ln(\langle x^2 \rangle_t - \langle x^2 \rangle_0)}{d \ln t}, \tag{79}$$

of the numerical fit of $\langle x^2 \rangle_t$, defined in equation (78), by a power law, that is,

$$\langle x^2 \rangle_t \underset{\text{fit}}{\simeq} \alpha t^\eta + \langle x^2 \rangle_0, \tag{80}$$

where α is some constant.

4.3.3. Numerical study. Consider an initial (Gaussian) positive-energy wavepacket, equation (C10) for $t = 0$, satisfying condition (74)²⁴, and let it evolve according to equation (36) with

$$\text{choice: } \gamma_1 = 0, \tag{81a}$$

$$\text{notation: } \gamma_2 = \gamma. \tag{81b}$$

We have implemented this evolution numerically, via an implicit scheme, described in appendix E. The dynamics displayed can be split into two or three regimes, as detailed further down. The simplest, two-regimes description is the following one: first, a *propagative* regime, in which propagation dominates over diffusion, and second, a *diffusive* regime, in which diffusion dominates over propagation. There are several possible criteria to precisely define the ‘domination’ one refers to. In the three-regimes description, illustrated in figure 1, there is transient regime, as we shall see in more detail. Let us characterize all the aforementioned regimes by analyzing all figures 1–3.

Let us focus on figure 2, displaying $\langle x \rangle_t$. One can easily check (not shown) that the initial time derivative of $\langle x \rangle_t$ is always v_g to a very good approximation. It is thus natural to introduce a time t_1 such that, up to this time, $\langle x \rangle_t$ is approximable $v_g t$. Of course, t_1 depends on the desired precision of this approximation. From 0 to t_1 , the dynamics is thus not only propagative, but also low-dispersion. One can then define a transient regime from t_1 to some t_2 such that for $t \geq t_2$, the mean position $\langle x \rangle_t \simeq \text{constant}$, a constant indeed manifestly reached as it can be seen on figure 2. Of course, t_2 depends on the desired precision of the constant fit of $\langle x \rangle_t$ for $t \geq t_2$. The regime from t_2 to infinity is a diffusive one, as we shall see below.

²⁴ So that, by extrapolating from the noiseless study of the previous section 4.3.1, we expect—when the Hamiltonian part of the Lindblad equation, equation (36), dominates over the noise part—to be in the low-dispersion regime (rather than the dispersive one).

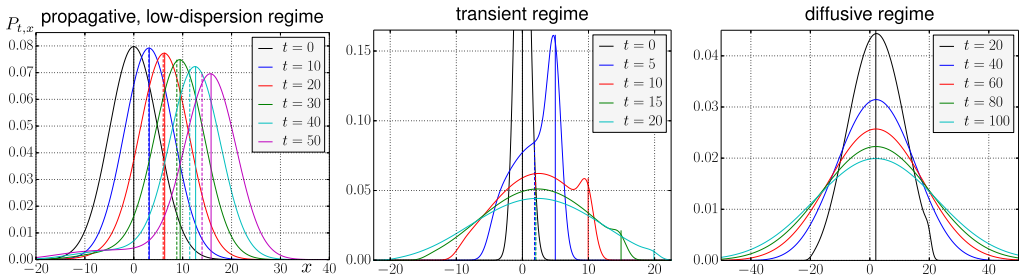


Figure 1. Probability density $P_{t,x} \equiv R_{t,x}^0$ (see equation (55)) of the massive, relativistic particle experiencing the (quantum) relativistic diffusion governed by the Dirac Lindblad equation (36) with $\gamma_1 = 0$, as a function of the position x on the line, for different times t . The first thing to mention is that the parameters and initial wavefunction—a (Gaussian) positive-energy wavepacket, equation (C10)), of the standard Dirac equation—have been chosen such that the dynamics is essentially classical, i.e., non-quantum, see the explanations in the main text. The dynamics clearly displays, as time evolves, three regimes. The first, propagative, low-dispersion regime, from $t = 0$ to a t_1 defined in section 4.3.3, is illustrated in the left panel, for which we have chosen $\gamma \equiv \gamma_2 = 0.05$, $p_0 = 1$ and $m = 3$, so that the group velocity $v_g \simeq 0.31$, and $\sigma = 0.1$, so that $\sigma/p_0 = 1/10$, which is why the global propagation dominates over dispersion: indeed, one can see that the mean position $\langle x \rangle_t$ of the distribution (see equation (77)), represented by dashed vertical lines, differs very little from the ballistic group motion $v_g t$, represented by solid vertical lines; Of course, the discrepancy between both increases with time. In the middle and right panels, we have chosen $\gamma = 0.5$, $p_0 = 5$ and $m = 0.5$, so that the group velocity $v_g \simeq 0.995$, and $\sigma = 0.5$ (so that $\sigma/p_0 = 1/10$ and we should still be, at least initially, in a low-dispersion case). Notice that the parameters used in the plots have been chosen in order to qualitatively better display each of the three regimes. The second, transient regime, from t_1 to a t_2 defined in 4.3.3, is illustrated in the middle figure: one can very clearly see how diffusion progressively takes over the ballistic motion of the initial density peak. The third, diffusive regime, from t_2 to infinity, is illustrated in the right figure: one can easily check numerically that this regime tends toward a standard diffusion, with variance $4Dt$, where $D = 1/\gamma$.

This was the three-regimes description. The interest of the two-regimes description is that we naturally introduce a time t_{mid} which, unlike t_1 and t_2 , is not arbitrary, i.e., depending on some desired precision, but *characteristic of the dynamics*. This t_{mid} could be, e.g., when the second derivative of $\langle x \rangle_t$ reaches its maximum (see figure 2), or when it is the second derivative of η_t which reaches its maximum (see figure 3).

Now, that the dynamics always tends toward an exact diffusion for $t \rightarrow +\infty$, i.e., with a variance scaling as t , seems to be expected from figure 3. One can easily check (not shown) that the diffusion coefficient is, in all shown cases, that of the massless case, $D = 1/\gamma$, i.e., that the variance equals $4Dt$, as expected from the fact that the Lindblad equation is linear and that there is no other diffusion term than that with diffusion coefficient D .

Let us comment on the limit position x_{max} seen on figure 2. In all the cases studied in figure 2, this limit position turns out to be very well approximated by

$$x_{max} \underset{fit}{\simeq} x_{lim}(v_g, \gamma) \equiv \frac{1}{v_g \gamma} \equiv \frac{D}{v_g}, \tag{82}$$

whose numerical values have been represented by black, dashed horizontal lines. Both the dependencies in v_g and D can be understood qualitatively by extrapolating from the massless case, where the probability density $P_{t,x} \equiv R_{t,x}^0$ follows a telegraph equation, equation (61), that

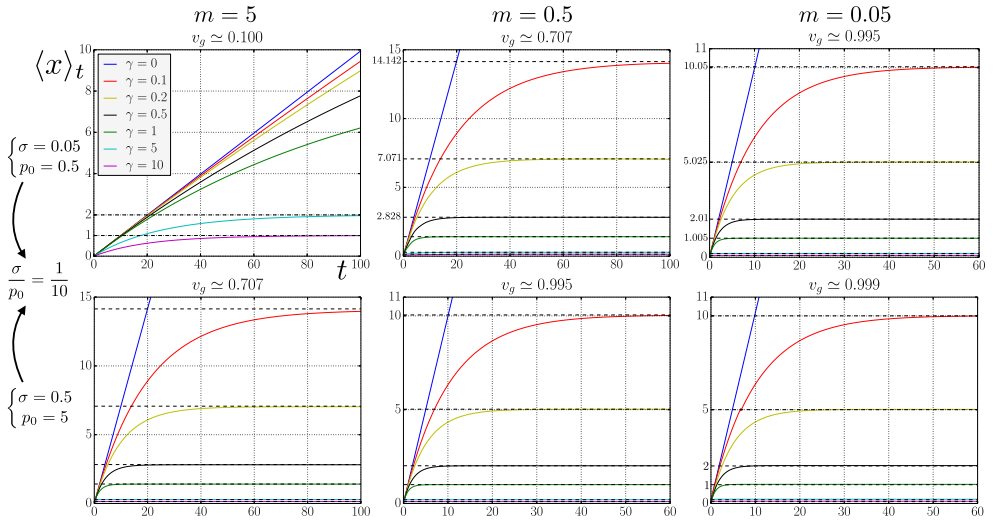


Figure 2. Time evolution of the mean position, $\langle x \rangle_t$ (see equation (77)), of an initial (Gaussian) positive-energy wavepacket of the standard Dirac equation, see appendix C, evolved through the Dirac Lindblad equation (36) with $\gamma_1 = 0$ and notation $\gamma_2 = \gamma$, i.e., a sole chirality-flip noise. The first (resp. second) row of plots corresponds to fixing a width $\sigma = 0.05$ and a mean momentum $p_0 = 0.5$ (resp. $\sigma = 0.5$ and $p_0 = 5$), and the ratio $\sigma/p_0 = 1/10$ is fixed on all plots. The first column of plots corresponds to $m = 5$, the second to $m = 0.5$, and the third to $m = 0.05$. We are in the low-dispersion regime, where the width of the initial wavepacket is much smaller than the initial average momentum, $\sigma \ll p_0$, so that the competition is expected to be between the global propagation of the wavepacket and its diffusion due to the noise, the second one increasingly dominating over the first one as time evolves. The wavepacket initially evolves ballistically at speed v_g , but later approaches asymptotically a limit position $x_{lim}(v_g, \gamma) \equiv 1/(v_g \gamma) \equiv D/v_g$, see equation (82), represented by dashed horizontal lines. After reaching the limit position, the probability distribution seems to experience an exact diffusion, see figure 3. One can see that the top–center (top–right) and bottom–left (bottom–center) figures seem to be almost the same, which suggests that the parameters that characterize the dynamics are (apart from γ), the ‘dispersion/(global propagation)’ ratio, i.e., σ/p_0 , which characterizes the degree of dispersiveness, and (ii) the group velocity v_g , which characterizes the initial global propagation. The role played by v_g , not only up to x_{lim} , but also after, is discussed further in the right-most series of plots of figure 3. Notice that, as v_g converges to 1, x_{lim} converges to D .

we rewrite here,

$$\frac{D}{c^2} \partial_t^2 P_x + \partial_t P_x = D \partial_x^2 P_x. \tag{83}$$

We recall that here the characteristic speed is $c = 1$. We have omitted the time index of $P_{t,x}$ as in equation (61).

What accounts for x_{max} diminishing when D does is the following. As D diminishes, the second time derivative in equation (83), $(D/c^2) \partial_t^2 P_x$, diminishes, while the first time derivative, $\partial_t P_x$, remains unaffected, so that propagation faints with respect to diffusion. This is a remarkable specificity of the telegraph equation. Indeed, D is involved not only in the usual diffusion term, $D \partial_x^2 P_x$, but also in the propagation term, $(D/c^2) \partial_t^2 P_x$, and both terms have the same variations as D (they are, more precisely, linear with D), so that a smaller D not only implies, via the usual diffusion term, a slower diffusion, but also, via the propagation term, that the diffusion regime is reached earlier. The telegraph

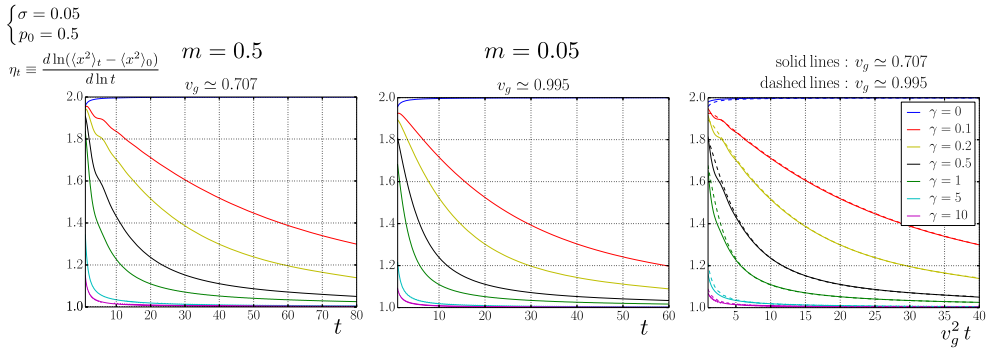


Figure 3. Time evolution of the exponent η_t (see equation (79)). The choices made are exactly the same as in the top row of figure 2, characterized by $\sigma = 0.05$ and $p_0 = 0.5$. We know that our numerical code fails for too small times. In the case $\gamma = 0$, the Fourier-transform solution is computationally easy to plot, and we have checked that in this case η_t is 2 whatever t . We believe that $\eta_{t=0}$ should be 2 (exact ballistic motion) whatever γ . It seems from the plot that η_t always tends to 1 when t tends to infinity, i.e., that the dynamics tends toward an exact diffusion. The left and middle plots manifestly coincide if plotted as a function of $v_g^2 t$.

equation thus appears as the particular case $d = D$ of the following, more general equation, $(d/c^2)\partial_t^2 f + \partial_t f = D\partial_x^2 f$, in which the diffusion coefficient D of the final diffusive regime is, this time, independent from the time taken to reach this diffusive regime, controlled by d (and c).

That x_{\max} diminishes when v_g increases could possibly seem counter-intuitive. The following explanation can actually account for it. In the telegraph equation, that the characteristic speed c increases makes propagation faint with respect to diffusion, i.e., makes the diffusive regime be reached earlier. Now, one can argue that in the massive case, the same mechanism happens, but with a characteristic speed which is not c anymore, but v_g .

It is interesting to put this limit-position effect in perspective with an effect predicted in the Stern–Gerlach experiment [77]. In this case, the system also experiences entanglement between the internal and the spatial degrees of freedom. However, the noise is assumed to be described by the Caldeira–Leggett model, so that it acts on the spatial part, not the internal one. One finds a limit momentum, rather than a limit position.

5. Continuum limit for discrete-time quantum walks with temporal coin noise depending smoothly on the position

5.1. Adding spatial randomness on top of the temporal randomness of the coin unitary

5.1.1. Introduction, and M -point function. We want to allow the temporally random coin unitaries of section 3.2 to be random also spatially. We thus introduce a random variable $\Omega_{t,x}^l$ for each lattice position $x \in \mathbb{L}$, where, for more definiteness, we have considered, instead of $\mathbb{Z}\epsilon$, a finite lattice

$$\mathbb{L} \equiv \{x_1, \dots, x_M\}, \tag{84}$$

with M some positive integer. From now on, we will omit the specification ‘ $\in \mathbb{L}$ ’ when writing ‘ $x \in \mathbb{L}$ ’. We keep the temporal independence of the random variables, i.e., $\Omega_{t_1,x}^l$ is independent on $\Omega_{t_2,x'}^{l'}$ for $t_2 \neq t_1$, whatever (l, x, l', x') (this, in particular, implies the classical Markovianity

of the noise). We assume l -independence in space, i.e., $\Omega_{t,x}^l$ is independent on $\Omega_{t,x'}^{l_2}$ for $l_2 \neq l_1$, whatever (x, x') . Now, we do *not* assume spatial independence at fixed t and l , i.e., a family of real numbers

$$(\omega_{t,x}^l)_x \equiv (\omega_{t,x_1}^l, \dots, \omega_{t,x_M}^l) \in \mathbb{R}^M, \tag{85}$$

where

$$M \equiv \text{number of sites of the lattice}, \tag{86}$$

is issued from a sampling of the family of random variables $(\Omega_{t,x}^l)_x$ according to some *arbitrary* M -point function (i.e., probability distribution), that we denote by $P_{t,(x)_x}^{l,(M)}$ ²⁵, where

$$(x)_x \equiv (x_1, \dots, x_M). \tag{87}$$

The family $(\omega_{t,x}^l)_x$ has thus a probabilistic weight $P_{t,(x)_x}^{l,(M)}((\omega_{t,x}^l)_x)$ ²⁶; in other words, $P_{t,(x)_x}^{l,(M)}((\omega_{t,x}^l)_x)$ is the probability (density) of the event ‘ $\Omega_{t,x_1}^l = \omega_{t,x_1}^l$ and $\Omega_{t,x_2}^l = \omega_{t,x_2}^l, \dots$, and $\Omega_{t,x_M}^l = \omega_{t,x_M}^l$ ’. As in section 3.2 for the spatially homogeneous noise, we assume the stationarity of the noise: $P_{t,(x)_x}^{l,(M)} = P_{(x)_x}^{l,(M)}$.

Instead of the evolution of equation (27), we thus have to consider an evolution of the form

$$\hat{\rho}_{t+\epsilon} = \int d\nu \mathcal{V}_{(\epsilon \bar{f}_{t,x} + \omega_{t,x})_x}^{\text{QW}}(\hat{\rho}_t), \tag{88}$$

where the integration measure $d\nu$, which satisfies the normalization condition $\int d\nu = 1$, is given by

$$d\nu \equiv (d\omega_t)^M P_{(x)_x}^{(M)}((\omega_{t,x})_x), \tag{89}$$

having introduced the notation

$$(d\omega_t)^M \equiv \prod_{l=0}^3 \prod_x d\omega_{t,x}^l, \tag{90}$$

and where, because of the l -independence in space,

$$P_{(x)_x}^{(M)}((\omega_{t,x})_x) = \prod_{l=0}^3 P_{(x)_x}^{l,(M)}((\omega_{t,x}^l)_x). \tag{91}$$

Since the $\omega_{t,x}$ s, varying x , are here mute (they are integration variables), and there is no ambiguity about the time t at which we are if we decide not to change, we will use the simplified notation

$$\lambda_x \equiv \omega_{t,x}. \tag{92}$$

²⁵ The temporal independence assumed above simply means being able to give oneself such a $P_{t,(x)_x}^{l,(M)}$ at any t , without knowing the past history, i.e., the values $(\omega_{t',x'}^l)_{\{t' \leq t\}, \{x'\}}$.

²⁶ That this M -point function is arbitrary implies, in particular, that it is not necessarily given, as it would be for independent random variables, by a product $P_{t,(x)_x}^{l,(M)}((\omega_{t,x}^l)_x) = \prod_x P_t^{l,(1)}(\omega_{t,x}^l)$. Notice that we have not allowed the 1-point function $P_t^{l,(1)}$ to depend on x , i.e., we have imposed translational invariance for the noise. Below in the main text, we extend the definition of translational invariance for non-vanishing correlations between the random variables.

Now, for each family $(\lambda_x^l)_x \in \mathbb{R}^M$, the random-unitaries superoperator is, naturally, given by

$$\mathcal{V}_{(\epsilon\bar{f}_{t,\bar{x}}+\lambda_x)_x}^{\text{QW}}(\hat{\rho}_t) \equiv \hat{V}_{(\lambda_x)_x}^{\text{QW}} \hat{\rho}_t \left(\hat{V}_{(\lambda_x)_x}^{\text{QW}} \right)^\dagger \tag{93}$$

where the random unitaries are, in the present DTQW case,

$$\hat{V}_{(\lambda_x)_x}^{\text{QW}} \equiv C_{\epsilon\bar{f}_{t,\bar{x}}+\lambda_x} \hat{S}, \tag{94}$$

with the position-dependent coin operator

$$C_{\epsilon\bar{f}_{t,\bar{x}}+\lambda_x} = \sum_x C_{\epsilon\bar{f}_{t,x}+\lambda_x} |x\rangle \langle x|, \tag{95}$$

and where, to lighten notations, we have used

$$\hat{S} \equiv S(\hat{p}), \tag{96}$$

given in equation (3). As in the spatially homogeneous case in section 3.2, the (densities of) Kraus operators are simply the random unitaries $\hat{V}_{(\lambda_x)_x}^{\text{QW}}$; there is one such operator for each $4M$ -uple $(\lambda_x)_x$.

5.1.2. We only need the 2-point function because the noise is local. We qualify a spatiotemporal noise $(\lambda_y)_y$ as local if the random unitary $\hat{V}_{(\lambda_y)_y}$, with *a priori* arbitrary dependence in $(\lambda_y)_y$, has matrix elements of the form

$$\langle x | \hat{V}_{(\lambda_y)_y} | x' \rangle = \sum_{z \in \mathbb{L}} V_{\lambda_z}^{xx'}, \tag{97}$$

that is, sums of terms depending, each, on a *single* λ_z . It is straightforward to check that the random unitary $\hat{V}_{(\lambda_y)_y}^{\text{QW}}$, equation (94), is local (with, moreover, the single term $z = x$ in the sum of equation (97)). For a few precisions on local noises, see appendix F.

Now, for a local noise as defined in equation (97), the matrix elements $\rho_{t+\epsilon}^{xx'} \equiv \langle x | \rho_{t+\epsilon} | x' \rangle$ are given by²⁷

$$\rho_{t+\epsilon}^{xx'} \equiv \sum_{y,y',z,z'} \int (d\lambda)^M P_{(\bar{x})\bar{x}}^{(M)}((\lambda_{\bar{x}})_{\bar{x}}) V_{\lambda_z}^{xy} \rho_t^{yy'} V_{\lambda_{z'}}^{y'x'} \tag{98a}$$

$$= \sum_{y,y',z,z'} \int d\lambda_z d\lambda_{z'} P_{z,z'}^{(2)}(\lambda_z, \lambda_{z'}) V_{\lambda_z}^{xy} \rho_t^{yy'} V_{\lambda_{z'}}^{y'x'}. \tag{98b}$$

In going from the first to the second line, we have integrated over the variables that do not appear in the integrand, and assumed that, at any order $n = 1, \dots, M$, there is a single marginal, i.e., not several ones that would be produced by having integrated the higher-order functions over different variables, which is ensured if we assume the M -point function to be fully symmetric (i.e., symmetric with respect to all pairs of variables), which, by a natural definition, is a

²⁷ To obtain this, just apply $\langle x |$ (resp. $|x\rangle$) on the left (resp. right) of equation (88) considered, more generally, for a local-noise superoperator \mathcal{V} , i.e., made of unitaries satisfying equation (97), not necessarily of the form \mathcal{V}^{QW} .

necessary feature of the M -point function if we require the noise to be translationally invariant; hence, a sole 2-point function appears,

$$P_{z,z'}^{(2)}(\lambda_z, \lambda_{z'}) \equiv \int \left(\prod_{r=0}^{R-1} \prod_{\tilde{x} \neq z, z'} d\lambda_{\tilde{x}}^r \right) P_{(\tilde{x})_{\tilde{x}}}^{(M)}((\lambda_{\tilde{x}})_{\tilde{x}}), \tag{99}$$

where $\lambda_x \equiv (\lambda_x^r)_{r=0, R-1}$, $R \in \mathbb{N}$ being the number of space (time)-dependent parameters which we consider random in space (in the case of the coin operator parametrized by 4 angles which has been considered in the present work, the maximum R that we can chose is $R = 4$, that is, all four angles random in space, and remember that we denoted $r = l$). The dynamics is completely determined by equation (98b), and, hence, by the knowledge of the 2-point function. Any M -point function, and hence Kraus-operators family $(\hat{V}_{(\lambda_x)_x})_{(\lambda_x)_x \in \mathbb{R}^{RM}}$, compatible with the 2-point function characterizing the model, is a valid one to describe that model.

5.1.3. Special form of the 2-point function for random variables associated to lattice sites, and for a translationally-invariant noise. By construction of our model, we do not only have a 2-point function $P_{z,z'}^{(2)}(\lambda, \lambda')$, but we also have that, when $z = z'$, then $\lambda = \lambda'$, so that the 2-point function must have the form [78]

$$P_{z,z'}^{(2)}(\lambda_z, \lambda_{z'}) = \delta_{zz'} P_z^{(1)}(\lambda_z) \delta(\lambda_z - \lambda_{z'}) + (1 - \delta_{zz'}) P_{z,z'}^{(2), \neq}(\lambda_z, \lambda_{z'}), \tag{100}$$

where $P_z^{(1)}(\lambda_z)$ is the 1-point function, and $P_{z,z'}^{(2), \neq}$ is a 2-point function which need only make sense for $z \neq z'$, i.e., $P_{z,z'}^{(2), \neq}(\lambda_z, \lambda_{z'})$ is, for $z = z'$, an arbitrary and irrelevant \mathbb{R}^+ -number.

Requiring the noise to be spatial translationally invariant means requiring

$$\forall(z, \lambda) \in \mathbb{L} \times \mathbb{R}, P_z^{(1)}(\lambda) = P^{(1)}(\lambda) \tag{101a}$$

$$\forall(z, z', \lambda, \lambda') \in \mathbb{L}^2 \times \mathbb{R}^2, P_{z,z'}^{(2)}(\lambda, \lambda') = w_{|z-z'|}(\lambda, \lambda') \tag{101b}$$

$$= w_{|z-z'|}(\lambda', \lambda), \tag{101c}$$

i.e., (i) that $P^{(1)}(\lambda)$ does not depend on the lattice position z , and (ii) that $P^{(2)}(\lambda, \lambda')$ actually depends only on the distance $|z - z'|$, and is an even function of (λ, λ') (i.e., is symmetric in (λ, λ')). For random, spatially independent variables, the first condition is of course sufficient, but if we allow non-vanishing 2-site correlations, the second is also needed.

5.2. Continuum limit for discrete-time quantum walks with temporal coin noise depending smoothly on the position

5.2.1. Condition for the temporal continuity of the density operator. Consider equation (98b) for the DTQW random unitary, equation (94):

$$\rho_{t+\epsilon}^{x'} = \int d\lambda_x d\lambda_{x'} P_{x,x'}^{(2)}(\lambda_x, \lambda_{x'}) C'_{\lambda_x} \langle x | \hat{S} \hat{\rho}_t \hat{S}^\dagger | x' \rangle C'_{\lambda_{x'}}, \tag{102}$$

where

$$C'_{\lambda_x} \equiv C_{\epsilon \vec{J}_{t,x} + \vec{\lambda}_x}. \tag{103}$$

As in section 3.2.2, we assume

$$\Lambda_x^l \equiv \sqrt{\epsilon} \tilde{\Lambda}_x^l, \quad l = 0, 3, x \in \mathbb{L}, \tag{104}$$

and change the integration measure in accordance. The above condition, equation (104), ensures, as in the case of a sole temporal noise, that $\hat{\rho}_{t+\epsilon} - \hat{\rho}_t$ scales as ϵ , i.e., that $\hat{\rho}$ is a continuous function of time, and hence that $\hat{\rho}$ is approximable by a *differentiable* function of time; it is in this sense that we can write $\partial_t \hat{\rho}$ ²⁸.

5.2.2. *About the difficulties to obtain, once we introduce spatial noise, a PDE description in a sensible continuum limit.* The question we ask ourselves is whether one can get a sensible limit to the spacetime continuum out of the noisy dynamics described by equation (88), i.e., more precisely, whether one can get a PDE for $\hat{\rho}$ in such a limit. Recall that this is indeed what we have obtained in the case of a purely temporal noise, see equation (36). Now, because the spacetime-dependent coin-operator parameters are sampled from random variables, $\tilde{\Lambda}_x^l$ s, which, for each point x of the 1D spatial lattice, are *different* from one another, then if we take the lattice spacing ϵ going to zero, the functions of the position resulting from this sampling, i.e., the *realizations* $(\tilde{\lambda}_x^l)_x$ of the spatial noise, will be *discontinuous everywhere on the line*. Hence, *for each realization* $(\tilde{\lambda}_x^l)_x$ of the spatial noise associated to the evolution $t \rightarrow t + \epsilon$ (i.e., each term in the integral of equation (88)), $\rho_{t,xx'} \equiv \langle x | \hat{\rho}_t | x' \rangle$ can *a priori* be considered a continuous function *neither* of x *nor* of x' . Now, at each time step, an average is made over all possible realizations $(\tilde{\lambda}_x^l)_x$ of the spatial noise, see equation (88), and it is possible that in certain cases, i.e., with certain constraints, this average *does* only produce continuous, and even differentiable functions $\rho_{t,xx'}$ of x and x' . That being said, this is a delicate topic which would require more work, and we will not treat it in the present article. Let us simplify the problem and ask ourselves: what are the constraints that one has to impose on the spatial part of the noise for *each* realization $(\tilde{\lambda}_x^l)_x$ of this spatial noise to induce a function $\rho_{t,xx'}$ differentiable in x and x' ? A sufficient condition answering this question is the following: such a differentiability of $\rho_{t,xx'}$ as a function of x and x' is trivially guaranteed if we impose all realizations $(\tilde{\lambda}_x^l)_x$ of the spatial noise to be differentiable functions of the position x themselves. But, imposing this implies that we *loose the notion of spatial noise in the continuum limit*, that is, in the continuum limit, the superimposed spatial noise introduced at the level of the DTQW, reduces to mere spatial dependence of the temporal noise. This is the case we are going to treat in the present work.

5.2.3. *Non-explicit Lindbladian form of the continuum limit.* In appendix G, we show that, if *all* sequences $(\lambda_x^l)_x$ involved in the integral of equation (88), correspond, *not* to outcomes of spatially-dependent random variables, but to values taken by differentiable functions of x (and with which they coincide in the continuum limit), then equation (102) admits the following dynamics in the continuum limit, $\epsilon \rightarrow 0$,

$$\partial_t \rho^{xx'} = -i \langle x | [\hat{H}^o, \hat{\rho}] | x' \rangle + \mathcal{N}_{\Gamma/2, \kappa_{|x-x'|}}(\rho^{xx'}), \tag{105}$$

²⁸ In the case where there is no spatial dependence of the parameters of the coin operator, we have also shown the existence of a formal continuum limit by Taylor expanding in that small parameter, $\sqrt{\epsilon}$, *before* making the Kraus integral, so that one may think that it is also only in the above-mentioned sense that we can write $\partial_t \hat{\rho}$. However, one can actually, in this case where there is no spatial dependence, perform the Kraus integral *before* Taylor expanding in $\sqrt{\epsilon}$, and the result actually yields functions which are differentiable in time, so that $\hat{\rho}$ also is, exactly, i.e., does not need to be approximated by a function exhibiting such a feature.

where the noise term is

$$\mathcal{N}_{\Gamma/2, \kappa_{|x-x'|}}(\rho^{xx'}) \equiv \sum_{l=0}^2 \gamma_l \mathcal{M}_{\kappa_{|x-x'|}}^l(\rho^{xx'}), \tag{106}$$

with

$$\Gamma \equiv (\gamma_0, \gamma_1, \gamma_2), \tag{107}$$

and

$$\mathcal{M}_{\kappa_{|x-x'|}}^l(\rho^{xx'}) \equiv \kappa_{|x-x'|}^l L_l \rho^{xx'} L_l - \frac{1}{2} \{L_l^\dagger L_l, \rho^{xx'}\}, \tag{108}$$

where the L_l s are given by equation (25) with $L_0 \equiv \mathbf{1}_2$, and where we have introduced the ‘variances’

$$\frac{\gamma_l}{2} \equiv \int d\tilde{\lambda}_y \tilde{p}^{l,(1)}(\tilde{\lambda}_y) (\lambda_y^l)^2, \tag{109}$$

and the ‘correlation coefficients’

$$\kappa_{|x-x'|}^l \equiv \frac{c_{xx'}^l}{\gamma_l/2} \in [-1, 1], \tag{110}$$

where the $c_{xx'}^l$ s are the 2-point ‘correlation functions’,

$$c_{xx'}^l \equiv \int d\tilde{\lambda}_x d\tilde{\lambda}_{x'} \tilde{p}_{xx'}^{l,(2)}(\tilde{\lambda}_x, \tilde{\lambda}_{x'}) \tilde{\lambda}_x^l \tilde{\lambda}_{x'}^l, \tag{111}$$

which actually depend on $|x - x'|$ only, because of condition (101b) for the translational invariance of the noise. Notice that, while the contribution of the noise $l = 0$ to the continuum limit was vanishing in section 3.2.2, here it does not, because of the spatial inhomogeneity. Indeed, it is because in general $\kappa_{|x-x'|}^0 \neq 1$, that the contribution $l = 0$ does not vanish:

$$\mathcal{M}_{\kappa_{|x-x'|}^0}^0(\rho^{xx'}) = (\kappa_{|x-x'|}^0 - 1) \rho^{xx'}. \tag{112}$$

One can check that equation (105) is trace preserving, by taking it at $x = x'$, and summing over all x s and over L, R . The left-hand side then becomes

$$\int_{\mathbb{R}} dx \sum_{L,R} \partial_t [(\rho^{uu})^{xx}] = \partial_t (\text{Tr } \hat{\rho}), \tag{113}$$

while the right-hand side is (since the Hamiltonian part is trace preserving)

$$\int_{\mathbb{R}} dx [(\rho^{LL})^{xx} + (\rho^{RR})^{xx}] \sum_{l=0}^2 \gamma_l (\kappa_{|x-x'|=0}^l - 1). \tag{114}$$

By construction of our 2-point function, see equation (100),

$$\kappa_{|x-x'|=0}^l = 1, \quad l = 0, \dots, 2. \tag{115}$$

The right-hand side, (114), thus vanishes, and hence so does the left-hand side, which yields trace preservation.

Notice that the fact that this continuum limit only makes sense for a sole temporal coin noise with smooth spatial variations, and is *not* valid for a superimposed spatial coin noise, implies that the ‘correlation coefficient’ $\kappa_{|x-x'|}^l$ is a differentiable function of $|x - x'|$, which in turn is consistent with the fact that our resulting PDE involves, in the Hamiltonian part, derivatives of ρ_t with respect to x and x' .

5.2.4. Explicit Lindbladian form. We are going to show that one can derive, from a certain, quite general family of random unitaries, a continuum Lindbladian limit. Consider the dynamical map ensuing from arbitrary temporal-noise random unitaries $\hat{Q}_\phi(\sqrt{\epsilon})$, (i) depending on an arbitrary sequence $\phi \equiv (\lambda_x)_x$ of values taken by a differentiable function of x , with which the sequence coincides in the continuum limit $\epsilon \rightarrow 0$, and (ii) being a function of the square root $\sqrt{\epsilon}$ of the spatiotemporal-lattice spacing ϵ ,

$$\hat{\rho}_{t+\epsilon} = \int d\nu \hat{Q}_\phi(\sqrt{\epsilon}) \hat{\rho}_t \hat{Q}_\phi^\dagger(\sqrt{\epsilon}), \tag{116}$$

where the integration measure satisfies $\int d\nu = 1$. Assume that the random unitaries have the following Taylor expansion,

$$\hat{Q}_\phi(\sqrt{\epsilon}) = \mathbb{1} + \sqrt{\epsilon} \hat{Q}_\phi^{(1/2)} + \epsilon \hat{Q}_\phi^{(1)} + O(\epsilon^{3/2}). \tag{117}$$

Equation (116) then reads

$$\hat{\rho} + \epsilon \partial_t \hat{\rho} = \hat{\rho} + \sqrt{\epsilon} \mathcal{H}(\overline{\hat{Q}}^{(1/2)} \hat{\rho}_t) + \epsilon \left[\mathcal{H}(\overline{\hat{Q}}^{(1)} \hat{\rho}_t) + \int d\nu \hat{Q}_\phi^{(1/2)} \hat{\rho}_t (\hat{Q}_\phi^{(1/2)})^\dagger \right] + O(\epsilon^{3/2}), \tag{118}$$

having introduced the mean value of an operator \hat{O}_ϕ ,

$$\overline{\hat{O}} \equiv \int d\nu \hat{O}_\phi, \tag{119}$$

and the Hermitian-symmetric part of an operator \hat{A} ,

$$\mathcal{H}(\hat{A}) \equiv \hat{A} + \hat{A}^\dagger. \tag{120}$$

For this expansion, equation (117), to make sense whatever $\epsilon \geq 0$, one needs

$$\mathcal{H}(\overline{\hat{Q}}^{(1/2)} \hat{\rho}_t) = 0, \tag{121}$$

for which it is sufficient that

$$\overline{\hat{Q}}^{(1/2)} \equiv \int d\nu \hat{Q}_\phi^{(1/2)} = 0, \tag{122}$$

and one then obtains the following PDE,

$$\partial_t \hat{\rho} = \overline{\hat{Q}}^{(1)} \hat{\rho}_t + \hat{\rho}_t (\overline{\hat{Q}}^{(1)})^\dagger + \int d\nu \hat{Q}_\phi^{(1/2)} \hat{\rho}_t (\hat{Q}_\phi^{(1/2)})^\dagger. \tag{123}$$

Now, $\overline{\hat{Q}}^{(1)}$ is in general not Hermitian, and can be decomposed into a Hermitian and an anti-Hermitian part,

$$\overline{\hat{Q}}^{(1)} = \hat{G} + (-i\hat{H}), \tag{124}$$

where

$$\hat{H} \equiv \frac{i}{2} \left[\overline{\hat{Q}}^{(1)} - \left(\overline{\hat{Q}}^{(1)} \right)^\dagger \right] \tag{125a}$$

$$\hat{G} \equiv \frac{1}{2} \left[\overline{\hat{Q}}^{(1)} + \left(\overline{\hat{Q}}^{(1)} \right)^\dagger \right], \tag{125b}$$

are both Hermitian. Equation (123) can then be rewritten as

$$\partial_t \hat{\rho} = -i[\hat{H}, \hat{\rho}] + \{\hat{G}, \hat{\rho}\} + \int d\nu \hat{Q}_\phi^{(1/2)} \hat{\rho}_t \left(\hat{Q}_\phi^{(1/2)} \right)^\dagger, \tag{126}$$

where $[\cdot, \cdot]$ is the commutator, and $\{\cdot, \cdot\}$ the anticommutator. Notice from this equation that \hat{H} is a Hamiltonian. Now, requiring that evolution (116) be trace preserving implies the following normalization condition,

$$\int d\nu \hat{Q}_\phi^\dagger(\sqrt{\epsilon}) \hat{Q}_\phi(\sqrt{\epsilon}) = 1, \tag{127}$$

which, using the Taylor expansion of equation (117), imposes

$$\hat{G} = -\frac{1}{2} \int d\nu \left(\hat{Q}_\phi^{(1/2)} \right)^\dagger \hat{Q}_\phi^{(1/2)}. \tag{128}$$

Plugging this expression of \hat{G} into equation (126) finally yields

$$\partial_t \hat{\rho} = -i[\hat{H}, \hat{\rho}] + \int d\nu \left[\hat{L}_\phi \hat{\rho}_t \hat{L}_\phi^\dagger - \frac{1}{2} \left\{ \hat{L}_\phi^\dagger \hat{L}_\phi, \hat{\rho} \right\} \right], \tag{129}$$

which is a Lindblad equation, with Lindblad operators

$$\hat{L}_\phi \equiv \hat{Q}_\phi^{(1/2)}. \tag{130}$$

One can apply this general result to recover (i) that of section 3.2.2, with a pure temporal coin noise, and (ii) that of section 5.2, with a temporal coin noise which depends smoothly on the position.

6. Conclusion

As we discussed in the introduction, the search for a correct description of diffusive dynamics in relativistic quantum systems has faced historically many difficulties, in the attempt to preserve essential features such as relativistic covariance or causality. In the non-quantum case, these difficulties have been overcome. In the quantum case, they are still under study. In the present paper, we do not address covariance. We present a model that can be used to simulate some features observed in more involved systems.

Our starting point, see section 2, is a DTQW on a one-dimensional lattice, whose walker is subject, see section 3, to noise *acting on its internal, coin (or chirality) degree of freedom*,

that makes it decohere. We consider two such models of decoherent DTQW. First, a model with both a coin-flip and a phase-flip channel. Second, a model of random coin unitary operators (so-called random coin unitaries). Noise acting on a two-level quantum system (such as the chirality part of a chiral system), appears in many physical scenarios, and is commonly described, microscopically, by spin-boson models²⁹. Such scenarios include the description of matter in a quantized radiation field, the motion of light particles in metals, or superconducting qubits which are coupled to propagating photons.

Given the update rules that govern the dynamics of DTQWs, their causality is guaranteed by construction. In fact, an important property of noiseless DTQWs is the ability to reproduce the dynamics of relativistic particles in the continuum limit, i.e., when both the lattice spacing and the time step go to zero. This also requires that the parameters of the coin operator that controls the dynamics follow this scaling in an appropriate manner. One can naturally ask the question of what is the continuum limit (if any) of the above decoherent-DTQW models. As expected, the existence of such a limit also imposes conditions on the behavior of the parameters that characterize the noise, as we approach the continuum. Within this assumption, we obtain that the two decoherent-DTQW models introduced above admit a common formal continuum limit, namely, a Lindblad equation with a Dirac-fermion Hamiltonian part and, as Lindblad jumps, a chirality flip and a chirality-dependent phase flip, which are two of the three standard error channels for a two-level quantum system. This, as we may call it, Dirac Lindblad equation, provides a model of quantum relativistic spatial diffusion, which is evidenced both analytically and numerically in section 4. The presence of the chirality, along with its entanglement with the spatial motion, is of course, in our noise model, a crucial ingredient in obtaining such a quantum relativistic system with spatial diffusion, given that the noise acts on the chirality.

We have investigated the resulting dynamics. For a particle with vanishing mass, the model reduces to the well-known telegraph equation, which yields propagation at short times, diffusion at long times, and exhibits no quantumness, in the sense that it can be described by a wave equation *on the density of presence of the particle*. On the other hand, the massive case has been analyzed numerically, and exhibits a rich phenomenology. We analyzed in detail the dynamics that appears when the initial state is Gaussian, and identified the relevant parameters of the problem. In the low-dispersion regime, corresponding to an initial momentum width which is much smaller than the initial average momentum, the average position first propagates ballistically, with a velocity that equals the group velocity and, after a transient regime, asymptotically approaches a limit position.

We also extended, in section 5, our formal-continuum-limit procedure to temporal noises which depend smoothly on position. We stress that this does not correspond to adding a spatial noise in any way.

Noiseless quantum walks have numerous applications. In quantum algorithmics, they are known to be universal computational primitives. In quantum simulation, they can emulate high-energy phenomena like particles propagating in external gauge fields (including a gravitational potential). And it has been suggested that quantum walks can also serve as building blocks for discrete models of gauge theories. Thus, stochastic quantum walks such as those considered in this article are useful tools to investigate the effects of decoherence, both in quantum algorithmics and in quantum simulation. To be fair, the results presented above are only partial and should be extended, not only to quantum walks on graphs, but also to many-particle quantum

²⁹ Reference [75] provides such a microscopic model in a framework which is very close to that of the present work; the only difference regarding the noise aspect is that they consider the depolarizing channel, which is an equally weighted sum of the three standard error channels for two-level systems, while we consider only two of these three channels, and with arbitrary weights.

walks, i.e. quantum cellular automata. But they reveal, through quantum walks, a profound and unexpected link between quantum algorithms running in a non ideal, ‘open’ quantum computer and relativistic diffusions. The link between decohering gauge theories and relativistic diffusions is perhaps less surprising, but it seems never to have been mentioned in the literature so far. Speaking quite generally, the results presented in this article show that the vast body of knowledge accumulated on classical relativistic diffusions can contribute to our understanding of open quantum systems, at least in situations where quantum walks play a natural role. And, vice-versa, studying decoherence of systems which can be modeled with quantum walks can teach us about relativistic diffusions.

Acknowledgments

We acknowledge fruitful discussions with José María Ibáñez and Isabel Cordero Carrión. PA thanks Alba María Tortosa Benito for her support, and Justin Gabriel for his friendship. This work has been funded by the CNRS PEPs Spain-France PIC2017FR6, the Spanish FEDER/MCIyU-AEI grant FPA2017-84543-P, SEV-2014-0398 and Generalitat Valenciana grant PROMETEO/2019/087. We also acknowledge support from CSIC Research Platform PTI-001.

Appendix A. Euler-angles parametrization of SU(2)

Consider the coin operator of equation (7) with, for simplicity, spacetime-independent entries. Up to the global phase ξ^0 , this arbitrary 2×2 unitary matrix,

$$C_{(\xi^0, \xi^1, \theta, \chi)} \equiv e^{i\xi^0} R_{(\xi^1, \theta, \chi)} \in U(2), \tag{A1}$$

is nothing but an arbitrary coin rotation, which can be written as

$$R_{(\xi^1, \theta, \chi)} \equiv e^{i\frac{\xi^1 + \chi}{2}\sigma^3} e^{i\theta\sigma^1} e^{i\frac{\xi^1 - \chi}{2}\sigma^3} \in SU(2). \tag{A2}$$

We have put the dependence on the angles between round brackets to indicate that these angles are constant in spacetime, i.e., only correspond, each, to one real variable.

We have chosen to parametrize this coin rotation with the angles ξ^1 , θ , and χ , which are the following linear combinations of the Euler angles of SO(3) for a passive rotation:

$$\psi = \xi^1 - \chi \tag{A3a}$$

$$\phi = \xi^1 + \chi \tag{A3b}$$

$$\Theta = 2\theta, \tag{A3c}$$

see reference [70], appendix F. Notice that θ is just half of the Euler angle giving the latitude. Notice also on equation (A2) that χ simply corresponds to a change of coin basis in the equatorial plane of the Bloch sphere. This parametrization is a compromise between (i) good visualization of the action of the coin rotation on the Bloch sphere, equation (A2), which is why we use *almost* the Euler angles—the only subtlety being, as the reader may have noticed, the

visualization of ξ^1 [70]—, and (ii) compactness of writing in a single-matrix form, equation (4), which is why we do the above linear combinations³⁰, equation (A3).

Appendix B. Quantum continuity equation

Equation (41) shows, in particular, (i) that³¹

$$\hat{r}_t^0 = \text{Tr}_c(\hat{\rho}_t) = \hat{\rho}_t^{\text{LL}} + \hat{\rho}_t^{\text{RR}}, \tag{B1}$$

is the operator corresponding to the probability of presence regardless of the internal state (partial trace of $\hat{\rho}_t$ over the internal d.o.f.), and (ii) that,

$$\hat{r}_t^3 = \hat{\rho}_t^{\text{LL}} - \hat{\rho}_t^{\text{RR}}, \tag{B2}$$

is the left-current operator. Points (i) and (ii) can be illustrated by the fact that one of the four coupled PDEs implied by equation (36) on the \hat{r}_t^μ s, is (we omit the time label to lighten notations),

$$\partial_t \hat{r}^0 = i[\hat{p}, \hat{r}^3], \tag{B3}$$

which is the quantum-operator version of the 1D continuity equation; indeed, in position space, i.e., applying $\langle x|$ on its left, and $|y\rangle$ on its right, equation (B3) delivers

$$\partial_t r_{xy}^0 = (\partial_x + \partial_y)r_{xy}^3, \tag{B4}$$

where $r_{xy}^\mu \equiv \langle x| \hat{r}^\mu |y\rangle$, and considering this equation, (B4), for $x = y$, yields (see equation (54)),

$$\partial_t R_x^0 - \partial_x R_x^3 = 0, \tag{B5}$$

where $R_x^\mu \equiv r_{xx}^\mu$. Equation (B5) is a standard continuity equation, not specific to a quantum setting. R_x^0 is the probability density, and R_x^3 the left-current density.

Notice the following. ‘How much’ quantum information contained in equation (B3) manifest itself (so that the equation cannot be reduced to its non-quantum version, equation (B5)), is conditioned to ‘how much’ the evolution equation for \hat{r}^3 contains quantum information as well. In the present case, we will see in section 4.2.1 see that this demands that the mass m does not vanish. Now, we know *a priori* that this condition is, although necessary, not sufficient, because in the non-relativistic limit, the internal and external d.o.f.s do not get entangled by the free dynamics, as mentioned early in section 4.1.1. So, another necessary condition for equation (B3) to contain purely quantum information is, for the present model, that the latter is relativistic.

³⁰ Indeed, if we had stuck strictly to using the Euler angles, we would have linear combinations of ψ and ϕ in the argument of the exponentials that appear in the matrix.

³¹ The four $\hat{\rho}_t^{\mu\nu}$ s, $u, v \in \{L, R\}$, are the components of $\hat{\rho}_t$ on this basis of the mixed coin states that we call canonical, which is induced by the LR basis of the coin pure states: $\hat{\rho} \equiv \sum_{u,v=L,R} \hat{\rho}_t^{\mu\nu} |u\rangle\langle v|$.

Appendix C. $m \neq 0, \Gamma = 0$: standard, massive Dirac fermions, a very brief reminder

C.1. General solution for a pure initial state

When $\Gamma = 0$, the dynamics is unitary. Hence, if we do not wish to evolve mixed initial states, the density-operator formalism is not necessary; we can work with the state-vector formalism. The evolution of an arbitrary pure state from time $t_0 = 0$ to time t is given by

$$\Psi_{t,x} = \frac{1}{\sqrt{2\pi}} \int_{\mathbb{R}} dp \tilde{\Psi}_{t,p} e^{ipx}, \tag{C1}$$

where

$$\tilde{\Psi}_{t,p} = \alpha_p^+ V_p^+ e^{-iE_p t} + \alpha_p^- V_p^- e^{iE_p t}, \tag{C2}$$

is the decomposition, at any time t , of the momentum amplitude distribution on the chirality eigenbasis of the considered Hamiltonian,

$$h(p) \equiv H_{m,0}^{\text{Dirac}}(p) = \begin{bmatrix} -p & m \\ m & p \end{bmatrix}, \tag{C3}$$

see equation (22). The eigenvalues are $\pm E_p$, with

$$E_p \equiv \sqrt{p^2 + m^2}, \tag{C4}$$

and two possible eigenvectors are³²

$$V_p^\pm \equiv \begin{pmatrix} 1 \\ \pm E_p + p \\ m \end{pmatrix}. \tag{C5}$$

The coefficients α^\pm of the decomposition, equation (C2), are, apart from the normalization condition,

$$\int_{\mathbb{R}} dp (|\alpha_p^+|^2 \|V_p^+\|^2 + |\alpha_p^-|^2 \|V_p^-\|^2) = 1, \tag{C6}$$

arbitrary complex-valued functions of p .

C.2. Choice of the initial condition

Unless otherwise mentioned, we choose a positive-energy initial state with Gaussian momentum distribution of center p_0 and spread σ , that is,

$$\alpha_p^+ = \beta_{p-p_0} \equiv \sqrt{N} \sqrt{g_{p-p_0}^\sigma} \tag{C7a}$$

$$\alpha_p^- = 0, \tag{C7b}$$

where

$$g_p^\sigma \equiv \frac{1}{\sqrt{2\pi}\sigma} e^{-\frac{p^2}{2\sigma^2}}, \tag{C8}$$

³² These are non-normalized in the internal space; there is no need of doing so.

and N is a normalization factor, such that (see equation (C6))

$$\int_{\mathbb{R}} dp N g_{p-p_0}^\sigma \left[1 + \left(\frac{E_p + p}{m} \right)^2 \right] = 1. \tag{C9}$$

C.3. Group and dispersion velocities

With the initial condition of equation (C7), the state evolution is

$$\Psi_{t,x} = \frac{1}{\sqrt{2\pi}} \int_{\mathbb{R}} dp A_{p-p_0} e^{i(px-E_p t)}, \tag{C10}$$

where

$$A_{p-p_0} \equiv \beta_{p-p_0} V_p^+. \tag{C11}$$

One can show that a sufficient condition for the dispersion relation, E_p , to be considered quadratical, i.e., for what we call the quadratical-dispersion-relation (QDR) approximation to be made, is

$$\sigma \ll p_0, \tag{C12}$$

which corresponds to A_{p-p_0} sharply peaked around $p = p_0$. Within the QDR approximation, the mean position and the centered spread are well approximated by the following, ballistic formulae [79]

$$X_t \equiv \langle x \rangle_t \simeq v_g t \tag{C13a}$$

$$\Sigma_t \equiv \sqrt{\langle x^2 \rangle_t - \langle x \rangle_t^2} \simeq \Sigma_0 \sqrt{1 + \frac{v_d^2}{\Sigma_0^2} t^2}, \tag{C13b}$$

with

$$\Sigma_0 \equiv \frac{1}{4\sigma^2} + a, \tag{C14}$$

and where the group and dispersion velocities are respectively given by

$$v_g \equiv \left. \frac{\partial E_p}{\partial p} \right|_{p=p_0} = \frac{p_0}{\sqrt{p_0^2 + m^2}} \tag{C15a}$$

$$v_d \equiv \Gamma|_{p=p_0} \sigma^2 + b, \tag{C15b}$$

where

$$\Gamma|_{p=p_0} \equiv \left. \frac{\partial^2 E_p}{\partial^2 p} \right|_{p=p_0}. \tag{C16}$$

The parameters a and b , intervening respectively in equations (C14) and (C15b), are a real numbers that can be computed analytically (within the QDR approximation).

Appendix D. Phase-change noise channel on a massless discrete-time quantum walk

In section 4.2.1, we have mentioned that the phase-flip noise, characterized by γ_1 , has *no effect* on the dynamics of R^0 and R^3 in the massless case. This would actually be the case of any *phase-change jump operator*, i.e., with the following properties, (i) it acts solely on the chirality, internal Hilbert space, (ii) it is diagonal, and (iii), it is unitary, that is, it has the form $J = \text{diag}(\exp(i\varphi_L), \exp(i\varphi_R))$, which adds, to each of the two wavefunction components (left- and right-moving), an arbitrary phase (φ_L and φ_R). Indeed, the phases of these two wavefunction components do simply not influence the spatial dynamics in the massless case.

Now, if we reintroduce a non-vanishing spacetime-lattice spacing ϵ , i.e., if the walker does experience the discreteness of spacetime, then any such J , e.g., even the identity $\text{diag}(1, 1)$, *does* modify the spatial dynamics, but this is simply because applying the noise term $\pi_1 J \hat{\rho}_t J$ in equation (19) makes in particular the walker stay, with probability π_1 , at his position during a *finite*, i.e., *non-vanishing* amount of time $\Delta t = \epsilon$, that is, the values of φ_L and φ_R are irrelevant to this phenomenon.

Appendix E. Numerical implementation of the Dirac Lindblad equation (36)

The Dirac Lindblad equation (36), which can be written as equation (42), is given, in position space, by the system of equations (51) and (52), which can be recast as

$$\partial_t \vec{r} + \mathbf{A} \partial_x \vec{r} + \mathbf{A}' \partial_{x'} \vec{r} = \mathbf{F} \vec{r}, \quad (\text{E1})$$

where (i) $\vec{r} \equiv (r^0, r^1, r^2, r^3)^\top$ (see equation (53)), (ii) the so-called Jacobian matrices are

$$\mathbf{A} \equiv i\mathbf{P} = \begin{bmatrix} \cdot & \cdot & \cdot & -1 \\ \cdot & \cdot & i & \cdot \\ \cdot & -i & \cdot & \cdot \\ -1 & \cdot & \cdot & \cdot \end{bmatrix}, \quad (\text{E2a})$$

$$\mathbf{A}' \equiv -i\mathbf{P}^\dagger = \begin{bmatrix} \cdot & \cdot & \cdot & -1 \\ \cdot & \cdot & -i & \cdot \\ \cdot & i & \cdot & \cdot \\ -1 & \cdot & \cdot & \cdot \end{bmatrix} = \mathbf{A}^\top, \quad (\text{E2b})$$

where the dots stand for zeros and \mathbf{P} is given in equation (44), and the so-called source-term matrix is, for $\gamma_1 = 0$,

$$\mathbf{F} \equiv \mathbf{Q}_{(\gamma_1=0, \gamma), m} = \begin{bmatrix} \cdot & \cdot & \cdot & \cdot \\ \cdot & \cdot & \cdot & \cdot \\ \cdot & \cdot & -\gamma & -2m \\ \cdot & \cdot & 2m & -\gamma \end{bmatrix}, \quad (\text{E3})$$

where \mathbf{Q} is given in equation (44). Given that the matrices \mathbf{A} and \mathbf{A}' are Hermitian and commute, there exists a unitary matrix,

$$\mathbf{U} \equiv \frac{1}{\sqrt{2}} \begin{bmatrix} 1 & \cdot & \cdot & 1 \\ \cdot & i & 1 & \cdot \\ \cdot & -i & 1 & \cdot \\ -1 & \cdot & \cdot & 1 \end{bmatrix}, \quad (\text{E4})$$

that simultaneously diagonalizes them,

$$\mathbf{\Lambda} \equiv \mathbf{U}\mathbf{A}\mathbf{U}^{-1} = \text{diag}(-1, -1, 1, 1) \tag{E5a}$$

$$\mathbf{\Lambda}' \equiv \mathbf{U}\mathbf{A}'\mathbf{U}^{-1} = \text{diag}(-1, 1, -1, 1). \tag{E5b}$$

This allows to rewrite the system of equations as

$$\partial_t \vec{v} + \mathbf{\Lambda} \partial_x \vec{v} + \mathbf{\Lambda}' \partial_{x'} \vec{v} = \mathbf{S} \vec{v}, \tag{E6}$$

where

$$\vec{v} \equiv (v^0, v^1, v^2, v^3)^\top \equiv \mathbf{U} \vec{r} \tag{E7a}$$

$$\mathbf{S} \equiv \mathbf{U}\mathbf{F}\mathbf{U}^{-1}. \tag{E7b}$$

System (E6) is a hyperbolic system of PDEs, and its solution is thus in particular solely determined by the initial condition $\vec{v}_{t=0}$.

We integrated this system numerically via the Strang operator-splitting method, which consists in splitting the single-time-step evolution into two parts: one corresponding to the homogeneous evolution of the system (i.e. $\mathbf{S} = 0$), and the other one corresponding to the evolution with null fluxes (i.e. $\mathbf{\Lambda} = \mathbf{\Lambda}' = 0$). This method is particularly adapted to the present case, since the homogeneous solution is exactly solvable,

$$v_{t,x,x'}^\mu = v_{0,x-\lambda^\mu t, x'-\lambda^{\mu'} t}^\mu, \tag{E8}$$

where the λ^μ s (resp. $\lambda^{\mu'}$ s), $\mu = 0, \dots, 3$, are the 4 eigenvalues of the matrix $\mathbf{\Lambda}$ (resp. $\mathbf{\Lambda}'$). For the second part of the evolution, one has to solve, as mentioned,

$$\partial_t \vec{v} = \mathbf{S} \vec{v}. \tag{E9}$$

This equation has a well-known explicit solution, which requires the exponentiation of the matrix \mathbf{S} . A direct numerical implementation of this exponential introduces well-known stiffness problems. To address this issue, we implement instead the following first-order (i.e., Euler) explicit-implicit scheme,

$$\frac{\vec{v}_{t+\epsilon} - \vec{v}_t}{\epsilon} = \alpha \mathbf{S} \vec{v}_t + (1 - \alpha) \mathbf{S} \vec{v}_{t+\epsilon}, \tag{E10}$$

where the parameter α has been adjusted by hand to $\alpha = 0.5$ ³³.

The accuracy of the splitting method can be improved from $O(\Delta t)$ to $O(\Delta t^2)$ by using the so-called Strang splitting, where we take half a step with the one-time-step source term evolution operator, $\mathbf{L}_{\epsilon/2}^s$, a full step with the one-time-step homogeneous evolution operator \mathbf{L}_ϵ^h , and finally half another step with the source term operator. During a time interval ϵ , the algorithm thus reads

$$\vec{v}_{t+\epsilon} = \mathbf{L}_{\epsilon/2}^s \mathbf{L}_\epsilon^h \mathbf{L}_{\epsilon/2}^s \vec{v}_t. \tag{E11}$$

³³ Our criterion to choose α has been to minimize, by hand, the discrepancy of the numerically obtained \vec{v}_t from the discretized equation of motion, equation (E6), at the final time of the simulation.

Appendix F. About local noises

A typical example of local noise, as defined by equation (97), would be

$$\hat{V}_{(\lambda_y)_y} = \hat{A} \hat{O}_{(\lambda_y)_y} \hat{B}, \tag{F1}$$

where the only operator, $\hat{O}_{(\lambda_y)_y}$, that depends on the noise, (i) is purely local, i.e.,

$$\hat{O}_{(\lambda_y)_y} \equiv \sum_z O_{(\lambda_y)_y}^z |z\rangle \langle z|, \tag{F2}$$

with $O_{(\lambda_y)_y}^z$ acting solely on the internal d.o.f. (which is why it has no hat), and (ii), depends locally on the noise, i.e., O^z actually only depends on λ_z ,

$$O_{(\lambda_y)_y}^z \equiv o_{\lambda_z}^z. \tag{F3}$$

Indeed, if the random unitary has the form of equation (F1) with the precisions (i) and (ii) given just above, the matrix elements would be of the form of equation (97), with

$$\hat{V}_{\lambda_z}^{xx'} \equiv \langle x | \hat{A} |z\rangle o_{\lambda_z}^z \langle z | \hat{B} |x'\rangle. \tag{F4}$$

Let us show that the fact that the operator $\hat{O}_{(\lambda_z)_z}$ is purely local is necessary for the noise to eventually be local without breaking the translational invariance of the system. We do a reduction to absurd. Assume that $\hat{O}_{(\lambda_z)_z}$ is not purely local, i.e., that, whatever³⁴ x , there exist $x' \neq x$ such that $O_{(\lambda_y)_y}^{xx'} \neq 0$. Imagine now that $O_{(\lambda_y)_y}^{xx'}$ only depends on some λ_z , i.e., $O_{(\lambda_y)_y}^{xx'} = o_{\lambda_z}^{xx'}$. Translational invariance imposes that, whatever x , (i) $x - z = \text{cte}$ (we also have $x' - z = \text{cte}_2$, but we will not need it). But, x and x' should not play a different role in a translationally invariant system, i.e., we must have $o_{\lambda_z}^{xx'} = o_{\lambda_z}^{x'x}$, so that (ii) $x' - z = \text{cte}$, which, together with (i), implies that $x' = x$, which contradicts the fact that $x' \neq x$, and completes the proof. That $\hat{O}_{(\lambda_z)_z}$ is purely local is thus necessary for the noise to be local. However, this condition is *a priori* not sufficient, one could imagine a unitary $O_{(\lambda_y)_y}$ that acts purely locally, i.e., only on the internal degree of freedom, but whose action depends on the random variables at all points, i.e., depends indeed on the whole family $(\lambda_y)_y$.

Notice that $\hat{V}_{(\lambda_y)_y}^{\text{QW}}$, equation (94), has a decomposition of the form of equation (F1) in which, more particularly, \hat{A} is the identity, so that the sum over z in equation (97) reduces to the single term $z = x$, namely,

$$\langle x | \hat{V}_{\lambda_x}^{\text{QW}} |x'\rangle \equiv C'_{\lambda_x} \langle x | \hat{S} |x'\rangle, \tag{F5}$$

where

$$C'_{\lambda_x} \equiv C_{\epsilon \bar{f}_{t,x} + \lambda_x}. \tag{F6}$$

Appendix G. Continuum limit of discrete-time quantum walks with temporal coin noise depending smoothly on the position

If, for each evolution $t \rightarrow t + \epsilon$, all sequences $(\lambda_x^t)_x$ involved in the integral of equation (88), correspond, *not* to outcomes of spatially-dependent random variables, but to values taken

³⁴ ‘Whatever’ is necessary, not only ‘there is’, because of the requirement of translational invariance.

by differentiable functions of x (and with which they coincide in the continuum limit), then the continuum limit of each of them exists, and is obtained via Taylor expansion in ϵ of the spacetime-lattice dynamics.

We know, from equation (33), that the following Taylor expansion holds,

$$C'_{\sqrt{\epsilon}\tilde{\lambda}_x} \langle x | \hat{S} = 1 - i\epsilon \langle x | \hat{H}_t^o + \left[i\sqrt{\epsilon} \sum_{l=0}^2 \tilde{\lambda}_x^l L_l - \frac{1}{2}(\sqrt{\epsilon})^2 \sum_{l=0}^2 (\tilde{\lambda}_x^l)^2 (L_l)^2 - (\sqrt{\epsilon})^2 \left[\tilde{\lambda}_x^0(\tilde{\lambda}_x^1\sigma^3 + \tilde{\lambda}_x^2\sigma^1) + \tilde{\lambda}_x^2\tilde{\lambda}_x^3(i\sigma^2) \right] + O(\epsilon^{3/2}) \right] \langle x |. \tag{G1}$$

Similarly, we have

$$\hat{S} |x'\rangle C'_{\sqrt{\epsilon}\tilde{\lambda}_{x'}} = 1 + i\epsilon \hat{H}_t^o |x'\rangle + |x'\rangle \left[-i\sqrt{\epsilon} \sum_{l=0}^2 \tilde{\lambda}_{x'}^l L_l - \frac{1}{2}(\sqrt{\epsilon})^2 \sum_{l=0}^2 (\tilde{\lambda}_{x'}^l)^2 (L_l)^2 - (\sqrt{\epsilon})^2 \left[\tilde{\lambda}_{x'}^0(\tilde{\lambda}_{x'}^1\sigma^3 + \tilde{\lambda}_{x'}^2\sigma^1) + \tilde{\lambda}_{x'}^2\tilde{\lambda}_{x'}^3(i\sigma^2) \right] + O(\epsilon^{3/2}) \right], \tag{G2}$$

Plugging equations (G1) and (G2) into equation (102) yields

$$\rho^{xx'} + \epsilon \partial_t \rho^{xx'} = \rho^{xx'} + \epsilon \left[-i \langle x | [\hat{H}^o, \hat{\rho}] |x'\rangle + \mathcal{F}_{xx'}(\rho^{xx'}) \right] + O(\epsilon^{3/2}), \tag{G3}$$

where we recognize a standard Hamiltonian part, and where the noise term is given by

$$\mathcal{F}_{xx'}(\rho^{xx'}) \equiv \sum_{l=0}^2 \mathcal{F}_{xx'}^l(\rho^{xx'}), \tag{G4}$$

where—using that $\tilde{p}_{x,x'}^{l(2)}(\tilde{\lambda}_x^l, \tilde{\lambda}_{x'}^l)$ is symmetric (for the functions $v^l : x \mapsto v_x^l$ and $v^l : x' \mapsto v_{x'}^l$, defined below, to indeed be the same), which is the feature (101c) of the translationally invariant noise defined in equation (101)—we obtain

$$\mathcal{F}_{xx'}^l(\rho^{xx'}) \equiv c_{x,x'}^l L_l \rho^{xx'} L_l^\dagger - \frac{1}{2} \left(v_x^l L_l^\dagger L_l \rho^{xx'} + v_{x'}^l \rho^{xx'} L_l^\dagger L_l \right), \tag{G5}$$

where the L_l s are given by equation (25) with $L_0 \equiv \mathbf{1}_2$, and with the 2-point ‘correlation functions’ and the ‘variances’ respectively given by

$$c_{x,x'}^l \equiv \int d\tilde{\lambda}_x d\tilde{\lambda}_{x'} \tilde{p}_{x,x'}^{l(2)}(\tilde{\lambda}_x^l, \tilde{\lambda}_{x'}^l) \tilde{\lambda}_x^l \tilde{\lambda}_{x'}^l \tag{G6a}$$

$$v_y^l \equiv \int d\tilde{\lambda}_y \tilde{p}_y^{l(1)}(\tilde{\lambda}_y^l) (\lambda_y^l)^2. \tag{G6b}$$

Now using (i) that $\tilde{p}_y^{l(1)}$ does not depend on y —which is the feature (101a) of the translationally invariant noise defined in equation (101)—, so that $v_y = v$, and (ii) assuming that $c_{x,x'}^l$ actually only depends on $|x - x'|$ and not (x, x') , which is guaranteed if $\tilde{p}_{x,x'}^{l(2)}$ behaves the same (feature (101b) of the translationally invariant noise defined in equation (101)), we obtain

$$\partial_t \rho^{xx'} = -i \langle x | [\hat{H}^o, \hat{\rho}] |x'\rangle + \mathcal{N}_{\Gamma/2, \kappa_{|x-x'|}}(\rho^{xx'}), \tag{G7}$$

where the noise term is now

$$\mathcal{N}_{\Gamma/2, \kappa_{|x-x'|}}(\rho^{xx'}) \equiv \sum_{l=0}^2 \gamma_l \mathcal{M}_{\kappa_{|x-x'|}}^l(\rho^{xx'}), \quad (\text{G8})$$

where we have renamed the ‘variances’ in accordance with section 3.2,

$$\gamma_l \equiv 2v^l, \quad (\text{G9})$$

and introduced the ‘correlation coefficients’,

$$\kappa_{|x-x'|}^l \equiv \frac{c_{x,x'}^l}{v^l} \in [-1, 1], \quad (\text{G10})$$

so that

$$\mathcal{M}_{\kappa_{|x-x'|}}^l(\rho^{xx'}) \equiv \kappa_{|x-x'|}^l L_l \rho^{xx'} L_l - \frac{1}{2} \{L_l^\dagger L_l, \rho^{xx'}\}. \quad (\text{G11})$$

ORCID iDs

Pablo Arnault  <https://orcid.org/0000-0003-2928-162X>

Andreu Anglés-Castillo  <https://orcid.org/0000-0003-2883-4851>

Giuseppe Di Molfetta  <https://orcid.org/0000-0002-1261-7476>

Reference

- [1] Einstein A 1905 Über die von der molekularkinetischen Theorie der Wärme geforderte Bewegung von in ruhenden Flüssigkeiten suspendierten Teilchen *Ann. Physik* **322** 549–60
- [2] Debbasch F and Chevalier C 2007 Relativistic stochastic processes: a review *Proc. Medyfinol 2006, Nonequilibrium Statistical Mechanics and Nonlinear Physics, XV Conf. on Nonequilibrium Statistical Mechanics and Nonlinear Physics, Dec 4-8 2006' Mar del Plata, Argentina (AIP Conf. Proc.)* vol 913 ed O Descalzi et al (Melville, NY: American Institute of Physics)
- [3] Percival I 1998 *Quantum State Diffusion* (Cambridge: Cambridge University Press)
- [4] Gardiner C W and Zoller P 2000 *Quantum Noise* 2nd edn (Berlin: Springer)
- [5] Schlosshauer M A 2007 *Decoherence and the Quantum-To-Classical Transition* (Berlin: Springer) (doi:10.1007/978-3-540-35775-9)
- [6] Breuer H-P and Petruccione F 2007 *The Theory of Open Quantum Systems* (Oxford: Oxford University Press)
- [7] Landau L D and Lifshitz E M 1887 *Fluid Mechnaics* 2nd edn (Oxford: Pergamon)
- [8] Eckart C 1940 The thermodynamics of irreversible processes. III. relativistic theory of the simple fluid *Phys. Rev.* **58** 919–24
- [9] Cattaneo C R 1949 Sulla conduzione del calore *Atti Sem. Mat. Fis. Univ. Modena* **3** 83–101
- [10] Grad H 1949 On the kinetic theory of rarefied gases *Commun. Pure Appl. Math* **2** 331–407
- [11] Israel W 1987 Covariant fluid mechanics and thermodynamics: an introduction *Relativistic Fluid Dynamics (Lecture Notes in Mathematics* vol 1385) ed A Anile and Y Choquet-Bruhat (Berlin: Springer)
- [12] Müller I and Ruggeri T 1993 Extended thermodynamics *Springer Tracts in Natural Philosophy* vol 37 (New York: Springer)
- [13] Debbasch F and van Leeuwen W 2009 General relativistic Boltzmann equation I. Covariant treatment *Physica A* **388** 1079–104
- [14] Debbasch F and van Leeuwen W 2009 General relativistic Boltzmann equation II. Manifestly covariant treatment *Physica A* **388** 1818–34

- [15] Dudley R M 1965 Lorentz-invariant Markov processes in relativistic phase space *Arkiv f. Mat.* **6** 241–68
- [16] Debbasch F, Mallick K and Rivet J P 1997 Relativistic Ornstein-Uhlenbeck process *J. Stat. Phys.* **88** 945–66
- [17] Debbasch F and Rivet J P 1998 A diffusion equation from the relativistic Ornstein-Uhlenbeck process *J. Stat. Phys.* **90** 1179–99
- [18] Debbasch F 2004 A diffusion process in curved space-time *J. Math. Phys.* **45** 2744–60
- [19] Franchi J and Le Jan Y 2004 Relativistic diffusions (arXiv:math/0403499)
- [20] Franchi J and Le Jan Y 2007 Relativistic diffusions and Schwarzschild geometry *Commun. Pure Appl. Math.* **60** 187–251
- [21] Dunkel J and Hänggi P (2005) Theory of relativistic Brownian motion: the $(1 + 1)$ -dimensional case *Phys. Rev. E* **71** 016124
- [22] Dunkel J and Hänggi P (2005) Theory of relativistic Brownian motion: the $(1 + 3)$ -dimensional case *Phys. Rev. E* **72** 036106
- [23] Chevalier C and Debbasch F 2007 Multi-scale diffusion on an interface *Europhys. Lett.* **77** 20005–9
- [24] Chevalier C and Debbasch F 2008 A unifying approach to relativistic diffusions and H -theorems *Mod. Phys. Lett. B* **22** 383–92
- [25] Chevalier C and Debbasch F 2008 Relativistic diffusions: a unifying approach *J. Math. Phys.* **49** 043303
- [26] Debbasch F, Espaze D and Foulonneau V 2012 Can diffusions propagate? *J. Stat. Phys.* **149** 37–49
- [27] Hakim R 1965 A covariant theory of relativistic Brownian motion I. local equilibrium *J. Math. Phys.* **6** 1482–95
- [28] Hakim R 1968 Relativistic stochastic processes *J. Math. Phys.* **9** 1805–18
- [29] Grover L K 1996 A fast quantum mechanical algorithm for database search *Proc. 28th Annual ACM Symp. on Theory of Computing - STOC96*
- [30] Chawla P, Mangal R and Chandrashekar C M 2019 Discrete-time quantum walk algorithm for ranking nodes on a network (arXiv:1905.06575)
- [31] Bialynicki-Birula I 1994 Weyl, Dirac, and Maxwell equations on a lattice as unitary cellular automata *Phys. Rev. D* **49** 6920–7
- [32] Arnault P and Debbasch F 2015 Landau levels for discrete-time quantum walks in artificial magnetic fields *Physica A* **443** 179–91
- [33] Arnault P and Debbasch F 2016 Quantum walks and discrete gauge theories *Phys. Rev. A* **93** 052301
- [34] Arnault P, Di Molfetta G, Brachet M and Debbasch F 2016 Quantum walks and non-Abelian discrete gauge theory *Phys. Rev. A* **94** 012335
- [35] Di Molfetta G and Pérez A 2016 Quantum walks as simulators of neutrino oscillations in a vacuum and matter *New J. Phys.* **18** 103038
- [36] Márquez-Martín I, Di Molfetta G and Pérez A 2017 Fermion confinement via quantum walks in $(2+1)$ -dimensional and $(3+1)$ -dimensional space-time *Phys. Rev. A* **95** 042112
- [37] Arrighi P, Di Molfetta G, Márquez-Martín I and Pérez A 2018 Dirac equation as a quantum walk over the honeycomb and triangular lattices *Phys. Rev. A* **97** 062111
- [38] Jay G, Debbasch F and Wang J B 2019 Dirac quantum walks on triangular and honeycomb lattices *Phys. Rev. A* **99** 032113
- [39] Di Molfetta G, Debbasch F and Brachet M 2014 Quantum walks in artificial electric and gravitational fields *Physica A* **397** 157–68
- [40] Arnault P and Debbasch F 2017 Quantum walks and gravitational waves *Ann. Physics* **383** 645–61
- [41] Arrighi P and Facchini S 2017 Quantum walking in curved spacetime: $(3+1)$ dimensions, and beyond *Quantum Inf. Comput.* **17** 810–24
- [42] Arrighi P and Facchini G D M F 2016 Quantum walking in curved spacetime: discrete metric (arXiv:1711.04662)
- [43] Arrighi P, Di Molfetta G, Márquez-Martín I and Pérez A 2019 From curved spacetime to spacetime-dependent local unitaries over the honeycomb and triangular quantum walks *Sci. Rep.* **9** 10904
- [44] Arrighi P, Facchini S and Forets M 2014 Discrete Lorentz covariance for quantum walks and quantum cellular automata *New J. Phys.* **16** 093007
- [45] Debbasch F 2019 Action principles for quantum automata and Lorentz invariance of discrete time quantum walks *Ann. Phys.* **405** 340–64
- [46] Debbasch F 2019 Discrete geometry from quantum walks *Condens. Matter* **4** 40
- [47] Márquez-Martín I, Arnault P, Di Molfetta G and Pérez A 2018 Electromagnetic lattice gauge invariance in two-dimensional discrete-time quantum walks *Phys. Rev. A* **98** 032333

- [48] Arnault P, Pérez A, Arrighi P and Farrelly T 2019 Discrete-time quantum walks as fermions of lattice gauge theory *Phys. Rev. A* **99** 032110
- [49] Cedzich C, Geib T, Werner A H and Werner R F 2019 Quantum walks in external gauge fields *J. Math. Phys.* **60** 012107
- [50] Di Molfetta G and Arrighi P 2019 A quantum walk with both a continuous-time and a continuous-spacetime limit (arXiv:1906.04483)
- [51] Hinarejos M, Bañuls M C and Pérez A 2013 A study of Wigner functions for discrete-time quantum walks *J. Comput. Theor. Nanosci.* **10** 1626–33
- [52] Hinarejos M, Bañuls M C and Pérez A 2015 Wigner formalism for a particle on an infinite lattice: dynamics and spin *New J. Phys.* **17** 013037
- [53] Debbasch F 2019 Relativistic Wigner function for quantum walks (arXiv:1902.11077)
- [54] Chandrashekar C M 2010 Discrete-time Quantum Walk - Dynamics and Applications *PhD Thesis* University of Waterloo (arXiv:1001.5326)
- [55] Pérez A 2016 Asymptotic properties of the Dirac quantum cellular automaton *Phys. Rev. A* **93** 012328
- [56] Konno N 2002 Quantum random walks in one dimension *Quantum Inf. Process.* **1** 345–54
- [57] Trzetrzelewski M 2015 On the mass term of the Dirac equation (arXiv:1101.3899)
- [58] Debbasch F 2019 Discrete geometry from quantum walks (arXiv:1902.11079)
- [59] Preskill J 2014 *Quantum Information and Computation* (Pasadena, CA: Caltech) ch 3
- [60] Cappellaro P 2012 *Quantum Theory of Radiation Interactions* (Cambridge, MA: MIT Press) ch 8
- [61] Di Molfetta G and Debbasch F 2016 Discrete-time quantum walks in random artificial gauge fields *Quantum Studies: Mathematics and Foundations* **3** 293–311
- [62] Barnett S M 2009 *Quantum Information* (Oxford: Oxford University Press)
- [63] Di Molfetta G, Debbasch F and Brachet M 2013 Quantum walks as massless Dirac fermions in curved space *Phys. Rev. A* **88** 042301
- [64] Roston G B, Casas M, Plastino A and Plastino A R 2005 Quantum entanglement, spin-1/2 and the Stern-Gerlach experiment *Eur. J. Phys.* **26** 657–72
- [65] Park S T 2012 Propagation of a relativistic electron wave packet in the Dirac equation *Phys. Rev. A* **86** 062105
- [66] Demikhovskii V Y, Maksimova G M, Perov A A and Frolova E V 2010 Space-time evolution of Dirac wave packets *Phys. Rev. A* **82** 052115
- [67] Randall G 2019 *Lecture 10: Persistent Random Walks and the Telegrapher's Equation* (Cambridge, MA: MIT Press)
- [68] Gaveau B, Jacobson T, Kac M and Schulman L S 1984 Relativistic extension of the analogy between quantum mechanics and Brownian motion *Phys. Rev. Lett.* **53** 419–22
- [69] Fukushima Y and Wada T 2017 A discrete transmission line model for discrete-time quantum walks *Interdiscipl. Inf. Sci.* **23** 87–93
- [70] Arnault P 2017 Discrete-time quantum walk and gauge theories *PhD Thesis* Université Pierre et Marie Curie (arXiv:1710.11123)
- [71] Cabrera R, Campos A G, Bondar D I and Rabitz H A 2016 Dirac open-quantum-system dynamics: formulations and simulations *Phys. Rev. A* **94** 052111
- [72] Haba Z 2009 Relativistic diffusion of massless particles (arXiv:0903.2622)
- [73] Haba Z 2009 Relativistic diffusion of elementary particles with spin *J. Phys. A: Math. Theor.* **42** 445401
- [74] Falci G, Morello Baganella M, Berritta M, D'Arrigo A and Paladino E 2010 Dynamics of Weyl wave-packets in a noisy environment *Physica E* **42** 584–9
- [75] Arsenijević M, Jeknić-Dugić J and Dugić M 2017 Generalized Kraus operators for the one-qubit depolarizing quantum channel *Braz. J. Phys.* **47** 339–49
- [76] Polyanin A D 2002 *Handbook of Linear Partial Differential Equations for Engineers and Scientists* (Boca Raton, FL: CRC Press)
- [77] Gomis P and Pérez A 2016 Decoherence effects in the Stern-Gerlach experiment using matrix Wigner functions *Phys. Rev. A* **94** 012103
- [78] Ahlbrecht A, Cedzich C, Matjesch R, Scholz V B, Werner A H and Werner R F 2012 Asymptotic behavior of quantum walks with spatio-temporal coin fluctuations *Quantum Inf. Process.* **11** 1219–49
- [79] Schwartz M 2016 *Lecture 11: Wavepackets and Dispersion* (Cambridge, MA: Harvard University Press)

Solitons in a photonic nonlinear quantum walk: lessons from the continuum

Andreu Anglés-Castillo,^{1,*} Armando Pérez,¹ and Eugenio Roldán²

¹*Departament de Física Teòrica & IFIC, Universitat de València-CSIC, 46100 Burjassot (València) Spain*

²*Departament d'Òptica i d'Optometria i Ciències de la Visió, Universitat de València, Dr. Moliner 50, 46100-Burjassot*

We analyze a nonlinear QW model which can be experimentally implemented using the components of the electric field on an optical nonlinear Kerr medium, which translates into a rotation in the coin operator, with an angle which depends (in a nonlinear fashion) on the state of the walker. This simple dependence makes it easy to consider the space-time continuum limit of the evolution equation, which takes the form of a nonlinear Dirac equation. The analysis of this continuum limit allows us, under some approximations, to gain some insight into the nature of soliton structures, which is illustrated by our numerical calculations. These solitons are stable structures whose trajectories can be modulated by choosing the appropriate initial conditions. We have also studied the stability of solitons when they are subject to an additional phase that simulates an external electric field, and also explored if they are formed in higher dimensional spaces.

I. INTRODUCTION

The quantum walk (QW) is a powerful toolbox with many applications. It can be shown to constitute a universal model of computation [1–3] with algorithmic applications, such as search problems [4–9] or element distinctness [10]. QWs manifest into two main categories. Continuous-time QWs (CQWs) are described by a local Hamiltonian originated from the adjacency matrix on some graph with a time evolution which is dictated by the Schrödinger equation, while discrete-time QWs (DQWs) are defined by a unitary evolution operator which relates two consecutive time instants in a stroboscopic way. Another important difference is that, in the case of DQWs, the Hilbert space associated to the graph needs to be enlarged with an additional degree of freedom (the so called “coin” space). In spite of this different formulation, it is possible to establish a connection between CQWs and DQWs [11–15]. In this work, we will concentrate on DQWs.

From a physical point of view, DQWs have also been used for the simulation of various physical theories and phenomena. Many of these applications are motivated from the fact that, under the appropriate conditions, the continuum limit of DQWs is the Dirac equation. In this way, DQWs can be used to simulate spin-1/2 particles in both external Abelian [16–18] and non-Abelian [19] gauge fields. Such simulations can also be applied to relativistic gravitational fields [20–24]. DQWs also show additional interesting phenomena [25–27].

QWs have been implemented using different setups [28], such as photons in various optical devices [29–35], atoms trapped in arrays of light [36], ion traps [37], or superconducting qubits [38].

In this work, we analyze a variant of the DQW which introduces nonlinearities on the angle of the coin operator, and shows some similar phenomena as in the Non-Linear Optical Galton Board (NLOGB) model introduced in [39], where such nonlinearities appeared as phases on the different components of the dynamical map. The main result in that reference was the appearance of soliton-like structures with a rich phenomenology that can be controlled by varying the coupling strength to the nonlinear Kerr medium. In the model that is proposed here, we also observe the formation of solitons with a characteristic profile. The continuum space-time limit can be easily obtained, and it turns out that it provides much information about the soliton nature, which is confirmed by our numerical simulations. It also allows to limit the conditions for stability for solitons. We observe that these solitons remain stable when they cross each other. Under the presence of an external electric field, we obtain different situations, depending on the strength of the field and the magnitude of the nonlinearity.

This paper is organized as follows. In Sect. II we first recall the setup for the linear DQW, and review the different proposals to account for a nonlinear DQW. In Sect. III we introduce our own proposal, and we discuss its experimental implementation based on nonlinear Kerr optical media. Sect. IV is devoted to the analysis of the continuum space-time limit, which is afterwards illustrated by our numerical calculations in Sect. V. We conclude in Sect. VI by summarizing our main findings.

II. OVERVIEW ON LINEAR AND NONLINEAR DQWS

We start by briefly revisiting the standard (linear) and nonlinear models to describe the DQW for a walker on a one-dimensional lattice.

* andreu.angles-castillo@uv.es

A. Linear DQW

Let us consider a particle (the walker) that can move along a discrete lattice with positions $x = j\epsilon$, $j \in \mathbb{Z}$, with ϵ the lattice spacing. A position Hilbert space \mathcal{H}_x is associated to this system, which is spanned by the basis $\{|x\rangle\}$, with x the lattice positions. As mentioned in the Introduction, we also need an additional degree of freedom that defines the coin Hilbert space \mathcal{H}_c , and will be spanned by two orthogonal states $\{|\uparrow\rangle, |\downarrow\rangle\}$. The total Hilbert space is, therefore, the tensor product $\mathcal{H} = \mathcal{H}_x \otimes \mathcal{H}_c$, and the basis that spans the whole space is $\{|x\rangle \otimes |\uparrow/\downarrow\rangle\}_{j \in \mathbb{Z}}$. For reasons that will be explained in Sect. IV, we define a time step evolution of the walker using the same amount ϵ , i.e. the state $|\psi_t\rangle$ at a given time t evolves as

$$|\psi_{t+\epsilon}\rangle = U |\psi_t\rangle, \quad (1)$$

with U the evolution operator. The operator U is the composition of two unitary operators,

$$U = SC, \quad (2)$$

where $C = \mathbb{I} \otimes R$ is the coin operator acting on \mathcal{H}_c . In the latter equation, S represents the conditional displacement operator, which can be formally written as

$$S = e^{-i\sigma_z \hat{p}}, \quad (3)$$

with \hat{p} the lattice quasi-momentum operator, and σ_i , $i = x, y, z$ the Pauli matrices acting on the $\{|\uparrow\rangle, |\downarrow\rangle\}$ states. As for the operator R , it will be represented by a 2×2 unitary matrix. An example is given by

$$R \equiv e^{-i\theta\sigma_y} = \begin{pmatrix} \cos\theta & -\sin\theta \\ \sin\theta & \cos\theta \end{pmatrix}. \quad (4)$$

In what follows, we will set $\epsilon = 1$, so that $x = j$. However, we will need to restore this parameter in Sect. IV, in order to derive the continuum limit of Eq. (1).

In terms of the tensor basis in \mathcal{H} , one can expand $|\psi_t\rangle$ as follows:

$$|\psi_t\rangle = \sum_x [u_{t,x} |x, \uparrow\rangle + d_{t,x} |x, \downarrow\rangle]. \quad (5)$$

In other words, the corresponding spinor is

$$\Psi(t, x) \equiv \langle x | \psi_t \rangle = u_{t,x} |\uparrow\rangle + d_{t,x} |\downarrow\rangle \equiv \begin{pmatrix} u_{t,x} \\ d_{t,x} \end{pmatrix}. \quad (6)$$

Finally, the operator S takes the form

$$S = \sum_x (|x+1\rangle \langle x| \otimes |\uparrow\rangle \langle \uparrow| + |x-1\rangle \langle x| \otimes |\downarrow\rangle \langle \downarrow|). \quad (7)$$

B. Nonlinear DQW

The discrete non-linear QW was not first introduced as such, but as a nonlinear Optical Galton Board [39], mainly because "nonlinear quantum walk" is close to be an oxymoron, being quantum mechanics a linear theory; however, the term Non-linear Quantum Walk (NLQW) has made its way through the literature and we adhere to it, but we must keep in mind that the waves used in a NLQW cannot be true quantum wave-functions but some other type of waves.

The NLOGB is a coined DQW on the line in which the wavefunction acquires an additional coin-state-dependent nonlinear phase $\phi_{c,NL}$ depending on the probability as $\phi_{c,NL} = i2\pi\alpha |c_{t,x}|^2$ with $c = u, d$ and α the nonlinearity strength. This is equivalent to either (i) replacing the standard QW coin operator R by the inhomogeneous non-linear coin operator

$$R_{t,x} = \begin{pmatrix} e^{i2\pi\alpha |u_{t,x}|^2} \cos\theta & -e^{i2\pi\alpha |d_{t,x}|^2} \sin\theta \\ e^{i2\pi\alpha |u_{t,x}|^2} \sin\theta & e^{i2\pi\alpha |d_{t,x}|^2} \cos\theta \end{pmatrix}, \quad (8)$$

or to (ii) generalizing the conditional displacement operator as

$$S = \sum_{x=-L}^L e^{i2\pi\alpha |u_{t,x}|^2} |x+1\rangle \langle x| \otimes |\uparrow\rangle \langle \uparrow| \quad (9)$$

$$+ e^{i2\pi\alpha |d_{t,x}|^2} |x-1\rangle \langle x| \otimes |\downarrow\rangle \langle \downarrow|. \quad (10)$$

In [39], the NLOGB was numerically studied and the existence of solitons and of rich spatio-temporal dynamics, including chaotic behaviour, was shown. The NLOGB was later experimentally implemented by Wimmer et al. [40] in a system involving the propagation of light pulses in optical fibres, an implementation in which the displacement operation consists in delaying or advancing the pulses, so that the QW occurs along the physical time dimension. More recently, the same group made a proposal of NLQW in optical mesh lattices [41], see also the related paper [42], a system that has been recently revisited by Yue et al. [43]. The NLOGB model has also been the subject of several theoretical studies, including the study of its continuous limit as a nonlinear Dirac equation [44–46]. Further numerical studies by Buarque and coworkers centred on self-trapping [47], breathing dynamics [48], and rogue waves [49]. There has also been made a rigorous mathematical study of the discrete model [50, 51] including the demonstration of long term soliton stability [52]. Recently, the NLOGB has been extended to three-state coins [53], and generalized to include the effect of perturbing potential barriers [54].

Moreover, NLQWs different from the NLOGB have been proposed. Shikano et al. [55] proposed a NLQW in which the nonlinearity is due to a feed-forward

quantum-coin mechanism such that the coin elements become $\cos \theta_{t,x} = |u_{t-1,x+1}| + i |d_{t-1,x-1}|$ and $\sin \theta_{t,x} = \sqrt{1 - |\cos \theta_{t,x}|^2}$. Lee et al. show how the dynamics of a nonlinear Dirac particle can be simulated by NLQWs with a measurement-based feed-forward scheme, slightly different from that of Shikano et al., considering both Gross-Neveu and Thirring types of nonlinear couplings. Gerasimenko et al. [56] introduced the nonlinearity through the operator $\exp[-i\kappa (|u_{t,x}|^2 - |d_{t,x}|^2) \sigma_y]$, so that the nonlinear phase-shift depends on the "population difference" $|u_{t,x}|^2 - |d_{t,x}|^2$, and concentrated in the study of the influence of zero modes on the formation of solitonic structures in the continuum limit. In [57] the work in [56] was generalized by using mathematical techniques appropriate for Floquet systems, which allowed for the finding of new bifurcations.

Another alternative is that of Mendonça et al. [58], who propose a non-linear displacement operator of the form

$$S = \sum_{x=-L}^L \frac{1}{\sqrt{1 + \alpha P_{t,x}}} [|x+1, \uparrow\rangle \langle x, \uparrow| + \alpha P_{t,x} |x, \uparrow\rangle \langle x, \uparrow|] + \sum_{x=-L}^L \frac{1}{\sqrt{1 + \alpha P_{t,x}}} [|x-1, \downarrow\rangle \langle x, \downarrow| + \alpha P_{t,x} |x, \downarrow\rangle \langle x, \downarrow|], \quad (11)$$

with

$$P_{t,x} = |u_{t,x}|^2 + |d_{t,x}|^2, \quad (12)$$

defined as the probability density of the walker at time t and at position x . They numerically find and describe a variety of nonlinear phenomena, which were further studied in [59].

As for Mallick et al. [60], they use the nonlinear map

$$u_{t+1,x} = \cos \theta u_{t,x-1} + e^{i\phi_{x-1}(t)} \sin \theta d_{t,x-1}, \quad (13)$$

$$d_{t+1,x} = -e^{-i\phi_{x+1}(t)} \sin \theta u_{t,x+1} + \cos \theta d_{t,x+1}, \quad (14)$$

with $\phi_x = \gamma P_x + \eta_x$, where η_x is a noise term, and study the breakdown of Anderson localization induced by the nonlinearity. Finally, in [61] single atoms are suggested as nonlinear beam-splitters in their proposal of a NLQW.

Closely related studies are those by Solntsev et al. [62], who incorporate biphoton generation –an intrinsic nonlinear process– in a photonic wave-guide array and study the potential of the system to generate entangled light, but the quantum walk is linear; Verga [63] studies edge-states in a QW with both linear and nonlinear disorder; Bisio et al. [64] analytically diagonalize a discrete-time on-site interacting fermionic cellular automaton in the two-particle sector; Adami et al. [65] study a NLQW naturally induced by a quantum graph with nonlinear

delta potentials; Templeman et al. [66] study topological protection in a strongly nonlinear interface lattice; and Held et al. [67] introduce Gaussian QWs, which are NLQWs in which the coins are substituted by two-mode squeezers. As stressed by the authors, this kind of NLQWs directly lead to accessible quantum phenomena, rendering possible the quantum simulation of nonlinear processes.

We must also mention works on continuous time NLQWs. In [68] the destruction of Anderson localization by nonlinearity is studied through discrete Anderson nonlinear Schrödinger equations that correctly describe the one-dimensional disordered waveguide lattices used in the experiments of Lahini et al. [69]. But most studies are related to the problem of database searching. Ebrahimi Kahou et al. study this problem with coupled discrete nonlinear Schrödinger equations, and discuss the implementability of the model with BECs [70]. Meyer and Gong study quantum search with the Gross-Pitaevskii equation [71, 72] concluding that it solves the unstructured search problem more efficiently than does the Schrödinger equation, because it includes a cubic nonlinearity, and Chiew et al. [73] demonstrate that the nonlinear quantum search can be more efficient than quantum search for graph comparison. Di Molffetta et al. [74] generalize the Meyer-Gross algorithm to two dimensions finding a clear advantage over the linear QW. Finally, in [75] the thresholds between modulational stability, rogue waves and soliton regimes are studied with coupled nonlinear Schrödinger equations with on site saturating non-linearity.

In the present paper, we introduce an alternative formulation of the NLQW which is appropriate for light polarization qubits propagating in Kerr media. Specifically, we introduce a nonlinear coin in which the rotation angle is given by $\theta = \theta_0 + \theta_{nl}$ with θ_0 constant and θ_{nl} depending on the light polarization state, hence in the coin state.

III. MODEL

A. NLQW coin and map

The non-linear Quantum Walk (QW) we propose introduces the non-linearity in the coin operator. The unitary operator R is now defined in a way that depends on the state of the walker

$$R(\theta_{t,x}) = e^{-i\theta_{t,x} \sigma_y} = \begin{pmatrix} \cos \theta_{t,x} & -\sin \theta_{t,x} \\ \sin \theta_{t,x} & \cos \theta_{t,x} \end{pmatrix}. \quad (15)$$

The angle of rotation is given by

$$\theta_{t,x} = \theta_0 + \alpha |u_{t,x}| |d_{t,x}| \sin \delta_{t,x}, \quad (16)$$

where we explicitly expressed the upper and lower components given by their modules and complex angle as

$u_{t,x} = |u_{t,x}|e^{i\varphi_{t,x}^u}$, $d_{t,x} = |d_{t,x}|e^{i\varphi_{t,x}^d}$ and $\delta_{t,x} = \varphi_{t,x}^u - \varphi_{t,x}^d$ is the phase difference. If we write how the components evolve explicitly after each time step, we get

$$\begin{aligned} u_{t+1,x} &= \cos(\theta_{t,x-1})u_{t,x-1} - \sin(\theta_{t,x-1})d_{t,x-1}, \\ d_{t+1,x} &= \sin(\theta_{t,x+1})u_{t,x+1} + \cos(\theta_{t,x+1})d_{t,x+1}. \end{aligned} \quad (17)$$

B. Experimental proposal

In proposing the nonlinear rotation term in Eq. (16), we are thinking in a QW photonic platform, using light-polarization qubits [76, 77], and including optical media with Kerr-type nonlinearity. It is well known that in an isotropic Kerr medium the normal modes of propagation are circularly polarized, their corresponding indexes of refraction are given by [78]

$$n_{\pm} = n_0 + \frac{1}{2n_0} \left[A |E_{\pm}|^2 + (A+B) |E_{\mp}|^2 \right], \quad (18)$$

where the subscripts + and - make reference to right- and left-circular polarization, respectively, n_0 is the linear refractive index, and A and B are the Maker-Terhune coefficients for the non-linear medium, whose ratio depends on the specific physical mechanism responsible for the Kerr effect (e.g., $A = B$ for nonlinear electronic response). In such a medium, the phenomenon of nonlinear polarization rotation occurs, by means of which a polarized monochromatic-wave that propagates a distance z along the nonlinear medium has the expression

$$\begin{aligned} \vec{E}(z) &= E_+ \hat{\sigma}_+ + E_- \hat{\sigma}_- \\ &= (A_+ \hat{\sigma}_+ e^{i\theta_{nl}} + A_- \hat{\sigma}_- e^{-i\theta_{nl}}) e^{ik_m z}, \end{aligned} \quad (19)$$

where $k_m = (n_+ + n_-)\omega/2c$ is the mean propagation constant, $\hat{\sigma}_{\pm} = (\hat{x} \pm i\hat{y})/\sqrt{2}$ are the unit circular polarization vectors, and

$$\theta_{nl} = \frac{1}{2} (n_+ - n_-) \frac{\omega}{c} z = \frac{B}{4n_0} \left(|E_-|^2 - |E_+|^2 \right) \frac{\omega}{c} z. \quad (20)$$

This expression shows that the polarization state of the light undergoes a rotation θ_{nl} after the propagation, the circular components changing from $\hat{\sigma}_{\pm}$ to $\hat{\sigma}'_{\pm} = \hat{\sigma}_{\pm} e^{i\theta_{nl}}$, and the linear components of the polarization passing from (x, y) at the entrance to

$$x' = x \cos \theta_{nl} - y \sin \theta_{nl}, \quad (21)$$

$$y' = x \sin \theta_{nl} + y \cos \theta_{nl}, \quad (22)$$

at the exit. Notice that for linearly polarized light $|E_-|^2 = |E_+|^2$, and hence $\theta_{nl} = 0$. Notice also that, the rotation does not change the proportion $|E_-|/|E_+|$.

Now, we take the linear polarization components as the coin state basis, so that the displacement operator acts on these linear components. It is then necessary the use of the additional standard coin rotation θ_0 in Eq. (16),

because, after the action of the displacement operator, the field is linearly polarized at the displaced positions, and we have seen that there is no nonlinear rotation for linear polarizations, which means that the nonlinear coin would not act but in the first step. Finally, by writing θ_{nl} in terms of the linear polarization components of the field, one arrives at the expression in Eq. (16).

IV. CONTINUUM LIMIT

The continuum limit of the QW is obtained by retaining the lowest order, i.e. $\mathcal{O}(\epsilon)$, in the unitary evolution defined by Eq. (1). To this purpose, we need to restore the parameter ϵ both in the lattice spacing and in the time step. The continuum limit of this quantum walk can be obtained following the standard method. Details and definitions are given in Appendix A.

The non-linear Dirac equation obtained from this limit reads

$$[i\gamma^\mu \partial_\mu - m(\Psi(t, x))] \Psi(t, x) = 0, \quad (23)$$

where the Dirac matrices are $\gamma^0 = \sigma_y$ and $\gamma^1 = i\sigma_x$ and the mass term is given by

$$m(\Psi(t, x)) = \tilde{\theta}_0 - \frac{\tilde{\alpha}}{2} \Psi^\dagger(t, x) \sigma_y \Psi(t, x), \quad (24)$$

where we defined the rescaled angle $\epsilon\tilde{\theta}_0 = \theta_0$ and non-linearity parameter $\epsilon\tilde{\alpha} = \alpha$. We notice that this mass term is different from that obtained from the NLOGB in [44]. We can write this equation in terms of the spinor components $\Psi(t, x) = (u(t, x), d(t, x))^T$ as

$$(\partial_x + \partial_t) u + \tilde{\theta} d = 0, \quad (25)$$

$$(\partial_x - \partial_t) d + \tilde{\theta} u = 0, \quad (26)$$

with

$$\tilde{\theta} \equiv \tilde{\theta}_0 + i\frac{\tilde{\alpha}}{2} (u^* d - u d^*), \quad (27)$$

where we alleviated the notation by not writing the explicit spatial and time dependence of each component. This system of equations can be rewritten in terms of the modulus and phases of the spinor components $u = U e^{i\varphi_u}$ and $d = D e^{i\varphi_d}$. After defining

$$\delta = \varphi_u - \varphi_d, \quad \sigma = \varphi_u + \varphi_d, \quad (28)$$

one easily gets

$$\begin{aligned} \partial_x \sigma + \partial_t \delta &= -\tilde{\theta} \frac{U^2 - D^2}{UD} \sin \delta, \\ \partial_x \delta + \partial_t \sigma &= \tilde{\theta} \frac{U^2 + D^2}{UD} \sin \delta, \\ (\partial_x + \partial_t) U &= -\tilde{\theta} D \cos \delta, \\ (\partial_x - \partial_t) D &= -\tilde{\theta} U \cos \delta, \end{aligned} \quad (29)$$

with

$$\tilde{\theta} \equiv \tilde{\theta}_0 + \tilde{\alpha} U D \sin \delta. \quad (30)$$

A. Homogeneous stationary solutions

In order to gain some insight into the solutions of the system, we first study the homogeneous stationary solutions and their stability. Let us focus on the last two equations of Eq. (29), which can be related as

$$\partial_t(U^2 + D^2) = -\partial_x(U^2 - D^2), \quad (31)$$

which for stationary solutions¹, and from the condition of normalization of the wavefunction, implies that $U = D$, and hence $\partial_t U = 0$. We can now define $I = U^2 = D^2$ to rewrite Eq. (29) as

$$\begin{aligned} \partial_x \sigma + \partial_t \delta &= 0, \\ \partial_x \delta + \partial_t \sigma &= 2\tilde{\theta} \sin \delta, \\ \partial_x I &= -2I\tilde{\theta} \cos \delta, \end{aligned} \quad (32)$$

with $\tilde{\theta} = \tilde{\theta}_0 + \tilde{\alpha}I \sin \delta$, and we used the fact that $\partial_t I = 0$. To further derive homogeneous stationary solutions, we impose $\partial_x I = \partial_x \delta = 0$, which implies that $\partial_t \sigma = 2\tilde{\theta} \sin \delta$ and $2I\tilde{\theta} \cos \delta = 0$. The latter equation admits several solutions: (i), $I = 0$ (trivial solution); (ii) $\tilde{\theta} = 0$, which implies $I \sin \delta = -\tilde{\theta}_0/\tilde{\alpha}$ that only exists for $I > |\tilde{\theta}_0/\tilde{\alpha}|$ and for which $\partial_t \sigma = 0$; and (iii), the two solutions $\delta = \pm\pi/2$ that exist for any value of I and for which $\partial_t \sigma = \pm 2\tilde{\theta} = 2(\tilde{\alpha}I \pm \tilde{\theta}_0)$. Notice that for positive (negative) $\tilde{\theta}_0/\tilde{\alpha}$, solution $\delta = -\pi/2$ ($\delta = \pi/2$) merges with solution $\tilde{\theta} = 0$ for $I = |\tilde{\theta}_0/\tilde{\alpha}|$.

We have performed the linear stability analysis of these solutions by analysing the linearized evolution of perturbations of the form $\delta v e^{\lambda t} e^{ikx}$ with δv small. The results can be summarized as follows: (i), the trivial solution, solution $\tilde{\theta} = 0$, and solution $\delta = \pi/2$ are all three neutrally stable with two pairs of complex conjugated purely imaginary eigenvalues (different for each solution); and (ii), solution $\delta = -\pi/2$ is unstable versus perturbations with wavenumber $0 < k^2 < \tilde{\theta}_0$ when $I < \tilde{\theta}_0/\tilde{\alpha}$, and unstable versus all perturbations, more unstable the larger k^2 is, when $I > \tilde{\theta}_0/\tilde{\alpha}$. All details are given in Appendix B.

Hence, there is a clear distinction between solution $\delta = \pi/2$, which is neutrally stable, and solution $\delta = -\pi/2$, which is unstable versus perturbations with non-null wave-number. This is reminiscent of the modulational instability occurring in optical fibres [78].

B. Solitons as stationary solution of the continuum equation

We aim to look for stationary solutions of the system of differential equations defined in Eq. (32). To obtain a closed stationary solution, we need to resort to assumptions that are backed up by the observations made for the discrete model in Section V A. First of, we observed that the phases sum σ is independent of the position inside the soliton-like structure in the discrete model of the QW, so that extending this observation to the first equation we can conclude that δ is time independent. We also observed that σ has a linear time dependence, and found that it was $\partial_t \sigma = -2\theta_0$, so that we end up with the following system of two equations

$$\begin{aligned} \partial_x \delta &= 2\tilde{\theta} \sin \delta + 2\theta_0, \\ \partial_x I &= -2I\tilde{\theta} \cos \delta. \end{aligned} \quad (33)$$

To further proceed we need to resort to an observation made for the discrete model again, which is that non-linear effects are enhanced when δ is close to $-\frac{\pi}{2}$, and assume that only small fluctuations about this value lead to soliton-like structures, that is, $\delta \approx -\frac{\pi}{2} + \Delta$. Approximating the trigonometric functions up to first order in Δ and $\tilde{\theta} = \tilde{\theta}_0 - \tilde{\alpha}I$ these equations reduce to

$$\begin{aligned} \partial_x \Delta &= 2\tilde{\alpha}I, \\ \partial_x I &= -2(\tilde{\theta}_0 - \tilde{\alpha}I)\Delta I \approx -2\tilde{\theta}_0\Delta I, \end{aligned} \quad (34)$$

where in the last equation we considered that the term $I^2\Delta$ is negligible². The solution of this system of equations is now exact and gives the following solution,

$$\begin{aligned} \Delta(x) &= \frac{\tilde{\alpha}}{2} \tanh\left(\frac{\tilde{\alpha}\tilde{\theta}_0}{2}x\right), \\ I(x) &= \frac{\tilde{\alpha}\tilde{\theta}_0}{8} \operatorname{sech}^2\left(\frac{\tilde{\alpha}\tilde{\theta}_0}{2}x\right), \end{aligned} \quad (35)$$

where we imposed the normalization condition to obtain the constants of integration. This solution is then confirmed to describe well a stationary soliton in the discrete model, which is numerically studied in Sect. V.

V. NUMERICAL

The appearance of soliton-like structures is ubiquitous in the study of NLQWs [39, 51, 54]. The key feature to keep the non-linearity of the walker present, that counteracts the natural dispersion of the walker and keeps the solitonic behaviour, is to have the relative phase of

¹ A stationary solution refers to a static probability distribution where the phases of the spinor components can still have time dependence.

² The probability density squared I^2 for an extended soliton structure is small, and Δ is also assumed to be small.

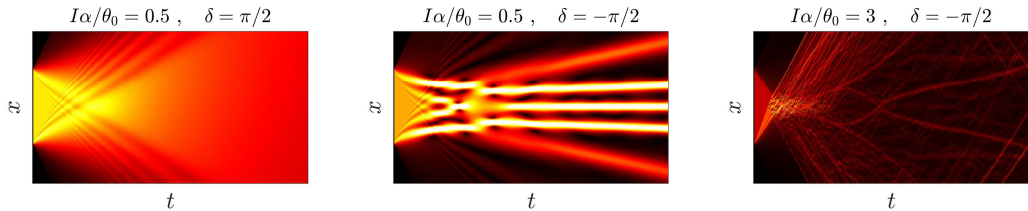


Figure 1. In this figure, we plot the evolution of the probability density (IIB) of an extended initial walker, where the spin states in locations $x = [-50, 50]$ all have the same initial coin state. The coin angle $\theta_0 = \pi/3$ and the non-linearity parameter is $\alpha = 2\pi$ in all panels. In the first panel, the initial coin state is $|\psi_0\rangle = (1, -i)^T/\sqrt{2}$ so that $\delta = -\pi/2$, while in the last two panels the initial coin state is $|\psi_0\rangle = (1, i)^T/\sqrt{2}$ with a corresponding $\delta = \pi/2$. The initial intensity of each initial condition is given in the title of each panel. The intensity of the walker is given by a heatmap, black indicates low probability density and brighter/hotter colours indicate higher probability density.

the walker components around $\delta_{t,x} \approx \pm\frac{\pi}{2}$, as can be seen from Eq. (16). For that reason, the spatial distribution of the relative phase between components will play an important role in the formation and stability of solitons. In order to explore the ability of this new proposed NLQW to form soliton-like structures, we consider in Fig. 1 an extended initial condition where the spin is uniformly distributed, where we plot the probability density, as defined by Eq. (IIB), in different situations.

We first study an initial condition with $\delta = \pi/2$. We found in the stability analysis of Sect. IV A that solutions with this phase difference were neutrally stable, meaning that perturbations are not enhanced nor diminished. It can be seen in the left panel of Fig. 1 that the probability density of the walker with this phase difference is mostly uniform after some initial interactions. When $\delta = -\pi/2$ the stability becomes dependent on the value of the intensity I . On the one hand, when $I\alpha/\theta_0 < 1$ only perturbations with small wave number ($0 < k < \theta_0$) are enhanced. In the central panel of Fig. 1 we can see the appearance of soliton-like structures that have an extended (low k) stable probability distribution. On the other hand, when $I\alpha/\theta_0 > 1$ perturbations of any wave number are enhanced. In the left panel of Fig. 1 it can be seen that no extended structures are formed, and most part of the probability is scattered.

A. Solitons

When the soliton-like structures of the central panel of Fig. 1 are formed, we observe that the probability distribution of the walker components are well described by the typical $\text{sech}^2(x)$ function. If we consider this distribution as an initial condition with relative phase between walker components corresponding to $\delta = -\pi/2$

$$\langle x | \psi_{0,x}^{\text{soliton}} \rangle = N_\beta \begin{pmatrix} \text{sech}(\beta x) \\ i \text{sech}(\beta x) \end{pmatrix}, \quad (36)$$

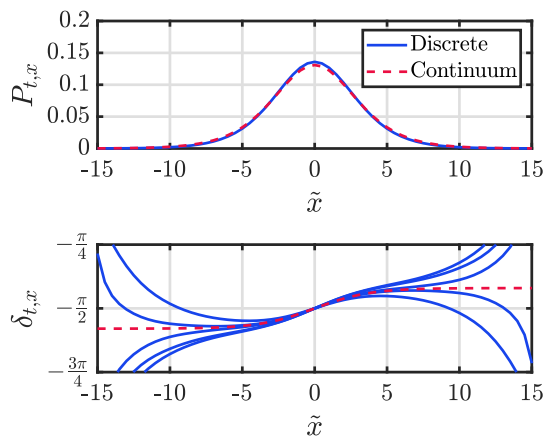


Figure 2. (Top) Probability distribution of the walker. (Bottom) Phase difference between walker components. The red dashed line represents the analytical solution obtained in Eq. (35) for both quantities. The initial condition is given by Eq. (36) and is evaluated at $t = 500, 501, 502, 503, 504$. The parameters of the quantum coin are $\tilde{\alpha} = 1$ and $\tilde{\theta}_0 = \pi/3$ and the initial width of the walker is given by $\beta = \tilde{\alpha}\tilde{\theta}_0/2$, for a spacing $\epsilon = 0.5$. The spatial coordinate has also been scaled as $\tilde{x} = \epsilon x$.

where N_β is a normalization constant that depends on β , we observe that the associated probability distribution remains stationary at different times. While this initial condition produces a soliton-like structure, it might not represent the stationary state of the evolved soliton.

In Fig. 2 we show the probability distribution of the walker and the difference of the walker phases $\delta_{t,x}$ after $t = 500$ and 4 subsequent steps. We also plot for comparison the stationary solution obtained in the continuum limit Eq. (35). The probability distribution is stationary and perfectly fits the analytical solution. The phase differences have oscillating values around the boundary of

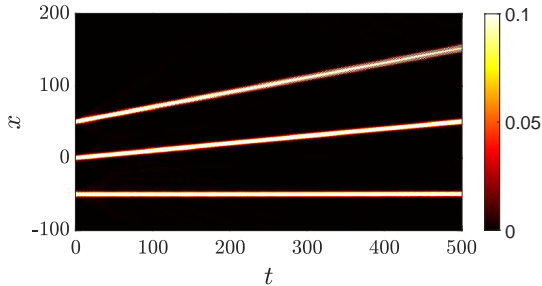


Figure 3. Density plot of the evolved probability distribution of three solitons initially localized at $x = 50$, $x = 0$ and $x = -50$ with different relative phase distributions, with $\nu = 2/3$, $\nu = 1/2$ and $\nu = 0$, respectively. They all have the same initial width with $\beta = 1/2$. The angle is $\theta_0 = \pi/4$, and the non-linearity parameter is $\alpha = \pi$.

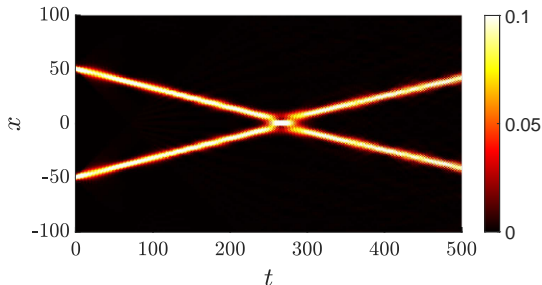


Figure 4. Density plot of the evolved probability distribution of two solitons initially localized at $x = 50$ and $x = -50$ that propagate in opposite directions with $\nu = -2/3$ and $\nu = 2/3$, respectively. They all have the same initial width $\beta = 1/2$. The angle is $\theta_0 = \pi/4$, and the non-linearity parameter is $\alpha = \pi$.

the soliton, but the behaviour around the centre of the soliton is well described by the analytical solution of the continuum model.

We also observed that the phase sum is constant in the x direction (inside the soliton), while it has a linear dependence in time. This dependence is observed to be

$$\sigma_{t,x}^{\text{soliton}} = \sigma_0 - 2\theta_0 t, \quad (37)$$

where σ_0 is the initial value the sum of the phases, and we notice that this expression is only valid in the regions inside the soliton. This observation is consistent with the assumptions made in Sect. IV B.

We also considered an initial condition of the form

$$\langle x | \psi_{0,x} \rangle = N_\beta \left(i e^{i\nu \tanh(\beta x)} \text{sech}(\beta x) \right). \quad (38)$$

In this case we did not observe a stationary soliton, but a soliton that propagates at a constant velocity. We ob-

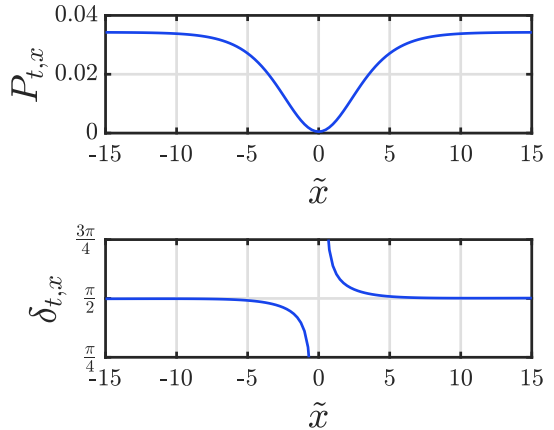


Figure 5. Probability distribution of the walker (upper panel), and phase difference between components (lower panel) with initial condition (39) evaluated after $t = 500$ steps. The parameters of the quantum coin are $\tilde{\alpha} = 1$ and $\tilde{\theta}_0 = \pi/3$. The initial width of the walker is given by $\beta = \tilde{\alpha}\tilde{\theta}_0/2$ and the intensity $I = \beta$, for a spacing $\epsilon = 0.5$. The spatial coordinate has also been scaled as $\tilde{x} = \epsilon x$.

served that if ν is positive, the initial soliton-like structure propagates to the right (positive x) and, if it is negative, it propagates to the left, i.e., ν plays the role of velocity on this initial condition. In Fig. 3 we present the evolution of three initial solitons propagating with different values of ν : two that propagate with different velocities, and another one with $\nu = 0$ that remains stationary. The probability distribution and relative phases are the same as in the static soliton, but with the centre displaced at a constant velocity. This initial condition produces a kick, after which the soliton propagates at a constant velocity.

Another feature that is characteristic of solitons is that the interaction between them leave the shape of their wave packets unaltered. This effect is also showcased by the solitons generated in this QW. In Fig. 4 we show the collision of two solitons propagating in opposite directions, and it can be observed that they cross each other without any significant modification after the crossing.

B. Dark solitons

While an initial condition with $\delta = \pi/2$ was not observed to form soliton-like structures, it was pointed out that, in the continuum limit, homogeneous solutions are marginally stable, i.e., there are no modulational instabilities (those that form patterns). This fact is indicative that if a constant amplitude I is a solution in some region, the amplitude $-I$ is also a solution. The front connecting these two regions, i.e., a domain wall type of initial

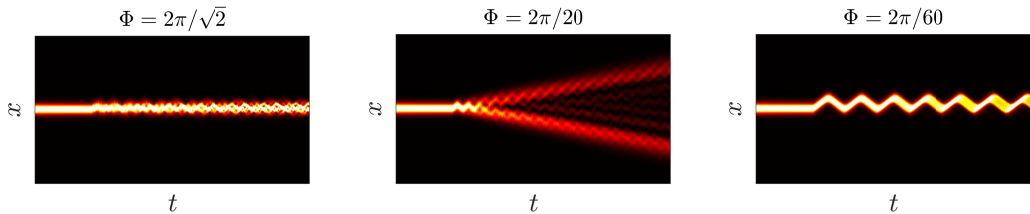


Figure 6. Evolution of the initial soliton considered in Fig. 2 which is subject to a constant electric field after $t = 100$. The intensity of the electric field is given in the title of each panel. The intensity of the walker is given by a heatmap, black indicates low probability density and brighter/hotter colours indicate higher probability density.

condition with $\delta = \pi/2$, should therefore be stable. In Fig. 5 we represent the stationary probability and phase difference obtained from an initial condition

$$\langle x | \psi_t^{\text{dark}} \rangle = I \begin{pmatrix} \tanh(\beta x) \\ -i \tanh(\beta x) \end{pmatrix}, \quad (39)$$

with a smooth transition between the two regions. It can be observed that the left and right regions remain constant and keep the initial phase difference $\delta = \pi/2$. The valley of the central part represents the dark soliton, and right in the centre, where the probability distribution is null, the phase difference is not well-defined.

C. Solitons in electric fields

We now explore whether these structures are robust against the presence of electric fields. To include the effect of an electric field we modify the step evolution defined in Eq. (1) by

$$|\psi_{t+1}\rangle = e^{i\Phi X} SC |\psi_t\rangle, \quad (40)$$

where X is the position operator, and Φ plays the role of the electric field intensity. In the limit where the non-linearity parameter α is null, this unitary evolution corresponds to a Dirac equation with constant electric field in the continuum limit. It was pointed out in [26, 79] that, for values of Φ that are small rational fractions of 2π , the walker displays oscillations around the initial position and if Φ is an irrational multiple of 2π the walker exhibits localization. If Φ is a large rational fraction of 2π the walker quickly exhibits dispersion. In Fig. 6 we explore the dynamics of a soliton under the effect of the electric field in these three regimes. It can be observed that for irrational values of Φ the walker remains localized, but the smooth structure of the initial soliton is lost. If Φ is a rational fraction of 2π the walker undergoes some oscillations but quickly disperses. And if Φ is a smaller fraction of 2π the oscillations of the walker are maintained for longer times.

In Fig. 7 we explore how the dispersion of the walker, characterized by the evolution of its standard deviation

$$\sigma_t = \sqrt{\langle x^2 \rangle - \langle x \rangle^2}, \quad (41)$$

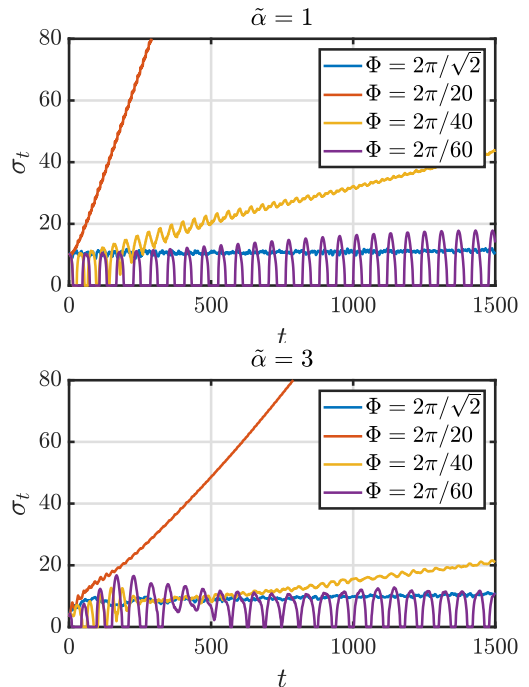


Figure 7. Dispersion of the walker for different values of the non-linearity parameter $\tilde{\alpha}$ and electric intensity Φ . The initial condition is given by Eq. (36), with a value of $\beta = \tilde{\alpha}\tilde{\theta}_0/2$ and the value $\theta_0 = \pi/3$ has been set for the coin.

evolves under these regimes for different values of the non-linearity parameter. On the one hand, it can be observed that for higher values of the non-linearity parameter α the dispersion produced by the values of $\Phi = 2\pi/20$ and $\Phi = 2\pi/40$ is slowed down, and the amplitude of the oscillations produced by $\Phi = 2\pi/60$ is reduced. On the other hand, when Φ is an irrational fraction of 2π the non-linearity parameter α does not seem to have any effect on the localization of the walker.

D. No solitons in 2D

This NLQW can be extended to a two-dimensional spatial Hilbert space as $\mathcal{H}_x \otimes \mathcal{H}_y$ with basis $\{|x\rangle \otimes |y\rangle\}$ together with the same 2 internal degrees of freedom as before, and spinor components $u_{t,x,y}$, $d_{t,x,y}$. The time step is defined as

$$|\psi_{t+1}\rangle = S_y C S_x C |\psi_t\rangle, \quad (42)$$

where $S_i = e^{-i\hat{p}_i \sigma_z}$ is the conditional shift operator in the direction $i = \{x, y\}$, and C is the same coin operators as before, with the rotation angle similarly defined as

$$\theta_{t,x,y} = \theta_0 + \alpha |u_{t,x,y}| |d_{t,x,y}| \sin(\varphi_{t,x,y}^u - \varphi_{t,x,y}^d), \quad (43)$$

where there is a dependence on the values of the walker in both dimensions.

It was discussed in [80] that non-linear QWs, that introduce the non-linearity in form of phases on the walker components, can be exploited to perform efficient search tasks on the two-dimensional grid. In line with those findings, we observed that the NLQW that introduces non-linearities in the coin rotation operator angle produces ballistic dispersion, indicating that no soliton-like structures are formed in the two-dimensional case.

VI. CONCLUSIONS

In this work, we have analysed a nonlinear QW model which can be experimentally implemented using the components of the electric field on an optical nonlinear Kerr medium. Differently to the Non Linear Optical Galton Board model studied in [39], where nonlinearities appear as two separate phases on the coin operator (or, equivalently, of the displacement operator), here they give rise to a rotation in the coin operator, with a single angle which depends (in a nonlinear fashion) on the state of the walker. This simple dependence makes it easy to consider the space-time continuum limit of the evolution equation, which takes the form of a nonlinear Dirac equation. The analysis of this continuum limit allows us, under some approximations, to gain some insight into the nature of the soliton structure, which is illustrated by our numerical calculations.

These solitons are stable structures whose trajectories can be modulated by choosing the appropriate initial conditions. From the continuum limit stability analysis, we were able to predict the existence of dark solitons which were numerically characterized. We have also studied the stability of solitons when they are subject to an additional phase that simulates an external electric field. For electric field intensities that are irrational the solitons remained localized but their smooth characterized structure is lost. For rational fractions of 2π electric field intensities, we characterized two regimes. For strong

electric fields, an initial soliton becomes slowly disrupted and the walker disperses, so that an increase of the non-linearity parameter slows down the dispersion produced by the strong electric field. For weak electric fields, oscillations of the soliton central position are present. Finally, we also explored a 2D version of these model, where no evidence of soliton formation was found.

To summarize, nonlinear quantum walks constitute an interesting field with a rich phenomenology that can be used for a better control of its algorithmic and simulation properties.

ACKNOWLEDGMENTS

This work has been funded by the Spanish MCIN/AEI/10.13039/501100011033 grant PID2020-113334GB-I00, SEV-2014-0398 and Generalitat Valenciana grant CIPROM/2022/66, the Ministry of Economic Affairs and Digital Transformation of the Spanish Government through the QUANTUM ENIA project call - QUANTUM SPAIN project, and by the European Union through the Recovery, Transformation and Resilience Plan - NextGenerationEU within the framework of the Digital Spain 2026 Agenda, and by the CSIC Interdisciplinary Thematic Platform (PTI+) on Quantum Technologies (PTI-QTEP+). This project has also received funding from the European Union's Horizon 2020 research and innovation program under grant agreement 101086123-CaLIGOLA. This work was funded by Spanish Ministerio de Ciencia Innovación y Universidades-Agencia Estatal de Investigación and European Union FEDER through Project PID2020-120056GB-C22 and by the Direcció General de Ciència i Investigació Generalitat Valenciana through Project CIAICO2021276.

Appendix A: Derivation of the continuum Limit

We can rewrite the walker time step of Eq. (1), using spinors, as

$$\Psi(t + \epsilon, x) = e^{-\epsilon \partial_x \sigma_x} e^{-i \sigma_y \epsilon \tilde{\theta}(t,x)} \Psi(t, x) \quad (A1)$$

where we have expressed it in terms of t and x that are both discretized by the same amount ϵ . When the limit $\epsilon \rightarrow 0$ is taken, the continuum limit of the equation is obtained. We have rescaled the original rotation angle by the same spacing $\tilde{\theta}(t,x)\epsilon = \theta_{t,x}$. These definitions allow us to write the l.h.s. of the equation as

$$\Psi(t + \epsilon, x) \approx \Psi(t, x) + \epsilon \partial_t \Psi(t, x), \quad (A2)$$

while we can approximate the r.h.s. as

$$\left(1 - \epsilon \sigma_z \partial_x\right) \left(1 - i \epsilon \tilde{\theta}(t, x) \sigma_y\right) \Psi(t, x). \quad (A3)$$

The zero order $O(\epsilon^0)$ exactly match in both sides, and the first order terms $O(\epsilon)$ define the following continuous equation

$$\partial_t \Psi(t, x) = -\sigma_z \partial_x \Psi(t, x) - i\bar{\theta}(t, x) \sigma_y \Psi(t, x), \quad (\text{A4})$$

which can be rewritten as Eq. (23).

Appendix B: Stability analysis

We start with Eqs. (29) and substitute in them $f_i(x, t) = \bar{f} + \delta f_i(x, t)$, $f_i \in \{U, D, \delta, \sigma\}$, with δf_i a small perturbation and \bar{f}_i the homogeneous-stationary solution values. After linearization of Eqs. (29) around the steady state (i.e. by neglecting nonlinear terms in the perturbations), the equations of evolution for the perturbations can be written as

$$\partial_t \vec{p} = \hat{L} \cdot \vec{p}, \quad (\text{B1})$$

$$\vec{p} = \text{col}(\delta U, \delta D, \delta \delta, \delta \sigma), \quad (\text{B2})$$

$$\hat{L}_{ij} = \left[\frac{\partial \dot{p}_i}{\partial p_j} \right]_{p_i = \bar{p}_i}, \quad (\text{B3})$$

where the matrix elements \hat{L}_{ij} are given by

$$\begin{aligned} \hat{L}_{11} &= -\hat{L}_{22} = (\theta_0 - \bar{\theta}) \cos \delta - \partial_x, \\ \hat{L}_{33} &= \hat{L}_{44} = \hat{L}_{14} = \hat{L}_{24} = 0, \\ \hat{L}_{12} &= \hat{L}_{21} = (\theta_0 - 2\bar{\theta}) \cos \bar{\delta}, \\ \hat{L}_{13} &= -\hat{L}_{23} = \sqrt{\bar{I}} (\bar{\theta} \sin \bar{\delta} - \alpha \bar{I} \cos^2 \bar{\delta}), \\ L_{31} &= -L_{32} = -2\bar{\theta} \sin \delta / \sqrt{\bar{I}}, \\ L_{34} &= -\partial_x, \\ \hat{L}_{41} &= \hat{L}_{42} = 2\sqrt{\bar{I}} \alpha \sin^2 \bar{\delta}, \\ L_{43} &= -2(\theta_0 - 2\bar{\theta}) \cos \bar{\delta} - \partial_x, \end{aligned}$$

with $\bar{\theta} = \theta_0 + \alpha \bar{I} \sin \bar{\delta}$, and the overbar indicating the homogeneous stationary solutions.

Equation (B1) admits solutions of the form

$$\vec{p}_j = \vec{p}_{0j} e^{\lambda_j t} e^{ikx}, \quad (\text{B4})$$

where λ_j are the eigenvalues of the matrix \hat{L} and \vec{p}_j are the eigenvectors. Clearly, whenever $\text{Re}(\lambda_j) > 0$, for a particular value of k , the corresponding steady state is unstable versus perturbations in the form of plane waves with wavenumber k .

Next, we detail the stability properties of the different homogeneous steady states. For the trivial solution $\bar{I} = 0$, as for solution $\bar{\theta} = 0$, the characteristic polynomial can be written as $\mathcal{P}(\lambda) = (\lambda^2 + k^2)^2 = 0$, hence $\lambda^2 = \pm ik$ and these solutions are consequently neutrally stable whenever they exist.

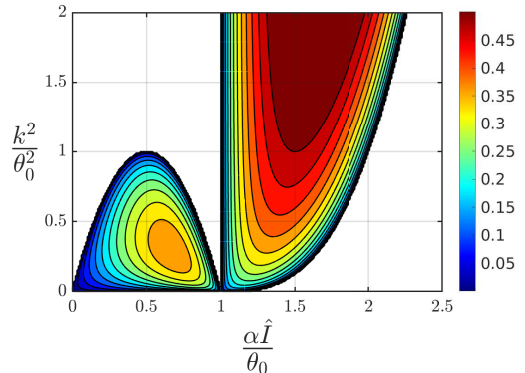


Figure 8. Real part of the eigenvalue that solves the characteristic equation $\mathcal{P}_-(\lambda) = 0$ and is scaled by θ_0 , i.e., we plot $\Re(\lambda/\theta_0)$. The white regions represent the space where the real part of λ is null.

For solutions $\delta = \pm\pi/2$, the characteristic polynomials read,

$$\begin{aligned} \mathcal{P}_\pm(\lambda) &= \lambda^4 + 2 \left[k^2 + 2(\alpha \bar{I} \pm \theta_0)^2 \right] \lambda^2 \\ &\quad + k^4 + 4k^2 \alpha \bar{I} (\alpha \bar{I} \pm \theta_0) = 0, \end{aligned} \quad (\text{B5})$$

where \pm corresponds to $\pm\pi/2$. It is not difficult to show that $\mathcal{P}_+(\lambda) = 0$ provides purely imaginary eigenvalues, hence the solution $\delta = +\pi/2$ is neutrally stable. Contrarily, $\mathcal{P}_-(\lambda)$ provides two couples of eigenvalues, one of which has a positive real part. In Fig. 8 we are representing the real part of the eigenvalue, multiplied by θ_0 , in the plane $(\alpha \bar{I}/\theta_0, k^2/\theta_0^2)$. It is clearly seen that: (i) for $\alpha \bar{I}/\theta_0 = 1$ the eigenvalue is zero for all k ; (ii) for $\alpha \bar{I}/\theta_0 < 1$ the eigenvalue is positive for $k^2/\theta_0^2 < 1$ and null for $k^2/\theta_0^2 > 1$; and (iii) for $\alpha \bar{I}/\theta_0 > 1$ the eigenvalue is positive for all k . Hence, we conclude that there is a long-wavelength modulational instability whenever $\alpha \bar{I}/\theta_0 < 1$, and a short-wavelength modulational instability whenever $\alpha \bar{I}/\theta_0 > 1$.

- [1] A. M. Childs. Universal computation by quantum walk. *Phys. Rev. Lett.*, 102:180501, 2009. I
[2] A. M. Childs, D. Gosset, and Z. Webb. Universal computation by multiparticle quantum walk. *Science*, 339:791–

794, 2013.

- [3] N. B. Lovett, S. Cooper, M. Everitt, M. Trevers, and V. Kendon. Universal quantum computation using the discrete-time quantum walk. *Phys. Rev. A*, 81(4):042330,

2010. I
- [4] A. M. Childs and J. Goldstone. Spatial search by quantum walk. *Phys. Rev. A*, 70(2):022314, 2004. I
- [5] A. Tulsi. Faster quantum-walk algorithm for the two-dimensional spatial search. *Phys. Rev. A*, 78(1):012310, 2008.
- [6] F. Magniez, A. Nayak, J. Roland, and M. Santha. Search via quantum walk. *SIAM J. Comput.*, 40(1):142–164, 2011.
- [7] A. Ambainis, A. Bačkurs, N. Nahimovs, R. Ozols, and A. Rivosh. Search by quantum walks on two-dimensional grid without amplitude amplification. In *Theory of Quantum Computation, Communication, and Cryptography*, pages 87–97. Springer Nature, 2013.
- [8] I. Foulger, S. Gnutzmann, and G. Tanner. Quantum walks and quantum search on graphene lattices. *Phys. Rev. A*, 91:062323, 2015.
- [9] M. Roget, S. Guillet, P. Arrighi, and G. Di Molfetta. Grover search as a naturally occurring phenomenon. *Phys. Rev. Lett.*, 124(18), May 2020. I
- [10] A. Ambainis. Quantum walk algorithm for element distinctness. *SIAM J. Comput.*, 37:210–239, 2007. I
- [11] F. W. Strauch. Relativistic quantum walks. *Phys. Rev. A*, 73:054302, 2006. I
- [12] F. W. Strauch. Relativistic effects and rigorous limits for discrete-time and continuous-time quantum walks. *J. Math. Phys.*, 48:082102, 2007.
- [13] A. M. Childs. On the relationship between continuous- and discrete-time quantum walk. *Commun. Math. Phys.*, 294(2):581–603, 2010.
- [14] P. Philipp and R. Portugal. Exact simulation of coined quantum walks with the continuous-time model. *Quantum Inf. Process.*, 16(14), 2016.
- [15] A. T. Schmitz and W. A. Schwalm. Simulating continuous-time hamiltonian dynamics by way of a discrete-time quantum walk. *Phys. Lett. A*, 380(11-12):1125–1134, 2016. I
- [16] F. Debbasch, G. Di Molfetta, D. Espaze, and V. Foulonéau. Propagation in quantum walks and relativistic diffusions. *Phys. Scripta*, 151:014044, 2012. I
- [17] P. Arnault and F. Debbasch. Landau levels for discrete-time quantum walks in artificial magnetic fields. *Physica A*, 443:179–191, February 2016.
- [18] P. Arnault and F. Debbasch. Quantum walks and discrete gauge theories. *Phys. Rev. A*, 93(5):052301, May 2016. I
- [19] P. Arnault, G. Di Molfetta, M. Brachet, and F. Debbasch. Quantum walks and non-Abelian discrete gauge theory. *Phys. Rev. A*, 94(1):012335, July 2016. I
- [20] G. Di Molfetta, M. Brachet, and F. Debbasch. Quantum walks as massless Dirac fermions in curved space. *Phys. Rev. A*, 88:042301, 2013. I
- [21] G. Di Molfetta, F. Debbasch, and M. Brachet. Quantum walks in artificial electric and gravitational fields. *Physica A*, 397:157–168, 2014.
- [22] P. Arnault and F. Debbasch. Quantum walks and gravitational waves. *Ann. Phys. (N. Y.)*, 383:645–661, August 2017.
- [23] P. Arrighi, S. Facchini, and M. Forets. Quantum walking in curved spacetime. *Quantum Inf. Process.*, 15(8):3467–3486, 2016.
- [24] P. Arrighi and S. Facchini. Quantum walking in curved spacetime: (3+1) dimensions, and beyond. *Quantum Info. Comput.*, 17(9-10):810–824, 2017. I
- [25] G. Di Molfetta and A. Pérez. Quantum walks as simulators of neutrino oscillations in a vacuum and matter. *New J. Phys.*, 18(10):103038, 2016. I
- [26] Pablo Arnault, Benjamin Pepper, and A. Pérez. Quantum walks in weak electric fields and bloch oscillations. *Phys. Rev. A*, 101:062324, Jun 2020. V C
- [27] I. Márquez-Martín, G. Di Molfetta, and A. Pérez. Fermion confinement via quantum walks in (2+1)-dimensional and (3+1)-dimensional space-time. *Phys. Rev. A*, 95(4):042112, 2017. I
- [28] K. Manouchehri and J. Wang. *Physical Implementation of Quantum Walks*. Springer, 2014. I
- [29] H. Trompeter, W. Krolikowski, D. N. Neshev, A. S. Desyatnikov, A. A. Sukhorukov, Y. S. Kivshar, T. Pertsch, U. Peschel, and F. Lederer. Bloch oscillations and Zener tunneling in two-dimensional photonic lattices. *Phys. Rev. Lett.*, 96:053903, 2006. I
- [30] A. Schreiber, K. N. Cassemiro, V. Potoček, A. Gábris, P. J. Mosley, E. Andersson, I. Jex, and Ch. Silberhorn. Photons walking the line. *Phys. Rev. Lett.*, 104:050502, 2010.
- [31] Alberto Peruzzo, Mirko Lobino, Jonathan C. F. Matthews, Nobuyuki Matsuda, Alberto Politi, Konstantinos Poullos, Xiao-Qi Zhou, Yoav Lahimi, Nur Ismail, Kerstin Wörhoff, Yaron Bromberg, Yaron Silberberg, Mark G. Thompson, and Jeremy L. O’Brien. Quantum walks of correlated photons. *Science*, 329(5998):1500–1503, 2010.
- [32] T. Kitagawa, M. A. Broome, A. Fedrizzi, M. S. Rudner, E. Berg, I. Kassal, A. Aspuru-Guzik, E. Demler, and A. G. White. Observation of topologically protected bound states in photonic quantum walks. *Nat. Commun.*, 3:882, 2012.
- [33] L. Sansoni, F. Sciarrino, G. Vallone, P. Mataloni, A. Crespi, R. Ramponi, and R. Osellame. Two-particle bosonic-fermionic quantum walk via 3D integrated photonics. *Phys. Rev. Lett.*, 108:010502, 2012.
- [34] A. Crespi, R. Osellame, R. Ramponi, V. Giovannetti, R. Fazio, L. Sansoni, F. De Nicola, F. Sciarrino, and P. Mataloni. Anderson localization of entangled photons in an integrated quantum walk. *Nat. Photonics*, 7:322–328, 2013.
- [35] Octavi Boada, Leonardo Novo, Fabio Sciarrino, and Yasser Omar. Quantum walks in synthetic gauge fields with three-dimensional integrated photonics. *Phys. Rev. A*, 95:013830, Jan 2017. I
- [36] M. Genske, W. Alt, A. Steffen, A. H. Werner, R. F. Werner, D. Meschede, and A. Alberti. Electric quantum walks with individual atoms. *Phys. Rev. Lett.*, 110:190601, 2013. I
- [37] Colin D. Bruzewicz, John Chiaverini, Robert McConnell, and Jeremy M. Sage. Trapped-ion quantum computing: Progress and challenges. *Applied Physics Reviews*, 6(2):021314, May 2019. I
- [38] Morten Kjaergaard, Mollie E. Schwartz, Jochen Braumüller, Philip Krantz, Joel I.-J. Wang, Simon Gustavsson, and William D. Oliver. Superconducting qubits: Current state of play. *Annu. Rev. Condens. Matter Phys.*, 11(1):369–395, March 2020. I
- [39] C. Navarrete-Benlloch, A. Pérez, and Eugenio Roldán. Nonlinear optical galton board. *Phys. Rev. A*, 75:062333, Jun 2007. I, II B, II B, V, VI
- [40] Martin Wimmer, Alois Regensburger, Christoph Bersch, Mohammad-Ali Miri, Sascha Batz, Georgy Onishchukov, Demetrios N. Christodoulides, and Ulf Peschel. Opti-

- cal diametric drive acceleration through action–reaction symmetry breaking. *Nature Phys*, 9(12):780–784, oct 2013. IIB
- [41] Martin Wimmer, Monika Monika, Iacopo Carusotto, Ulf Peschel, and Hannah M. Price. Superfluidity of light and its breakdown in optical mesh lattices. *Phys. Rev. Lett.*, 127:163901, Oct 2021. IIB
- [42] Hannah M. Price, Martin Wimmer, Monika Monika, Ulf Peschel, and Iacopo Carusotto. Theory of hydrodynamic phenomena in optical mesh lattices. *arXiv*, 2022. IIB
- [43] Sambhu Jana, Kojam Monika Devi, and Dibakar Roy Chowdhury. Obstruction immune topological propagation in 3d-printed metal-based photonic crystals. *Optics Communications*, 529:129111, 2023. IIB
- [44] Giuseppe Di Molfetta, Fabrice Debbasch, and Marc Brachet. Nonlinear optical galton board: Thermalization and continuous limit. *Phys. Rev. E*, 92:042923, Oct 2015. IIB, IV
- [45] Chang-Woo Lee, Pawel Kurzyński, and Hyunchul Nha. Quantum walk as a simulator of nonlinear dynamics: Nonlinear dirac equation and solitons. *Phys. Rev. A*, 92:052336, Nov 2015.
- [46] Masaya Maeda and Akito Suzuki. Continuous limits of linear and nonlinear quantum walks. *Reviews in Mathematical Physics*, 32(04):2050008, 2020. IIB
- [47] A. R. C. Buarque and W. S. Dias. Self-trapped quantum walks. *Phys. Rev. A*, 101:023802, Feb 2020. IIB
- [48] A. R. C. Buarque and W. S. Dias. Probing coherence and noise tolerance in discrete-time quantum walks: Unveiling self-focusing and breathing dynamics. *Phys. Rev. A*, 103:042213, Apr 2021. IIB
- [49] A. R. C. Buarque, W. S. Dias, F. A. B. F. de Moura, M. L. Lyra, and G. M. A. Almeida. Rogue waves in discrete-time quantum walks. *Phys. Rev. A*, 106:012414, Jul 2022. IIB
- [50] Masaya Maeda, Hironobu Sasaki, Etsuo Segawa, Akito Suzuki, and Kanako Suzuki. Weak limit theorem for a nonlinear quantum walk. *Quantum Inf Process*, 17(9), jul 2018. IIB
- [51] Masaya Maeda, Hironobu Sasaki, Etsuo Segawa, Akito Suzuki, and Kanako Suzuki. Dynamics of solitons for nonlinear quantum walks. *J. Phys. Commun.*, 3(7):075002, jul 2019. IIB, V
- [52] Masaya Maeda. Asymptotic stability of small bound state of nonlinear quantum walks. *Physica D: Nonlinear Phenomena*, 439:133408, 2022. IIB
- [53] P. R. N. Falcão, J. P. Mendonça, A. R. C. Buarque, W. S. Dias, G. M. A. Almeida, and M. L. Lyra. Nonlinear three-state quantum walks. *Phys. Rev. A*, 106:042202, Oct 2022. IIB
- [54] F. S. Passos and A. R. C. Buarque. Nonlinear flip-flop quantum walks through potential barriers. *Phys. Rev. A*, 106:062407, Dec 2022. IIB, V
- [55] Yutaka Shikano, Tatsuaki Wada, and Junsei Horikawa. Discrete-time quantum walk with feed-forward quantum coin. *Sci Rep*, 4(1), mar 2014. IIB
- [56] Y. Gerasimenko, B. Tarasinski, and C. W. J. Beenakker. Attractor-repeller pair of topological zero modes in a nonlinear quantum walk. *Phys. Rev. A*, 93:022329, Feb 2016. IIB, IIB
- [57] Ken Mochizuki, Norio Kawakami, and Hideaki Obuse. Stability of topologically protected edge states in nonlinear quantum walks: additional bifurcations unique to floquet systems. *J. Phys. A: Math. Theor.*, 53(8):085702, jan 2020. IIB
- [58] J. P. Mendonça, F. A. B. F. de Moura, M. L. Lyra, and G. M. A. Almeida. Emergent nonlinear phenomena in discrete-time quantum walks. *Phys. Rev. A*, 101:062335, Jun 2020. IIB
- [59] Longyan Gong, Xuan Guo, Jingye Sun, Weiwen Cheng, and Shengmei Zhao. Wave packet spreading with periodic, fibonacci quasiperiodic, and random nonlinear discrete-time quantum walks. *Quantum Inf Process*, 21(12), nov 2022. IIB
- [60] Arindam Mallick and Sergej Flach. Logarithmic expansion of many-body wave packets in random potentials. *Phys. Rev. A*, 105:L020202, Feb 2022. IIB
- [61] Xinyuan Zheng and Edo Waks. A strongly interacting photonic quantum walk using single atom beam splitters, 2023. IIB
- [62] Alexander S. Solntsev, Frank Setzpfandt, Alex S. Clark, Che Wen Wu, Matthew J. Collins, Chunle Xiong, Andreas Schreiber, Fabian Katzschmann, Falk Eilenberger, Roland Schiek, Wolfgang Sohler, Arnan Mitchell, Christine Silberhorn, Benjamin J. Eggleton, Thomas Pertsch, Andrey A. Sukhorukov, Dragomir N. Neshev, and Yuri S. Kivshar. Generation of nonclassical biphoton states through cascaded quantum walks on a nonlinear chip. *Phys. Rev. X*, 4:031007, Jul 2014. IIB
- [63] Alberto D. Varga. Edge states in a two-dimensional quantum walk with disorder. *Eur. Phys. J. B*, 90(3), mar 2017. IIB
- [64] Alessandro Bisio, Giacomo Mauro D’Ariano, Paolo Perinotti, and Alessandro Tosini. Thirring quantum cellular automaton. *Phys. Rev. A*, 97:032132, Mar 2018. IIB
- [65] Riccardo Adami, Reika Fukuizumi, and Etsuo Segawa. A nonlinear quantum walk induced by a quantum graph with nonlinear delta potentials. *Quantum Inf Process*, 18(4), mar 2019. IIB
- [66] Joshua R. Tempelman, Kathryn H. Matlack, and Alexander F. Vakakis. Topological protection in a strongly nonlinear interface lattice. *Phys. Rev. B*, 104:174306, Nov 2021. IIB
- [67] Philip Held, Melanie Engelkemeier, Syamsundar De, Sonja Barkhofen, Jan Sperling, and Christine Silberhorn. Driven gaussian quantum walks. *Phys. Rev. A*, 105:042210, Apr 2022. IIB
- [68] A. S. Pikovsky and D. L. Shepelyansky. Destruction of anderson localization by a weak nonlinearity. *Phys. Rev. Lett.*, 100:094101, Mar 2008. IIB
- [69] Yoav Lahini, Assaf Avidan, Francesca Pozzi, Marc Sorel, Roberto Morandotti, Demetrios N. Christodoulides, and Yaron Silberberg. Anderson localization and nonlinearity in one-dimensional disordered photonic lattices. *Phys. Rev. Lett.*, 100:013906, Jan 2008. IIB
- [70] Mahdi Ebrahimi Kahou and David L. Feder. Quantum search with interacting bose-einstein condensates. *Phys. Rev. A*, 88:032310, Sep 2013. IIB
- [71] David A Meyer and Thomas G Wong. Nonlinear quantum search using the gross-pitaevskii equation. *New J. Phys.*, 15(6):063014, jun 2013. IIB
- [72] David A. Meyer and Thomas G. Wong. Quantum search with general nonlinearities. *Phys. Rev. A*, 89:012312, Jan 2014. IIB
- [73] M. Chiew, K. de Lacy, C. H. Yu, S. Marsh, and J. B. Wang. Graph comparison via nonlinear quantum search. *Quantum Inf Process*, 18(10), aug 2019. IIB

- [74] Giuseppe Di Molfetta and Basile Herzog. Searching via nonlinear quantum walk on the 2d-grid. *Algorithms*, 13(11):305, nov 2020. IIB
- [75] L. J. R. Bezerra, D. Morais, A. R. C. Buarque, F. S. Passos, and W. S. Dias. Thresholds between modulational stability, rogue waves and soliton regimes in saturable nonlinear media. *Nonlinear Dyn*, 111(7):6629–6638, dec 2022. IIB
- [76] Peter L. Knight, Eugenio Roldán, and J. E. Sipe. Quantum walk on the line as an interference phenomenon. *Phys. Rev. A*, 68:020301, Aug 2003. IIIB
- [77] Andreas Schreiber, Aurél Gábris, Peter P. Rohde, Kaisa Laiho, Martin Štefaňák, Václav Potoček, Craig Hamilton, Igor Jex, and Christine Silberhorn. A 2d quantum walk simulation of two-particle dynamics. *Science*, 336(6077):55–58, apr 2012. IIIB
- [78] Robert W. Boyd. *Nonlinear Optics, Third Edition*. Academic Press, Inc., USA, 3rd edition, 2008. IIIB, IV A
- [79] C. Cedzich, T. Rybár, A. H. Werner, A. Alberti, M. Genske, and R. F. Werner. Propagation of quantum walks in electric fields. *Phys. Rev. Lett.*, 111:160601, Oct 2013. VC
- [80] Di Molfetta Giuseppe, Giuseppe Di Molfetta, and Basile Herzog. Searching via Nonlinear Quantum Walk on the 2D-Grid. *Algorithms*, 13(11):305, November 2020. VD